Stage 5 Approved Version

March 2006

Research Report: UCPRC-RR-2006-02

Construction and Test Results on Dowel Bar Retrofit HVS Test Sections 556FD, 557FD, 558FD, and 559FD: State Route 14, Los Angeles County at Palmdale

Authors:

Yi Bian, John Harvey, and Abdikarim Ali

This work was completed as part of Partnered Pavement Research Program Strategic Plan Item 4.8 "Dowel Bar Retrofit of Rigid Pavements"

PREPARED FOR:

California Department of Transportation
Sacramento

PREPARED BY:

University of California
Pavement Research Center
UC Davis and Berkeley

DOCUMENT RETRIEVAL PAGE			**Report No: UCPRC-RR-2006-02**
Title: Construction and Test Results on Dowel Bar Retrofit HVS Test Sections 556FD, 557FD, 558FD and 559FD: State Route 14, Los Angeles County at Palmdale			
Authors: Y. Bian, J. Harvey, and A. Ali			
Prepared for: Caltrans	**FHWA No.:** S/CA/RI-2006/27b		**Date**: March 2006
Strategic Plan Element No: 4.8	**Status:** Final		**Status:** Final, approved by Caltrans

Abstract: This report presents the results of construction, Heavy Vehicle Simulator (HVS) tests, deflection tests, post-HVS forensic testing, and analysis on dowel bar retrofitted (DBR) concrete pavement test sections at Palmdale, California. This project was originally proposed in 2000 by the Caltrans Headquarters Division of Design. Benefits expected from this research are to provide Caltrans with information about design and construction of DBR to help determine where DBR may be a cost-effective strategy for rehabilitating rigid pavement and to help obtain best performance where DBR is selected as the preferred rehabilitation strategy.

HVS Tests: Pavement sections include retrofitted joints and transverse cracks with three and four epoxy-coated steel dowels, four hollow stainless steel dowels, and four fiber-reinforced polymer dowels per wheelpath. HVS and FWD results at Palmdale also are compared with the results from previous HVS testing. HVS testing showed that joint performance with four epoxy-coated steel dowels was generally the best of all the sections in terms of load transfer efficiency (LTE) and joint deflection. Three dowels per wheelpath was substantially worse than the other test sections that had four dowels per wheelpath in terms of load transfer efficiency (LTE), however, it was substantially better than before DBR. Joint deflections were substantially better for four epoxy-coated steel dowels per wheelpath than for the other sections. HVS results show that for each of the DBR alternatives, LTE was not substantially affected by heavy HVS loading and that the slabs failed by fatigue cracking before LTE dropped substantially.

FWD Tests: The primary performance criteria are LTE and vertical deflection of the joints. Larger joint vertical deflections and lower LTE are strongly correlated with increased rate of faulting and roughness development. FWD deflection measurements agree with those under HVS wheel loading, showing that LTE was substantially improved by DBR and was not substantially affected by HVS trafficking. Results are presented showing sensitivity of deflections and LTE to dowel type, number of dowels per wheelpath, and slab temperature based on FWD measurements.

Construction and materials: Observations about DBR construction and materials presented indicate variability in depth of dowel bar placement, overall good condition of the slots and grout, and test results showing that the grout met Caltrans specifications for flexural and compressive strength.

Keywords:
Dowel bar retrofit, concrete pavement, load transfer efficiency, fiber-reinforced polymer dowels, hollow stainless steel dowels

Proposals for Implementation:

Related documents: UCPRC-RR-2003-03

Signatures:

J Harvey **1st Author**	E. Kohler **Technical Review**	D. Spinner **Editor**	J Harvey **Principal Investigator**	M. Samadian **Caltrans Contract Manager**

DISCLAIMER

The contents of this report reflect the views of the authors who are responsible for the facts and accuracy of the data presented herein. The contents do not necessarily reflect the official views or policies of the State of California or the Federal Highway Administration. This report does not constitute a standard, specification, or regulation.

ACKNOWLEDGMENTS

The University of California Pavement Research Center would like to acknowledge the cooperation and work devoted to this project by California Department of Transportation (Caltrans) District 7, especially Gary Laurent, Construction Resident Engineer, and the Maintenance Superintendents and crews who supported this study.

The Caltrans Division of Research and Innovation (DRI) Contract Monitor was Michael Samadian, under the direction of Tom Hoover and Nick Burmas. David Bush was the Dynatest site manager during HVS testing, and Peter Millar was the HVS operator.

Construction of the dowel bar retrofits was performed by PenHall, under the direction of Casey Holloway. Field site sampling support was performed under the direction of Clark Scheffy. The researchers would also like to thank the suppliers of the various types of dowels.

EXECUTIVE SUMMARY

This report presents the results of Heavy Vehicle Simulator (HVS) tests, deflection tests, post-HVS forensic testing, and analysis on dowel bar retrofitted (DBR) concrete pavement test sections at Palmdale, California. This project was originally proposed in 2000 by the Caltrans Headquarters Division of Design. Other stakeholder Caltrans units included Headquarters METS Office of Rigid Pavement Materials and Structural Concrete as well as Caltrans Districts 1 and 7. Benefits expected from this research are to provide Caltrans with information needed for decisions about design and construction of DBR in order (1) to help determine where DBR may be a cost-effective strategy for rehabilitating rigid pavement and (2) to help obtain best performance where DBR is selected as the preferred rehabilitation strategy. This work was completed as part of Partnered Pavement Research Program Strategic Plan Item 4.8, "Dowel Bar Retrofit of Rigid Pavements."

Tasks for this project focus on four objectives agreed upon with Caltrans. This report completes the requirements for the first objective. This report augments information provided in 2003 about HVS and related tests at Ukiah (10).

1. Field Accelerated Pavement Testing with the HVS: Full-scale data tests of several types of dowels to compare performance of retrofitted joints and cracks with those not retrofitted. Observations and results are presented in this report.
2. Field Live Traffic Testing: Collecting field data on a long-term basis (approximately two years) under real loads will enable calibration of HVS and analysis results. Results will be presented in a separate report.
3. Laboratory testing of materials: A report on completed corrosion tests was submitted to Caltrans in 2005. A separate report on laboratory testing of FRP dowels will be provided.
4. Modeling (future reports will present results for the following tasks):

- Finite element analysis of doweled concrete pavement joint
- Compilation of performance data from existing DBR projects throughout the U.S.
- Life Cycle Cost analyses

Results for the first objective are presented in the report in sections that describe the HVS test sections, results of HVS tests, results of FWD tests, and observations about construction and materials.

OVERVIEW OF HVS TEST SECTIONS

Pavement sections tested include retrofitted joints and transverse cracks with three and four epoxy-coated steel dowels, four hollow stainless steel dowels, and four fiber-reinforced polymer dowels per wheelpath. The results of the HVS testing and other testing and analysis on the dowel bar retrofit sections at Palmdale also are compared with the results from previous HVS testing of the following test sections:

- DBR sections at Ukiah,
- Sections of new pavement at Palmdale where dowels were installed during construction of the slab, and
- Sections of new pavement at Palmdale that were constructed without dowels.

The dowel bar retrofit HVS tests were conducted on previously untrafficked portions of what is referred to as "Section 7" of the North Tangent at Palmdale. The pavement in Section 7 has cement-treated base (CTB), undoweled, jointed, plain concrete slabs with untied shoulders, and a standard width of 3.7 m. Four sections on Section 7 were dowel bar retrofitted for HVS test sections as summarized below in Table A.

Trafficking of the four HVS test sections proceeded under similar temperature and rainfall to enable the following comparisons:

- Four epoxy-coated steel dowels per wheelpath (556FD) versus three dowels per wheelpath (557FD), and
- Epoxy-coated steel dowels (559FD, Joint 32) versus hollow stainless steel dowels (559FD, Joint 33) versus fiber-reinforced polymer (FRP) dowels (558FD), all with four dowels per wheelpath.

Trafficking consisted of 60 kN (13,500 lb) and 90 kN (20,250 lb) dual-wheel truck-tire loading and 150 kN (33,750 lb) aircraft, single-wheel loading.

Table A Summary of Palmdate Dowel Bar Retrofit Test Sections

HVS Test Section	Joint or Crack Number	Type of Dowels	Number of Dowels	Number of HVS load repetitions
558FD	Joint 41	Epoxy-coated steel	Four per wheelpath	2,208,578
	Crack 2	Fiber reinforced polymer		
	Joint 42	Fiber reinforced polymer		
556FD	Joint 38	Epoxy-coated steel	Four per wheelpath	2,208,546
	Joint 39	Epoxy-coated steel		
557FD	Joint 35	Epoxy-coated steel	Three per wheelpath	1,121,600
	Joint 36	Epoxy-coated steel		
559FD	Joint 32	Epoxy-coated steel	Four per wheelpath	2,001,497
	Crack 1	Hollow stainless steel in one wheelpath; epoxy-coated steel in other wheelpath		
	Joint 33	Hollow stainless steel		

RESULTS OF HVS TESTS

HVS tests followed the three failure criteria shown below.

- Fatigue cracking of the concrete slab,
- Major damage to the DBR joints, or
- Loss of LTE of the loaded joint or crack.

The primary performance criteria for the HVS test sections is load transfer efficiency (LTE) of the joints and vertical deflection of the joints. Highlighted here are deflections and LTE results, from both FWD and Joint Deflection Measurement Devices (JDMDs).

Comparison of DBR alternatives: Fatigue life under HVS loads. All of the HVS test sections failed by fatigue cracking of the concrete slab. Neither of the other two failure types occurred on any of the test sections. Sections with four dowels per wheelpath withstood a similar number of HVS load repetitions before failing by fatigue cracking.

HVS results show that for each of the DBR alternatives, load transfer efficiency was not substantially damaged by heavy HVS loading and that the slabs failed by fatigue cracking before the LTE dropped substantially. These results, where DBR outlasted the structural effectiveness of the concrete slabs, are representative of the materials, quality, conditions, and workmanship in these test sections. HVS trafficking was not applied to any of the Palmdale test sections until at least one month after construction and after more than a year for some of the sections.

Comparison of DBR alternatives with three vs. four dowels per wheelpath: Fatigue life under HVS loads. Fatigue life of the slab with three dowels per wheelpath was substantially shorter than the other test sections that had four dowels per wheelpath. Longer fatigue life, higher LTE, and lower deflections indicated better performance under these test conditions by four dowels per wheelpath when compared to three dowels per wheelpath.

Comparison of DBR alternatives: Maximum joint deflections. Under HVS loading all of the DBR joints but one showed an increase in joint maximum deflection after HVS trafficking. This deflection is not attributed to temperature changes. The increases came under the 90 kN and 150 kN loading. The only joint not showing an increase had FRP dowels in Section 558FD. The other joint with FRP dowels in the same section behaved the same as all the other joints.

Comparison of DBR alternatives: Joint vertical deflections. The four epoxy-coated steel dowels had much smaller joint vertical deflections than the others. Deflections for the alternatives (four FRP dowels per wheelpath, four hollow stainless steel dowels per wheelpath, and three epoxy-coated steel

dowels per wheelpath) showed deflections similar to each other. At comparable temperatures, three epoxy-coated steel dowels showed the largest deflections.

Comparison of DBR alternatives: LTE under HVS loads. All of the sections showed a slight increase in initial LTE with increase in HVS wheel load (from 60 to 90 to 150 kN). LTE is nearly always higher than 90 percent on the DBR joints, regardless of temperature and load, under HVS loading (using the moving wheel definition of LTE described in this report).

Comparison of DBR alternatives: LTE after HVS trafficking (JDMDs). All of the DBR joints showed little or no decrease in LTE after HVS trafficking, based on measurements under the 60 kN HVS wheel load.

Comparison of DBR with three vs. four dowels per wheelpath: Deflection and LTE results. Under HVS loading, LTE values were lower with three epoxy-coated steel dowels per wheelpath than all of the joints with four dowels per wheelpath, regardless of the type of dowel. Joint deflections were higher with three dowels per wheelpath than with four dowels.

Comparison of DBR to undoweled joints: LTE sensitivity to temperature. All but one of the joints showed a sensitivity of LTE to temperature, with LTE increasing with increased temperature. This is expected, and is caused by slab expansion closing the joint and increasing aggregate interlock at the joint. The temperature susceptibility was very low compared to undoweled joints. The one joint that did not show temperature sensitivity of LTE had hollow stainless cylinder dowels.

Comparison of DBR at Ukiah vs. Palmdale: LTE results. Both locations showed similar lack of damage to LTE under HVS trafficking. Comparison of results between the Palmdale DBR sections and the Ukiah DBR sections show a tendency toward higher LTE at Palmdale than Ukiah. This trend correlates with higher temperatures at Palmdale.

RESULTS OF FWD TESTS

As noted in the section “Results of HVS Tests,” the primary performance criteria for the HVS test sections are load transfer efficiency of the joints and vertical deflection of the joints. Larger joint vertical deflections and lower LTE are strongly correlated with increased rate of faulting and roughness development. Deflections were measured under the HVS loading (discussed above) and with the FWD before and after DBR as well as before and after HVS testing. Though the definitions of LTE are somewhat different under HVS and FWD loading, correlation with performance is consistent in both loading conditions. In addition to measuring joint deflections to calculate LTE, deflections were measured at center slab to backcalculate concrete stiffness, support layer (base + subgrade) stiffness, and subgrade k-values.

Comparison of DBR alternatives: LTE after HVS trafficking. FWD deflection testing performed after HVS testing showed that the HVS trafficking caused almost no change in LTE for all of the DBR joints. This observation is the same as shown by LTE results with data from JDMD measurements mentioned above.

Comparison of undoweled joints before DBR vs. joints with dowels originally installed: Average LTE. Deflection tests prior to DBR showed that the average LTE was 91 percent in the Palmdale test sections with originally installed dowels in the joints (including a widened lane and others with a tied shoulder). LTE values were consistent, with almost no difference between day and night measurements. Measurements at different times of the year showed that the joints with originally installed dowels never had less than 90 percent LTE. Many of these joints had been heavily trafficked during previous HVS tests. The average LTE on the undoweled sections was 33 percent in the day at an average surface temperature of 10°C, and 25 percent at night at an average surface temperature of 3°C.

Comparison of undoweled, DBR, and originally doweled joints: Temperature effects on Average LTE. At higher temperatures, deflection testing after DBR on joints and cracks showed the LTE of the undoweled and DBR joints was nearly the same as that of the originally installed dowel joints. The average LTE was 97 percent at 34°C, with no difference between undoweled and DBR joints. At 23°C, the average undoweled LTE was 85 percent, and the average DBR LTE was 82 percent.

The influence of temperature on LTE of undoweled joints was evident under cooler temperatures. The average LTE for the undoweled joints was 73 percent at 13°C and dropped to 57 percent at 9°C. At 9°C, individual undoweled joint LTE values ranged between 27 and 93 percent, indicating the inconsistency of relying on aggregate interlock for LTE.

The DBR strategy significantly improved the LTE of the previously undoweled joints and cracks, and reduced the sensitivity of the LTE to different temperatures. The average LTE after DBR was 83 percent at 13°C and 79 percent at 9°C.

Comparison of DBR vs. originally installed dowels: Temperature effects on LTE. Comparison of originally installed dowel performance with that of DBR showed that when the temperature is above 33°C all joints have consistently high LTE, likely mostly carried by aggregate interlock, making the presence and installation (original or DBR) of dowels irrelevant. At lower temperatures, the DBR joints had somewhat lower LTE than joints with originally installed dowels, although it is still always greater than 80 percent and usually 85 to 90 percent when there are four dowels per wheelpath. There is also greater variability in the LTE between different DBR joints than between different joints with originally installed dowels.

Comparison of Undoweled vs. DBR with three dowels per wheelpath: LTE results. Three dowels per wheelpath typically had much better LTE than undoweled joints. However, three dowels per wheelpath had lower nighttime LTE than that of four dowels per wheelpath, regardless of the dowel type.

Comparison of DBR: Curling based on LTE. Built-in slab curling, which results from greater concrete shrinkage on the surface of the slab than at the bottom, may have been reduced by DBR by about 2°C, although the results were not conclusive. This built-in curling was measured in terms of the Equivalent Built-In Temperature Difference (EBITD), which is backcalculated from FWD deflections performed at different times of day in order to eliminate the effect of temperature gradients on curling. High EBITD increases tensile stresses in the slab that cause longitudinal and corner cracking. It is possible that any potential reduction in EBITD may only occur when the DBR backfill grout sets during late afternoon and early evening when the temperature gradient in the slab is most positive (hotter on top) and the slab is the closest to being flat. Future measurement of FWD deflections before and after DBR may provide data to check for similar results and to see if it is dependent on the slab temperature gradient at the time that the backfill grout sets and more conclusively determine the significance of changes in EBITD caused by DBR.

Comparison of Ukiah vs. Palmdale: Temperature effects on LTE and backcalculated stiffness. Similar to results on the Ukiah test sections (10), FWD results show backcalculated stiffness and LTE are highly dependent on temperature and temperature gradient. Low mid-slab temperature causes the concrete slabs to contract, causing joints to open and greatly reducing LTE unless there are dowels in the joint. Increasing mid-slab temperatures causes the slabs to expand, causing the joints to close, which increases aggregate interlock, and may even place the joint faces in compression. At higher temperatures, LTE is greater than 90 percent for all joints, regardless of their condition.

Deflections taken at center slab to backcalculate stiffness show the effects of temperature gradients. Positive temperature gradients, with the slab hotter on top than on the bottom, result in lower backcalculated moduli for the concrete slab and the underlying support layers. The change in the shape of the slab caused by positive temperature gradients results in smaller deflections at the joints and corners. Negative temperature gradients, with the slab cooler on the top than the bottom, result in greater backcalculated moduli for the concrete slab and the underlying support layers. This shape also results in greater deflections at the joints and corners.

OBSERVATIONS ABOUT CONSTRUCTION AND MATERIALS

Accuracy of placement. Dowel bar placement accuracy was measured on cores taken after all testing was completed. The results showed that all dowels cored were above the mid-depth of the slab and some were very near the top of the slab. Most of these cores were from the HVS wheelpath. These results

indicate that the test sections were not "perfect" and resemble possible field construction in terms of dowel placement variability.

Slot and grout condition. The condition of the grout backfill material in the dowel bar slots was inspected periodically on both the wheelpath trafficked by the HVS and the wheelpath that was not trafficked. Many of the dowel slots showed the grout to be in good condition, except for slightly out of place foam back board on several of the joints.

Grout appearance. Some slots showed what appeared to be a lack of fine materials in the grout. Inspection two years after construction and after all HVS testing was completed showed some transverse cracking in the grout in the dowel slots. The grout did not come out of any of the slots, and the cracks remained tightly interlocked.

Grout tests. Beam and cylinder specimens of the mixed backfill grout material were made from material sampled at the site. The beams and cylinders were measured for 3rd point loading modulus of rupture and compressive strength. The results showed that the grout met Caltrans specifications for flexural strength and for compressive strength at twenty-four hours. The specification for compressive strength at three hours (0.125 days) could not be checked because of a travel delay for the testing contractor. The test at eight hours (0.33 days) indicated high early strength for the mix, but conformity with the three-hour strength requirement can not be determined.

Early opening to traffic. Early opening on DBR projects was not included by Caltrans in the scope of this study. Observations are not possible based on this project because trafficking was not applied to any of the Palmdale test sections until at least one month after construction and after more than a year for some sections.

TABLE OF CONTENTS

LIST OF FIGURES

LIST OF TABLES

1 INTRODUCTION

1.1 Purpose of This Report

The purpose of this report is to present the results of a set of Heavy Vehicle Simulator (HVS) tests, deflection tests, post-HVS forensic testing and analysis on dowel bar retrofitted (DBR) concrete pavement test sections at Palmdale, California. The test sections included retrofitted joints and transverse cracks with three and four epoxy-coated steel dowels, four hollow stainless steel dowels, and four fiber-reinforced polymer dowels per wheelpath. The results of the HVS testing and other testing, and the analysis on the dowel bar retrofit sections at Palmdale are also compared with the results from previous HVS testing of the following test sections:

- DBR sections at Ukiah
- Sections of new pavement at Palmdale where dowels were installed during construction of the slab and
- Section of new pavement at Palmdale that were constructed without dowels.

This project was originally proposed in 2000 by the Caltrans Headquarters Division of Design. Other stakeholder Caltrans units included Headquarters METS Office of Rigid Pavement Materials and Structural Concrete, as well as Caltrans Districts 1 and 7. Benefits expected from this research are to provide Caltrans with information needed for decisions about design and construction of DBR in order (1) to help determine where DBR may be a cost-effective strategy for rehabilitating rigid pavement and (2) to help obtain best performance where DBR is selected as the preferred rehabilitation strategy. This work was completed as part of Partnered Pavement Research Program Strategic Plan Item 4.8, "Dowel Bar Retrofit of Rigid Pavements."

Tasks for this project focus on four objectives agreed upon with Caltrans. This report completes the requirements for the first objective and presents observations and results only for the first objective. This report augments information provided in 2003 about HVS and related tests at Ukiah (10).

5. Field Accelerated Pavement Testing with the HVS: To collect full-scale data quickly, although with heavier loads than normally occur under real traffic. This will compare performance of retrofitted joints and cracks with those not retrofitted. This testing also includes measurement of load transfer efficiency (LTE) and other pavement properties with the Falling Weight Deflectometer (FWD). Several generic types of dowels will be included in the field test sections.

6. Field Live Traffic Testing: To collect field data on a long-term basis (approximately two years) under real loads. This testing enables calibration of HVS and analysis results.
7. Laboratory testing of materials: Permits evaluation of additional variables that cannot be included in the HVS testing, such as corrosion of the dowels and dowel types not included in the field test sections. Laboratory testing is also used to characterize materials used in the HVS test sections.
8. Modeling

- Finite element analysis of doweled concrete pavement joints: allows for performance prediction of other options without testing; enables extrapolation of HVS results.
- Compilation of performance data from existing DBR projects throughout the U.S.: allows for calibration of HVS and analysis results to field project results.
- Life Cycle Cost analyses.

1.2 Background

1.2.1 Roughness on Rigid Pavements

Rigid pavements, also referred to as concrete pavements or portland cement concrete (PCC) pavements, make up a large and important portion of the state highway network owned and maintained by the California Department of Transportation (Caltrans). They represent approximately 18 percent of the centerline-kilometers in the state network and 32 percent of the lane-kilometers (1). The difference between the centerline-kilometers and the lane-kilometers indicates the extent to which rigid pavements have been used for multilane facilities in urban areas. Rigid pavements have also been used extensively for the interstate system and other routes with heavy truck traffic in California.

Much of the rigid pavement network has performed well beyond its original twenty-year design life. It has been estimated that approximately 90 percent of the states' rigid pavement were constructed in the fifteen years between 1959 and 1974 (2), and they are therefore now forty to fifty-five years old. Because they have been subjected to many years of heavy truck traffic many of these pavements are now in need of maintenance or rehabilitation. In 2003, rigid pavements made up 27 percent of the distressed pavement lane-kilometers. (1)

Smoothness is the primary means by which the public evaluates pavement condition (3, 4, 5, 6, 7), and it is a significant variable controlling vehicle operating costs for both passenger and freight vehicles (8, 9). Smoothness is also one of the three variables by which Caltrans prioritizes pavement maintenance and rehabilitation, the others being the amount of traffic and the extent of cracking.

The smoothness of newly constructed rigid pavements is controlled by the paving process. The primary cause of increases in roughness (or lack of smoothness) on rigid pavements after construction is the development of faulting on transverse joints, and faulting of transverse cracks when they occur. The smoothness of a concrete pavement through its life is therefore controlled by its initial smoothness and the development of faulting under traffic loading. Faulting, sometimes referred to as "step-faulting," is the difference in height between two concrete slabs at a transverse joint or crack, as shown in Figure 1.1. As faulting develops, the edge of the "upstream" slab at the joint becomes higher than the edge of the "downstream" slab.

Figure 1.1. Upstream view showing faulting on an undoweled concrete pavement (courtesy of L. Khazanovich).

A previous report presented analyses using empirical models relating faulting to International Roughness Index (IRI, the measure of ride quality used by Caltrans) that showed that a relatively low level of faulting (3 mm or more) can lead to levels of roughness that cause discomfort to drivers, increase

vehicle operating costs and freight damage, and that exceed Caltrans IRI criteria for triggering maintenance or rehabilitation. (10)

The conclusion that roughness is primarily controlled by faulting is reinforced by other recent work. The IRI model in the recently released draft report on the pavement design guide developed by NCHRP Project 1-37A (11) shows that faulting is the most important factor controlling ride quality in jointed plain concrete pavement (JPCP), the type of concrete pavement built by Caltrans. The report states that:

> By far the most sensitive factor affecting JPCP [ride quality] is joint faulting and the most critical factor affecting joint faulting is dowel diameter.

That report also states that:

> The use of properly sized dowels is the most reliable and cost-effective way to control joint faulting. Studies have shown that properly sized dowels with adequate consolidation will reduce faulting dramatically.

These statements are based on analysis of new rigid pavement.

Historically, Caltrans has relied on improving the non-erodability of base materials through cement stabilization as well as aggregate interlock between the slabs at the joint to control faulting development. Empirical models developed from field data indicate that although the use of non-erodible bases, usually meaning cement treated base or asphalt treated base, improves faulting performance, their use is not as effective as the use of dowels. The field data and models indicate that the best faulting performance is obtained by using dowels with non-erodible bases (12, 13, 14, 15).

Caltrans has not used dowels except for a few projects built since 1999. The decision not to use dowels during initial construction of most of the rigid pavements in the state network was primarily based on the results of test sections evaluated in the late 1940s (16). There were construction difficulties at that time, primarily an inability to place dowels straight and level, which can lead to early failure of the pavement.

Typical dowel practice at that time also included the use of small diameter dowels, typically 19 to 25 mm. Recent studies have shown that effectiveness of dowels placed in new highway pavements is greatly improved when the diameters are at least 32 mm, although 25 mm dowels still perform better than undoweled pavements (11, 13).

Small diameter dowels result in high bearing stresses in the surrounding concrete under traffic loading, which causes the concrete to not hold the dowel as tightly as when originally constructed. As dowels become loose in the concrete they lose their ability to perform their intended function, which is to transfer loads from one slab to another across the transverse joint. Load transfer efficiency (LTE) is

typically measured by deflection testing across joints and cracks, and has been found to be highly correlated with the development of faulting (11, 13). The details of the mechanism of faulting development were presented in detail in a previous report (10), and are also discussed in various other reports (11, 13, 14, 15).

1.2.2 Rehabilitation Strategies for Rigid Pavements

Caltrans is interested in finding the most cost-effective rehabilitation strategies for concrete pavements. In the five fiscal years, 1998/99 through 2002/03, Caltrans made a major effort to improve smoothness on the rigid pavement network by performing diamond grinding on about 12 percent (3,220 ln-km) of its rigid pavement network, and placing asphalt concrete overlays on about 8 percent (2,089 ln-km), which reduced the lane-kilometers with poor ride quality but no major structural defects to 790 ln-km by the time of the 2003 State of the Pavement. Dowel bar retrofit (DBR) has also been used by Caltrans on some projects (1).

It was found that reflection cracking appears on the surface of asphalt concrete overlays of rigid pavements approximately seven to eight years after construction, on average. This finding was based on analysis of Caltrans PMS data for the years 1978 to 1993, and only considering initial overlays. There was a wide variance of the reflection cracking lives around the average, with the variance likely dependent on climate, traffic, and the distresses present at the time of overlay (17). Significant increases in roughness typically do not occur until some time after the appearance of reflection cracking, after the extent and severity of the reflection cracking has increased. The time to triggering of maintenance or rehabilitation for asphalt concrete overlays of rigid pavements due to roughness, as measured by IRI, has not been definitively established with Caltrans PMS data. It has also not been established for diamond grinding projects on Caltrans pavements. The time to reach trigger values of roughness is also expected to be dependent on climate, traffic, and existing pavement condition. The condition of cement-treated bases and asphalt-treated permeable bases under older pavements and its effect on the lives of grinding and asphalt concrete overlays is of concern because of the variability of the durability of some Caltrans bases, particularly those designed and constructed before Caltrans began using lean concrete base. (15, 18, 19, 20).

While it is clear that the use of properly constructed dowels in new pavements significantly reduces the rate of fault development, the long-term performance of DBR is not clear. Whether dowel bar retrofit provides similar performance, as measured by Load Transfer Efficiency, is the purpose of this research, as is how can dowel bar retrofit be made more cost-effective. The information presented in this report compares the results of Heavy Vehicle Simulator (HVS) testing and other testing, and analysis of

dowel bar retrofit sections with that of new doweled sections and undoweled sections. This information will later be used with information presented in other reports that are part of this research project in order to estimate the life of dowel bar retrofit sections and their life-cycle cost for comparison with alternative rehabilitation strategies.

1.2.3 Alternative DBR Strategies

The information in this report also examines the performance of various dowel bar retrofit designs. Corrosion of epoxy-coated dowels has been identified as a risk that could shorten the life of DBR projects in locations where the pavement is exposed to high chloride contents, particularly where salt is used to melt ice and snow. This risk has been identified through accelerated laboratory testing and observation of some field sections (21). Alternative dowels have been proposed that are expected to have better corrosion resistance. Alternatives tested in the HVS sections included in this study were dowels made of grout–filled, hollow stainless steel cylinders and dowels made of fiber-reinforced polymer (FRP).

Caltrans has used four dowels per wheelpath for DBR, which is the design originally used in Washington State. The Washington State Department of Transportation (WSDOT) and other states have also used three dowels per wheelpath with the intention of reducing the cost of DBR. This study includes a comparison under HVS loading of four and three dowels per wheelpath.

1.3 Scope of This Report

The original construction of the pavement sections is summarized from previous reports, and the details of the DBR design, materials, and construction are presented in Chapter 2. The analysis and comparison of HVS and Falling Weight Deflectometer (FWD) testing data are described in Chapters 3 through 6. Chapter 3 presents an overview of the FWD and HVS testing performed. Chapter 4 summarizes FWD test data from the sections prior to dowel bar retrofit. Chapter 5 presents FWD test data from the sections after DBR, but before HVS testing. Chapter 6 presents the HVS test data and FWD test data from the sections after DBR and after HVS testing. Chapter 7 compares the FWD and HVS results between the different Palmdale DBR test pavements, and between the Ukiah and Palmdale DBR and Palmdale LLPRS test pavements. Chapter 8 presents the conclusions and recommendations drawn from this study.

Appendix A presents the layout of the HVS test sections in detail. Appendix B includes overhead photographs of all test sections with cracks marked on the pavement at the conclusion of HVS testing. Appendix C contains details of grout strength testing. Appendix D includes detailed deflection test data. Appendix E includes the test section construction specifications and special provisions.

2 DESIGN, MATERIALS, AND CONSTRUCTION OF ORIGINAL PAVEMENT AND DOWEL BAR RETROFIT SECTIONS

This chapter presents the details regarding the design, materials, and construction of the original Palmdale test sections, and of the DBR sections.

Two sections of pavement were built in June 1998 for Heavy Vehicle Simulator testing to investigate concrete pavement design features for Long-Life Pavement Rehabilitation Strategies (LLPRS). Both sections are on State Route 14, approximately six kilometers south of Palmdale in northeastern Los Angeles County, as shown in Figure 2.1. Each section is 210 m long. Both were built as an outside lane tied to the existing traffic lanes, one in the southbound direction and one in the northbound direction, and they are referred to as the South Tangent and North Tangent, respectively. All of the sections are jointed plain concrete pavement (JPCP).

The South Tangent sections were used to evaluate the fatigue performance of Fast-Setting Hydraulic Cement Concrete (FSHCC). The North Tangent sections were built to evaluate the performance of undoweled pavements, doweled pavements with tied shoulders, and doweled pavements with a wide lane. (22, 23)

2.1 Design, Materials, and Construction of Original Pavement

2.1.1 Cross-Sections

The dowel bar retrofit HVS tests were conducted on previously untrafficked portions of what is referred to as "Section 7" of the North Tangent. As can be seen in Figure 2.2, the pavement in Section 7 has cement-treated base (CTB), undoweled jointed plain concrete slabs with untied shoulders, and a standard width of 3.7 m.

The concrete slabs on Section 7 were nominally 200 mm thick. All slab joints were sawed at 90° with spacing matching that of the adjacent slabs on SR 14. The joint spacing for the entire North Tangent approximately follows the pattern of 3.7, 4.0, 5.5, and 5.8 m. Figure 2.3 shows the slab numbering for Section 7 of the North Tangent, and the location and dimensions of the HVS test sections on the original pavement.

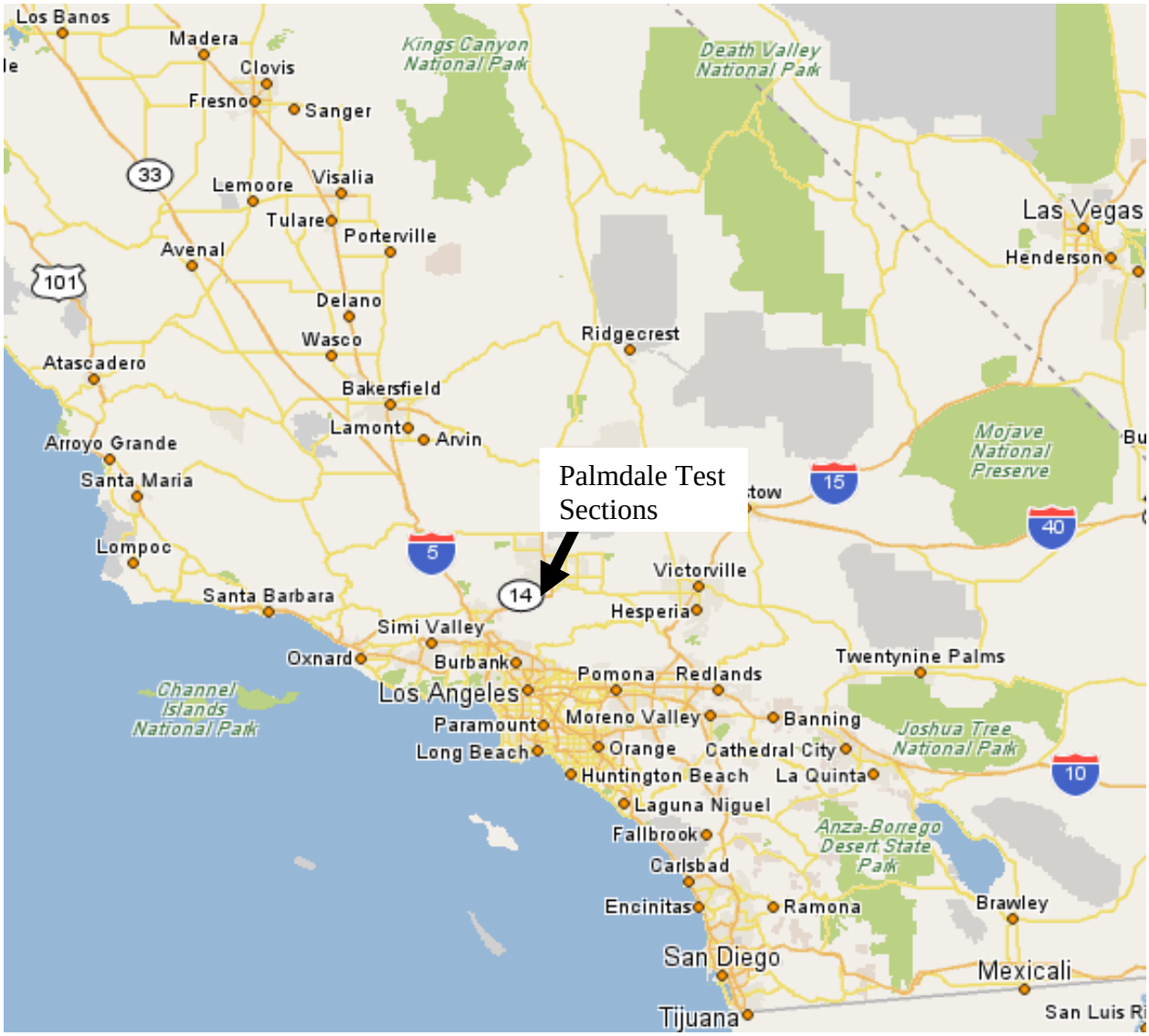

Figure 2.1. Location of Palmdale test sections.

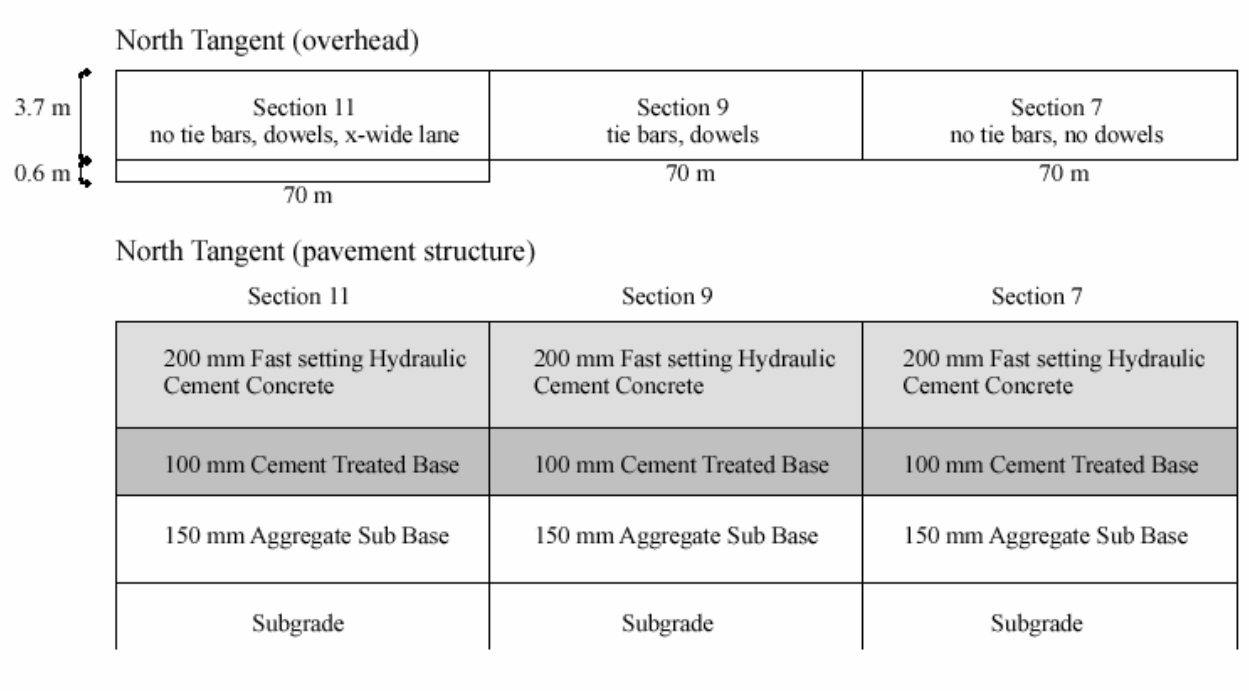

Figure 2.2. Pavement Structure Diagram for North Tangent (23).

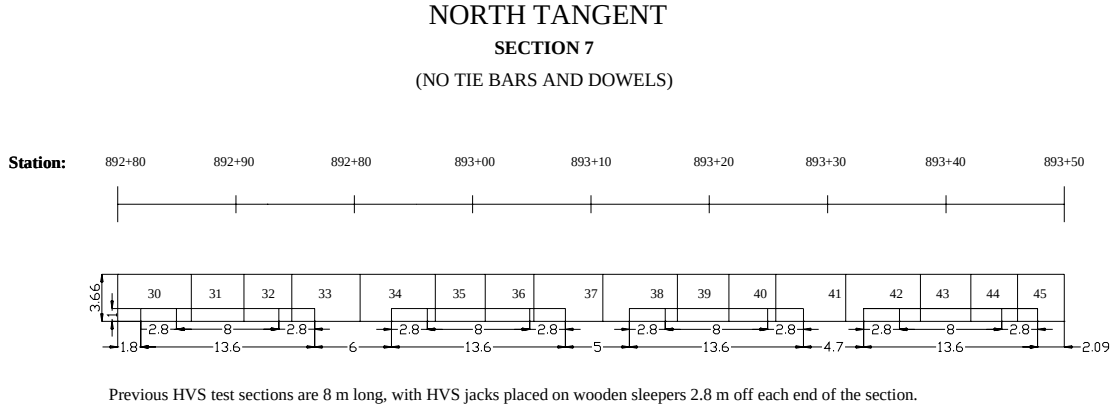

Figure 2.3. Slab and joint numbering and dimensions of slabs in Section 7 of North Tangent.

2.1.2 Materials

Visual examination of the subgrade material indicated that it consists of uplifted alluvial deposits with large stones (> 5 cm diameter) included and some weak-to-relatively strong cementing of the sand and gravel. Dynamic Cone Penetrometer (DCP) measurements were performed on the South Tangent at the

time of original construction. The results were highly variable, which was attributed to the presence of stiff rock material at relatively shallow depths — sometimes as shallow as 0.3 m below the top of the subgrade. The stiffness of the subgrade on the South Tangent was estimated to be between 118 and 447 MPa at those locations where the DCP did not reach the bedrock. It was assumed that results of the North Tangent would be similar because both the North and South Tangents are in similar deep cuts and are very close to each other. However, DCP measurements were not possible on the North Tangent. Subgrade stiffnesses backcalculated from Falling Weight Deflectometer deflections measured seven to ninety days after construction averaged for Section 7 were between 159 and 255 MPa. (23)

The North Tangent was constructed with 150 mm of Class 2 aggregate subbase (ASB) placed on subgrade compacted to Caltrans specifications. A 100-mm thick layer of Class A cement-treated base (CTB) was placed on the aggregate subbase. The CTB was designed to have a seven-day compressive strength of 1.895 MPa (275 psi) ± 0.345 MPa when tested with CT 312 to simulate material meeting the pre-1964 Caltrans specification. The CTB mix design is shown in Table 4.1 of Reference 23.

The mix design for the concrete is described in Section 4.3 of Reference 23 and Section 3.2 of Reference 24. The specification called for a minimum cement content of 375 kg/m3. The specification called for flexural strengths of 2.8 MPa after eight hours and 4.1 MPa after seven days in accordance with Caltrans Test 523 (center-point loading). The specifications also called for a three-hour compressive strength of 17.2 MPa and a three-day compressive strength of 34.5 MPa in accordance with ASTM C 109. Before the test sections were constructed, the contractor had to demonstrate through a trial slab that the eight-hour and seven-day flexural strength specifications could be met with the proposed mix design.

The concrete mix design includes the following constituents: one coarse and fine aggregate, two cement types (Type I/II portland cement and fast-setting hydraulic cement produced by Ultimax), water, air entraining agent, DelvoTM liquid, or solid retarder. Table 4.2 of Reference 23 shows the proportion of each mix constituent for one cubic meter. Ultimax is a proprietary cement with its main chemical constituent being calcium sulfoaluminate. The contractor used a blend of the two cements to achieve the required strength specifications. After trying several trial slabs with blends of cements ranging from 100 percent Ultimax and zero percent portland to 70 percent Ultimax and 30 percent portland, the contractor finally chose a blend of 80 percent Ultimax and 20 percent portland. The 80/20 blend was used on all of the test sections.

2.1.3 Measured Concrete Properties

The subgrade, subbase, and base materials were prepared in May and early June 1998. The slabs in Section 7 were placed on June 18, 1998.

Various fresh mix properties were tested at the time of construction, and specimens for strength tests were prepared. Flexural and compressive strengths were measured from two different trucks on each section at eight hours, seven days, ninety days, and long-term (575 days for flexural and 636 days for compressive). Flexural strength tests were performed following ASTM C 78 (third-point loading) with some additional tests performed following CT 523 (center-point loading). Compressive strength tests were performed following ASTM C 39. The test information relevant to the DBR test sections is summarized below from information in Reference 23.

Two specimens from each truck were tested at each age for each type of strength. Specimens tested at eight hours were cured on site in a mold placed under wet burlap next to the pavement. Specimens for later testing were demolded at forty-eight hours and sprayed with water, then wrapped in wet burlap and plastic and cured at room temperature.

Tests were performed on material from the trucks that placed materials on Slabs 33 and 41 in Section 7 of the North Tangent, which are on or are very close to the DBR sections, as can be seen in Figures A1 through A3 in Appendix A.

Air entrainment test values were 2 percent and zero percent for the two trucks. Slump test results were greater than six inches and four inches.

Flexural and compressive strength results averaged for the two trucks are shown in Table 2.1. The results show that there was almost no long-term strength gain after ninety days.

Table 2.1. Summary of Flexural and Compressive Strengths from Specimens Prepared in the Field during Construction of Section 7 of North Tangent (23)

Age	Flexural Strength (ASTM C 78)		Compressive Strength (ASTM C 39)	
	Average (MPa)	Coefficient of Variation (%)	Average (MPa)	Coefficient of Variation (%)
8 hours	1.91	5	12.4	6
7 days	3.66	4	28.3	11
90 days	5.20	13	48.3	4
Long-term 575 days flexural 636 days compressive	5.20	5	50.1	18

Caltrans performed center-point flexural beam strength tests on beams cured at the site. The average strength at eight hours was 1.17 MPa with a coefficient of variation of 44 percent. The average strength at seven days was 3.87 MPa with a coefficient of variation of 9 percent.

Compressive strength tests were also performed on cores taken from the site from several slabs on the opposite edge of the slab from the location of the future HVS wheel track. The cores were taken and tested several weeks after construction. The results for Section 7 are summarized in Table 2.2.

Table 2.2. Summary of Thicknesses and Compressive Strengths from Cores from Section 7 of North Tangent (23) Taken Several Weeks after Construction

Slab	Length (mm)	Density (g/cm^3)	Compressive Strength Corrected for Dimensions (MPa)
32	220	2.46	32.4
35	228	2.31	41.3
39	220	2.24	17.5
43	237	2.36	33.1

The results indicate that the slabs where typically somewhat thicker than the design thickness of 203 mm. The strengths indicate a fairly large degree of variation between different slabs.

Roesler and Rao reported an average elastic modulus of the concrete slabs backcalculated from Falling Weight Deflectometer deflections on the North Tangent of approximately 42,500 MPa (24).

Coefficient of Thermal Expansion (COTE) was measured on concrete specimens prepared in the laboratory using raw materials collected at the site during construction (25). The average coefficient of thermal expansion, in dry condition, was 8.03 (10^{-6}) ε/ ºC.

Laboratory shrinkage tests indicated that the cement used for construction of the original HVS test sections resulted in high concrete free shrinkage as measured using Caltrans and ASTM tests. Static strain gauges cast in the concrete slabs also showed high differential shrinkage between the locations 50 mm above the bottom of the slabs and 50 mm below the top of the slabs. Very low humidity and low rainfall greatly contributed to the differential shrinkage, which resulted in warped slabs with the edges warped upward (25).

2.2 Condition after Original HVS Testing

All of the original slabs in the North Tangent that were 5.5 and 5.8 m in length had top-down transverse cracking within three months of construction under shrinkage and curling stresses and before the HVS was brought onto the site (25). HVS testing was performed on the shorter slabs. The slabs and joints selected for DBR and subsequent HVS testing for this study were those that had not been

significantly damaged by the HVS testing during the previous experiment. Slabs tested in Section 7 as part of the original experiment are shown in Figure 2.3.

2.3 Design, Materials, and Construction of Dowel Bar Retrofit

2.3.1 Dowel Bar Retrofit Design and Layout

Four sections on Section 7 were dowel bar retrofitted for later Heavy Vehicle Simulator (HVS) test sections. Details of the four HVS test sections are shown in Tables Table 2.3 and Table 2.4, and in Appendix A. It can be seen in the two tables and in Figure 2.3 that two of the test sections, 558FD and 559FD, had long slabs with transverse cracks caused by shrinkage and temperature gradients and that the cracks were dowel bar retrofitted.

2.3.2 Dowel Bar Types

Three types of dowels were included in the HVS test sections: epoxy-coated steel; grout-filled, hollow, stainless steel cylinders; and fiber-reinforced polymer (FRP).

2.3.2.1 Epoxy-coated steel

The epoxy-coated steel dowels were made of carbon steel coated with flexible epoxy (green color code). Epoxy-coated bars were also epoxy coated at the ends. The epoxy-coated dowels are 38 mm in diameter and 457 mm long. One of the dowels is shown in Figure 2.4.

2.3.2.2 Hollow stainless steel dowel

The hollow stainless steel dowels consisted of a hollow-type A316 stainless steel cylinder approximately 5 mm thick, filled with a cementitious grout. The hollow stainless steel dowels are 38 mm in diameter and 457 mm long. One of the dowels is shown in Figure 2.5.

2.3.2.3 Fiber-reinforced polymer

Glass FRP (GFRP) dowels were used for this project. The fiber-reinforced polymer consists of a polyester matrix with 70 percent glass fibers by volume. The FRP dowels are 38 mm in diameter and 457 mm long. This type of dowel is shown in Figure 2.6.

Table 2.3. HVS Dowel Bar Retrofit Test Sections, Test Durations, Slab Numbers and Joint Numbers

HVS Test Section	Slab Number	Joint (Crack) Number
556FD (March 2002 – August 2002)	38	38
	39	39
	40	
557FD (August 2002 – October 2002)	35	35
	36	36
	37	
558FD (August 2001 – March 2002)	41	41
	42	Crack 2
		42
	43	
559FD (October 2002 – March 2003)	32	32
	33	Crack 1
		33
	34	

Table 2.4. Type and Number of Dowels Retrofitted on Each Joint or Crack

Joint or Crack Number	HVS Test Section	Type of Dowels	Number of Dowels
Joint 32	559FD	Epoxy-coated steel	Four per wheelpath
Crack 1	559FD	Hollow stainless steel in one wheelpath; epoxy-coated steel in other wheelpath	Four per wheelpath
Joint 33	559FD	Hollow stainless steel	Four per wheelpath
Joint 35	557FD	Epoxy-coated steel	Three per wheelpath
Joint 36	557FD	Epoxy-coated steel	Three per wheelpath
Joint 38	556FD	Epoxy-coated steel	Four per wheelpath
Joint 39	556FD	Epoxy-coated steel	Four per wheelpath
Joint 41	558FD	Epoxy-coated steel	Four per wheelpath
Crack 2	558FD	Fiber-reinforced polymer	Four per wheelpath
Joint 42	558FD	Fiber-reinforced polymer	Four per wheelpath

Figure 2.4. Epoxy-coated steel dowel.

Figure 2.5. Hollow stainless steel dowel.

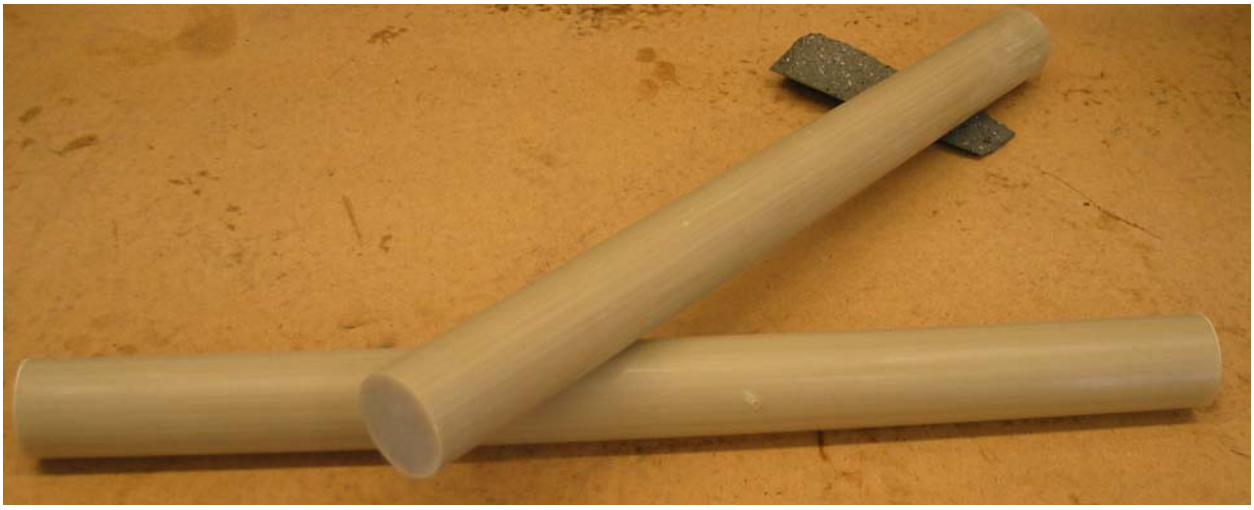

Figure 2.6. Glass fiber-reinforced dowel.

2.3.3 Dowel Bar Retrofit Construction

The DBR construction was performed June 28–30, 2001 by the PenHall Company. The construction specification is included in Appendix E. The construction inspection was performed by the UCPRC based on training provided earlier by the Washington State Department of Transportation for the construction of DBR test sections at Ukiah (10).

2.3.3.1 Construction Process

A specially designed machine was used to cut the dowel bar slots (see Figure 2.7 and Figure 2.8). The machine has a system to vacuum up cutting water to prevent storm water contamination. The machine also has a removable arbor on which the saw blades are mounted (Figure 2.9). The blade configuration was changed during construction to permit sawing of the sections with four dowels per wheelpath and those with three dowels per wheelpath.

Quality control of saw cut depths was performed by the contractor as shown in Figure 2.10, and some of the dowels were checked by UCPRC staff prior to chipping out of the dowel bar slots, as shown in Figure 2.11 and Figure 2.12. A high-pressure air hose was then used to clean debris from the slots, as Figure 2.13 shows. The joint was sealed with DAP™ 25-year Painter's Acrylic Latex Caulk (Figure 2.14).

Dowel bar retrofit assemblies were put together for each crack or joint (Figure 2.15). The assemblies consisted of the dowel, two end caps, two chairs, and a joint separator made of foam backer board (Figure 2.16). The assemblies were then sprayed with bond-breaker material, as shown in Figure

2.17, and placed into the slots, as shown in Figure 2.18 and Figure 2.19. Dowel bar depth and uniformity of depth were then checked (Figure 2.20).

Backfill grout was prepared on site using a small portable batch mixer, shown in Figure 2.21. The backfill grout was dumped out of the mixer into a small front loader bucket and driven along the shoulder to the dowel bar assembly. At the joint or crack the grout was pulled out of the loader into the slots with shovels (Figure 2.22 and Figure 2.23), and vibrated with a small stinger (Figure 2.24). The next day a grinding machine ground the grout flush with the surface of the pavement, resulting in the texture shown in Figure 2.25 and Figure 2.26. The blue lines in the photographs indicate future HVS wheelpath center over the dowel bar set.

Figure 2.7. Dowel bar slot cutting machine (rear view).

Figure 2.8. Dowel bar slot cutting machine (side view, blade arbor and vacuum between front and back wheels).

Figure 2.9. Removable saw blade arbor.

Figure 2.10. Quality control of dowel bar slot cut depth.

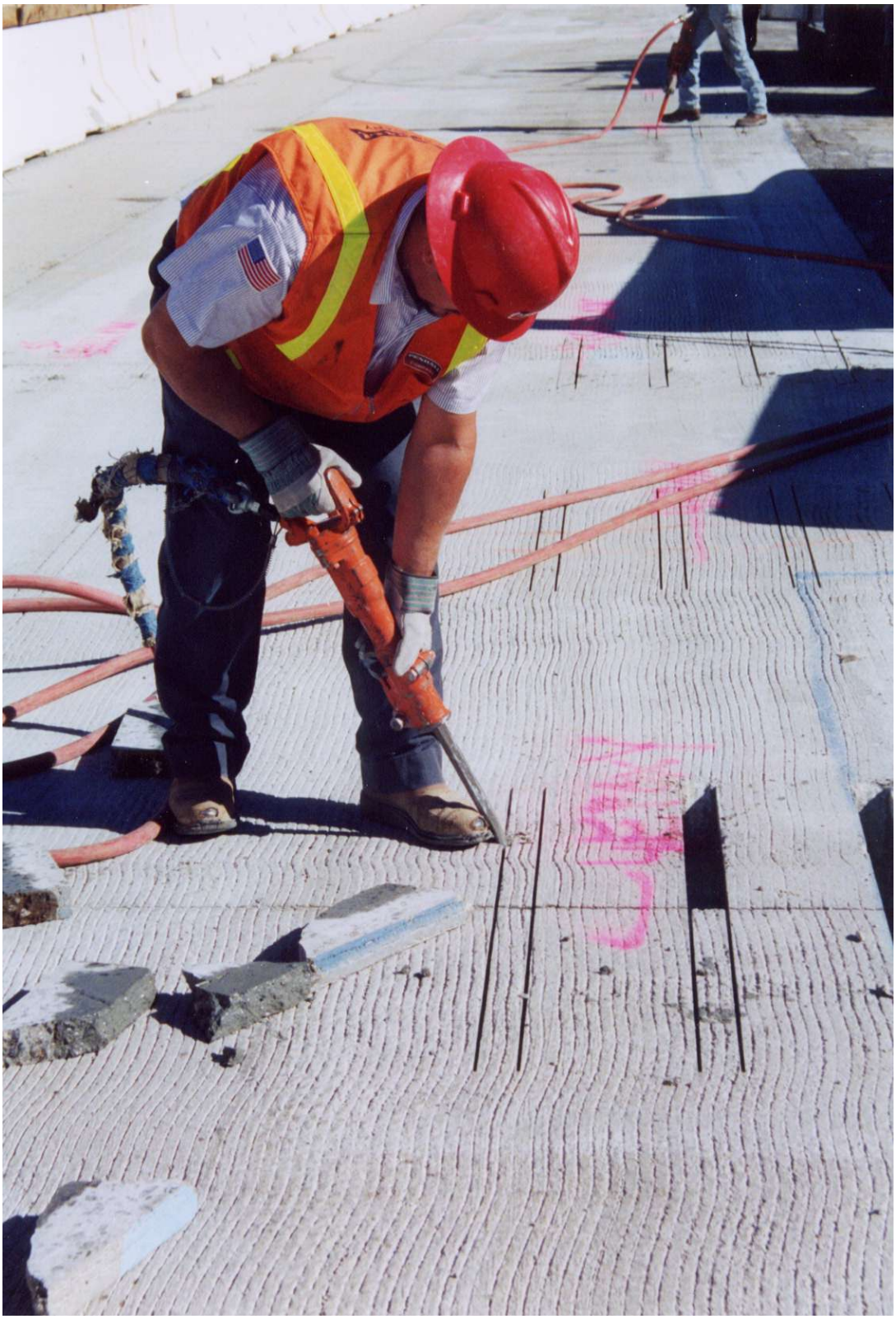

Figure 2.11. Chipping out of dowel bar slots.

Figure 2.12. Removal of concrete from dowel bar slots.

Figure 2.13. Cleaning dowel bar slots with air hose.

Figure 2.14. Sealing joints with caulk.

Figure 2.15. Putting together dowel bar retrofit assemblies.

Figure 2.16. Dowel bar retrofit assembly.

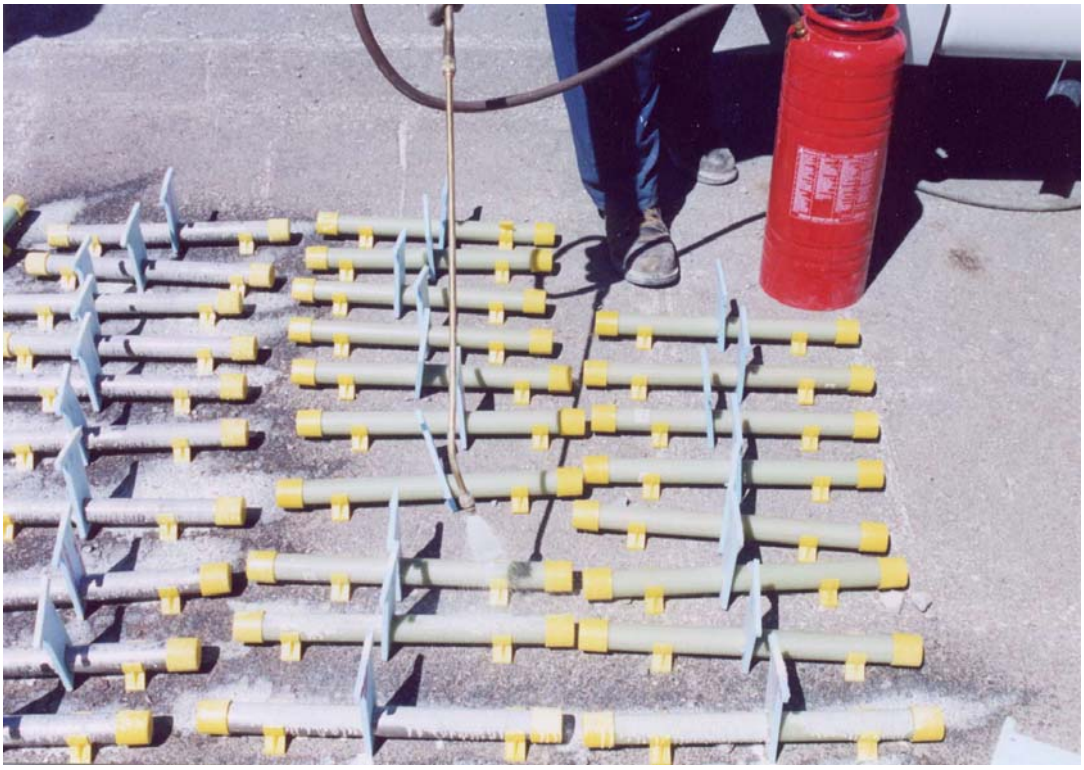

Figure 2.17. Spraying bond-breaker material on dowel bar retrofit assemblies.

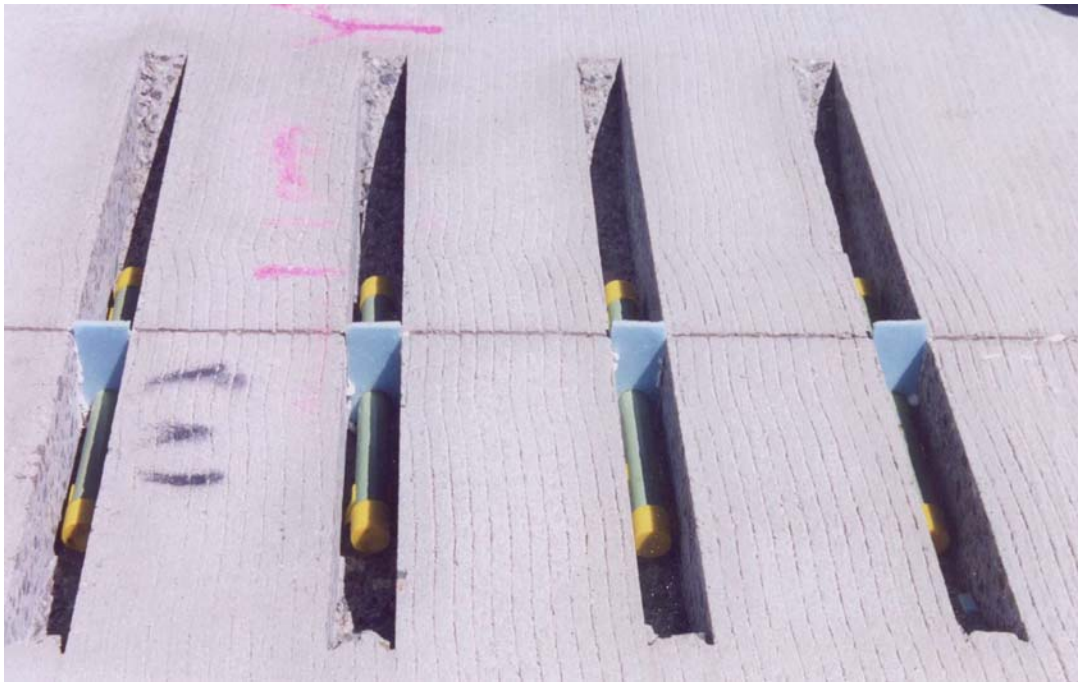

Figure 2.18. Dowel bar retrofit assemblies in slots (epoxy-coated steel dowels).

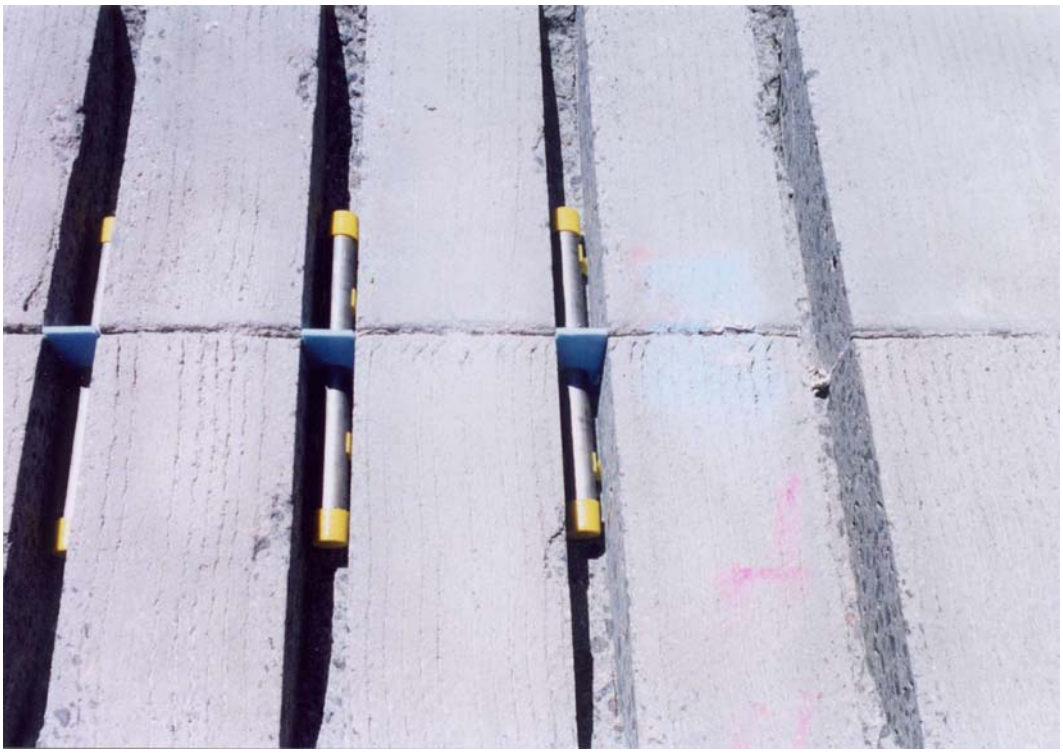

Figure 2.19. Dowel bar retrofit assemblies in slots (hollow stainless steel dowels).

Figure 2.20. Checking dowel bar depth and uniformity of depth.

Figure 2.21. Batching backfill grout material into mixer.

Figure 2.22. Placement of backfill grout in dowel bar slots.

Figure 2.23. Pulling backfill grout into slots with shovels.

Figure 2.24. Vibration of backfill grout with small stinger.

Figure 2.25. Sections 559FD (Slabs 32, 33, and 34 in foreground), 557FD (background), and 556FD (far background under front of HVS) after dowel bar retrofit and grinding, and before HVS testing.

Figure 2.26. Close-up of surface texture of Section 557FD after dowel bar retrofit and grinding, and before HVS testing (blue lines painted on surface indicate future HVS wheeltrack).

2.3.3.2 Backfill Grout Material

The backfill material was prepared from aggregate, sacks of cement, and water brought to the site by the contractor. The material was required to meet the specifications included in Appendix E of this report. The contractor used Five Star Highway Patch for the cement.

Beam and cylinder specimens of the mixed backfill material were made from material sampled at the site following ASTM C 31. The beam dimensions were 152 by 152 by 457 mm, and the cylinder dimensions were 203 mm in height and 102 mm in diameter. The specimens were vibrated using a small mechanical vibrating rod. Curing compound was placed on the surface of the specimens immediately after finishing. The same curing compound used on the dowel bar retrofit locations was also used on the specimens.

The first specimens were tested at the site by a commercial laboratory. One day after construction the remaining specimens were transported to the UC Pavement Research Center laboratory in Richmond and placed in a room with 97 percent humidity and a temperature of 20°C. The beams and cylinders were measured for third-point loading modulus of rupture following ASTM C 78 and compressive strength following ASTM C 39, respectively. The curing times and measured flexural and compressive strengths are shown in Table 2.5 and are plotted in Figure 2.27.

From the results it can be seen that the grout met Caltrans specifications for flexural strength and for compressive strength at twenty-four hours. The specification for compressive strength at three hours (0.125 days) could not be checked because of a travel delay for the testing contractor. The test at eight hours (0.33 days) indicates high early strength for the mix, but it cannot be concluded as to whether it met the three-hour strength requirement.

The strength for the backfill grout at the Ukiah DBR test sections is shown in Table 2.6 and plotted for comparison against the Palmdale data in Figure 2.28 and Figure 2.29. It can be seen that the Palmdale grout had greater compressive strength than the Ukiah grout. It can also be seen that the Palmdale flexural strength was generally greater at each age, although the ultimate flexural strengths appear to be approximately the same.

Table 2.5. Grout Flexural Beam (Modulus of Rupture) and Compressive Strength Results from Field Prepared Specimens at Palmdale

Grout Curing Time (days)	Flexural Beam Strength (MPa)	Average	Caltrans Specification (minimum)	Compressive strength (MPa)	Average	Caltrans Specification (minimum)
0.33	3.16	3.4		0.33	37	21 (at 0.125 days)
0.33	3.71			0.33		
1	3.65	3.8	3.5	1	42	35
1	3.55			1		
1	4.11			1		
7	5.47	5.3		7	52	
7	5.19			7		
7	5.13			7		
14	6.40	6.5		14	58	
14	6.54			14		
14	6.53			14		
28	6.61	6.4		28	63	
28	6.31			28		
28	6.35			28		
165	7.48	7.1				
165	6.83					
165	6.92					

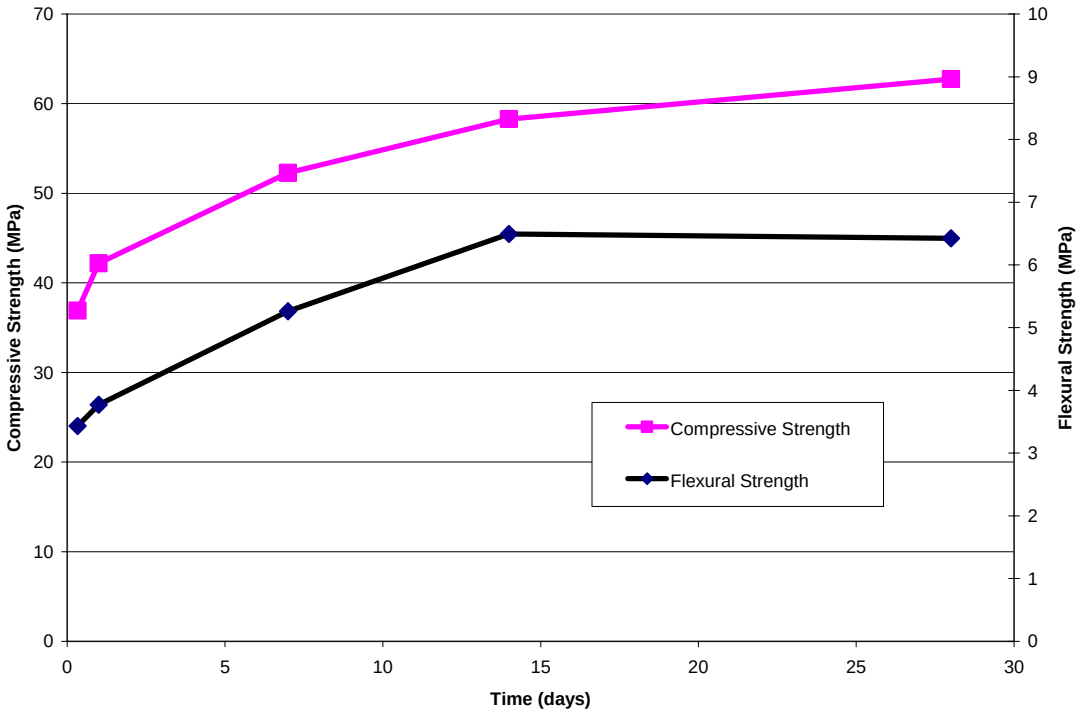

Figure 2.27. Average compressive and flexural strengths from field-prepared backfill grout specimens.

Table 2.6. Grout Flexural Beam (Modulus of Rupture) and Compressive Strength Results from Field Prepared Specimens at Ukiah

Grout Curing Time (days)	Flexural Beam Strength (MPa)	Average	Caltrans Specification (minimum)	Compressive Strength (MPa)	Average	Caltrans Specification (minimum)
1.125	3.9	3.8		21	21	21
0.125	3.8			21		
1	2.2	2.5	3.5			35
1	2.7					
8	3.5	3.7		39	39	
8	3.9			39		
14				47	44	
14				41		
37	6.8	6.7		53	54	
37	6.5			55		

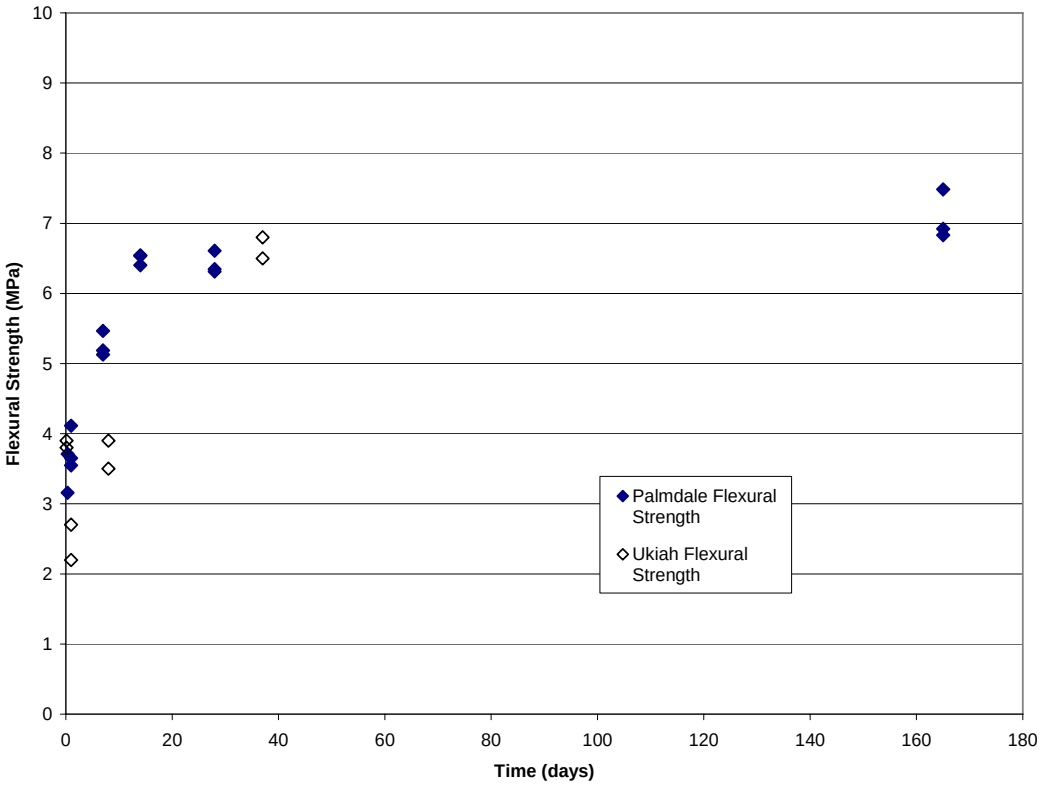

Figure 2.28. Comparison of long-term flexural beam strength for Palmdale and Ukiah DBR backfill grout.

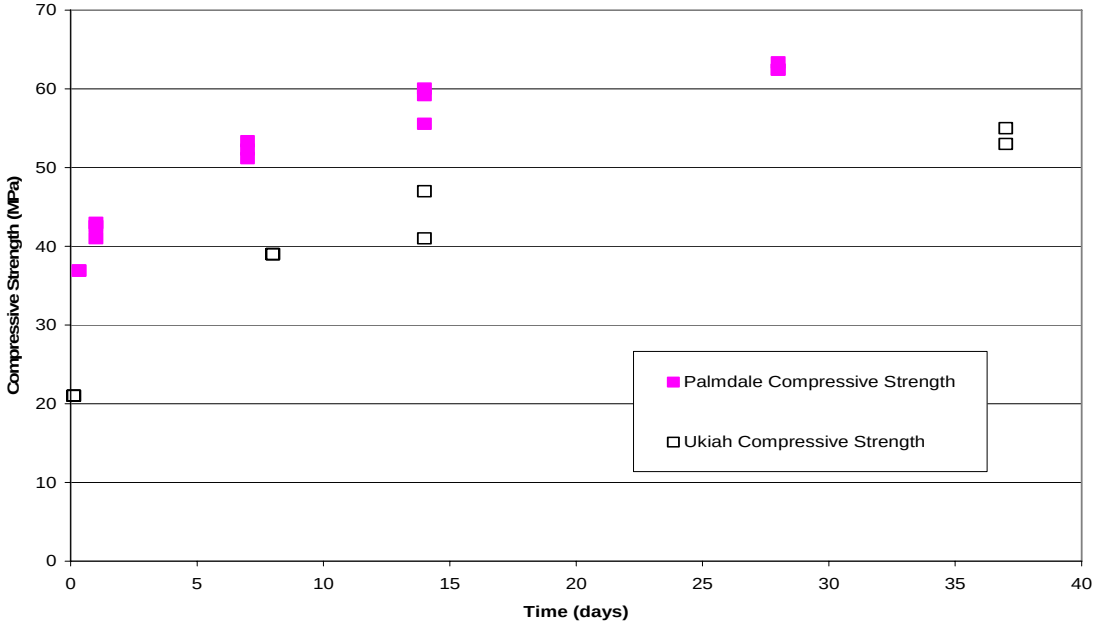

Figure 2.29. Comparison of long-term compressive strength for Palmdale and Ukiah DBR backfill grout.

2.3.3.3 Other Materials

Other materials used on the project, including backer board, chairs, end caps, etc., appeared to meet the specifications for the project.

2.3.3.4 Slab Thickness and Dowel Position After Construction

After HVS tests, twenty-six cores were obtained from the DBR sections in June 2003, including fourteen with retrofitted dowels. All the cores were measured to determine the slab thicknesses; the average results are shown in Table 2.7.

Table 2.7. Average Concrete Slab Thicknesses in DBR Sections

Slab No.	**32**	**33**	**35**	**36**	**38**	**39**	**41**	**42**
Thickness (mm)	212.5	220.4	227.4	233.5	227	220.6	220.8	229.3

For the cores that had dowels, the distances from the slab surface to the dowel (cover depths)are shown in Table 2.8, as is the deviation from placement at the mid-depth of the slab. Some examples are shown in Figure 2.30, Figure 2.31, Figure 2.32, and Figure 2.33. The dowels were cored between the dowel end and the dowel center, as can be seen in the overhead photographs in Appendix B that are marked with the dowel core locations. The results show that all of the dowels cored were above the mid-depth of the slab, and some were very near the surface of the slab. These results indicate that the test sections were not “perfect” and probably resemble field construction in terms of dowel placement variability. Most of the cores in Table 2.8 were taken from the HVS wheelpath.

Table 2.8. Distance from Top to Center of Dowel from Cores with Dowels

Joint Description	Core No.	Actual Cover Depth [a] (mm)	Slab Thickness (mm)	Deviation from slab center [b] (mm)
Joint 39, epoxy-coated steel dowel, 4/wheelpath	DBR39NW	76	213	-12
Joint 38, epoxy-coated steel dowel, 4/wheelpath	DBR38NW	77	227	-18
Joint 32, epoxy-coated steel dowel, 4/wheelpath	DBR32NW	73	214	-15
Joint 36, epoxy-coated steel dowel, 3/wheelpath	DBR36NW	75	236	-24
Joint 35, epoxy-coated steel dowel, 3/wheelpath	DBR35NE	91	226	-3
Joint 35, epoxy-coated steel dowel, 3/wheelpath	DBR35NW	83	227	-12
Joint 36, epoxy-coated steel dowel, 3/wheelpath	DBR36NE	74	227	-21
Joint 42, FRP dowel, 4/wheelpath	DBR42NWC	38	238	-62
Joint 42, FRP dowel, 4/wheelpath	DBR42NNW	74	232	-23
Joint 42, FRP dowel, 4/wheelpath	DBR42NNE	66	223	-27
Joint 33, hollow stainless steel dowel, 4/wheelpath	DBR33NW2	73	226	-21
Joint 33, hollow stainless steel dowel, 4/wheelpath	DBR33NE2	86	221	-6
Joint 41, epoxy-coated steel dowel, 4/wheelpath	DBR41NE	81	226	-13
Joint 41, epoxy-coated steel dowel, 4/wheelpath	DBR41NW	78	216	-11

[a] Compares to expected cover depth of 83mm (based on design slab thickness of 203mm)
[b] Vertical deviation of dowel center from slab center = cover depth + (dowel diameter/2)- (slab thickness/2); positive value indicates dowel below slab center, negative value indicates dowel above slab center.

Figure 2.30. Core DBR33NE2 with hollow stainless steel dowel located 6 mm above mid-depth of slab.

Figure 2.31. Core DBR33NW with epoxy-coated steel dowel located 12 mm above mid-depth of slab.

Figure 2.32. Core DBR42NWC with FRP dowel located 62 mm above mid-depth of slab.

Figure 2.33. Core DBR42NNW with FRP dowel located 23 mm above mid-depth of slab.

2.3.3.5 Longer-Term Grout Condition

The condition of the grout backfill material in the dowel bar slots was inspected periodically on both the wheelpath trafficked by the HVS and the wheelpath that was not trafficked. Many of the dowel slots showed the grout to be in good condition. For example, Figure 2.34 and Figure 2.35 show a photographs taken in March 2002, ten months after construction, and it can be seen that the only apparent problems with the construction are slightly out-of-place foam backer boards on several of the joints.

However, some the slots showed what appear to be a lack of fine materials in the grout. This can be seen in Figure 2.36, which shows the DBR slots on a set of transverse cracks. Some of the cracking on this slot may be due to placement of the DBR on unconnected transverse cracks without a clear joint or crack on which to place the foam backer board. A little of the apparent lack of fines can be seen in Figure 2.37, which shows a joint.

Photographs taken in June 2003, two years after construction and after HVS testing was completed on all sections, showed some transverse cracking in the grout in the dowel slots. The grout did not come out of any of the slots, and the cracks remained tightly interlocked. This can be seen in Figure 2.38, which shows transverse cracking in the grout and slab and a very small amount of separation of the grout from the slab. Figure 2.39 shows another slot with some separation of grout and slab. Figure 2.40 shows transverse cracks in the grout.

Figure 2.34. Photograph of Joint 38, Section 556FD, in March 2002, showing generally good condition. (Blue line painted on surface shows HVS wheelpath).

Figure 2.35. Photograph of Joint 36, Section 557FD, in March 2002, showing generally good condition.

Figure 2.36. Photograph of Crack 1, Section 559FD, in March 2002, showing lack of fines, transverse cracking, and separation at edges.

Figure 2.37. Photograph of Joint 33, Section 559FD, in March 2002, showing a small amount of lack of fines and separation at the edges of the dowel slot closest to the slab center.

Figure 2.38. Photograph of DBR slot, Section 557FD, in June 2003, showing tight transverse cracks in grout and slab.

Figure 2.39. Photograph of DBR slot, Section 559FD, Slab 39, in June 2002, showing some separation of grout and slab.

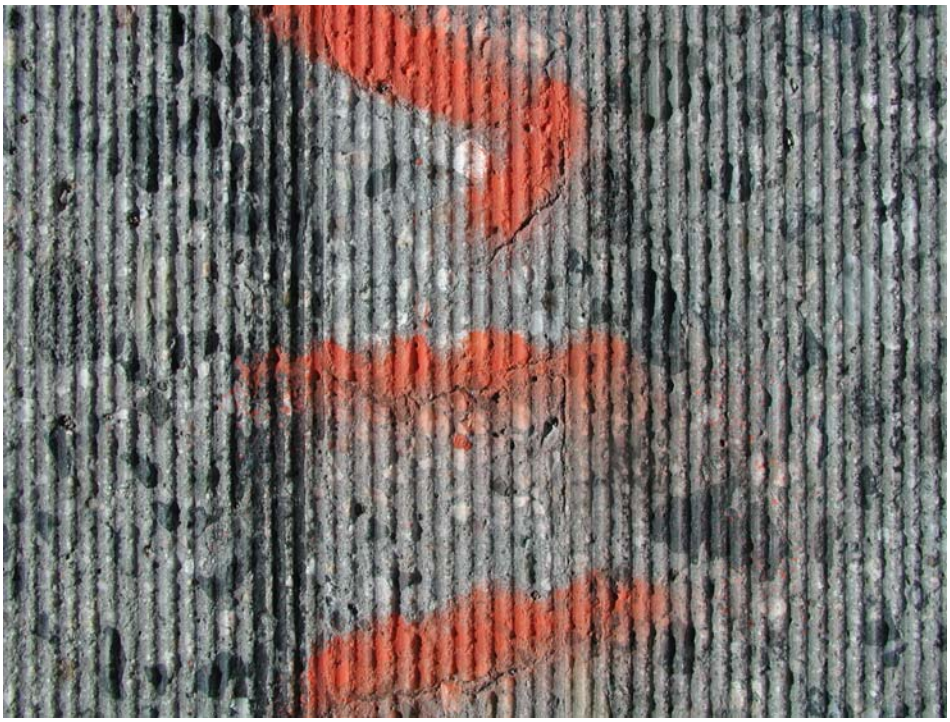

Figure 2.40. Photograph of DBR slot, Section 558FD, Slab 42, in June 2002, showing some transverse cracking in grout.

3 OVERVIEW OF FWD AND HVS TESTING

This chapter presents details of the testing program on the Palmdale DBR sections and adjacent sections using the Heavy Vehicle Simulator (HVS) and the Falling Weight Deflectometer (FWD). The mobile deflection testing device used for this project is a Heavy Weight Deflectometer (HWD) which is the same as an FWD except that it is capable of applying heavier loads. Because it is a more commonly known term, the HWD is referred to as an FWD in this report.

3.1 Measurement of Load Transfer Efficiency (LTE)

As implied by the name "load transfer efficiency" (LTE), this property is measured through application of load, and is a measure of what proportion of the load is transferred to the adjoining slab. LTE is normally expressed as a percentage, with one hundred percent meaning that the two adjoining slabs act as if they are one continuous slab, and zero percent meaning that the two slabs act entirely independently.

However, for most testing it is not possible to calculate this value with the actual loads because deflections, not the loads, are measured on the slabs. Thus this measure must be approximated using calculations based on the deflections of the slabs.

Separate definitions of LTE were used for measurements taken using Joint Deflection Measurement Devices (JDMD) during HVS testing and for measurements taken using the FWD, because the former uses a moving load and the latter uses a load dropped in one place.

3.1.1 Calculation Using JDMDs

JDMDs are used to measure the vertical movement of a single point on a concrete slab with a moving wheel load (normally the HVS wheel). JDMDs are attached to the side of the slab on both sides of the joint, and a full deflection bowl is recorded as the wheel moves from one slab to another across the joint. An example of the data is shown in Figure 3.1. Because a moving wheel is used, there is an "approach LTE," which is the load transfer as the load approaches the slab, and a "departure LTE," which is the load transfer as the load leaves the slab. Thus there are four possible LTE values for each joint (two slabs, with two LTE values each) on an HVS section because the wheel can traffic in both directions. On an in-service pavement there can only be two, since the traffic is unidirectional for each slab.

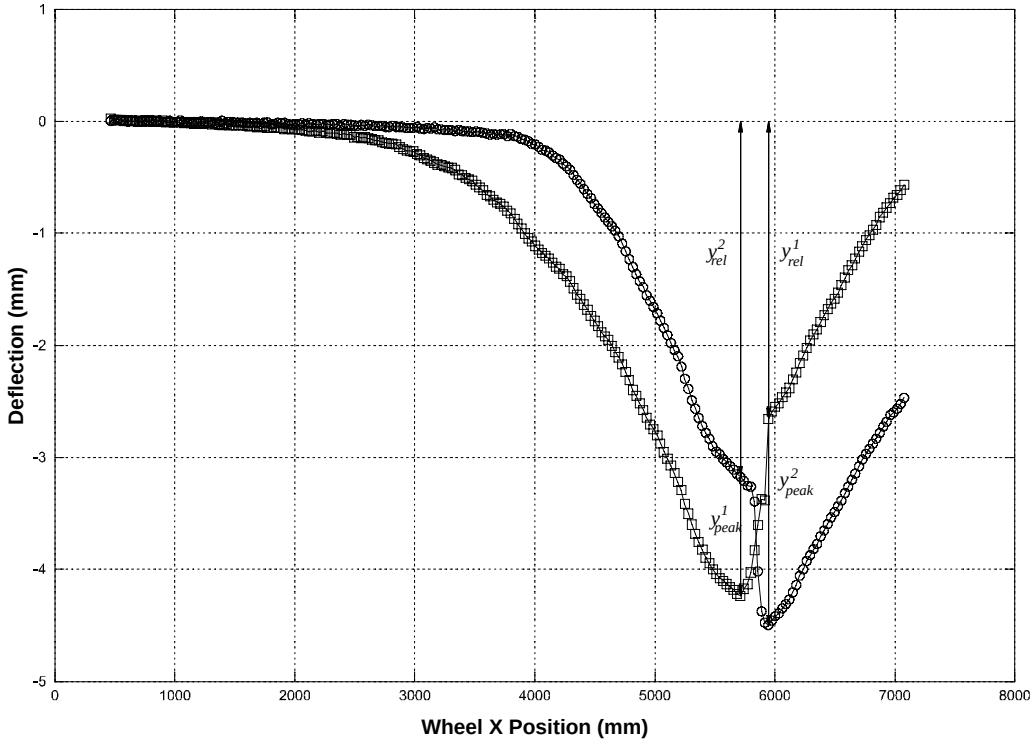

Figure 3.1. Example of LTE calculation from JDMD measurements.

However, there are a number of different ways of defining LTE based on deflection. Normally, there are four deflection values: the two peak values (the superscripts in Figure 3.1 and in Equation 1 indicate the instrument) and the two relative values, which are the deflection of each instrument when the other is at its peak. If the instrument experiences its relative deflection before its peak, then it is an "approach LTE;" if it experiences its relative deflection after its peak deflection then it is a "departure LTE." There are four possible calculations (two per instrument) that can be performed from the four data values above:

$$LTE^{approach}_{pair} = \frac{y^2_{rel}}{y^1_{peak}} \quad LTE^{depart}_{pair} = \frac{y^1_{rel}}{y^2_{peak}}$$
$$LTE^{approach}_{single} = \frac{y^2_{rel}}{y^2_{peak}} \quad LTE^{depart}_{single} = \frac{y^1_{rel}}{y^1_{peak}} \qquad \textbf{(1)}$$

The "pair" definitions shown in Equation 1 use the deflections of both instruments, when the wheel is at the same location; the "single" definitions use the deflection of only one instrument when the wheel is at different locations. There are arguments for the use of both of these definitions: the *single* definition in Equation 1 only uses the deflection of one slab, and so it cannot exceed a value of one, while the *pair* definition has the load at a single location, and so compares the deflections of the two slabs under

the same loading condition. The *pair* definition as been implemented in the HVS database and used in this report, because it provides more stable results, and therefore makes it easier to track changes in LTE with damage.

Negative LTE is also possible when the approach slab is being pushed upwards by pumping. With the *pair* definition, an LTE value greater than one is possible for the departure slab if it has a high deflection (caused by cracking, voids, or curling), and the approach slab has a low deflection.

3.1.2 Calculation Using the FWD

The FWD applies a single, dynamic load pulse to a slab close to the joint, and the peak deflection is measured on either side of the joint. This loading is shown in Figure 3.2.

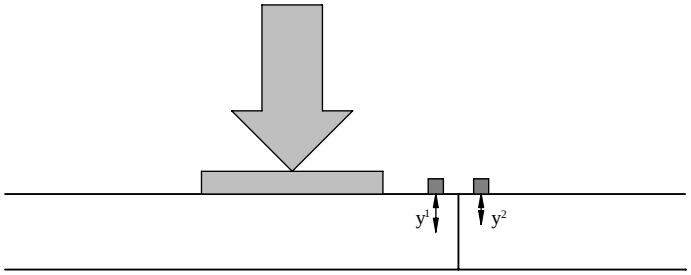

Figure 3.2. LTE testing using the FWD.

Load Transfer Efficiency (LTE) is typically defined for FWD measurements as:

$$LTE = y^2 / y^1 \qquad \textbf{(2)}$$

where y^2 and y^1 are the peak deflections under the dynamic load.

The program *Elmod 3* (26) was used to calculate LTE from FWD deflections for this report. To calculate LTE, *Elmod 3* makes use of Westergaard's "load transfer efficiency factor," j, which is defined by the equation:

$$j = 2\ y^2 / (y^1 + y^2) \qquad \textbf{(3)}$$

Westergaard's equation for stress at the bottom of a slab is given for a free edge. This stress can be calculated with j at a joint with load transfer. The relationship between LTE and j is defined as:

$$LTE = j / (2-j) \qquad \textbf{(4)}$$

This calculation is close to the "approach pair" LTE for the JDMDs, but it uses the peak deflections of the slabs at both measuring points. Because of this it is less likely to provide values out of the zero to one range.

3.2 Maximum Deflections

One other parameter was measured to evaluate the condition of load transfer at the transverse joints and cracks: maximum deflection. Maximum deflection provides an indication of the energy applied by the deflected slab to the underlying materials as well as to any water that is in the joint and under the slabs. An approach for evaluating faulting based on the energy applied to the underlying layers by the action of the joint was proposed by Hoerner (14), and a similar approach has been implemented in the NCHRP 1-37A software (11). This approach will be used to estimate faulting performance using the data from these and other test sections in a later report.

Maximum deflection, referred to as "peak deflection" in this report, is the maximum vertical downward movement of the loaded slab. Under FWD loading this would be the maximum movement of y^1 in Figure 3.2. Under Heavy Vehicle Simulator (HVS) loading this is the deflection of the approach slab when the wheel is on the approach slab, which would be y^1 in Figure 3.1, as the wheel passes from left to right.

3.3 Schedule and Conditions of FWD and HVS Tests

3.3.1 Chronology of Testing

The chronology of deflection testing, HVS testing, and coring of the original HVS tests and DBR sections at Palmdale is shown in Table 3.1.

3.3.2 FWD Test Conditions

The Dynatest Model 8082 Falling Weight Deflectometer (FWD) Test System was used to generate the nondestructive testing data analyzed for this report. The FWD generates a transient, impulse-type load of 25–30 millisecond duration at any desired load level between 27 kN (6,000 lbf) and 245 kN (55,000 lbf), thereby approximating the effect of a 50–80 kph (30–50 mph) moving wheel load. For this project, test loads were normalized to 44 kN (10 kip) and 67 kN (15 kip). All the FWD tests were performed separately in daytime and nighttime, and included testing along the center and the left edge of each slab. The stationing for this project was carried out in units of feet. The starting point (Station 0) is located at the southern end of the test section, with stationing increasing northward.

Table 3.1. Timetable of Testing on Palmdale Sections

Event	Time
Construction of Doweled and Undoweled Pavements	June 1998
FWD Test No. 1	June 19 1998
FWD Test No. 2	June 23 1998
FWD Test No. 3	August 1998
FWD Test No. 4	September 1998
FWD Test No. 5	January 1999
FWD Test No. 6	March 1999
HVS Test 532FD	June – July 1999
HVS Test 533FD	August – November 1999
HVS Test 534FD	December 1999 – March 2000
HVS Test 535FD	March – April 2000
HVS Test 536FD	April – July 2000
HVS Test 537FD	July – August 2000
HVS Test 539FD	August – September 2000
HVS Test 540FD	October – November 2000
HVS Test 538FD	December 2000 – January 2001
FWD Test No. 7	February 2001
DBR Construction on Untested Undoweled Joints and Cracks	June 28-30 2001
HVS Test 558FD	August 2001 – March 2002
HVS Test 556FD	March – August 2002
FWD Test No. 8	April 2002
HVS Test 557FD	August – October 2002
FWD Test No. 9	October 2002
HVS Test 559FD	October 2002 – March 2003
FWD Test No. 10	April 2003
FWD Test No. 11	June 2003
Coring of DBR Section	June 2003
FWD Test No. 12	February 2004

During FWD tests, the 300-mm diameter loading plate is located at the slab corner. The deflections under the loading plate and across the transverse joint (or transverse crack) are measured by

geophones on the FWD. The spacing of geophones starting from the center of the loading plate is: 0, 200, 300, 800, 1200, 1600, and 2000 mm, with geophone numbering beginning with Geophone 1 at the 0 mm distance, and Geophone 7 at the 2000 mm position. To measure deflections across a joint/crack, the FWD is positioned such that the joint/crack of interest is between Geophone 2 (200 mm from loading plate) and Geophone 3 (300 mm from loading plate). A summary of all FWD testing results is shown in Appendix D.

3.3.3 HVS Test Conditions

The HVS is a 60 tonne mobile loading device that has one wheel (dual or single) with variable load and an 8-m long loading span. It can be run in a bi- or a unidirectional mode, channelized or with programmed lateral wander.

The HVS loading was initiated under a 60-kN (13,500 lb) load (on dual truck tires (Goodyear G159A radials) and then increased to 90 kN (20,250 lb) on dual truck tires with the tire pressure kept constant at 689.5 kPa (100 psi). The final load used was 150 kN (33,750 lb) on an aircraft wheel, with tire pressure maintained at 1450 kPa (210 psi). Channelized (no wander), bidirectional loading was conducted on the wheelpath for all tests over the center of the dowel bar group. The roof panels and some of the side panels of the temperature control chamber were in place during the HVS tests to provide shading to the test sections. The temperature control system was not used because it was previously shown to not completely control temperatures and curling in the slabs (28); in addition some temperature variability was desired during the testing.

3.3.4 Use of the HVS to Evaluate Joint Performance

Two important differences between HVS loading and highway loading are: bidirectional versus unidirectional trafficking and the speed of the wheel. Bidirectional loading, which is used with the HVS, does not cause faulting; unidirectional loading, which occurs under highway traffic, causes faulting by moving material from under the downstream slab to under the upstream slab. Since faulting is highly correlated with LTE (27), it is used as a surrogate under HVS loading. Deflections and LTE determine the energy applied to the underlying layers that moves material and causes faulting.

Bidirectional HVS results have been compared with unidirectional HVS results, and the conclusion is that the bidirectional loading causes damage to the aggregate interlock and the degradation of the dowel/concrete interface, which leads to loss of LTE through the dowels (28). Calibration from HVS to field has to be done for both unidirectional and bidirectional loading because the wheel speeds (load dynamics), the traffic wander, and the temperatures are different.

Differences in loading time between the HVS and the FWD should not significantly change LTE and deflection measurements, assuming that the response of the concrete slab, steel dowels, and underlying layers is primarily elastic.

3.4 Expected Effects of Pavement Temperature on Deflections, Backcalculated Stiffnesses, and Load Transfer Efficiency

Temperature and temperature gradient are expected to have significant effects on deflections, backcalculated stiffnesses, and load transfer efficiency.

Decreasing mid-slab temperature causes the concrete slabs to contract, which causes the joints between slabs to open. Increasing mid-slab temperatures causes the slabs to expand, which causes the joints to close, which increases aggregate interlock and may even place the joint faces into compression. Opening of the joints under cold temperatures will reduce their load transfer efficiency and increase the vertical joint deflections under loading.

Positive temperature gradients, with the slab hotter on the top than the bottom, cause the top of the slab to expand relative to the bottom of the slab. Positive temperature gradients typically occur in the late afternoon and evening. This shape forces the edges, and especially the corners of the slab, into closer contact with the underlying layers. This will tend to reduce contact between the center of the slab and the base and increase the center-slab deflections. The increased center-slab deflections will result in lower backcalculated moduli for the concrete slab and the underlying support layers. This shape also results in smaller deflections at the joints and corners.

Negative temperature gradients, with the slab cooler on the top than on the bottom, cause the bottom of the slab to expand relative to the top of the slab. These temperature gradients typically occur in the night and morning. This shape results in the edges and corners moving up relative to the rest of the slab, placing the center of the slab in close contact with the underlying layers, and decreasing measured center-slab deflections. This results in greater backcalculated moduli for the concrete slab and the underlying support layers. This shape also results in greater deflections at the joints and corners.

4 FWD TEST DATA PRIOR TO DOWEL BAR RETROFIT

The slab deflections before DBR construction were measured by FWD in February 2001 (FWD Test No. 7 in Table 3.1). Deflections were measured twice in a twenty-four-hour period: once from 2:30 p.m. to 4:16 p.m. (daytime) on February 7 and once from 12:01 a.m. to 1:17 a.m. (nighttime) on February 8. The measured deflections were used to backcalculate the concrete stiffness, support layer (base + subgrade) stiffness, subgrade k-values, and joint load transfer efficiency (LTE).

4.1 Backcalculated Stiffness

Pavement surface temperatures and air temperatures from February 2001 are summarized in Table 4.1. Backcalculated stiffness values are shown in Table 4.2 and Figure 4.1 through Figure 4.3. The average pavement surface temperature was around 9.5^{o}C for daytime tests, and around 3.5^{o}C for nighttime tests. It is expected that under lower temperature, stiffness values would be greater than those under higher temperature because the slab center is in better contact with underlying layer due to temperature-induced curl. However, as can be seen from Table 4.1 and Figure 4.1 through Figure 4.3, the backcalculated daytime and nighttime stiffness values are quite close. The unexpected lack of difference between the daytime and nighttime values could be due to the fact that the temperature difference between daytime and nighttime for this FWD test is only approximately 6^{o}C, so the resulting stiffness difference is not obvious.

Table 4.1. Summary of Pavement Surface Temperature from February 2001

Location		Daytime		Nighttime	
		Average	Standard Deviation	Average	Standard Deviation
Center slab	Surface temperature (^{o}C)	9.47	1.01	3.56	0.80
	Air temperature (^{o}C)	6.22	0.63	-1.18	0.39
Transverse joint	Surface temperature (^{o}C)	9.56	0.98	3.44	0.89
	Air temperature (^{o}C)	6.24	0.61	-1.08	0.29

Table 4.2. Summary of Backcalculated Stiffness

		Daytime		Nighttime	
		Average	**Standard Deviation**	**Average**	**Standard Deviation**
Section 11 (Wide truck lane)	Concrete Stiffness E_{pcc} (MPa)	58,071	39,341	60,968	44,332
	Support stiffness $E_{sg+base}$ (MPa)	328	67	306	73
	Support k-value (MPa/m)	192	93	168	73
Section 9 (Doweled)	Concrete Stiffness E_{pcc} (MPa)	37,731	25,358	58,612	31,285
	Support stiffness $E_{sg+base}$ (MPa)	282	104	232	72
	Support k-value (MPa/m)	186	124	110	37
Section 7 (Un-doweled)	Concrete Stiffness E_{pcc} (MPa)	52,421	17,149	47,786	26,982
	Support stiffness $E_{sg+base}$ (MPa)	214	58	197	71
	Support k-value (MPa/m)	100	30	95	37
All	Concrete Stiffness E_{pcc} (MPa)	49,408	29,732	55,789	34,671
	Support stiffness $E_{sg+base}$ (MPa)	275	91	245	84
	Support k-value (MPa/m)	159	99	124	60

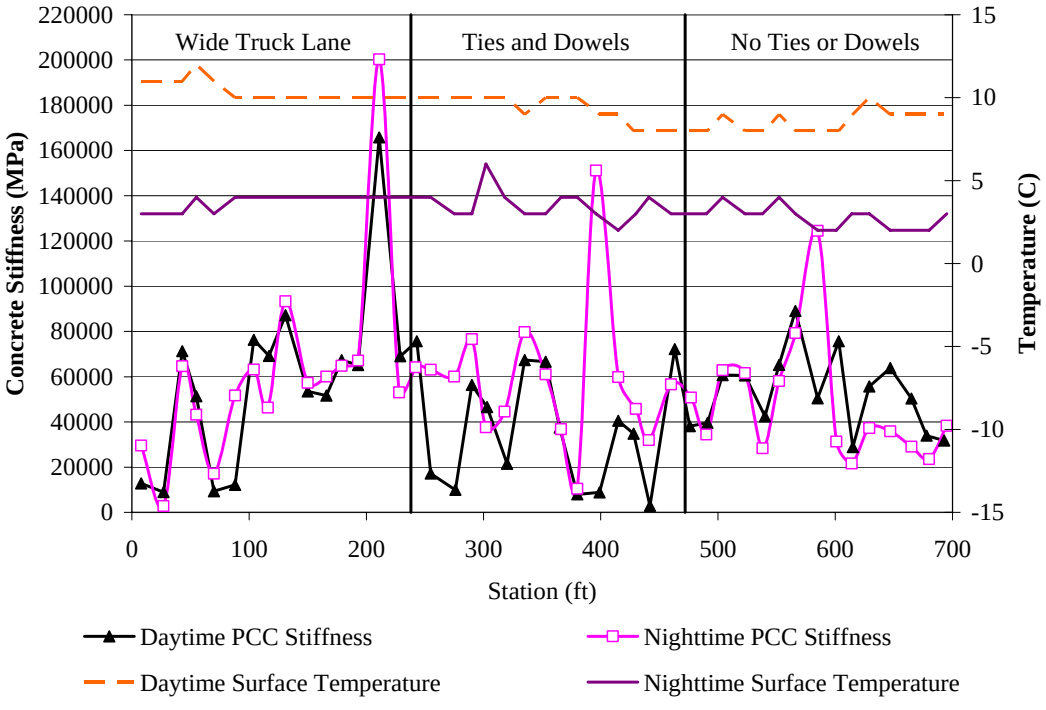

Figure 4.1. Backcalculated concrete stiffness from center slab deflections, Feb. 2001.

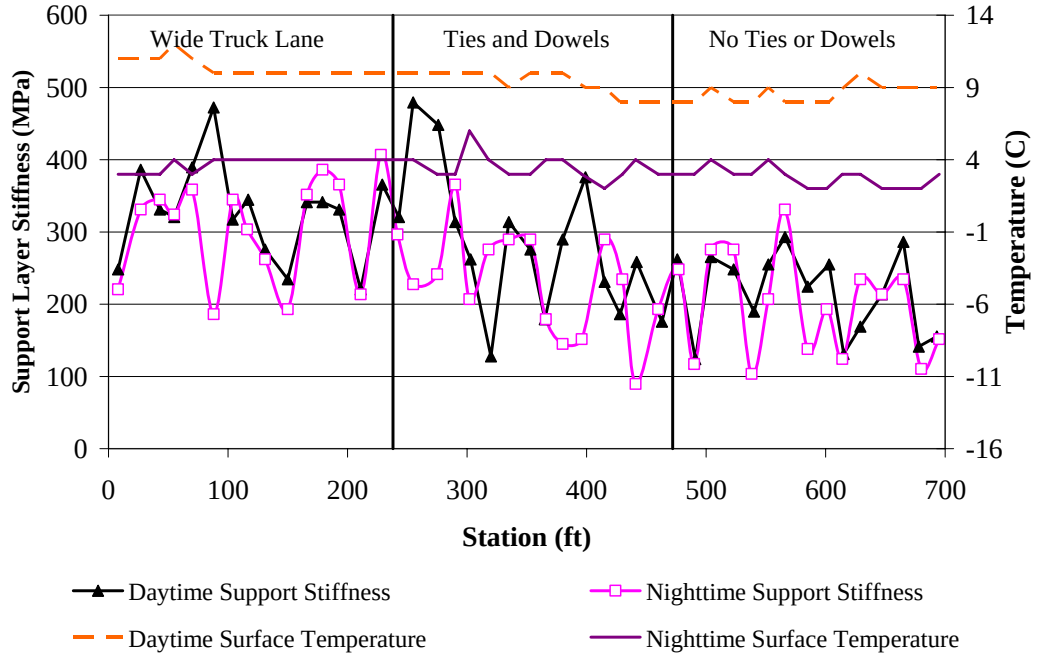

Figure 4.2. Backcalculated support layer stiffness from center slab deflections, Feb. 2001.

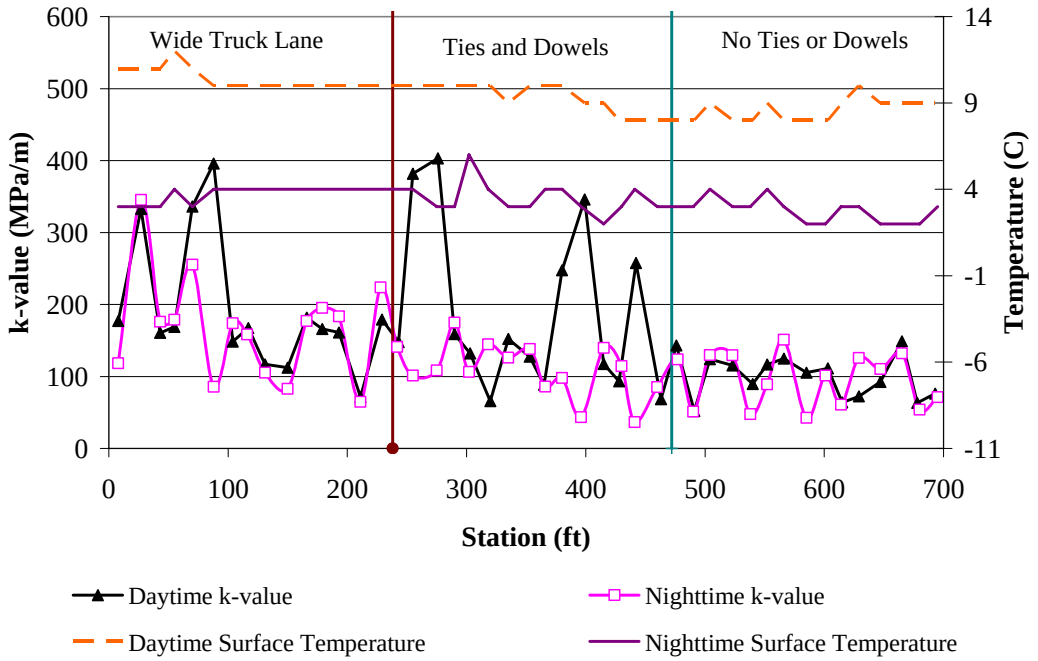

Figure 4.3. Backcalculated subgrade k-value from center slab deflections, Feb. 2001.

4.2 Load Transfer Efficiency

The daytime and nighttime measured load transfer efficiencies (LTE) for the North Tangent set are summarized in Table 4.3, and the LTE value for each joint is shown in Figure 4.4. For this FWD test section, both daytime and nighttime temperatures are relatively low. However, LTEs for testing sections with a wide truck lane (Section 11) or with ties and dowels (Section 9) are still high (around 90 percent). For Section 7 (without ties or dowels), the slab joints showed much lower LTE: 33.41 percent for the daytime average and 25.33 percent for the nighttime average.

Table 4.3. LTE Summary from FWD Tests in February 2001

	Daytime		Nighttime	
	Average	**Standard Deviation**	**Average**	**Standard Deviation**
Section 11	90%	2%	90%	2%
Section 9	92%	2%	92%	2%
Section 7	33%	14%	25%	14%
All	72%	29%	69%	32%

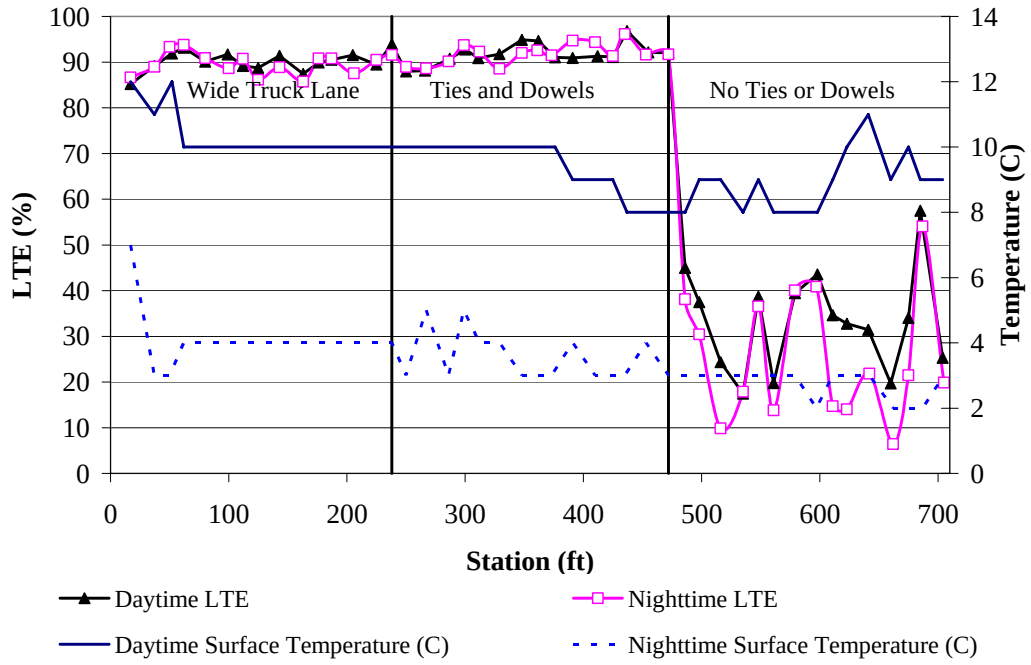

Figure 4.4. Load Transfer Efficiency, Feb. 2001.

5 FWD TESTS AFTER DBR AND BEFORE HVS TESTING

This chapter presents details of FWD tests performed six months apart, after the joints and cracks had been retrofitted but prior to accelerated traffic loading.

5.1 April 2002 FWD Test

5.1.1 Backcalculated Stiffness

Pavement surface temperatures from April 2002 are summarized in Table 5.1. Stiffness for concrete, support layer (base and subgrade), and subgrade k-values for the whole test set are shown in Table 5.2.

Table 5.1. Summary of Pavement Surface Temperature from April 2002

Location		Daytime		Nighttime	
		Average	Standard Deviation	Average	Standard Deviation
Center slab	Surface temperature (^{o}C)	33.6	1.2	13.1	0.5
	Air temperature (^{o}C)	20.4	0.8	12.5	0.3
Transverse joint	Surface temperature (^{o}C)	33.6	1.2	13.2	0.8
	Air temperature (^{o}C)	20.4	0.7	12.6	0.3

The FWD tests were performed between 2:20–3:40 p.m. on April 8, 2002 (daytime), and between 2:30–3:30 a.m. on April 10, 2002 (nighttime). Details of temperature and stiffness values for all the test joints are shown in Figure 5.1 through Figure 5.3. The data for the Section 7 are summarized in Table 5.2 and Figure 5.1 through Figure 5.3, and include all joints in this section (DBR joints and non-DBR joints).

It is expected that nighttime stiffness values would be higher than those from daytime because the slab center is in better contact with the underlying layer under nighttime conditions (the curl caused by negative temperature gradients). For the whole test set, the difference between day and night pavement surface temperatures is around 20^{o}C. The average nighttime PCC stiffness is 19.7 percent higher than that of the daytime, the average nighttime support layer stiffness is 7.9 percent higher, and the average nighttime k-value is 7.4 percent higher. Also, the measured stiffness and k-values do not change much with different FWD loads, which indicates that the subgrade/base support have a linear response to load changes for this test set.

Table 5.2. Summary of Backcalculated Stiffness

		Daytime		Nighttime	
		Average	**Standard Deviation**	**Average**	**Standard Deviation**
Section 11 (Wide truck lane)	Concrete stiffness E_{pcc} (MPa)	49,910	9,429	61,486	24,170
	Support stiffness $E_{sg+base}$ (MPa)	236	38	309	93
	Support k-value (MPa/m)	116	28	155	53
Section 9 (Initially doweled and tied)	Concrete stiffness E_{pcc} (MPa)	53,030	7,200	67,639	27,635
	Support stiffness $E_{sg+base}$ (MPa)	261	34	245	76
	Support k-value (MPa/m)	128	19	113	44
Section 7 (DBR section)	Concrete Stiffness E_{pcc} (MPa)	45,129	9,464	41,207	21,696
	Support stiffness $E_{sg+base}$ (MPa)	240	30	236	103
	Support k-value (MPa/m)	121	19	128	81
All	Concrete stiffness E_{pcc} (MPa)	50,135	9,003	60,026	26,891
	Support stiffness $E_{sg+base}$ (MPa)	246	36	266	93
	Support k-value (MPa/m)	122	23	131	59

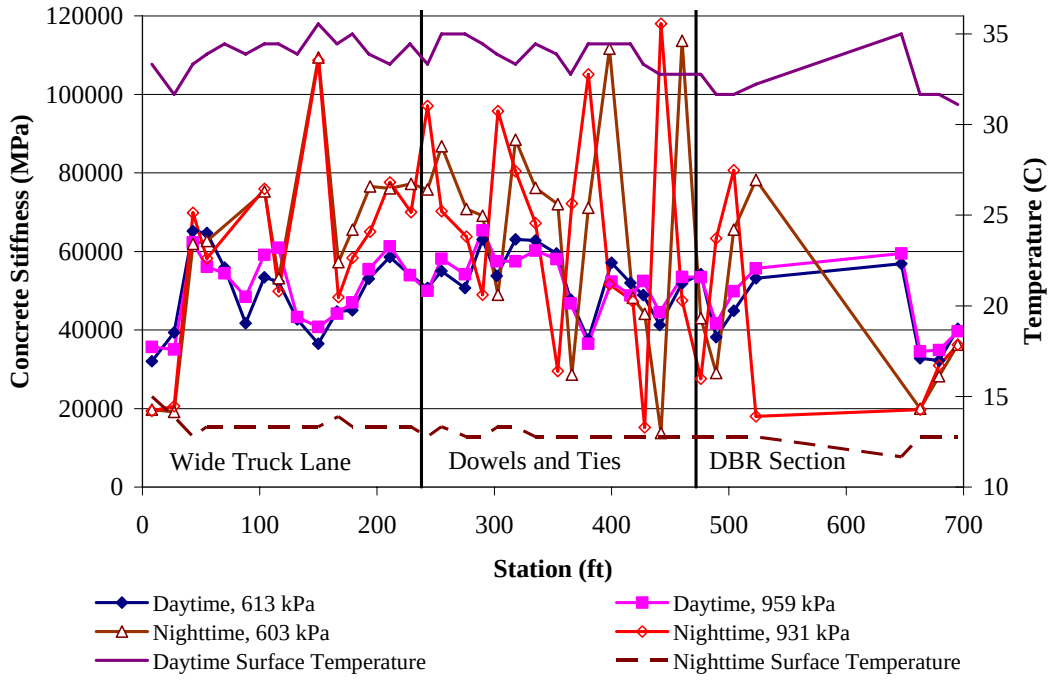

Figure 5.1. Backcalculated concrete stiffness from center-slab deflections, April 2002.

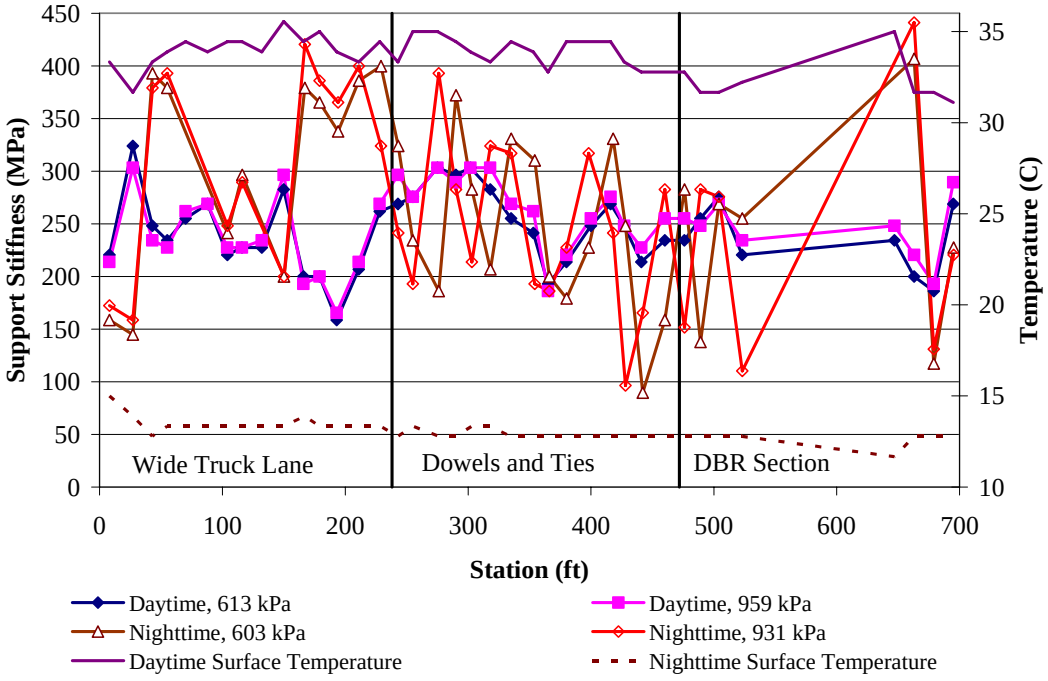

Figure 5.2. Backcalculated support layer stiffness from center-slab deflections, April 2002.

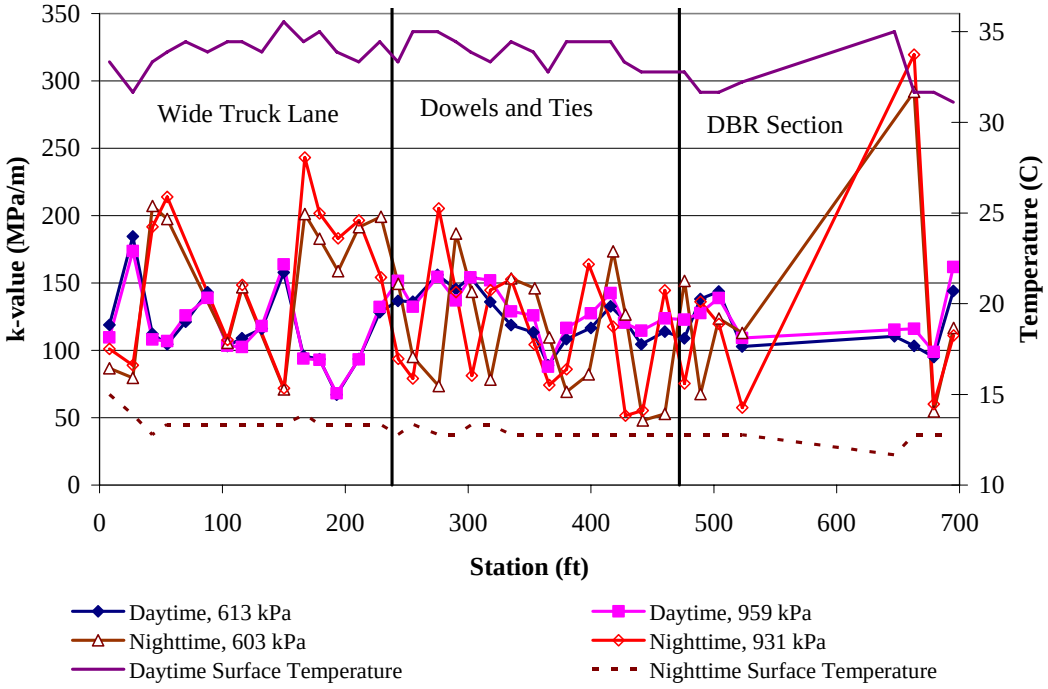

Figure 5.3. Backcalculated subgrade k-value from center-slab deflections, April 2002.

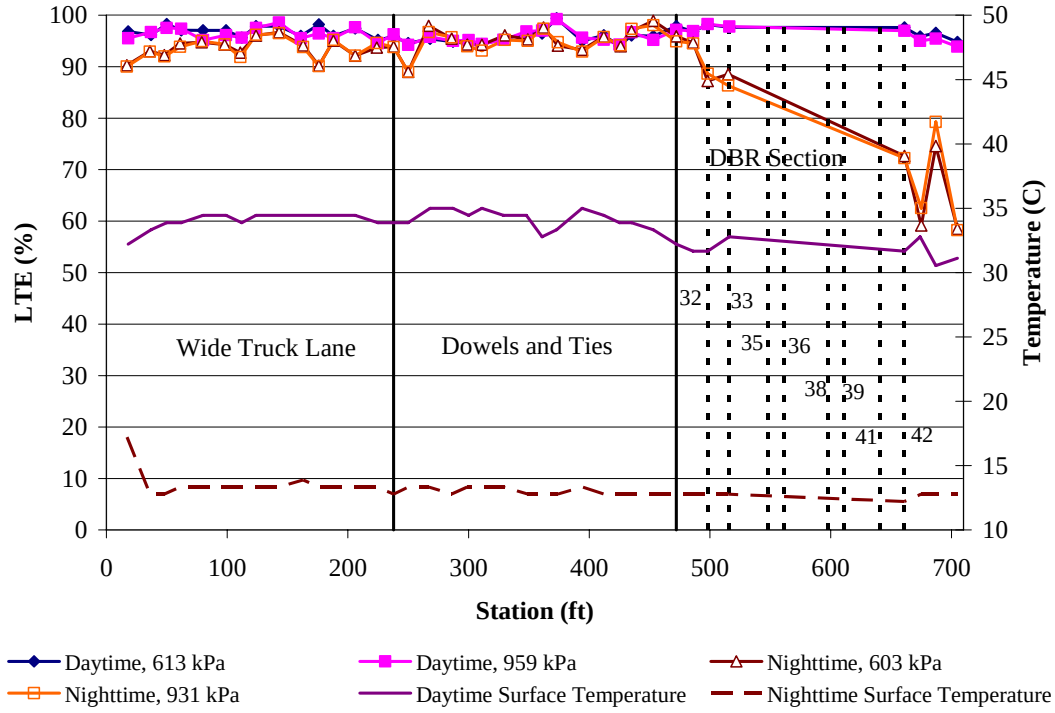

Figure 5.4. Load Transfer Efficiency, April 2002 (with joint numbers shown in DBR section).

5.1.2 Load Transfer Efficiency

The daytime and nighttime measured load transfer efficiencies (LTE) for the North Tangent set are summarized in Table 5.3. During daytime, the high pavement surface temperature (33.62°C) causes the slabs to expand, closing the joint and increasing aggregate interlock. From Table 5.3, it can be seen that all the joints exhibit high daytime LTE. For joints in Section 11 (wide truck lane) and Section 9 (initially doweled and tied), nighttime LTE are also high. For Section 7 (DBR section), only some of the joints were retrofitted by dowel bars, so the average nighttime LTE is relatively low and the standard deviation is high. The LTE value for each joint is shown in Figure 5.4 and Table 5.4, and DBR joint details are shown in Table 5.5. In this FWD test Joints 34–41 were not tested; therefore, the LTE values for these joints are not available. From Table 5.4, it can be seen that the average doweled joint nighttime LTE is 13.51 percent higher than that of undoweled joint nighttime LTE. Like backcalculated stiffness and k-value, LTE is also independent of the load level being used in the FWD test (Figure 5.4).

Table 5.3. LTE Summary from FWD Tests in April 2002

	Daytime		Nighttime	
	Average	**Standard Deviation**	**Average**	**Standard Deviation**
Section 11	97%	1%	94%	2%
Section 9	96%	1%	95%	2%
Section 7	97%	1%	77%	13%

Table 5.4. Nighttime LTE of Section 7 (DBR Section)

	Joint No.	Nighttime LTE	Average	Standard Deviation
Doweled	32	87%	83%	9%
	33	89%		
	42	72%		
Undoweled	31	95%	73%	20%
	43	59%		
	44	79%		
	45	58%		

Table 5.5. DBR Joint Details

Joint Number	Dowel Bar Type
32	Epoxy-coated steel dowel, 4/wheelpath
33	Hollow stainless steel dowel, 4/wheelpath
42	FRP dowel, 4/wheelpath

5.2 October 2002 FWD Test

5.2.1 Backcalculated Stiffness

Pavement surface temperatures from October 2002 are summarized in Table 5.6. Stiffness for concrete, support layer (base and subgrade), and subgrade k-values for the whole test set are shown in Table 5.7.

The FWD tests were performed between 2:24 a.m. and 4:00 p.m. on October 24, 2002 (daytime), and between 2:22 a.m. and 3:45 a.m. on October 25, 2002 (nighttime). Details of temperature and stiffness values for all the test joints are shown in Figure 5.5 through Figure 5.7.

The pavement surface temperature difference between daytime and nighttime in October is about 14^{o}C, and it is expected that pavement layers will exhibit higher nighttime stiffness values due to the nighttime curl. As can be seen in Table 5.7, concrete stiffness is always higher during the nighttime than the daytime. The average nighttime concrete stiffness for the whole North Tangent set is 18.4 percent higher than the average daytime concrete stiffness. However, the backcalculated nighttime support layer stiffness and subgrade k-values are slightly lower than the daytime values. On average for the whole test

set, the nighttime support layer stiffness is 3.6 percent lower and the nighttime subgrade k-value is 7.7 percent lower than the daytime values. It appears that the daytime and nighttime support stiffness and subgrade k-values are very close. For this test, the pavement surface temperature difference (14°C) is smaller than that of April 2002 (20°C), and this temperature difference will be even smaller in the base and subgrade layers. Thus, the properties of the support layers may not be influenced much by the temperature changes and can be fairly close. Again, the measured stiffness and k-values change little with different FWD loads, which indicates that the subgrade/base support is highly linear for this test set.

Table 5.6. Summary of Pavement Surface Temperature from October 2002

Location		Daytime		Nighttime	
		Average	Standard Deviation	Average	Standard Deviation
Center slab	Surface temperature (°C)	23.1	1.9	9.3	0.7
	Air temperature (°C)	15.4	1.0	7.9	0.3
Transverse joint	Surface temperature (°C)	23.2	2.0	9.4	0.6
	Air temperature (°C)	15.5	1.0	7.9	0.3

Table 5.7. Summary of Backcalculated Stiffness

		Daytime		Nighttime	
		Average	Standard Deviation	Average	Standard Deviation
Section 11 (Wide truck lane)	Concrete stiffness E_{pcc} (MPa)	48,959	18,541	60,913	28,253
	Support stiffness $E_{sg+base}$ (MPa)	339	89	311	173
	Support k-value (MPa/m)	185	50	162	107
Section 9 (Initially doweled and tied)	Concrete stiffness E_{pcc} (MPa)	46,680	20,213	54,026	28,895
	Support stiffness $E_{sg+base}$ (MPa)	238	108	232	124
	Support k-value (MPa/m)	121	61	115	75
Section 7 (DBR section)	Concrete stiffness E_{pcc} (MPa)	49,112	21,959	55,386	18,749
	Support stiffness $E_{sg+base}$ (MPa)	252	114	245	81
	Support k-value (MPa/m)	134	89	120	45
All	Concrete stiffness E_{pcc} (MPa)	48,269	20,131	57,142	26,679
	Support stiffness $E_{sg+base}$ (MPa)	276	112	267	143
	Support k-value (MPa/m)	146	74	135	87

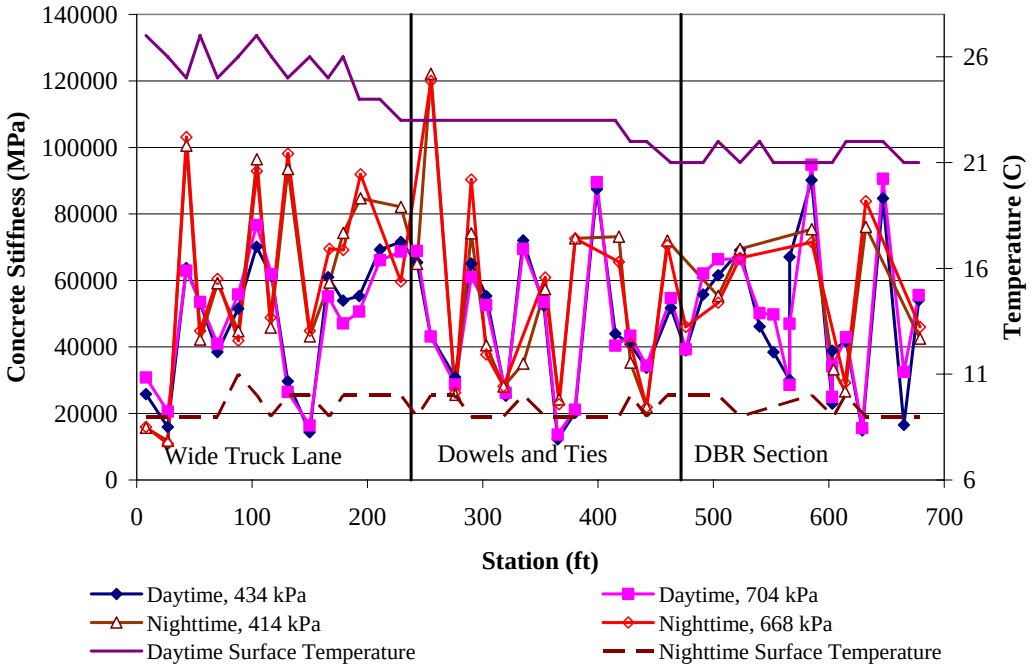

Figure 5.5. Backcalculated concrete stiffness from center-slab deflections, October 2002.

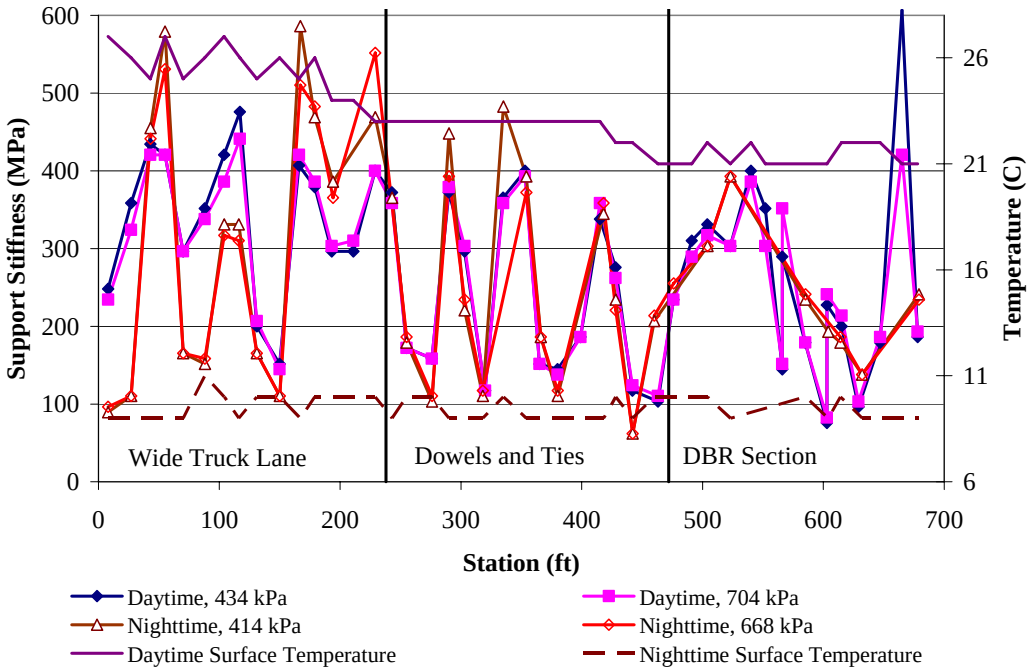

Figure 5.6. Backcalculated support layer stiffness from center-slab deflections, October 2002.

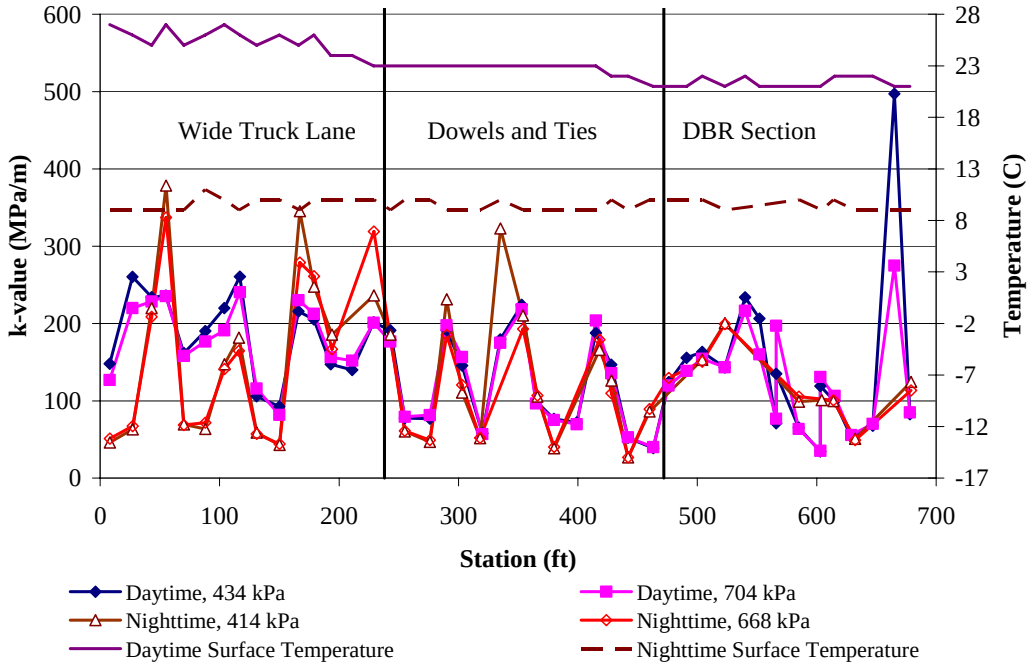

Figure 5.7. Backcalculated support layer k-value from center-slab deflections, October 2002.

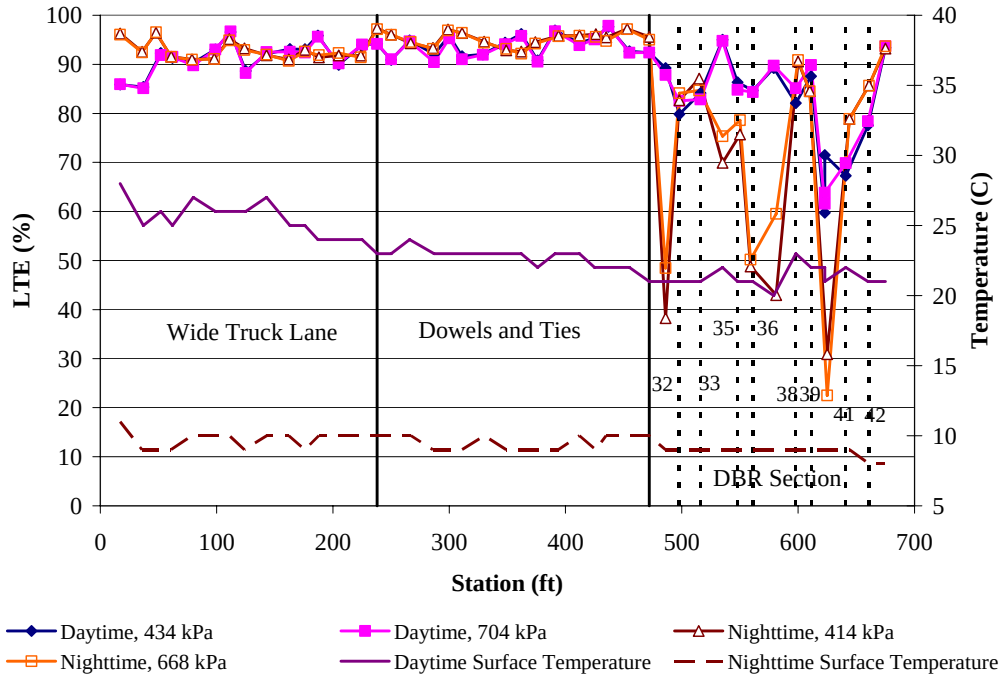

Figure 5.8. Load Transfer Efficiency, October 2002 (joint numbers shown in DBR section).

5.2.2 Load Transfer Efficiency

The daytime and nighttime measured load transfer efficiencies (LTE) in October 2002 for the North Tangent set are summarized in Table 5.8 and Figure 5.8. For Section 11 (wide truck lane) and Section 9 (initially doweled and tied), joint LTEs are always higher than 85 percent, regardless of whether they were measured in the daytime or the nighttime. For Section 7, the average LTE values shown in Table 5.8 include the LTEs for both retrofitted joints and unretrofitted joints, and it can be seen that the LTEs are considerably lower than those of Sections 9 and 11. Details of DBR-section joint LTEs are shown in Figure 5.8, Table 5.9, Table 5.10, and Table 5.11. Compared with the results from April 2002, the daytime pavement surface temperature is approximately 10^{o}C lower. As a result, daytime LTEs for the DBR section are also much lower than those from the April 2002 FWD test. More detailed comparisons among the different FWD test results will be shown in later sections.

From Tables Table 5.10 and Table 5.11, it can be concluded that for DBR section, the daytime LTE for doweled joints and undoweled joints are very close due to the relatively high temperature. However, during nighttime, average doweled LTE is 38 percent higher than average undoweled LTE. The data presented in Table 5.11 indicates that the LTE values are much lower for three dowel bars (Joints 35 and 36) for each wheelpath compared with using four dowel bars per wheelpath.

Table 5.8. LTE Summary from FWD Tests in October 2002

Section	Daytime		Nighttime	
	Average	Standard Deviation	Average	Standard Deviation
Section 11	92%	3%	93%	2%
Section 9	94%	3%	95%	1%
Section 7	83%	9%	71%	21%

Table 5.9. DBR Joint Details

Joint Number	Dowel Bar Type
32	Epoxy-coated steel dowel, 4/wheelpath
33	Hollow stainless steel dowel, 4/wheelpath
35	Epoxy-coated steel dowel, 3/wheelpath
36	Epoxy-coated steel dowel, 3/wheelpath
38	Epoxy-coated steel dowel, 4/wheelpath
39	Epoxy-coated steel dowel, 4/wheelpath
41	Epoxy-coated steel dowel, 4/wheelpath
42	FRP dowel, 4/wheelpath

Table 5.10. Average Daytime LTE of Section 7 (DBR Section), October 2002

	Dowel Type	Joint no.	LTE	Average LTE	Overall Average LTE	Standard Deviation
Doweled	ECS[1] dowel, 4 pw[2]	32	81%	81%	82%	6%
		38	84%			
		39	89%			
		41	69%			
	ECS dowel, 3pw	35	86%	86%		
		36	85%			
	HSS[3] dowel, 4pw	33	83%	83%		
	FRP dowel, 4pw	42	78%	78%		
Un-doweled	31		89%	85%		13%
	34		95%			
	37		89%			
	40		61%			
	43		94%			

[1]ECS: epoxy-coated steel.
[2]pw: per wheelpath.
[3]HSS: hollow stainless steel.

Table 5.11. Average Nighttime LTE of Section 7 (DBR Section), October 2002

	Dowel Type	Joint no.	LTE	Average LTE	Overall Average LTE	Standard Deviation
Doweled	ECS[1] dowel, 4 pw[2]	32	83%	85%	79%	12%
		38	91%			
		39	85%			
		41	79%			
	ECS dowel, 3pw	35	77%	64%		
		36	50%			
	HSS[3] dowel, 4pw	33	86%	86%		
	FRP dowel, 4pw	42	86%	86%		
Un-doweled	31		48%	57%		25%
	34		73%			
	37		51%			
	40		27%			
	43		93%			

[1]ECS: epoxy-coated steel.
[2]pw: per wheelpath.
[3]HSS: hollow stainless steel.

6 HVS TESTS AND FWD TESTS AFTER DBR AND AFTER HVS TESTING

This chapter presents detailed results of performance and measured properties of the Palmdale test sections during HVS testing and using the FWD after HVS testing was completed.

6.1 HVS Results Analysis

6.1.1 Failure Criteria for HVS Tests

The definition of failure for the HVS test sections at Palmdale consisted of three criteria:

- Cracking of the concrete slab due to fatigue,
- Major damage to the retrofitted dowel bars, or
- Loss of load transfer efficiency of the loaded joint or crack.

The test sections were considered to have failed when any of these criteria was met. All four test sections, 556FD, 557FD, 558FD, and 559FD, failed by the first criterion, fatigue cracking of the concrete slab.

6.1.2 Balancing of Environmental Conditions in Experiment Execution

The trafficking of the four HVS test sections was scheduled to provide similar temperature and rainfall conditions for the following two comparisons:

- Four epoxy-coated steel dowels per wheelpath (556FD) versus three dowels per wheelpath (557FD),
- Epoxy-coated steel dowels (559FD, Joint 32) versus hollow stainless steel dowels (559FD, Joint 33) versus fiber-reinforced polymer dowels (558FD), all with four dowels per wheelpath.

This was generally achieved, as can be seen in Figure 6.1.

Various test loads were using during HVS testing, and two types of wheels: a dual truck wheel and a single aircraft wheel. During HVS testing deflection data was taken periodically. Deflection were measured under two loads each time data was taken: the load being used for trafficking at that time, referred to as the “trafficking load”, and at a common load used to provide continuity of measurements across the entire test, referred to as the “measuring load”. The measuring load was always 60 kN (13,500 lb).

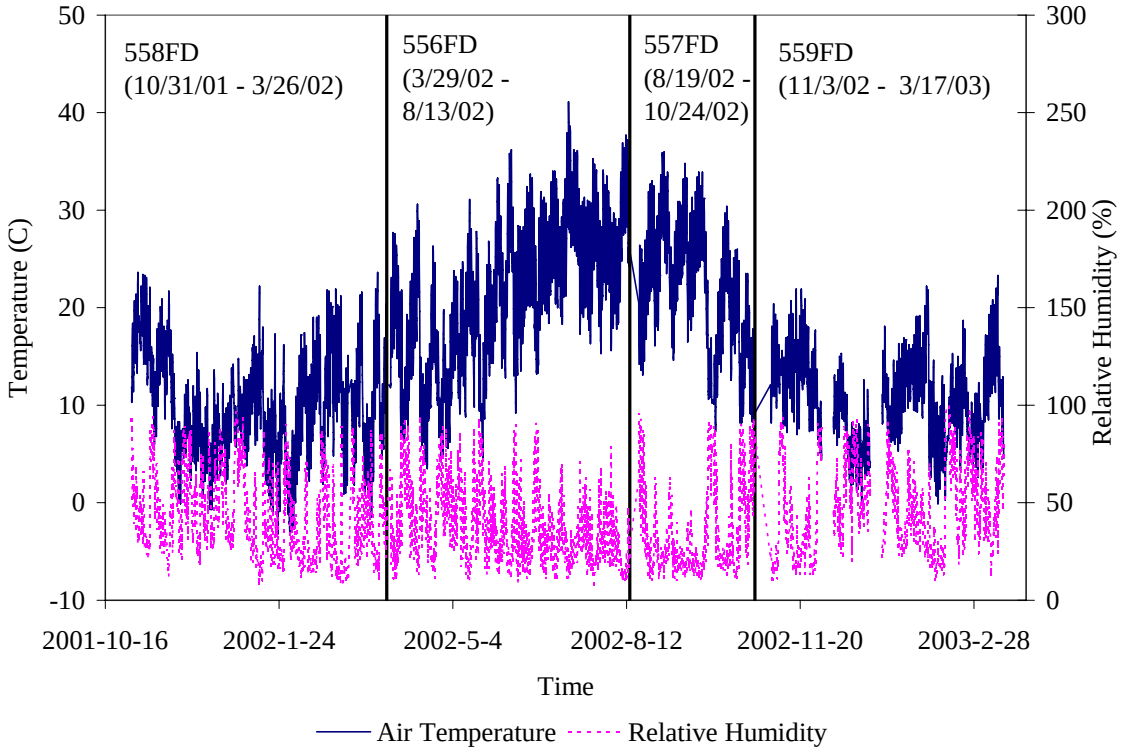

Figure 6.1. Air temperature and relative humidity across all Palmdale DBR HVS tests.

6.1.3 556FD HVS Test

The condition of Section 556FD prior to HVS testing in March 2002 is shown in Figure 6.2. Figure 6.3 shows a close-up of Joint 38 and Figure 6.4 shows a close-up of Joint 39.

Figure 6.2. HVS Test Section 556FD prior to HVS testing.

Figure 6.3. HVS Test Section 556FD, Joint 38, prior to HVS testing.

Figure 6.4. HVS Test Section 556FD, Joint 39, prior to HVS testing.

JDMD locations and numbering for Section 556FD are shown in Figure 6.5.

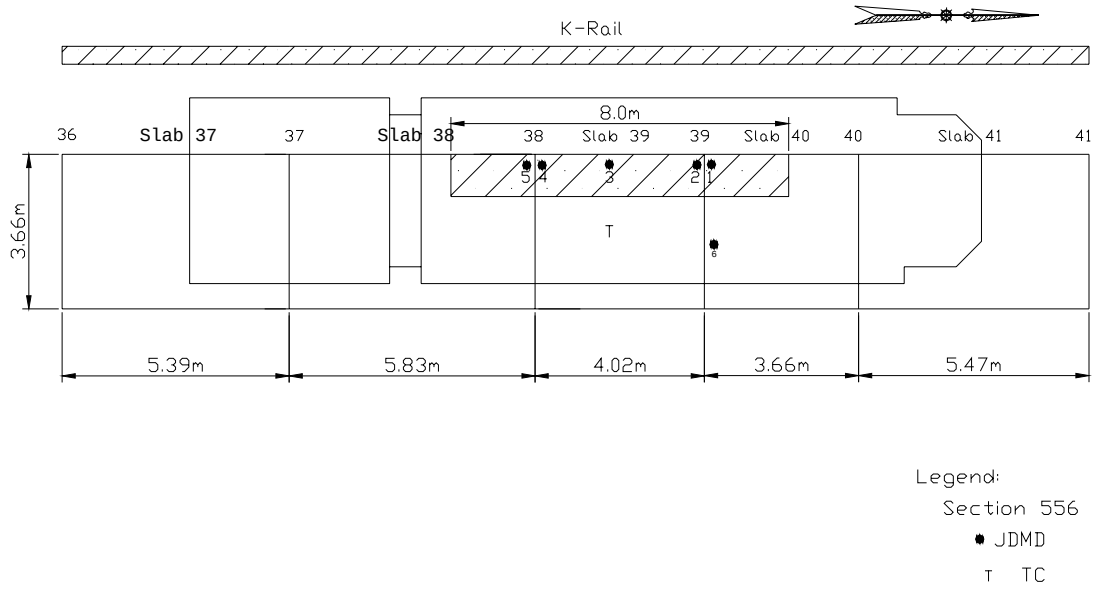

Figure 6.5. JDMD locations and numbering for Section 556FD.

The load history on Section 556FD is shown in Table 6.1. HVS loading on Section 556FD was started with a 60 kN dual wheel load, followed by a 90 kN dual wheel load and a 150 kN aircraft wheel load, for a total of 2,208,546 repetitions, as shown in Table 6.1. During repetitions with a wheel load of 90 kN, five repetitions were tested with the common test load of 60 kN; and for repetitions with a wheel load of 150 kN, nineteen repetitions were tested at 60 kN. The testing obtained from repetitions with same test load (40 kN) throughout the HVS testing will be used to evaluate how the HVS repetitions damage the test section. In this way, the damage caused by different test loads can be evaluated in terms of deflections and LTE under a standard measurement load.

Table 6.1. Load History on Section 556FD

Load (kN)	Tire/Wheel Type	Inflation Pressure (kPa)	From Repetition	To Repetitions	Repetitions
60	Dual truck	689.5	1	81,202	81,202
90	Dual truck	689.5	81,203	419,411	338,209
150	Single Aircraft	1,450	419,412	2,208,546	1,789,135

Air temperature and relative humidity during testing of 556FD are shown in Figure 6.6. Extreme environmental conditions for 556FD are summarized in Table 6.2. The environmental conditions during this test can be summarized as warm and continuously dry. Only 6 days out of the total 137 testing days had measurable rainfall. Mid-slab temperatures and slab temperature gradients are summarized in Figure 6.7 and Figure 6.8, respectively.

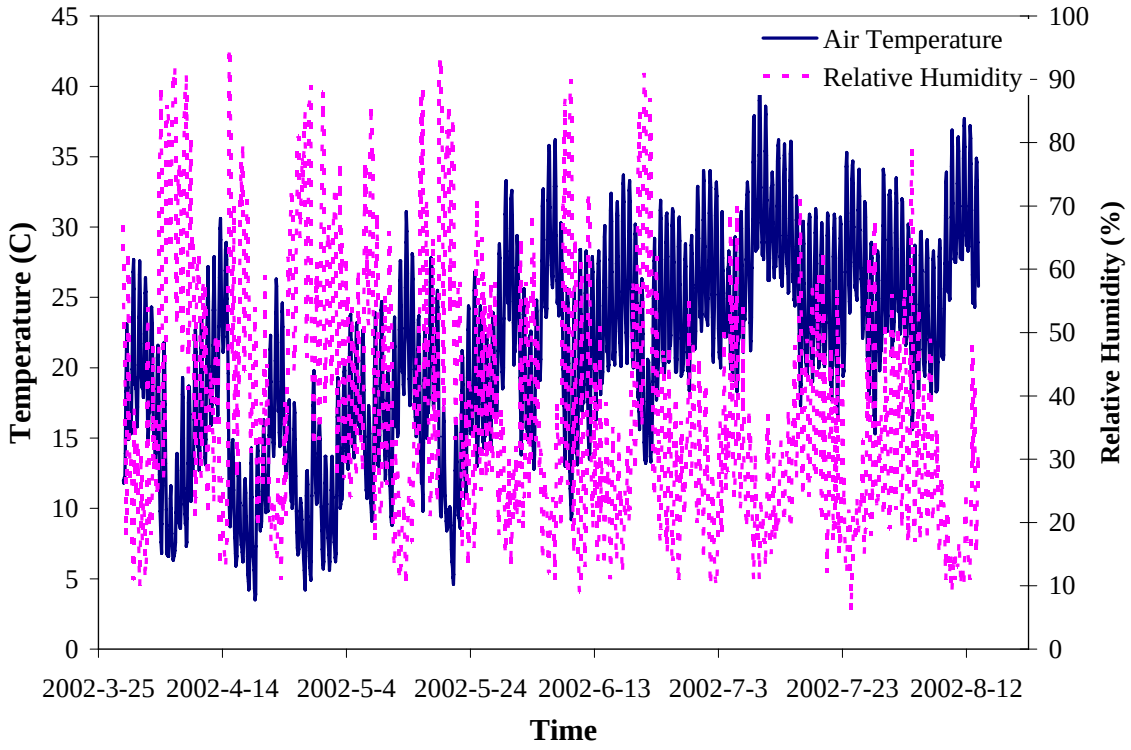

Figure 6.6. Air Temperature and relative humidity on Section 556FD during HVS testing.

Table 6.2. Extreme Environmental Conditions During HVS Testing of Section 556FD

	Air Temperature (°C)	Rainfall (mm)	Relative Humidity (%)
Maximum	41.1	1.52	95
Minimum	3.5	0	6
Average	20.9	0.002139 (6 days over the course of the test)	37.25

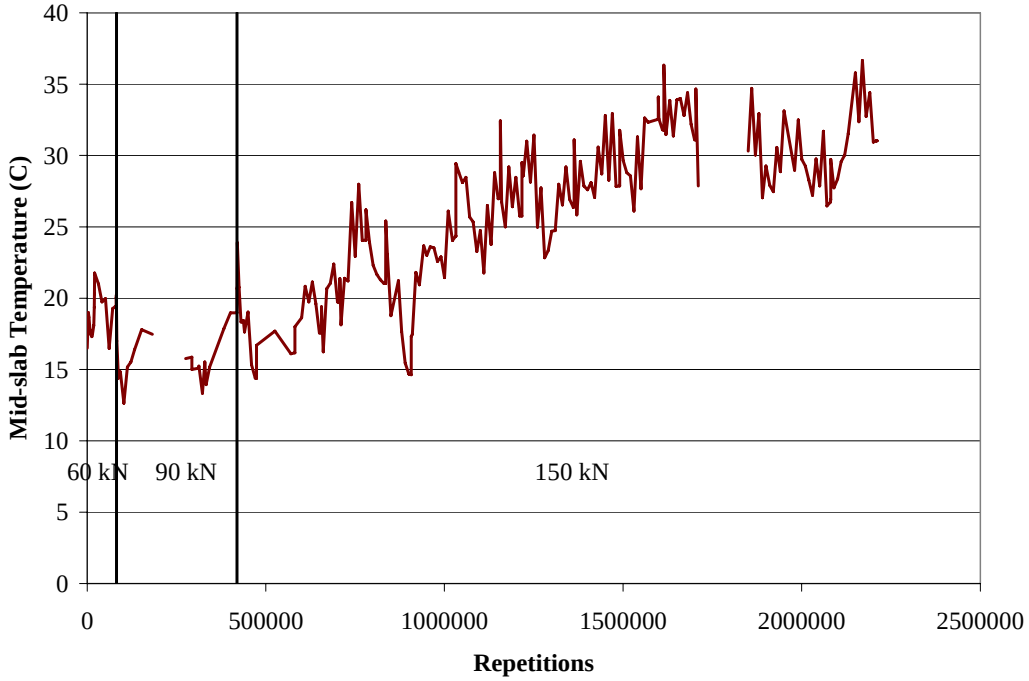

Figure 6.7. Mid-slab temperatures for HVS Test Section 556FD.

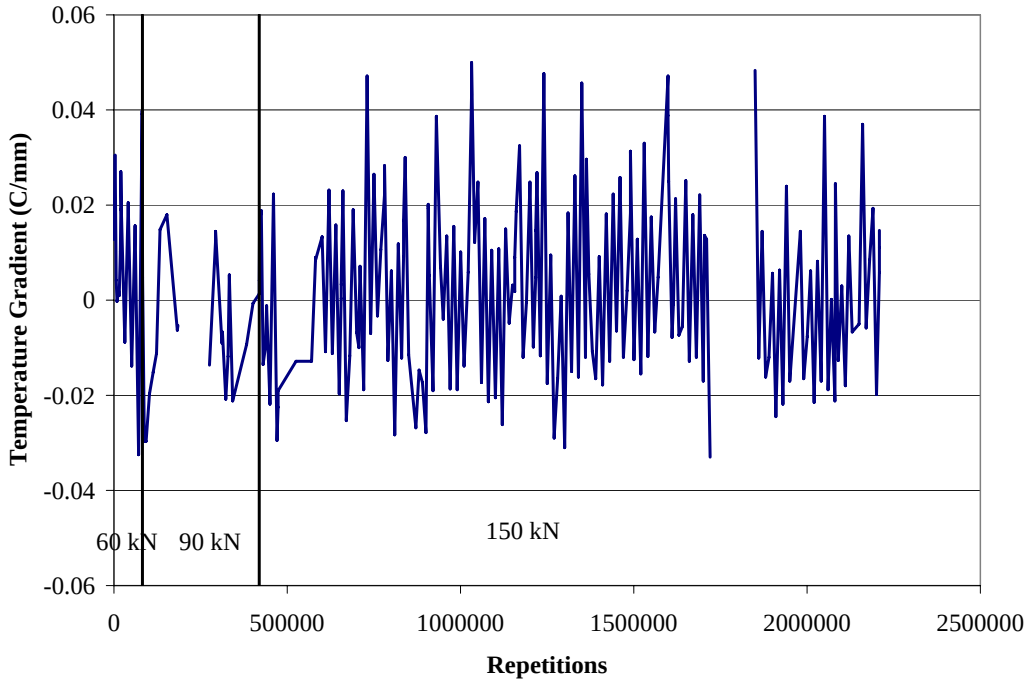

Figure 6.8. Slab temperature gradient for HVS Test Section 556FD.

6.1.3.1 Joint Maximum Deflections

Maximum JDMD deflections at the joints for all the repetitions and mid-slab temperatures for Section 556FD are shown in Figure 6.9 under the trafficking load (60, 90, or 150 kN). Maximum joint deflections with measuring load loads of 60 kN are shown in Figure 6.10.

From Figure 6.9, the vertical deflections (JDMD 1, 2, 4, and 5) under 90 kN and 150 kN loads are obviously higher than those under 60 kN loads. However, from Figure 6.10 it can be seen that when an identical measuring load of 60 kN was applied, the vertical deflections after repetitions with trafficking load of 90 kN and 150 kN are also considerably higher than the earlier deflections under 60 kN trafficking loads, indicating some damage from the trafficking. Under the same wheel loads, the joints exhibited greater vertical deflections with lower mid-slab temperature. It is observed that the JDMD peak deflection is dependent on mid-slab temperature instead of slab temperature gradient, so mid-slab temperature for this test section is also shown in Figure 6.9 and Figure 6.10.

From both Figure 6.9 and Figure 6.10, the horizontal deflections (JDMD 6) remain fairly constant throughout the whole HVS test. Vertical deflections midway along the longitudinal edge of the slab (JDMD 3) follow the same trend with the other vertical deflections at the transverse joints, and they also change with fluctuating mid-slab temperature: they increase with lower temperature and decrease with higher temperature.

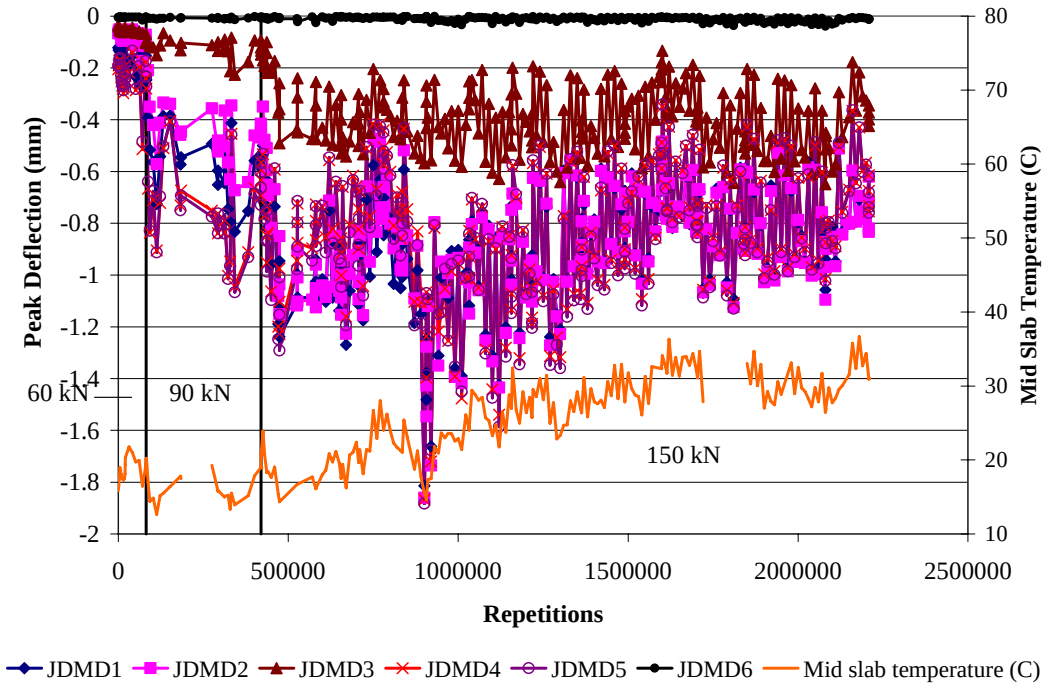

Figure 6.9. Maximum joint deflections under HVS trafficking load on Section 556FD.

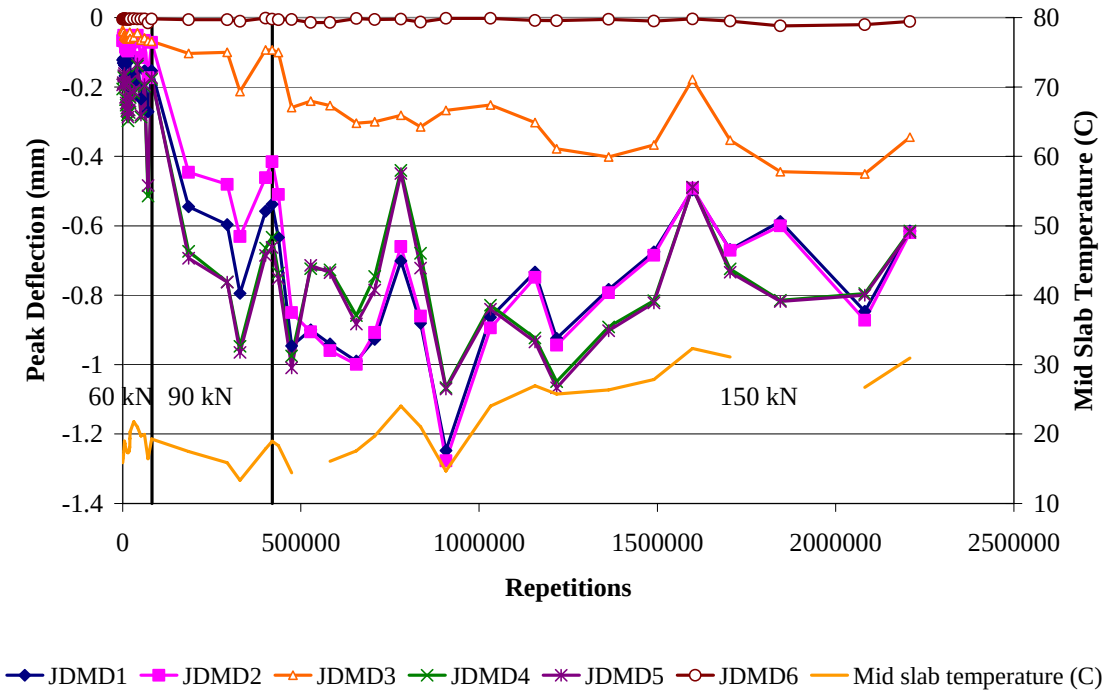

Figure 6.10. Maximum joint deflections under HVS loading with measurement load of 60 kN on Section 556FD.

6.1.3.2 Vertical Joint Deflections vs. Mid-Slab Temperatures

The vertical deflections against the corresponding mid-slab temperature are shown in Figure 6.11 through Figure 6.14. Only deflections obtained under the measuring load of 60 kN are included in these figures. From the figures it can be concluded that in general, vertical deflection decreases with increased temperature, reflecting increased aggregate interlock as the slabs expand and the joint faces come closer or even go into compression. From repetitions 23 to 81,202 (with wheel load of 60 kN), the relationship between vertical deflections and measured mid-slab temperatures can be roughly regressed by a straight line. With similar mid-slab temperatures, the vertical deflections after many more repetitions with higher wheel loads are significantly higher than those under a wheel load of 60 kN. This indicates that the joints had some damage after these HVS wheel repetitions.

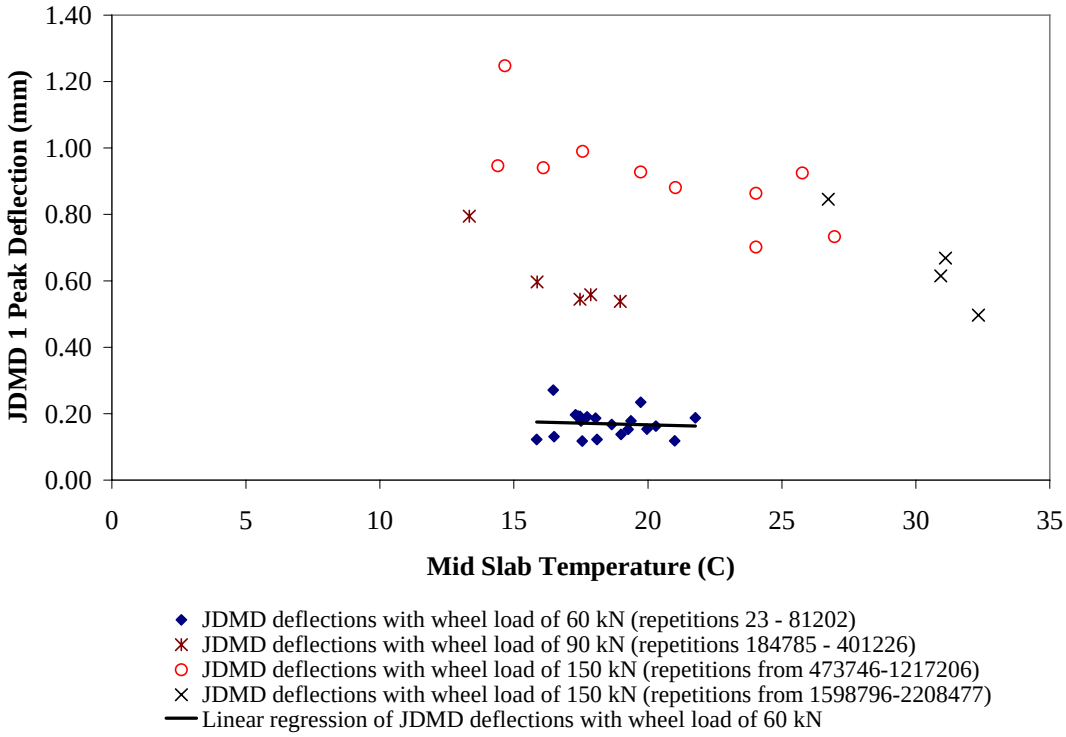

Figure 6.11. JDMD 1 Peak Deflection vs. mid-slab temperature on Section 556FD under measuring load of 60 kN (Joint 39, epoxy-coated steel dowel, 4/wheelpath).

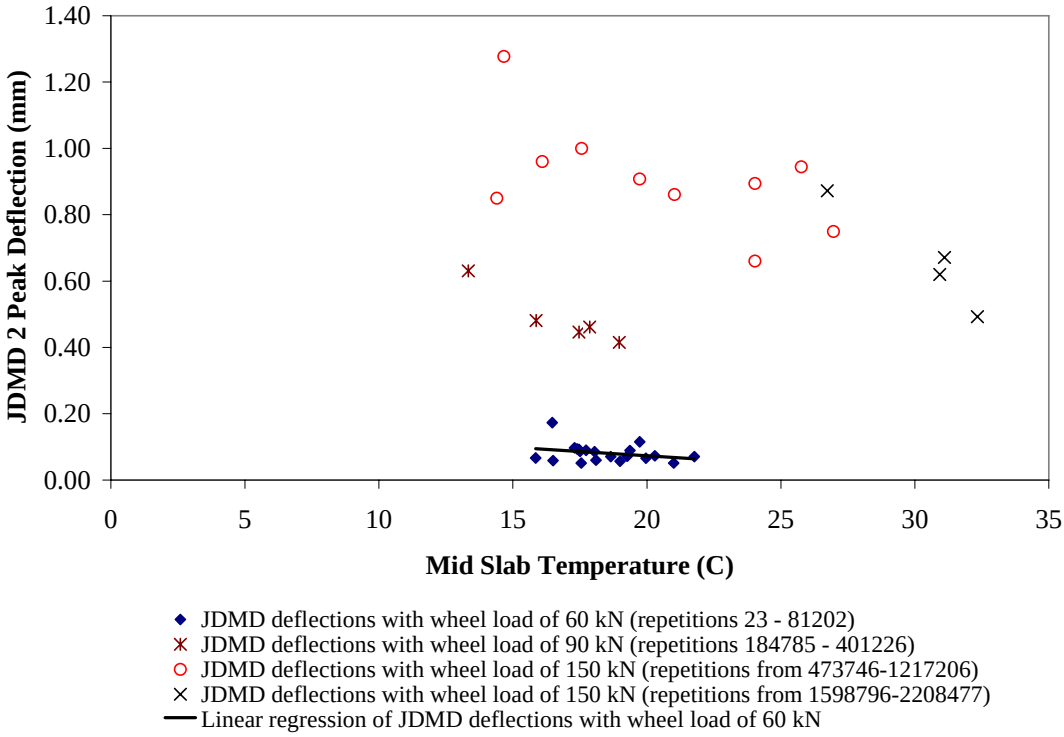

Figure 6.12. JDMD 2 Peak deflection vs. mid-slab temperature on Section 556FD under measuring load of 60 kN (Joint 39, epoxy-coated steel dowel, 4/wheelpath).

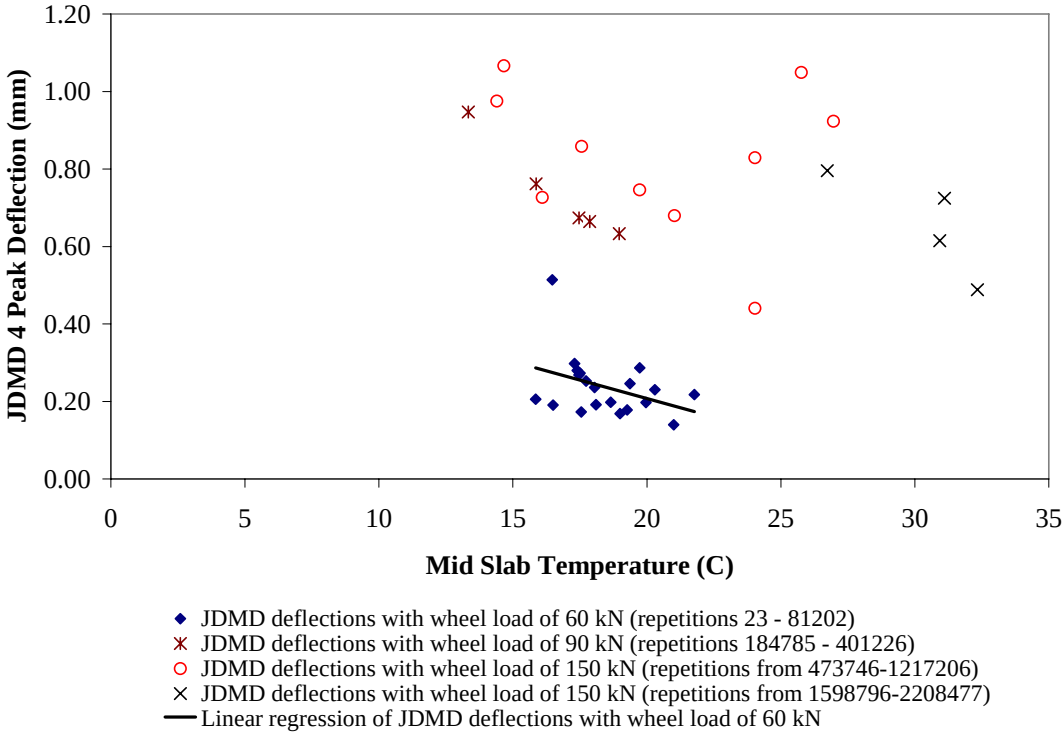

Figure 6.13. JDMD 4 peak deflection vs. mid-slab temperature on Section 556FD under measuring load of 60 kN (Joint 38, epoxy-coated steel dowel, 4/wheelpath).

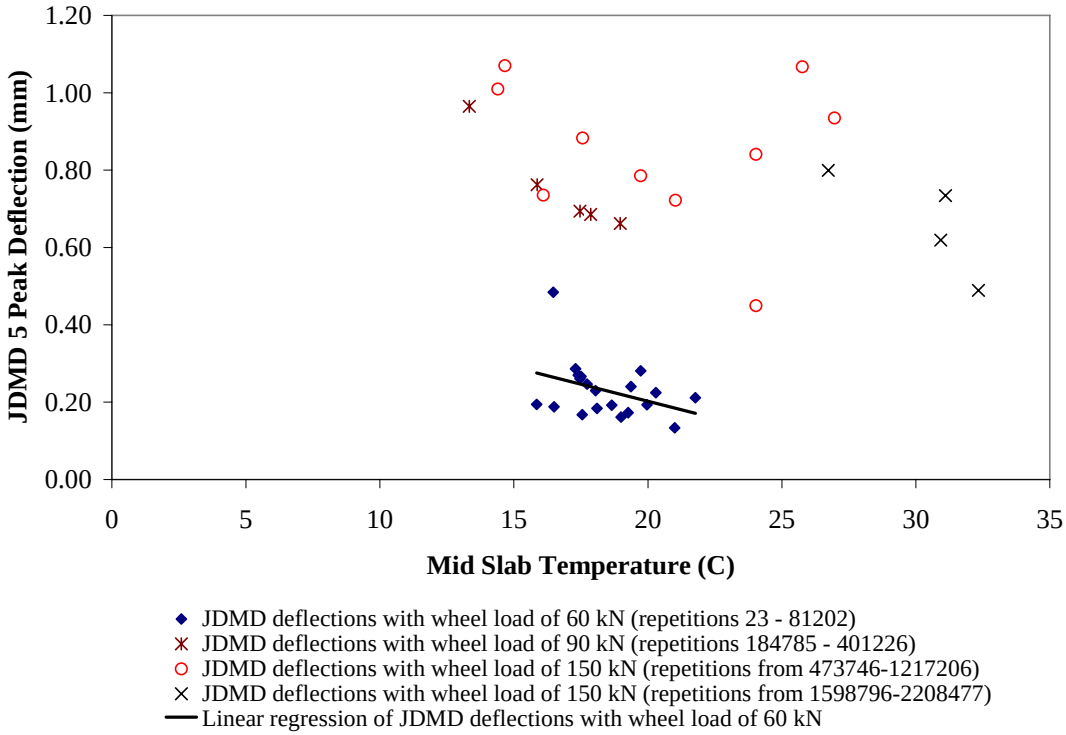

Figure 6.14. JDMD 5 Peak deflection vs. mid-slab temperature on Section 556FD under measuring load of 60 kN (Joint 38, epoxy-coated steel dowel, 4/wheelpath).

6.1.3.3 Load Transfer Efficiency

Load transfer efficiency (LTE) for all the repetitions and mid-slab temperatures for Section 556FD are shown in Figure 6.15 under the trafficking loads. LTEs with measuring load of 60 kN load are shown in Figure 6.16. From the figures, it appears that joint LTE increases with temperature; however, it doesn't change much with HVS wheel load and HVS repetitions. For all the measured data, joint LTEs for Section 556FD are always higher than 95 percent. This LTE value is considerably higher than that obtained from FWD tests. However, this could be due to the different LTE definitions employed by HVS testing and FWD testing and the different loads.

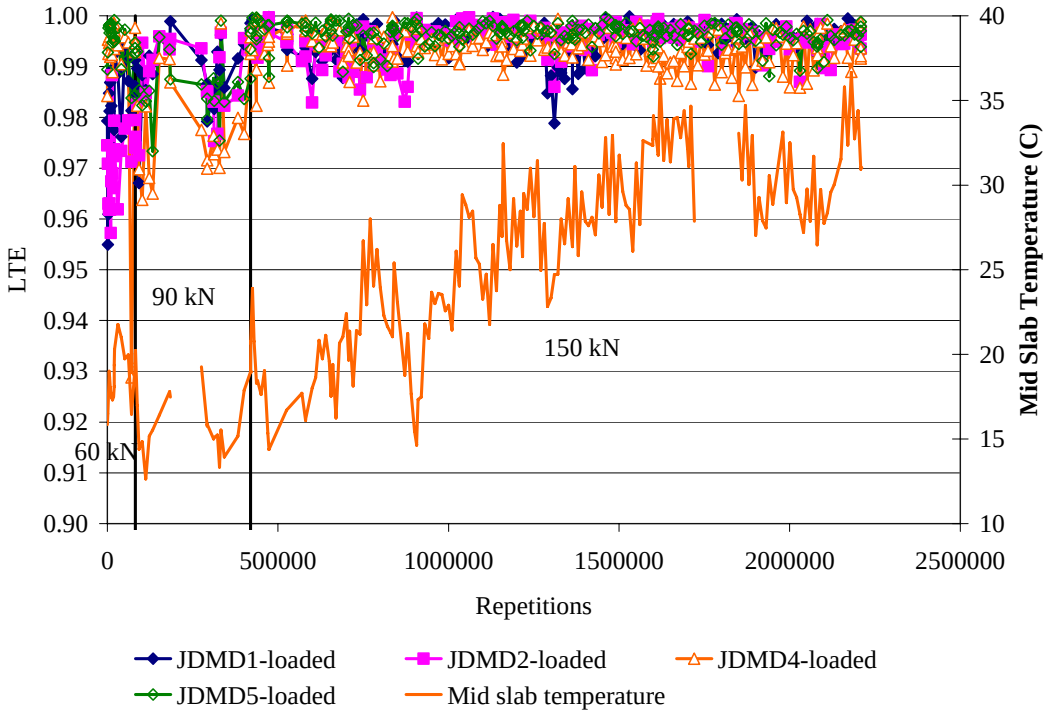

Figure 6.15. LTE under HVS trafficking load on Section 556FD.

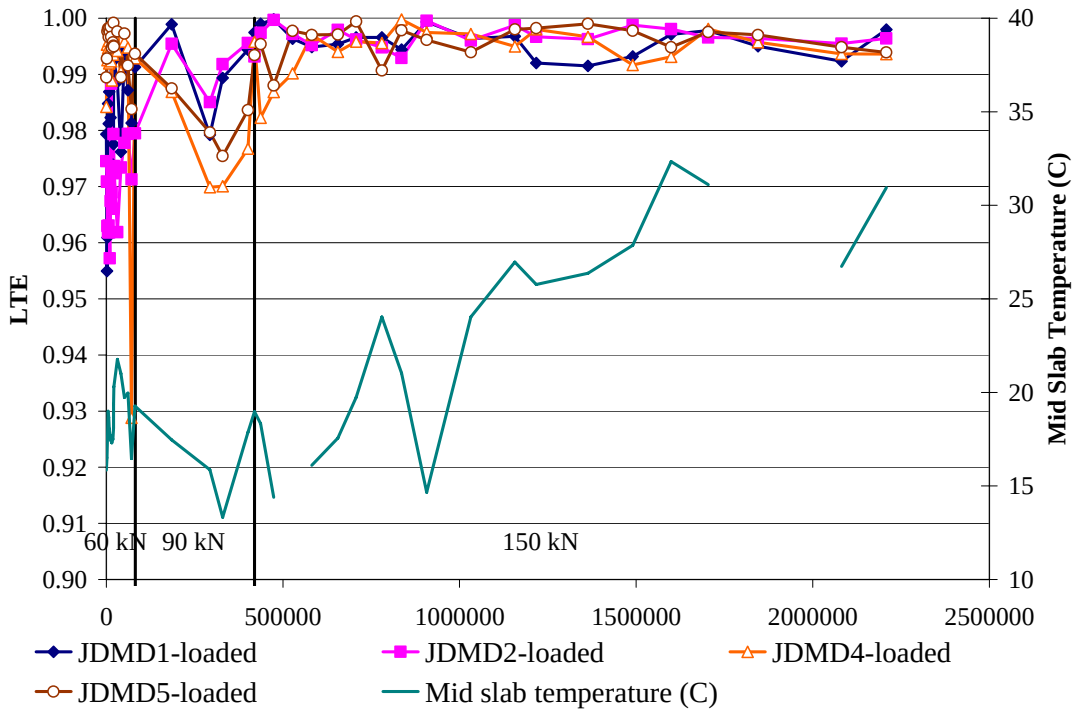

Figure 6.16. LTE under HVS loading with measuring load of 60 kN on Section 556FD.

6.1.3.4 LTE vs. Mid-Slab Temperatures

The joint LTE against the corresponding mid-slab temperature are shown in Figure 6.17 through Figure 6.20. Only LTEs obtained under the measuring load of 60 kN are included in these figures. From the figures, it appears that joints show higher LTE values when temperature increases. However, for the data measured from repetitions 23 to 81,202 (with measuring load of 60 kN), the relationship between LTE and mid-slab temperature is not so linearly well-defined as that between peak joint vertical deflection and temperature. Also, although it was stated in Section 6.1.3.1 that the joint vertical deflections increased considerably after HVS load repetitions, it can be observed from Figure 6.17 through Figure 6.20 that such repetitions didn't reduce the joint LTE much. From these results, it can be concluded that after numerous load repetitions, the vertical deflections on both sides of the joint increased together. The high LTE throughout the HVS test is the consequence of dowel bar retrofitting of the joints.

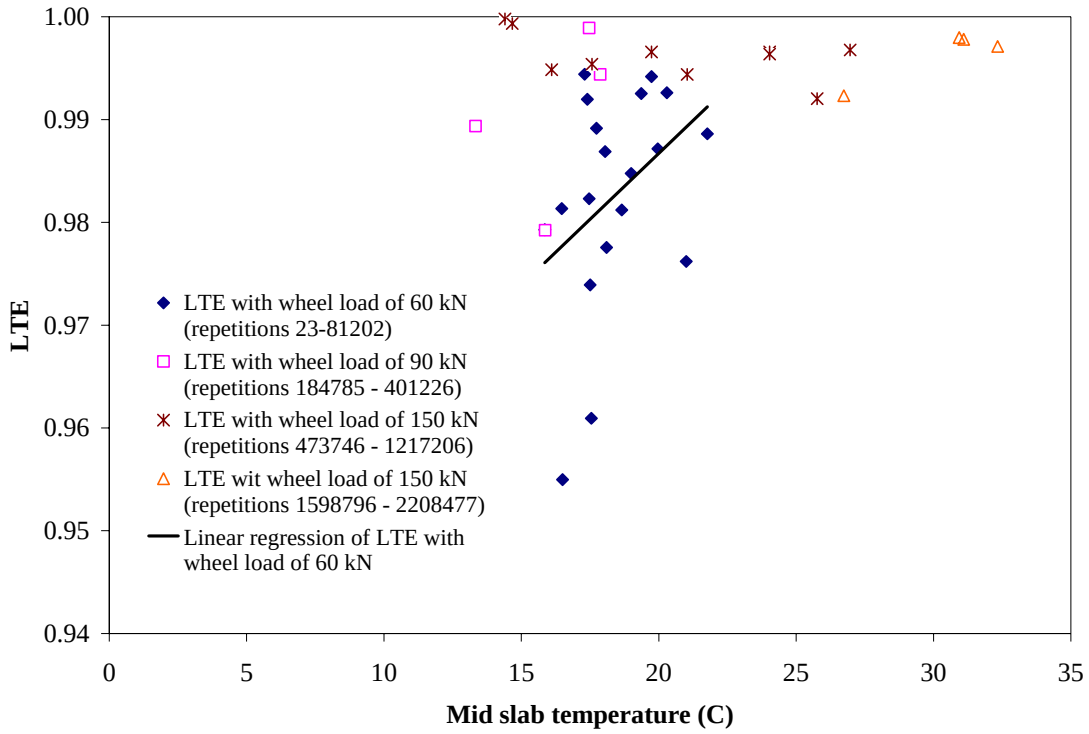

Figure 6.17. JDMD 1 LTE vs. mid-slab temperature on Section 556FD (with measuring load of 60 kN; Joint 39, epoxy-coated steel dowel, 4/wheelpath).

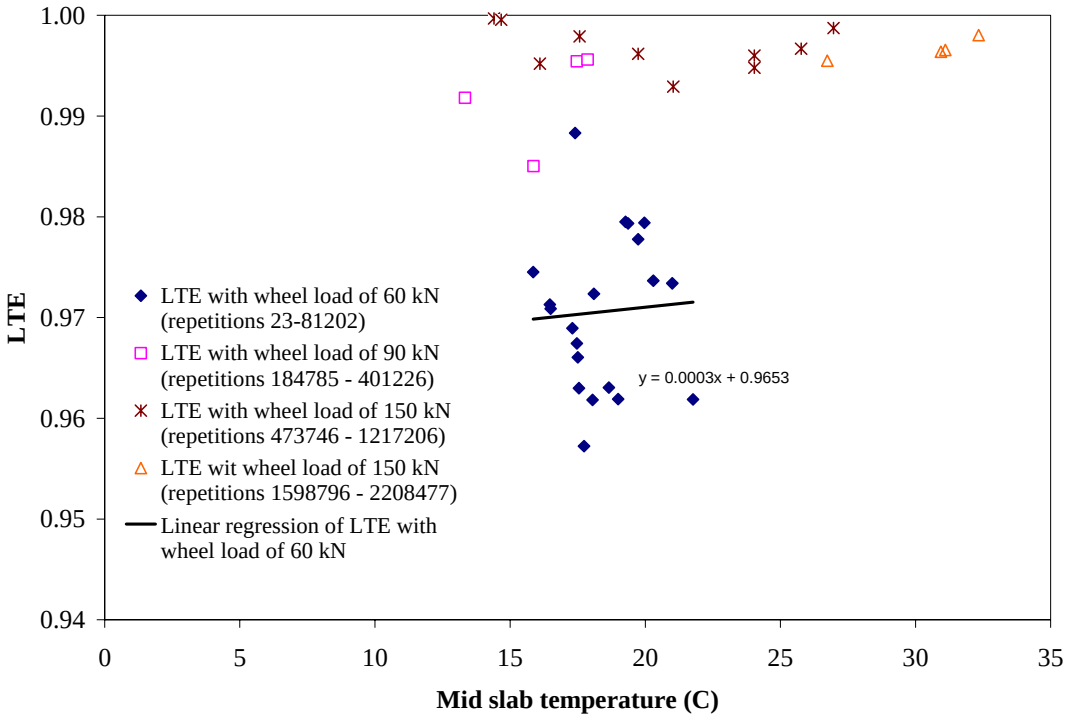

Figure 6.18. JDMD 2 LTE vs. mid-slab temperature on Section 556FD (with measuring load of 60 kN; Joint 39, epoxy-coated steel dowel, 4/wheelpath).

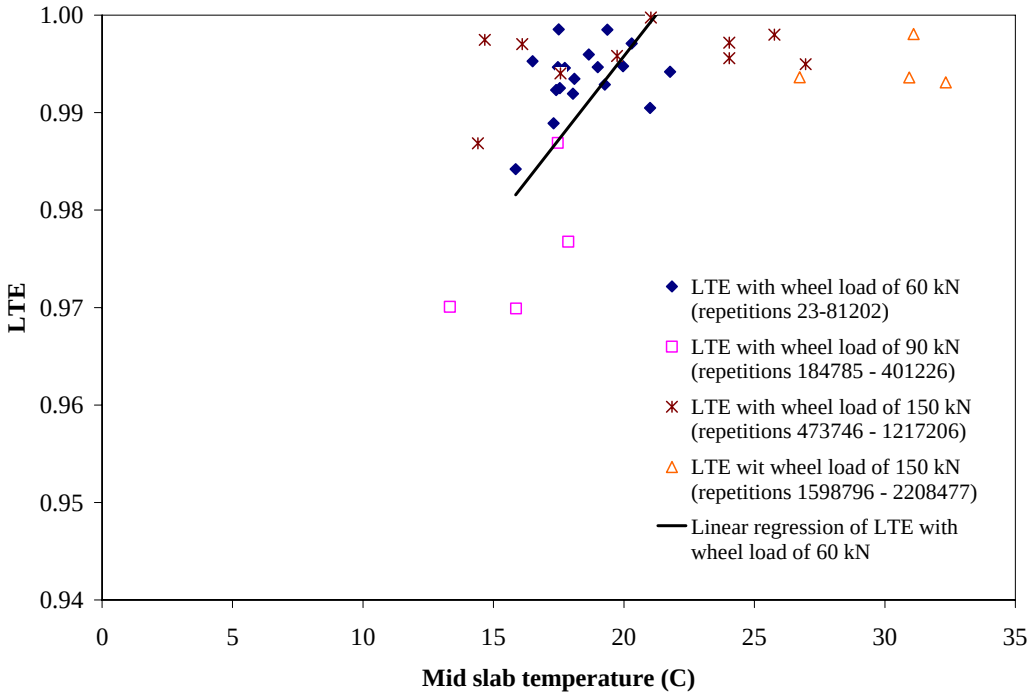

Figure 6.19. JDMD 4 LTE vs. mid-slab temperature on Section 556FD with measuring load of 60 kN (Joint 38, epoxy-coated steel dowel, 4/wheelpath).

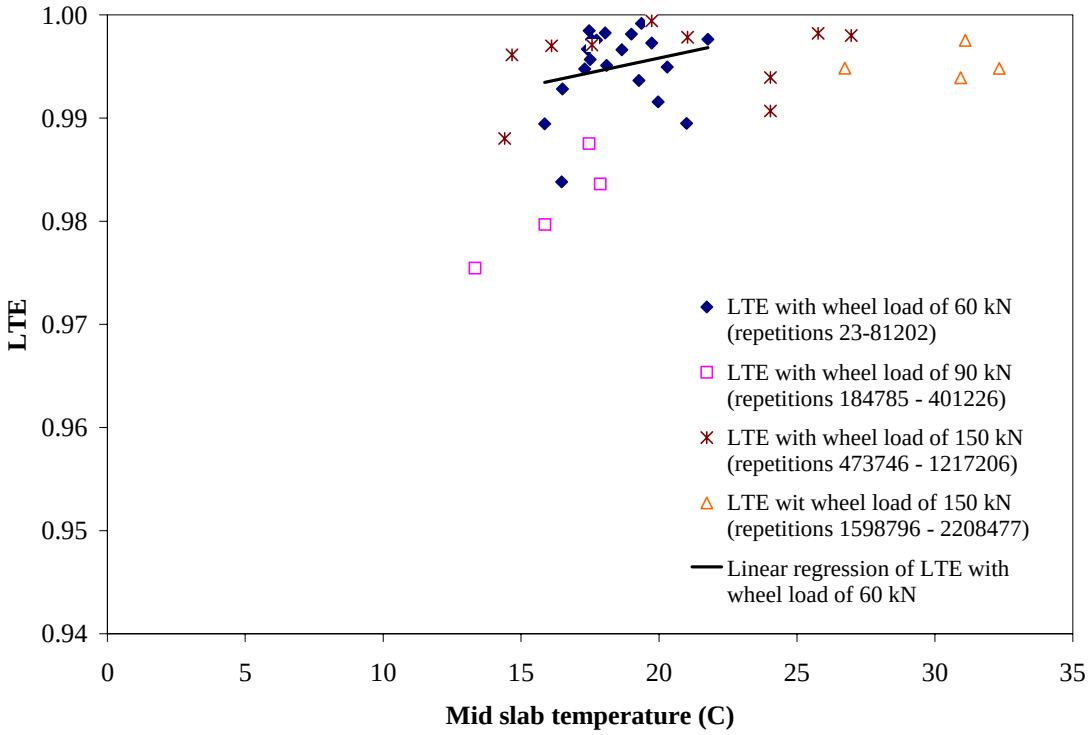

Figure 6.20. JDMD 5 LTE vs. mid-slab temperature on Section 556FD with measuring load of 60 kN (Joint 38, epoxy-coated steel dowel, 4/wheelpath).

6.1.3.5 Slab Cracking and Final Condition

The initial condition of Section 556FD is shown in Figure 6.21. The existing cracks in Slabs 38 and 40, the slabs on either end of the center slab, can be seen in the photograph. Figure 6.22 shows the transverse crack that appeared on the surface of Slab 40 at the end of the wheelpath after 1.291 million load repetitions. Figure 6.23 shows the transverse crack that appeared on the surface of the center slab (Slab 39) after 1.759 million repetitions, indicating fatigue failure of the concrete slab. Figure 6.24 shows propagation of the transverse crack towards the transverse joint with additional loading to 2.064 million repetitions. This turning of the transverse crack towards the joint with additional propagation occurred on all other prior HVS test sections at Palmdale and is due to the use of a half axle as opposed to a full axle (24). The final state of cracking in the section is shown in Figure 6.25, and the final state of Joint 39 is shown in Figure 6.26. Final condition of Slabs 38, 39, and 40 is shown in overhead photos in Appendix B.

Figure 6.21. Initial condition of slabs in Section 556FD with existing cracking in adjacent slabs marked in red.

Figure 6.22. Cracking in Slab 40 at end of wheelpath after approximately 1.291 million repetitions.

Figure 6.23. Cracking in the center slab (Slab 39) after 1.759 million repetitions.

Figure 6.24. Cracking in Slab 39 after 2.066 million repetitions.

Figure 6.25. Cracking in all slabs at end of HVS loading on Section 556FD after 2.209 million repetitions.

Figure 6.26. Close-up of Joint 39 at end of HVS loading after 2.209 million repetitions.

6.1.4 557FD HVS Test

The condition of Section 557FD in March 2002, prior to HVS testing is shown in Figure 6.27. Figure 6.28 shows a close-up of Joint 35 and Figure 6.29 shows a close-up of Joint 36.

JDMD locations and numbering for Section 557FD are shown in Figure 6.30.

Figure 6.27. HVS Test Section 557FD prior to HVS testing.

Figure 6.28. HVS Test Section 557FD, Joint 35, prior to HVS testing.

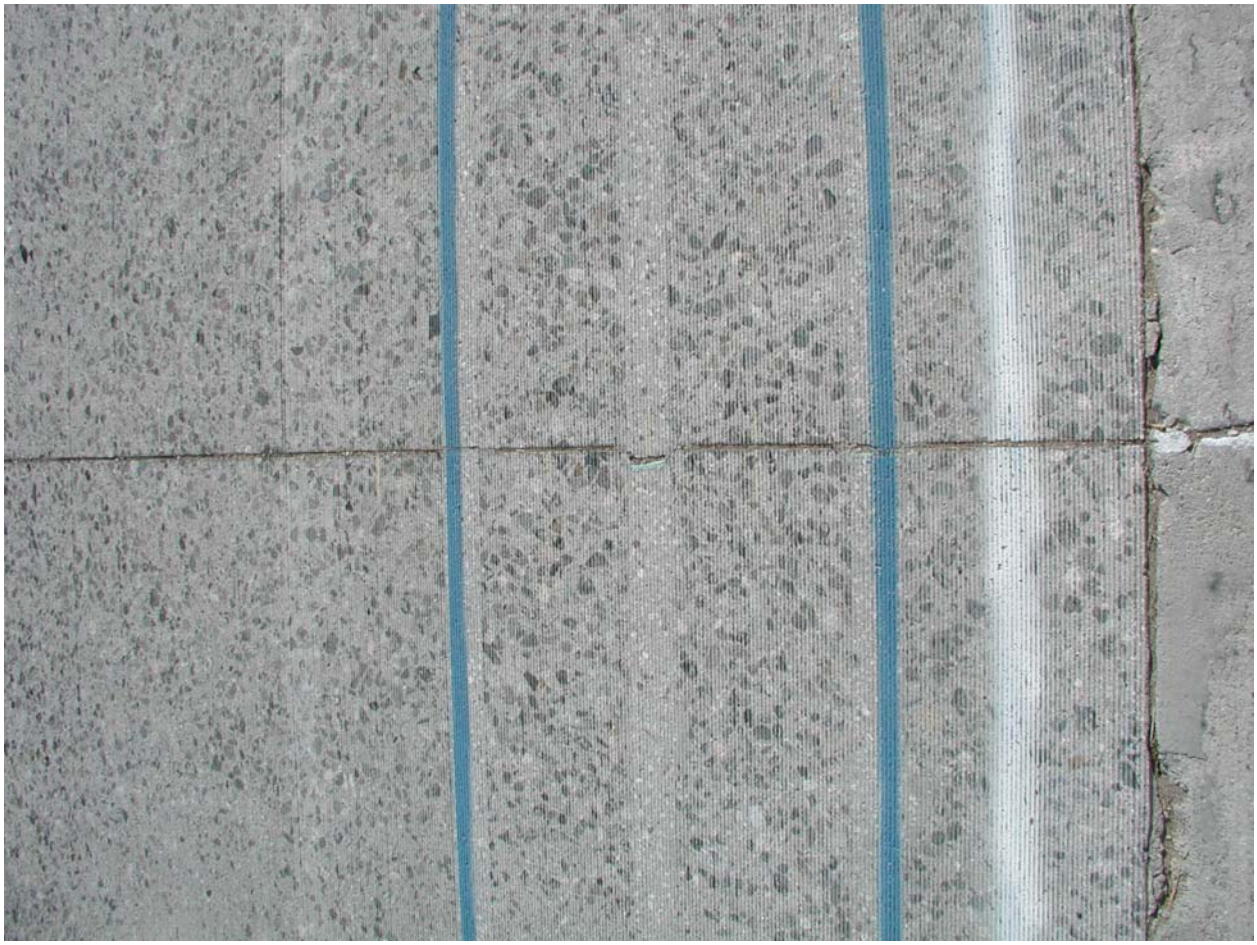

Figure 6.29. HVS Test Section 557FD, Joint 36, prior to HVS testing.

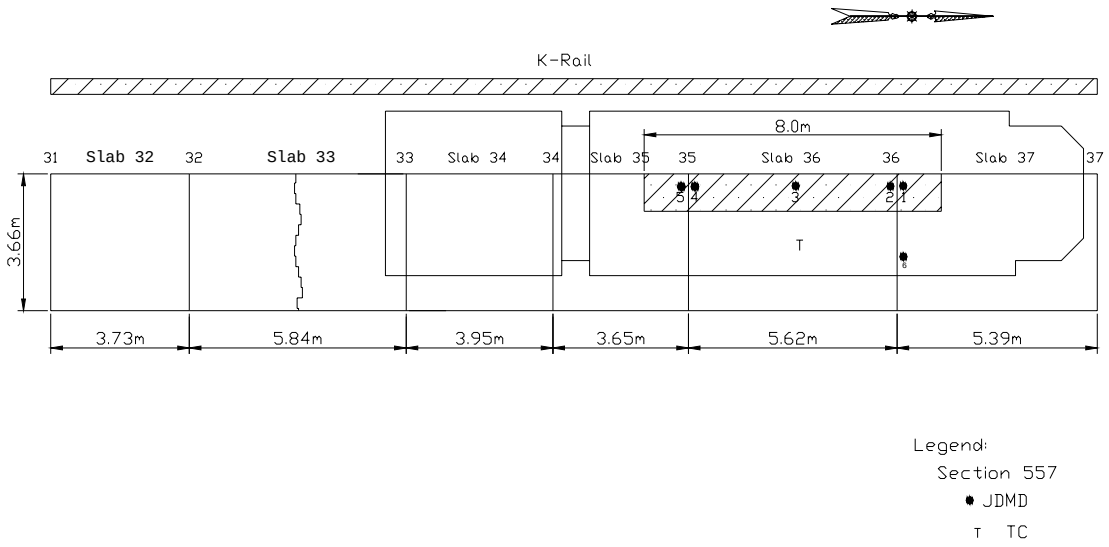

Figure 6.30. JDMD locations and numbering for Section 557FD.

The load history on Section 557FD is shown in Table 6.3. HVS loading on Section 557FD the 60 kN and 90 kN dual tire truck wheel and the 150 kN single aircraft wheel. Similar with HVS 556FD, seven repetitions were periodically taken with the measuring load of 60 kN during trafficking with the wheel load of 150 kN to normalize the influence induced by different loading levels.

Table 6.3. Load history on Section 557FD

Load (kN)	Tire/Wheel Type	Inflation Pressure (kPa)	From Repetition	To Repetitions	Repetitions
60	Dual truck	689.5	1	68,806	68,806
90	Dual truck	689.5	68,807	264,632	195,286
150	Single aircraft	1,450	264,633	1,121,600	856,968

Air temperature and relative humidity during Section 557FD HVS testing are shown in Figure 6.31, and extreme environmental conditions are summarized in Table 6.4. The environmental conditions during this test can be generally described as warm and dry. Only one day out of the sixty-seven testing days had measurable rainfall. Mid-slab temperatures and slab temperature gradients are shown in Figure 6.32 and Figure 6.33. The environmental conditions on Section 557FD are very similar to those on Section 556FD, which was the intention of the test scheduling so that four and three dowels per wheelpath could be compared under roughly similar environmental conditions.

Table 6.4. Extreme Environmental Conditions during HVS Testing of Section 557FD

	Air Temperature (°C)	Rainfall (mm)	Relative Humidity (%)
Maximum	36	0.51	96
Minimum	7.3	0	10
Average	21.5	0.000641 (1 day over the course of the test)	35.44

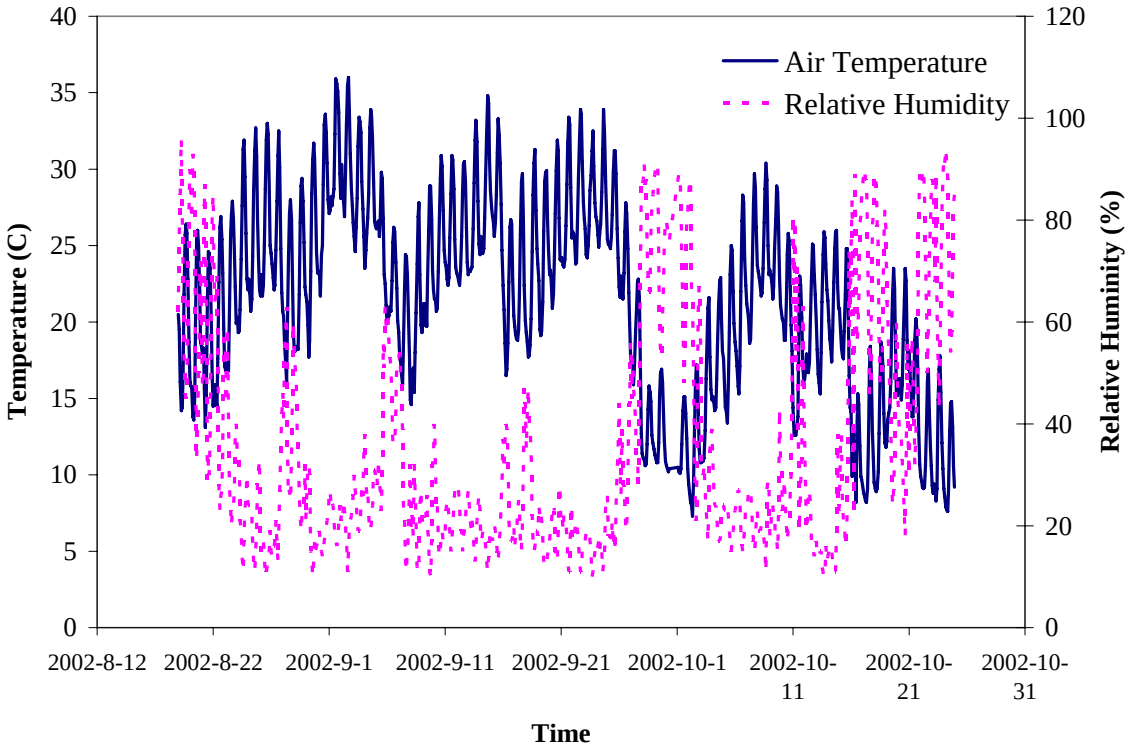

Figure 6.31. Air temperature and relative humidity on Section 557FD during HVS testing.

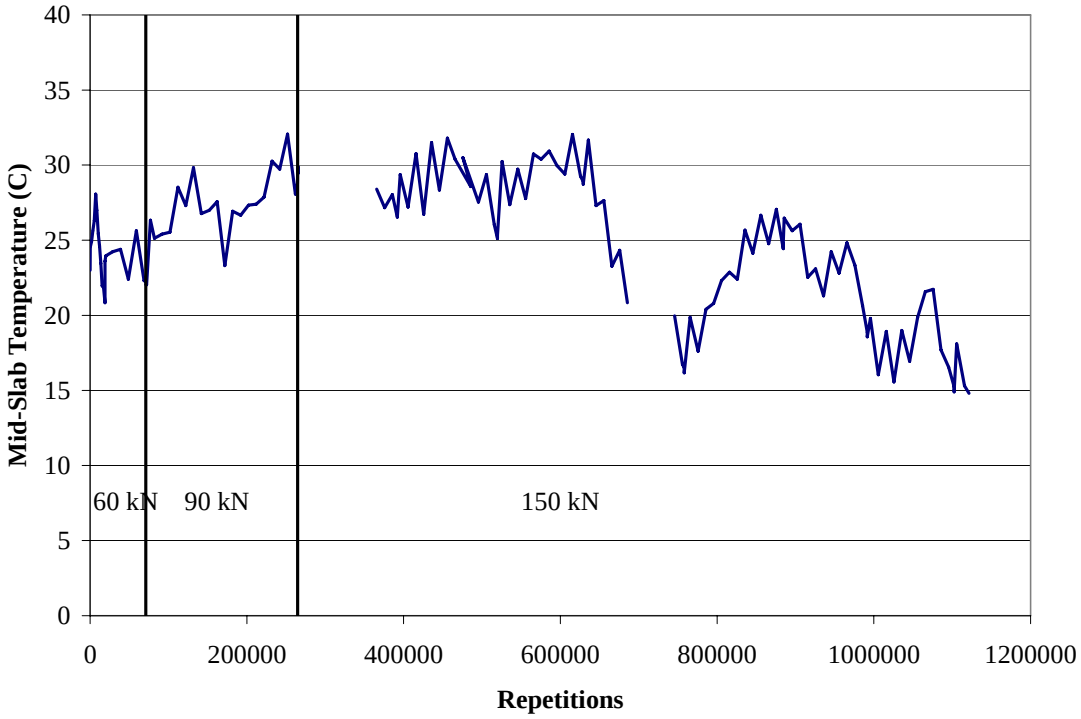

Figure 6.32. Mid-slab temperature for HVS Test Section 557FD.

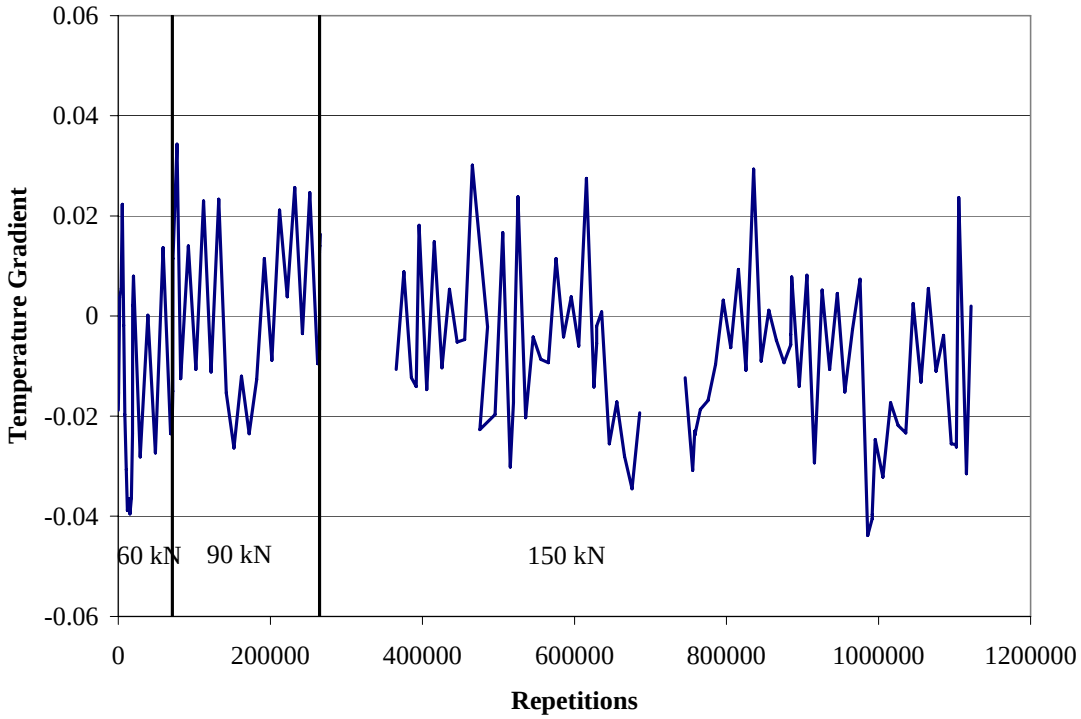

Figure 6.33. Slab temperature gradients for HVS Test Section 557FD.

6.1.4.1 Joint Maximum Deflections

Maximum JDMD deflections for all repetitions together with mid-slab temperatures for Section 557FD are shown in Figure 6.34 under the trafficking load. Maximum JDMD deflections with measurement loads of 60 kN are shown in Figure 6.35.

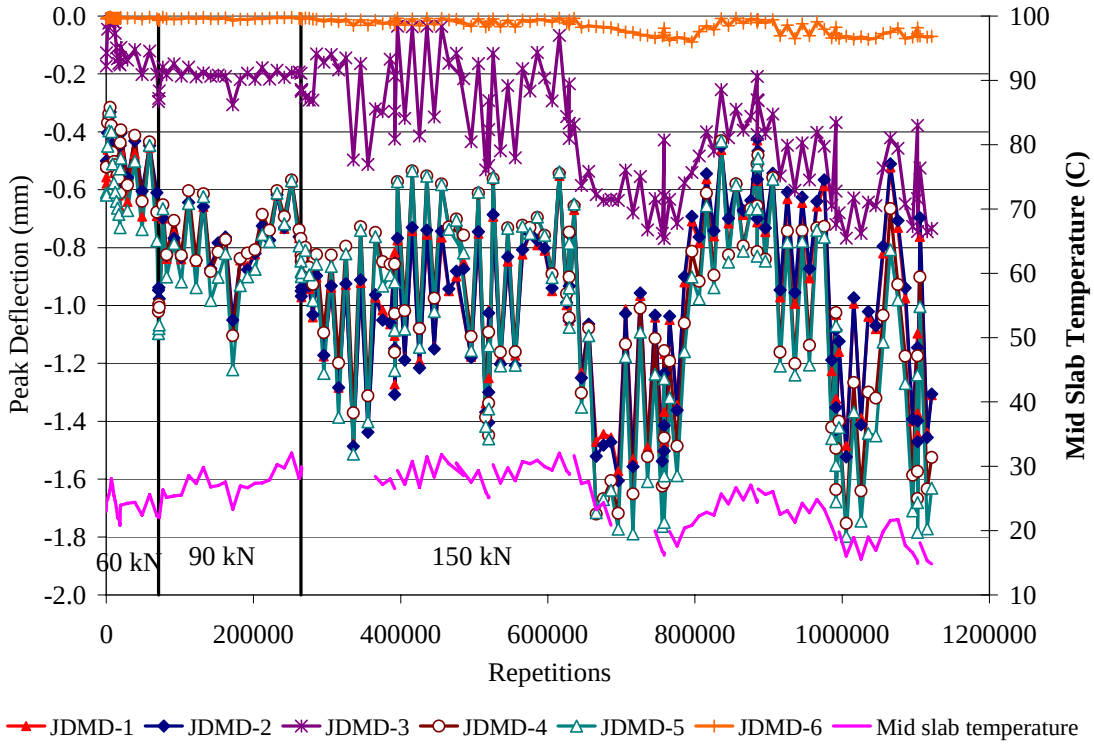

Figure 6.34. Maximum joint deflections under HVS trafficking load on Section 557FD.

It can be seen from Figure 6.34 that the vertical joint deflections (JDMD 1, 2, 4, and 5) under wheel load of 60 kN are much lower than those under 90 and 150 kN. With identical test load of 60 kN, the joint deflections after the wheel load repetitions of 90 kN and 150 kN are still considerably higher than those with wheel load of 60 kN (Figure 6.35) indicating damage to the joint. From both figures it can be seen that vertical joint deflections are higher under lower mid-slab temperatures, as expected.

Compared with vertical joint deflections, the horizontal deflection (JDMD 6) remains quite constant throughout the whole HVS test (Figure 6.34 and Figure 6.35). Vertical deflection midway along the longitudinal edge of the slab (JDMD 3) increases under wheel repetitions of 90 and 150 kN, and it also shows a higher value under lower temperature, likely due to temperature gradient induced upward curling of the pavement edges.

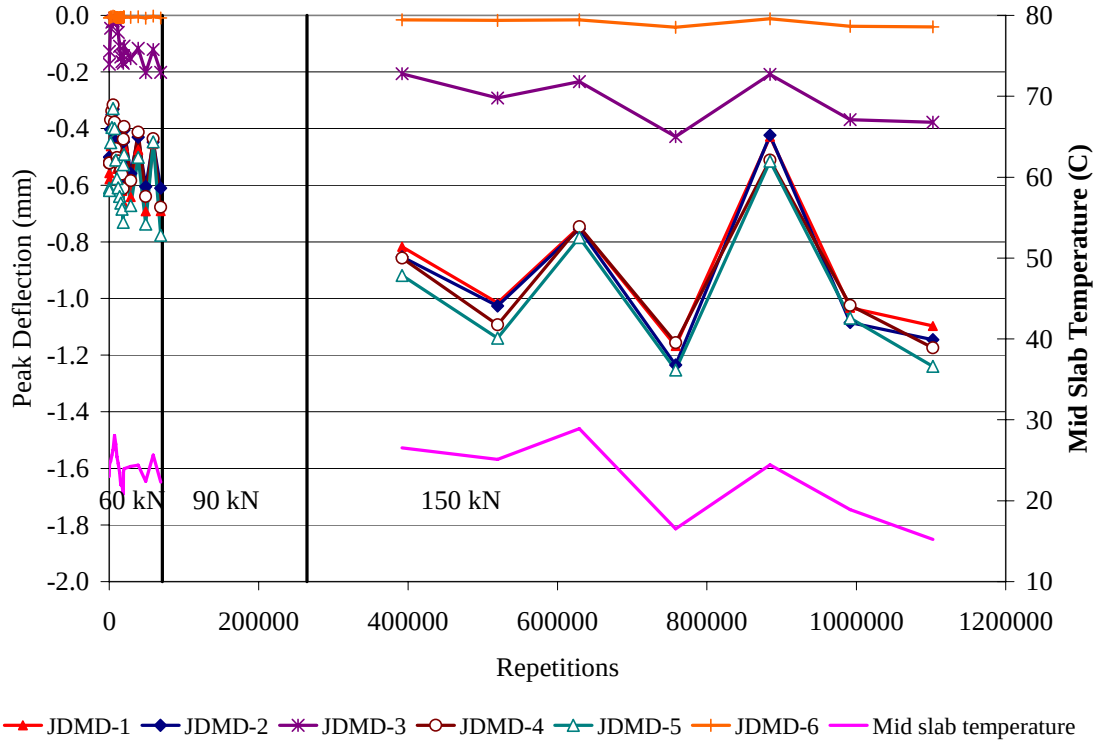

Figure 6.35. Maximum joint deflections with HVS test load of 60 kN on Section 557 FD.

6.1.4.2 Vertical Joint Deflections vs. Mid-Slab Temperature

The vertical deflection against mid-slab temperature is shown in Figure 6.36 through Figure 6.39, and only data obtained under the measuring load of 60 kN are included in these figures. As has been found from Section 556FD, from Figure 6.36 through Figure 6.39, it can be seen that vertical deflection is lower under higher temperature, as expected. From repetitions 32–68,806 (with wheel load of 60 kN), the relationship between vertical deflection and mid-slab temperature can be roughly regressed by a straight line. Within a similar temperature range, the vertical deflections after more repetitions of higher wheel loads are much higher than those from repetitions 32–68,809. This indicates damage to the joint under the HVS repetitions.

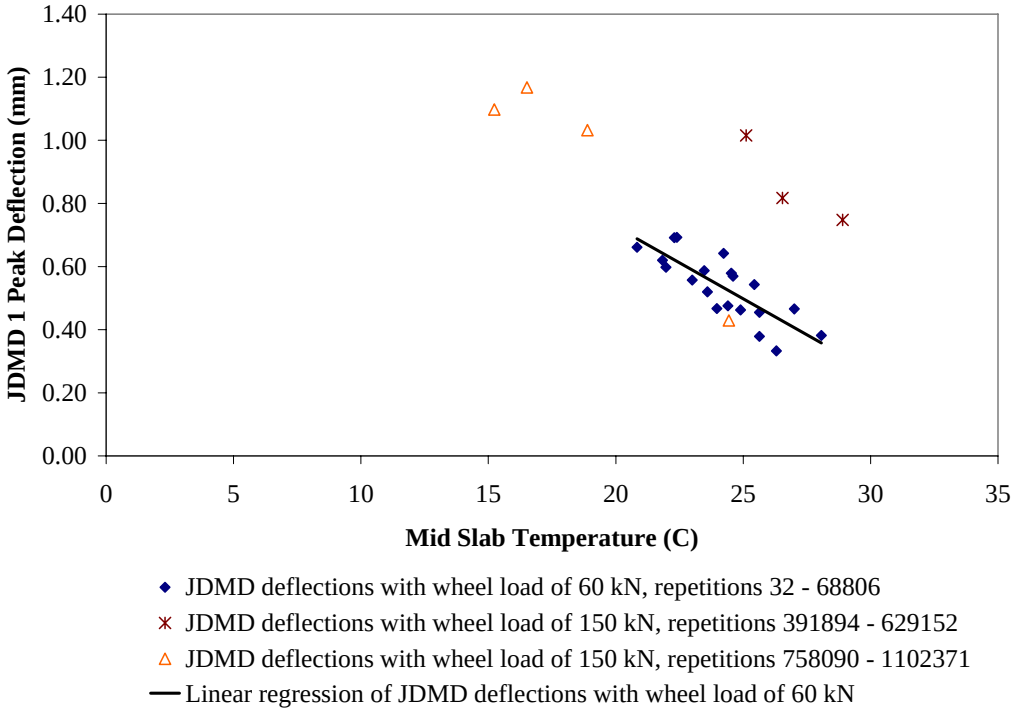

Figure 6.36. JDMD 1 peak deflection vs. mid-slab temperature on Section 557FD with measuring load of 60 kN (Joint 36, epoxy-coated steel dowel, 3/wheelpath).

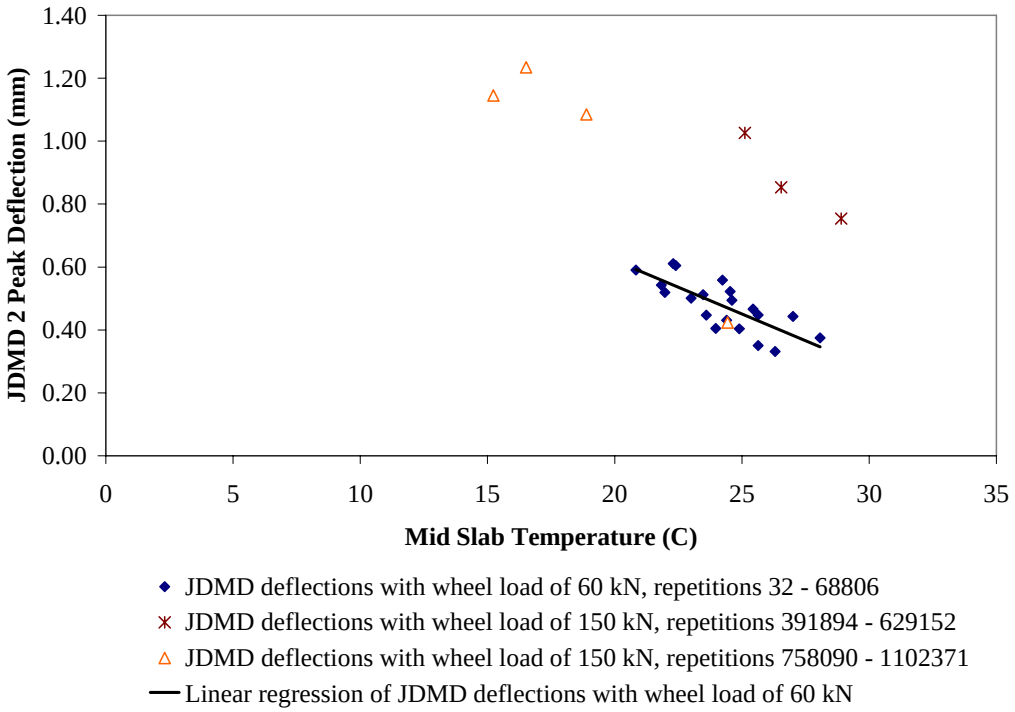

Figure 6.37. JDMD 2 peak deflection vs. mid-slab temperature on Section 557FD with measuring load of 60 kN (Joint 36, epoxy-coated steel dowel, 3/wheelpath).

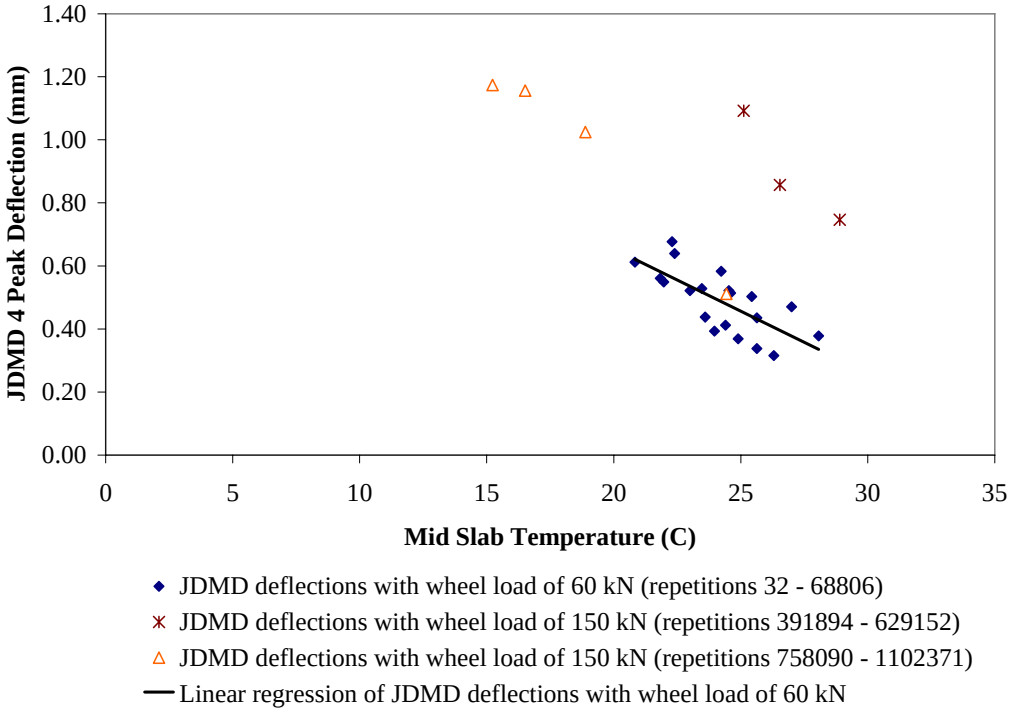

Figure 6.38. JDMD 4 peak deflection vs. mid-slab temperature on Section 557FD with measuring load of 60 kN (Joint 35, epoxy-coated steel dowel, 3/wheelpath).

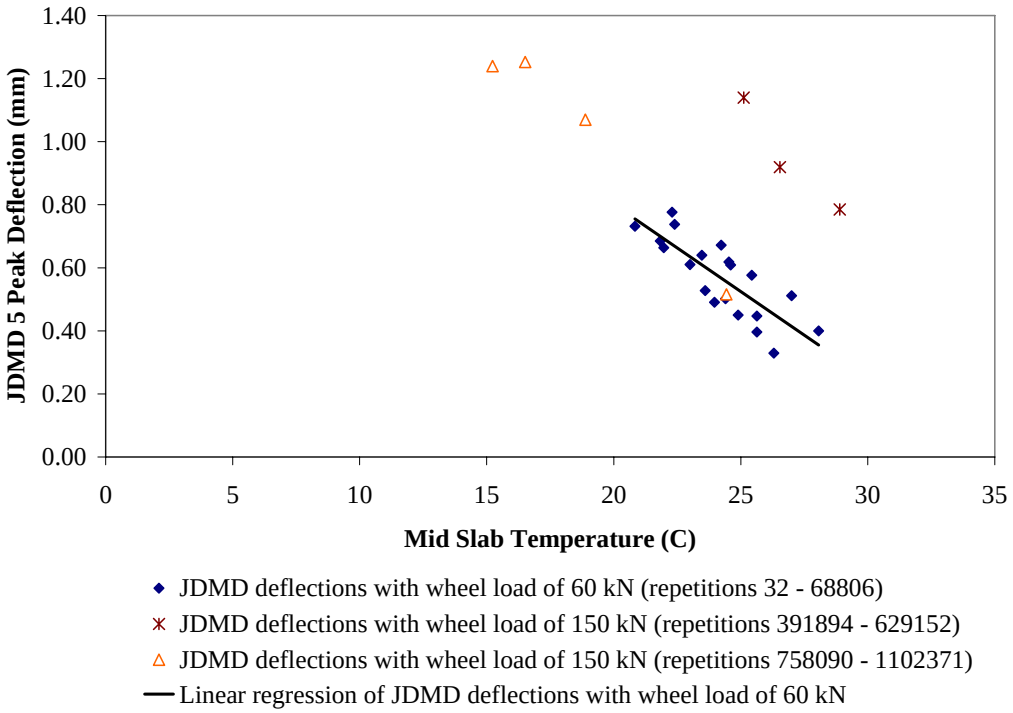

Figure 6.39. JDMD 5 peak deflection vs. mid-slab temperature on Section 557FD with measuring load of 60 kN (Joint 35, epoxy-coated steel dowel, 3/wheelpath).

6.1.4.3 Load Transfer Efficiency

Load transfer efficiency (LTE) for all repetitions together with mid-slab temperature for Section 557FD are shown in Figure 6.40 under the trafficking loads, and LTE with the 60 kN measuring load are shown in Figure 6.41. The LTE for all repetitions shown in Figure 6.40 are higher than 88 percent and the joints show greater LTE values under higher temperature. However, the joint LTEs don't decrease after HVS repetitions. The two joints (Joint 35 and 36, Table 6.1) tested in Section 557FD only have three dowels per wheelpath, and the measured LTEs are generally lower than those obtained from Section 556FD. Detailed comparison among LTE from different HVS test sections will be described in Chapter 7 of this report.

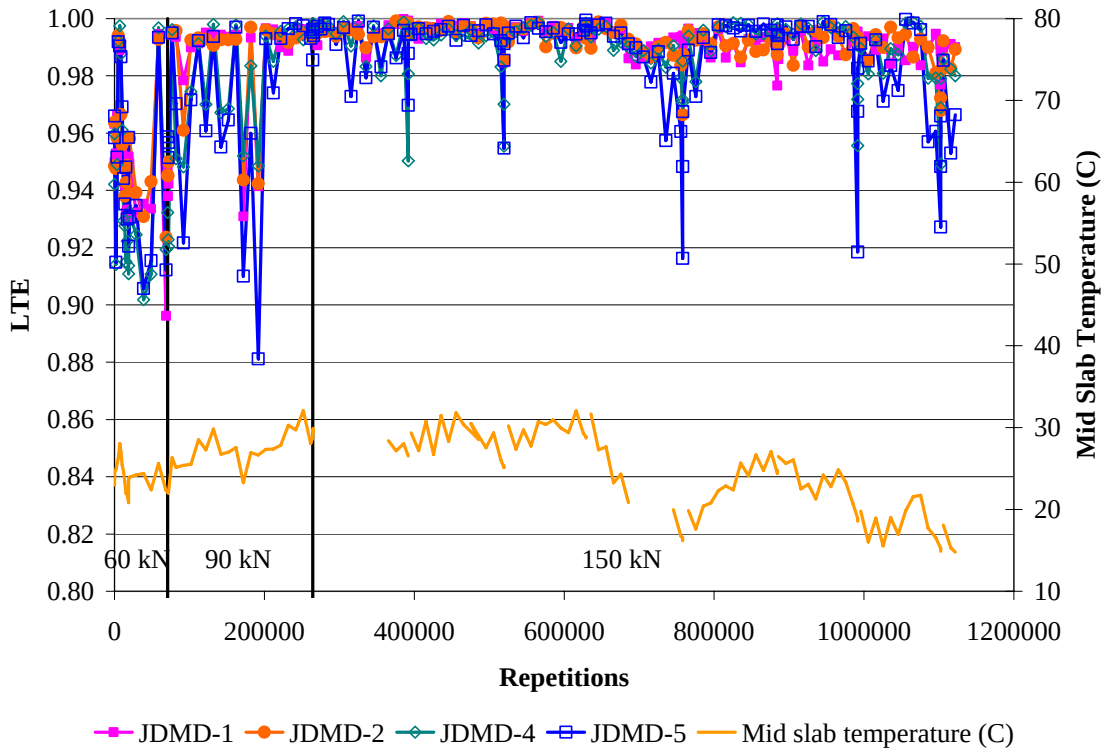

Figure 6.40. LTE under HVS trafficking load on Section 557FD.

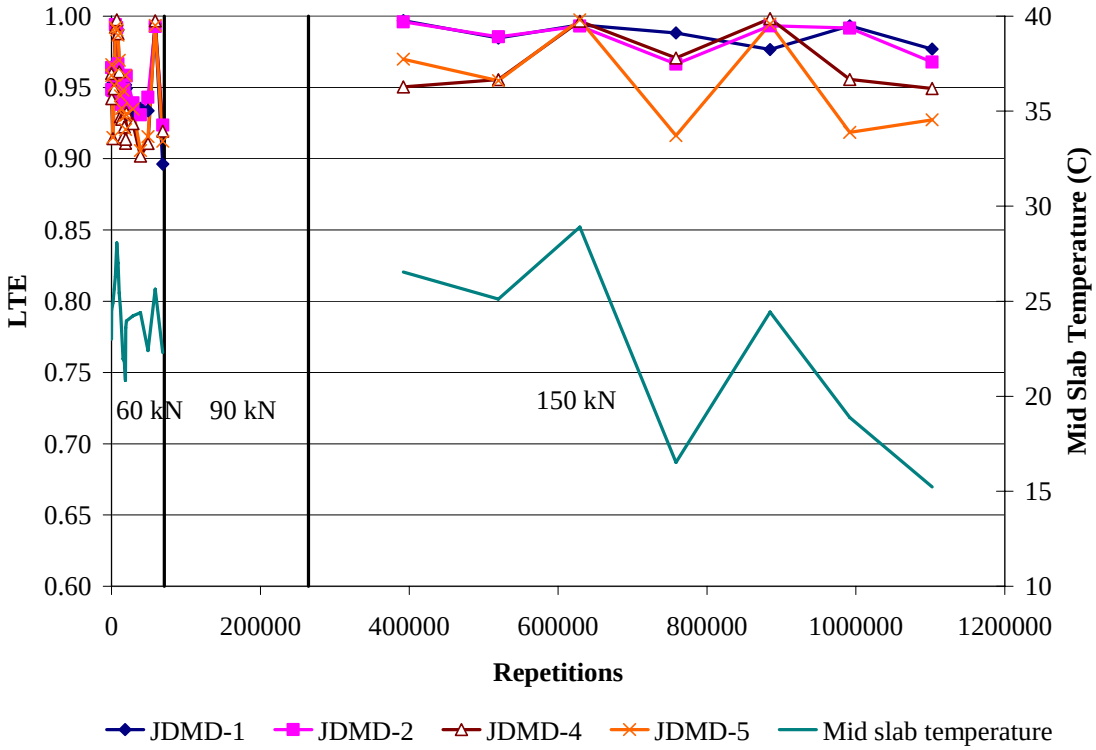

Figure 6.41. LTE under HVS loading with test load of 60 kN on Section 557FD.

6.1.4.4 LTE vs. Mid-Slab Temperature

The joint LTE against the corresponding mid-slab temperature are shown in Figure 6.42 to Figure 6.45. Only LTEs obtained under the measuring load of 60 kN are included in these four figures. The conclusions drawn from Figure 6.42 to Figure 6.45 are similar to those from Figure 6.17 through Figure 6.20 (Section 556FD): the joint LTE show almost no decrease under HVS load repetitions.

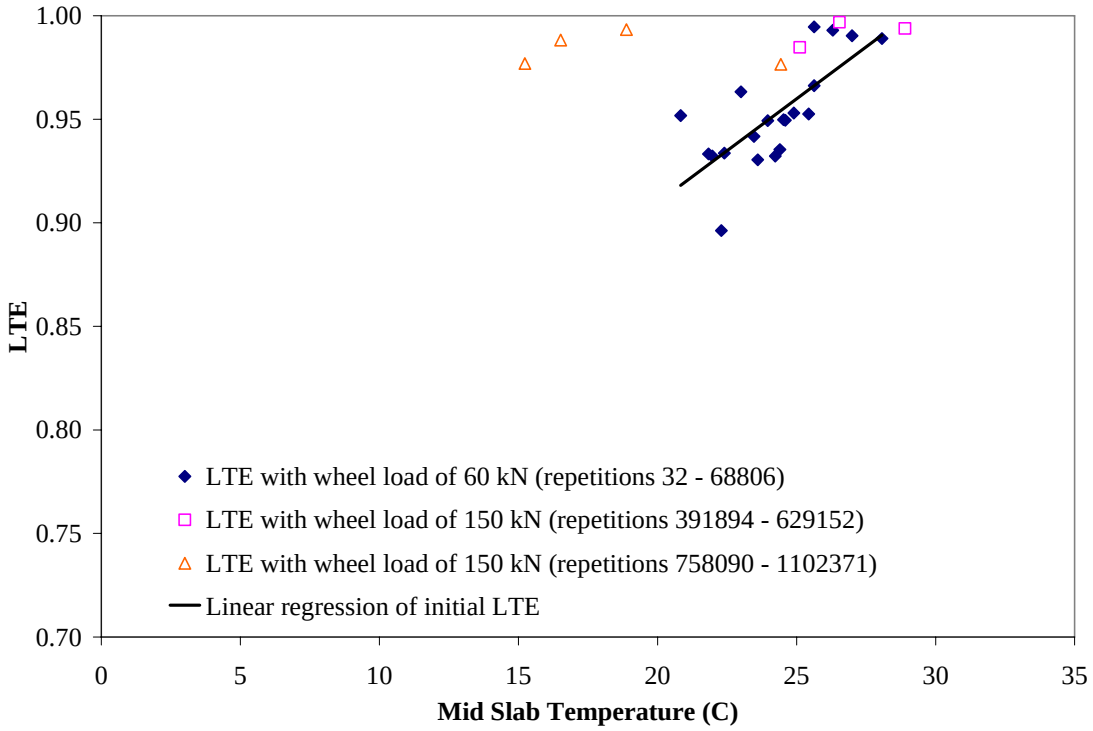

Figure 6.42. JDMD 1 LTE vs. mid-slab temperature on Section 557FD (with measuring load of 60 kN; Joint 36, epoxy-coated steel dowel, 3/wheelpath).

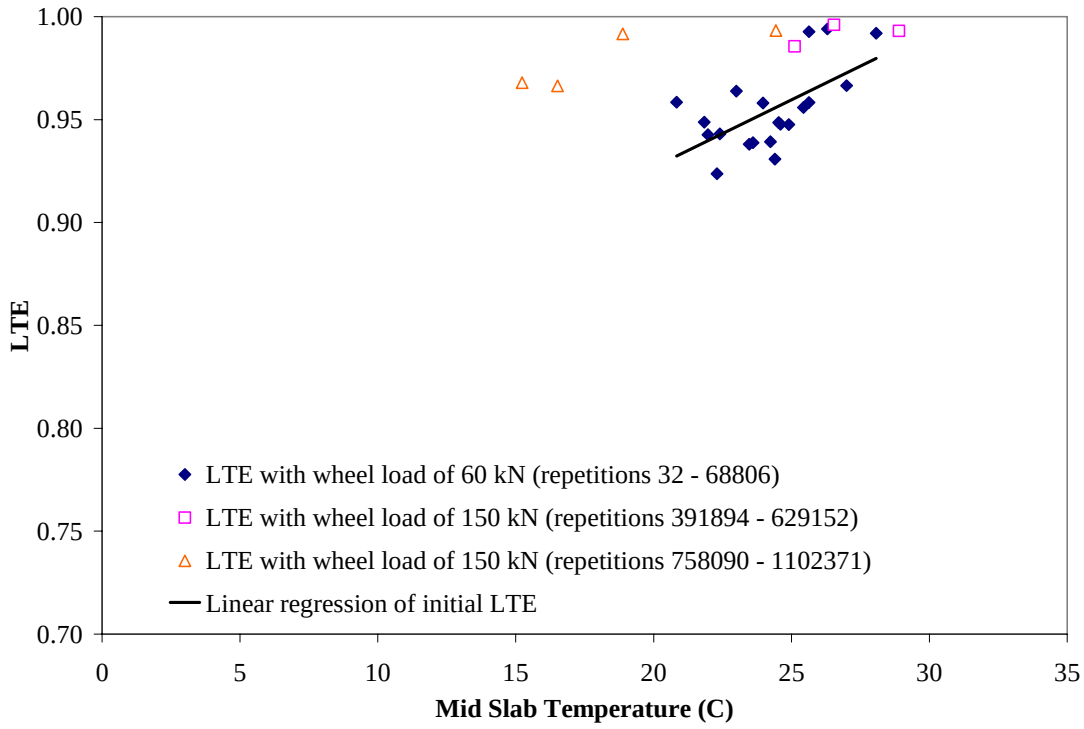

Figure 6.43. JDMD 2 LTE vs. mid-slab temperature on Section 557FD (with measuring load of 60 kN; Joint 36, epoxy-coated steel dowel, 3/wheelpath).

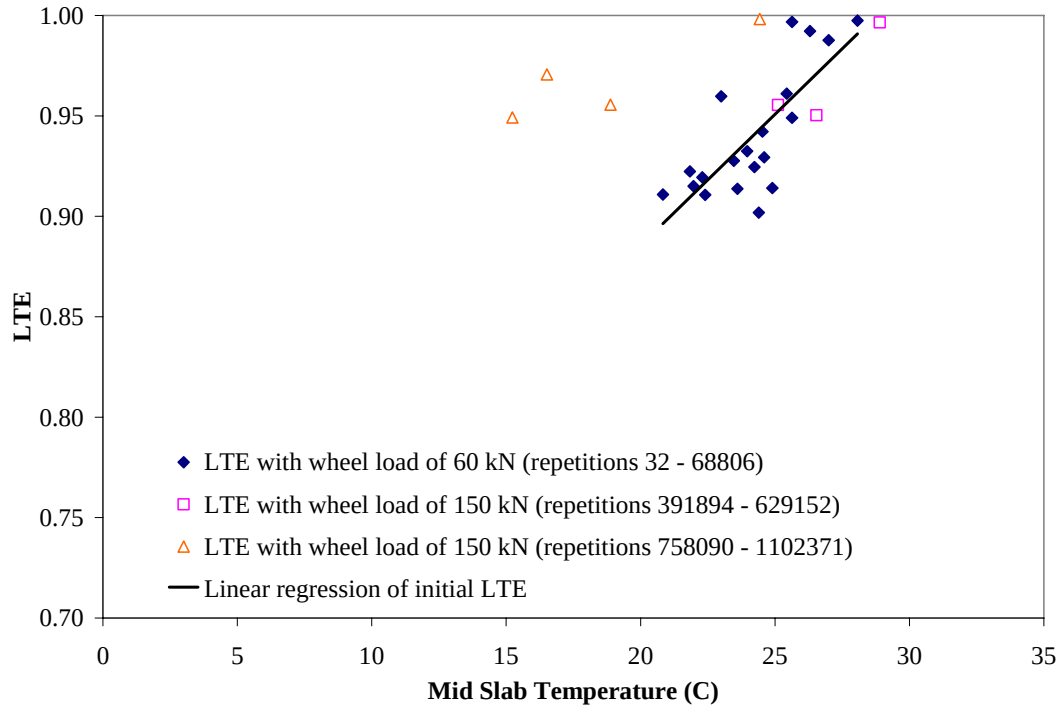

Figure 6.44. JDMD 4 LTE vs. mid-slab temperature on Section 557FD with measuring load of 60 kN (Joint 35, epoxy-coated steel dowel, 3/wheelpath).

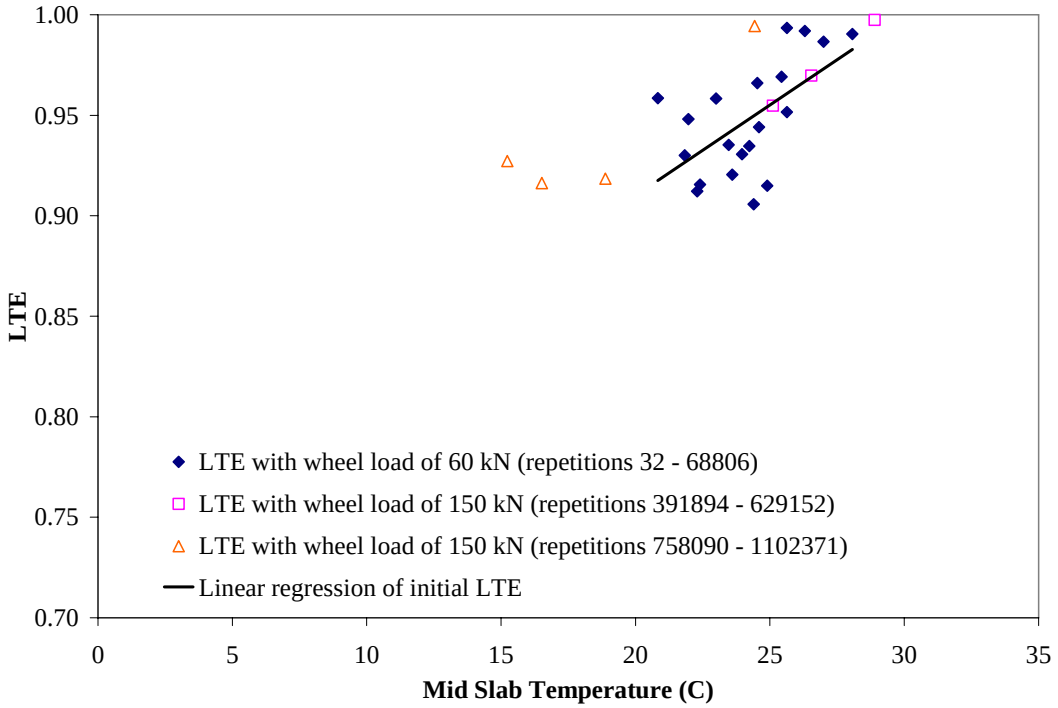

Figure 6.45. JDMD 5 LTE vs. mid-slab temperature on Section 557FD with measuring load of 60 kN (Joint 35, epoxy-coated steel dowel, 3/wheelpath).

6.1.4.5 Slab Cracking and Final Condition

The initial condition of Section 557FD, with no existing cracking, is shown in Figure 6.46. Figure 6.47 shows a mid-slab transverse crack that appeared on the surface of Slab 36 after 722,290 load repetitions, indicating fatigue failure of the concrete slab. The transverse crack shows that familiar turning towards the transverse joint due to the half axle loading. Figure 6.48 shows transverse cracking at the end of the wheelpath that appeared in Slab 35 after 776,068 repetitions. The final state of cracking in the section is shown in Figure 6.49, after 1.122 million repetitions. Final condition of Slabs 35, 36, and 37 is shown in overhead photos in Appendix B.

Figure 6.46. Initial condition of slabs in Section 557FD showing no existing cracking.

Figure 6.47. Mid-slab transverse cracking in Slab 36 after 722,290 repetitions.

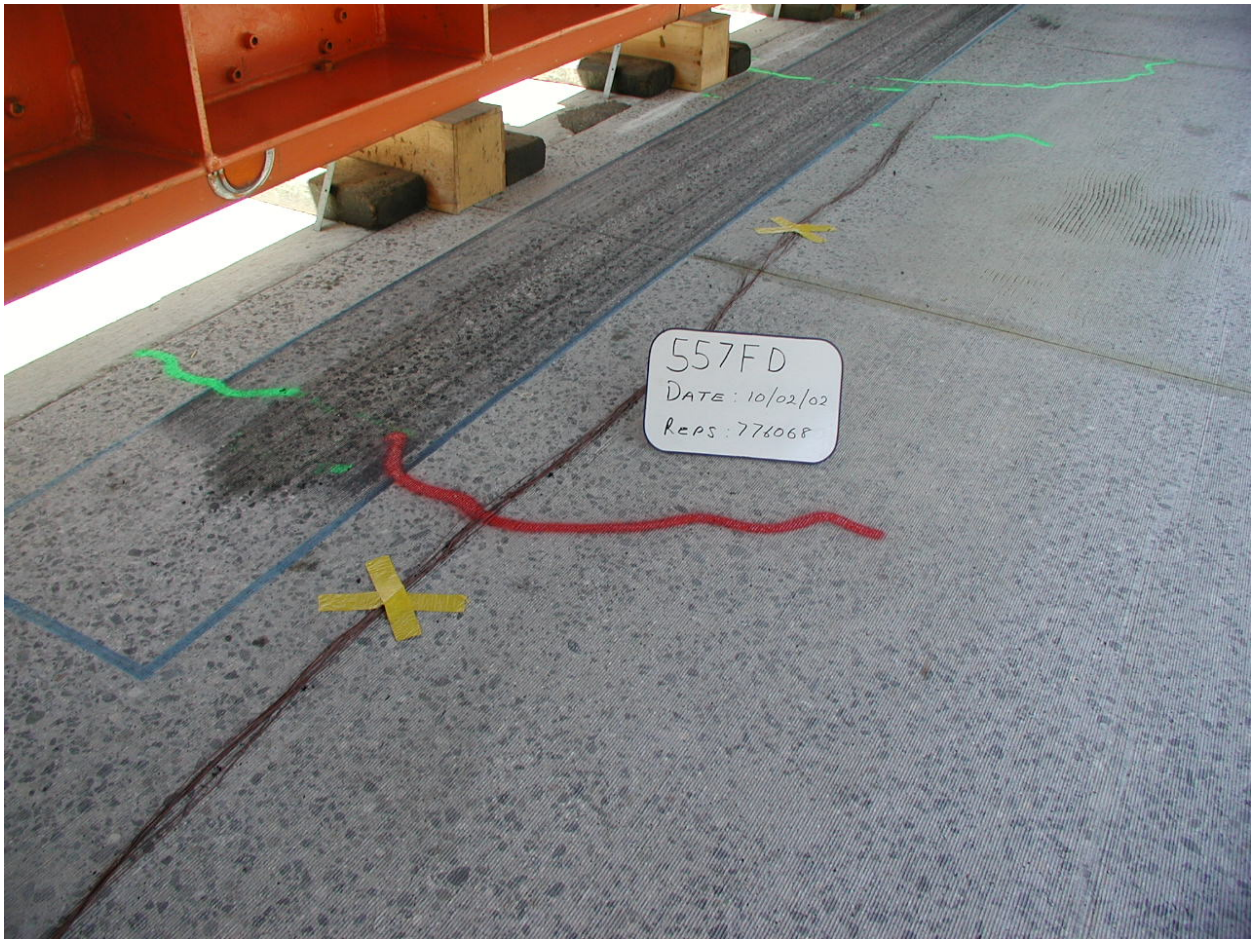

Figure 6.48. Cracking at the end of the wheelpath in Slab 35 after 776,068 repetitions.

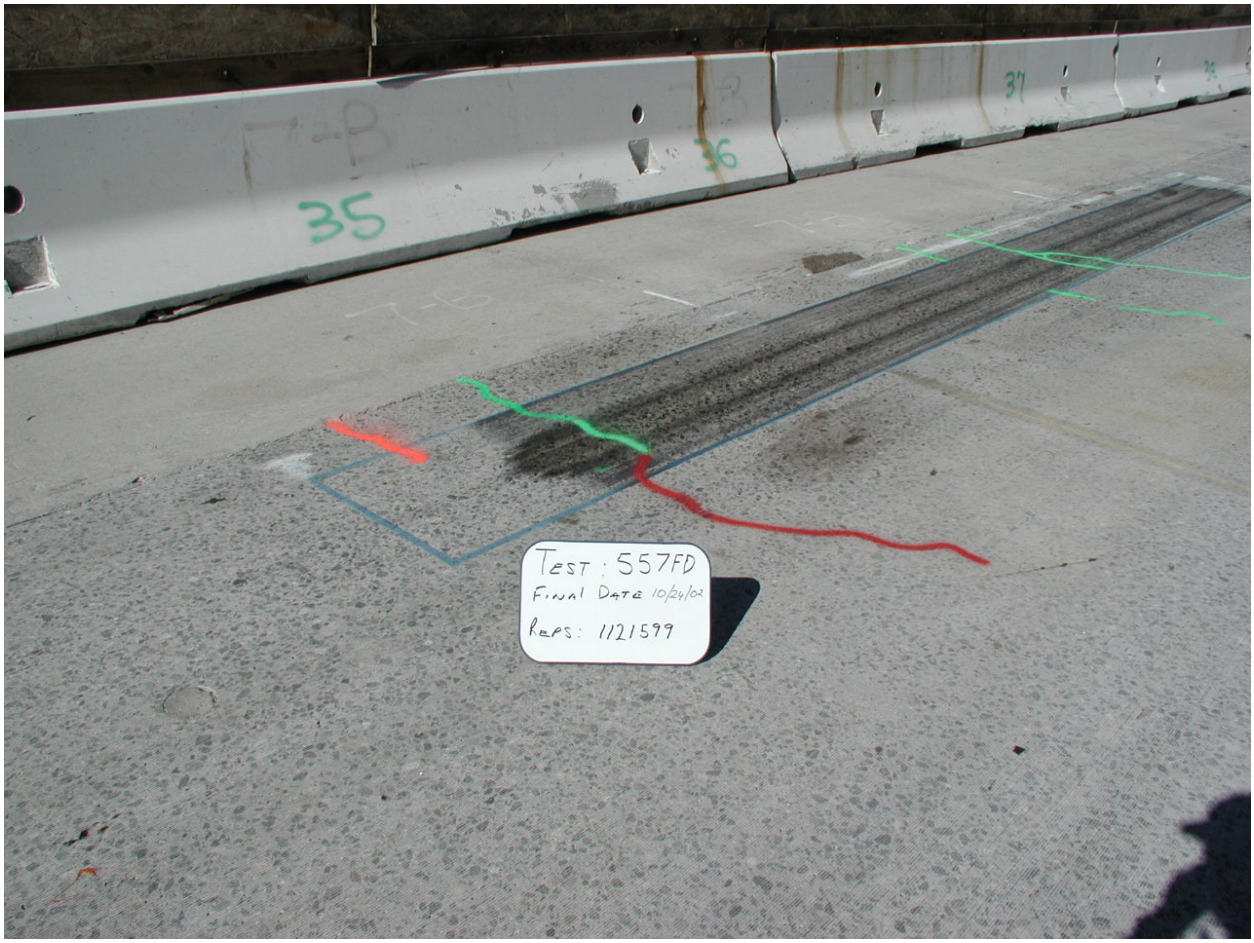

Figure 6.49. Final condition of Section 557FD after 1.122 million repetitions.

6.1.5 558FD HVS Test

Section 558RF had a large transverse crack (Crack 2) across the center of Slab 42 which was dowel bar retrofitted prior to HVS testing. The cracks present prior to DBR on Slab 42 can be seen near Joint 41 on Section 558FD in Figure 6.50, taken in March 2002 during HVS testing. Figure 6.51 shows a close-up of Slab 43 near Joint 42 taken at the same time. Figure 6.52 shows a close-up of Joint 42, Figure 6.53 shows a close-up of Joint 41, and Figure 6.54 shows a close-up of Crack 2, all taken at the same time in March 2002 after 2.002 million load repetitions. Vertical and horizontal JDMDs can be seen in the photographs of the joints and crack.

Figure 6.50. Slab 42 near Joint 41 on Section 558FD after 2.002 million repetitions.

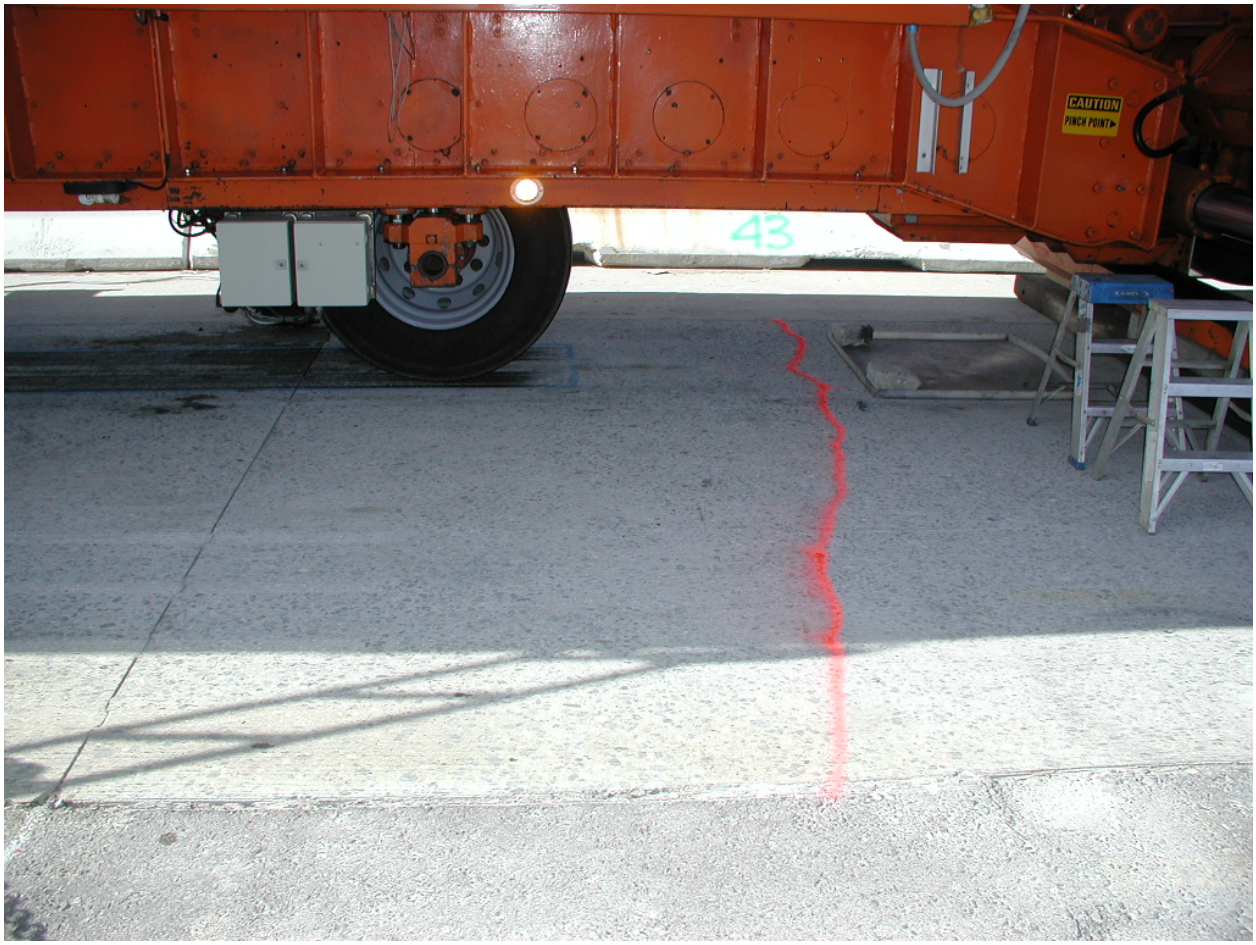

Figure 6.51. Slab 43 near Joint 42 on HVS Test Section 558FD after 2.002 million repetitions.

Figure 6.52. HVS Test Section 558FD, Joint 42 after 2.002 million repetitions.

Figure 6.53. HVS Test Section 558FD, Joint 41 after 2.002 million repetitions.

Figure 6.54. HVS Test Section 558FD, Crack 2 after 2.002 million repetitions.

JDMD locations and numbering for Section 558FD are shown in Figure 6.55.

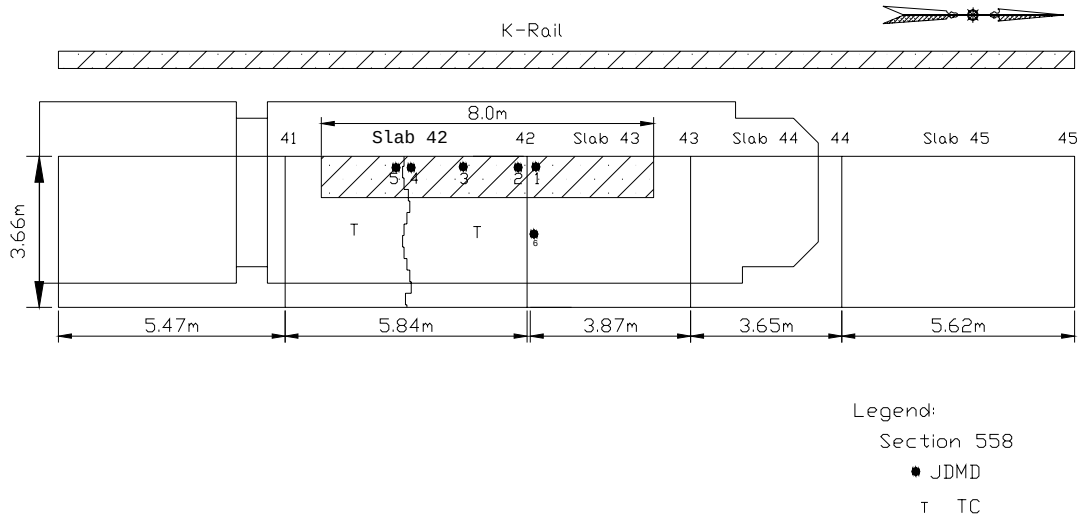

Figure 6.55. JDMD locations and numbering for Section 558FD.

The load history on Section 558FD is shown in Table 6.5. HVS loading on Section 558FD was applied using the 60 kN dual wheel load, followed by the 90 kN dual wheel load and the 150 kN single

aircraft wheel load, for a total of 2,208,578 repetitions. For this test section, only one repetition under the trafficking load of 150 kN was tested with the measurement load of 60 kN.

Table 6.5. Load history on Section 558FD

Load (kN)	Tire/Wheel Type	Inflation Pressure (kPa)	From Repetition	To Repetitions	Repetitions
60	Dual truck	689.5	1	63,283	63,283
90	Dual truck	689.5	63,284	1,219,868	1,156,585
150	Single aircraft	1,450	1,219,869	2,208,578	988,710

Air temperature and relative humidity during the testing of 558FD are shown in Figure 6.56. Extreme environmental conditions for 558FD are summarized in Table 6.6. During this test, 57 days out of the total 147 testing days had measurable rainfall. Mid-slab temperatures and slab temperature gradients are shown in Figure 6.57 and Figure 6.58, respectively.

Table 6.6. Extreme Environmental Conditions during HVS Testing of Section 558FD

	Air Temperature (^{o}C)	Rainfall (mm)	Relative Humidity (%)
Maximum	23.6	13.72	97
Minimum	-3.2	0	7
Average	9.50	0.0835 (57 days over the course of the test)	43.57

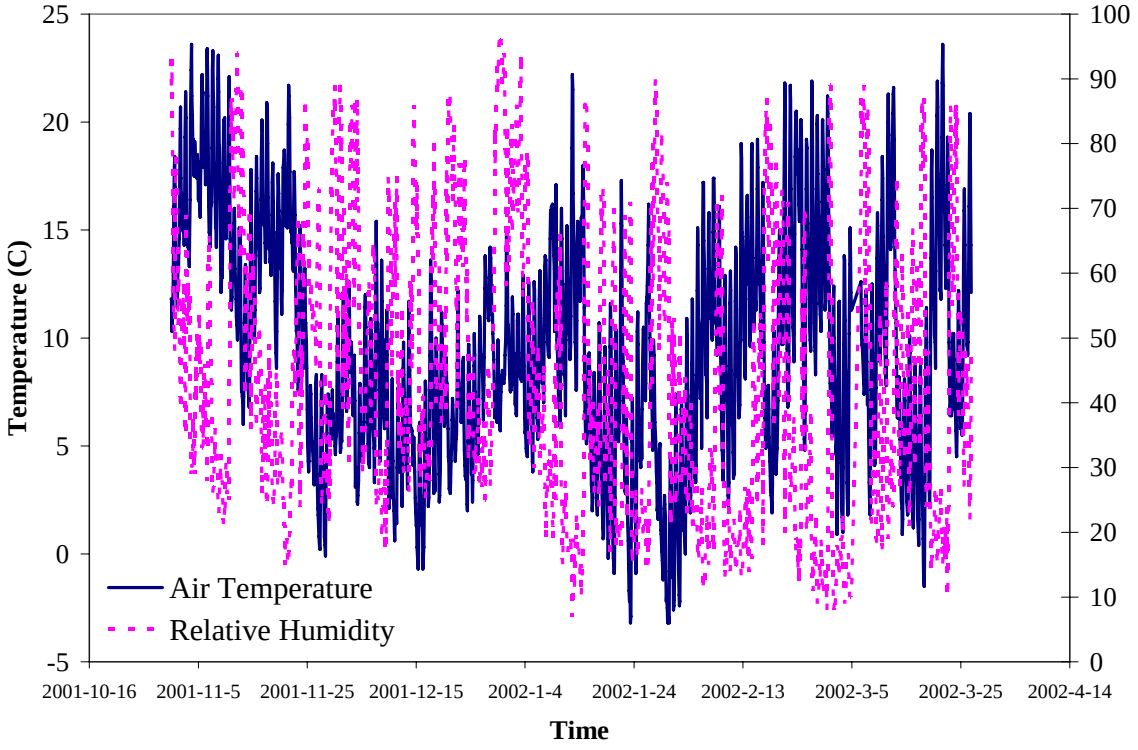

Figure 6.56. Air temperature and relative humidity on Section 558FD during HVS testing.

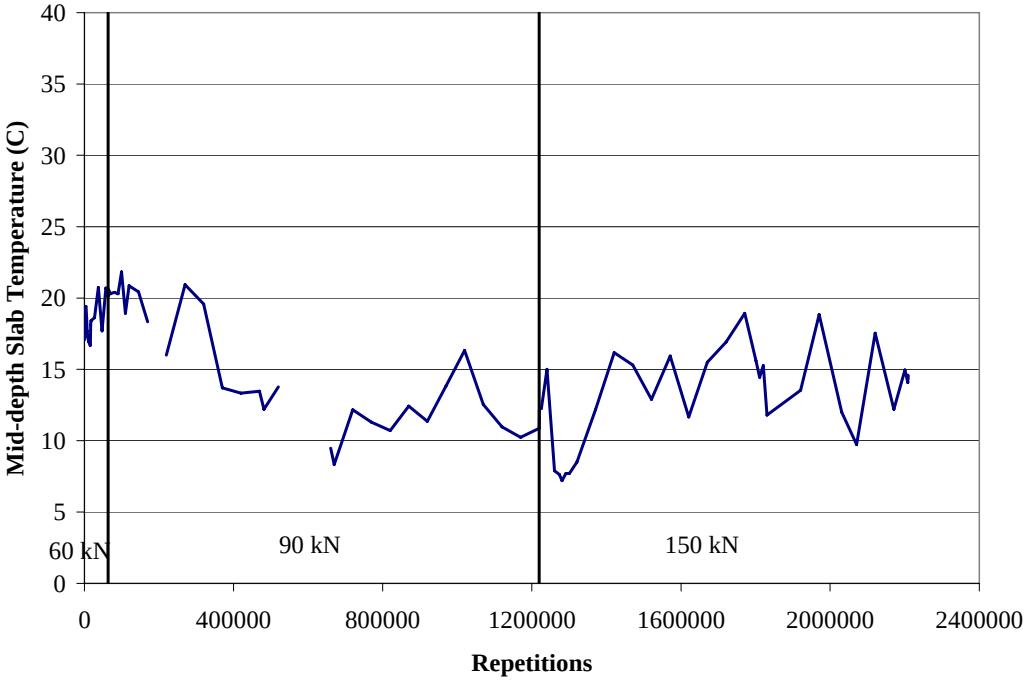

Figure 6.57. Mid-slab temperature for HVS Test Section 558FD.

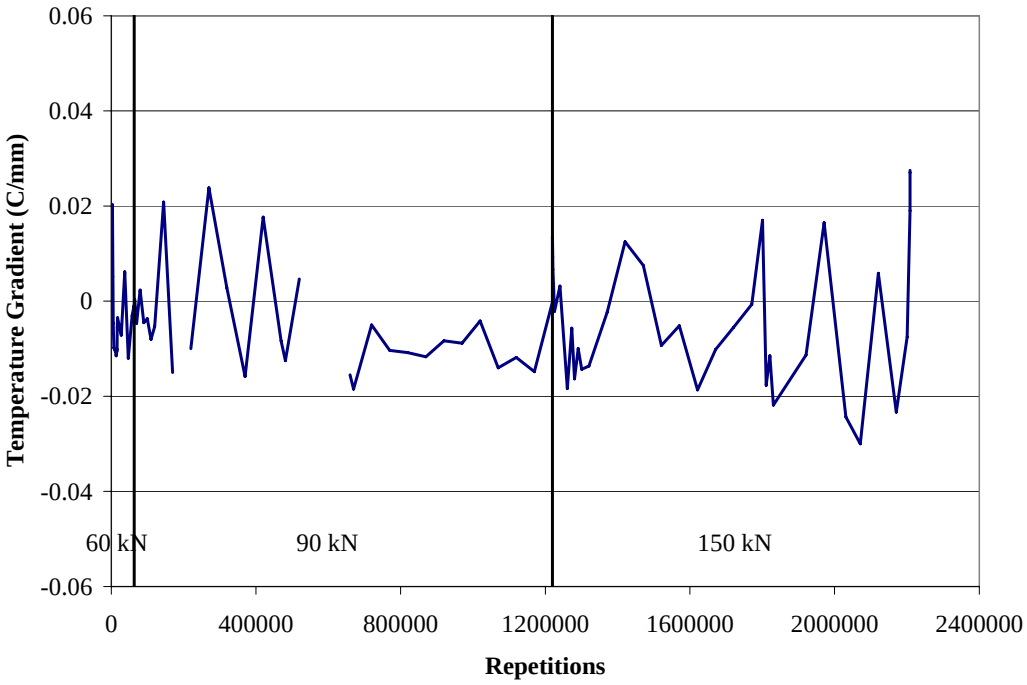

Figure 6.58. Slab temperature gradient for HVS Test Section 558FD.

6.1.5.1 Joint Maximum Deflection

Maximum JDMD deflections for all HVS repetitions and mid-slab temperatures for Section 558FD are shown in Figure 6.59 under the trafficking load. Maximum joint deflections with measurement load (60 kN) are shown in Figure 6.60.

From Figure 6.31, the vertical deflections (JDMD 1, 2, 4, and 5) under wheel loads of 90 kN and 150 kN are significantly higher than those under wheel load of 60 kN. Also, the vertical deflections fluctuate with temperature changing and show higher values under lower temperatures, which is expected.

From Figure 6.59, the horizontal deflection (JDMD 6) keeps fairly stable throughout the whole HVS test. Vertical deflections midway along longitudinal slab edge (JDMD 3) show higher values after HVS repetitions with trafficking loads of 90 kN and 150 kN, and also under lower temperatures.

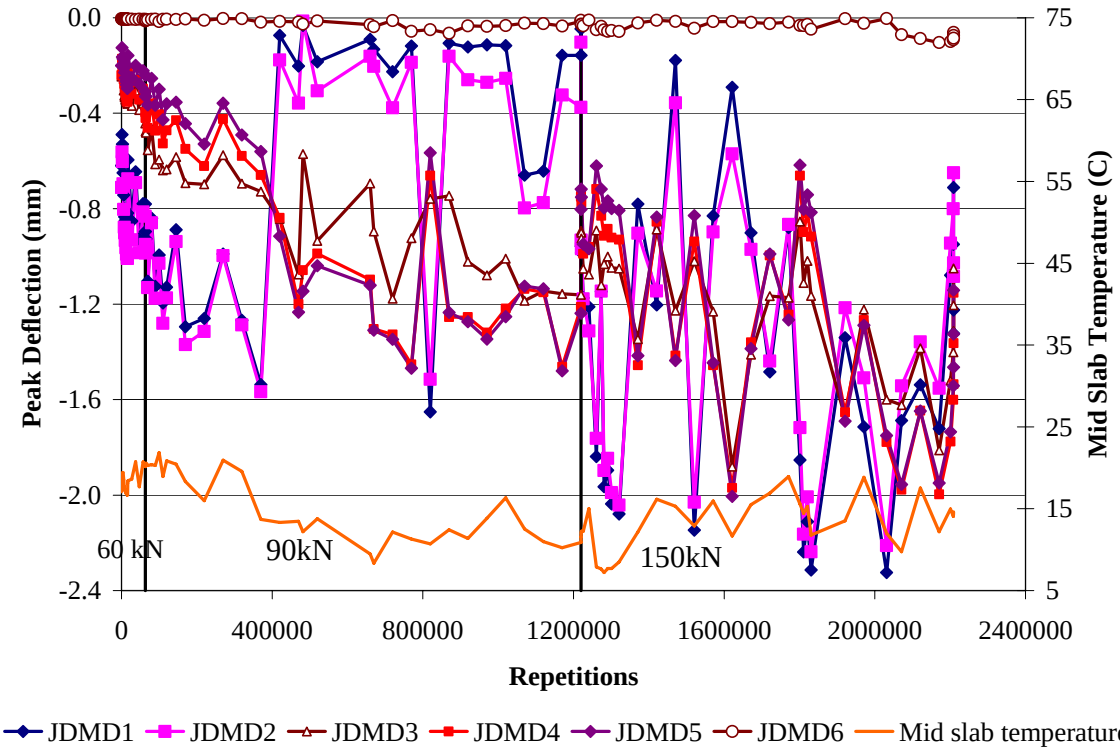

Figure 6.59. Maximum JDMD Deflections on HVS Test Section 558FD under trafficking loads.

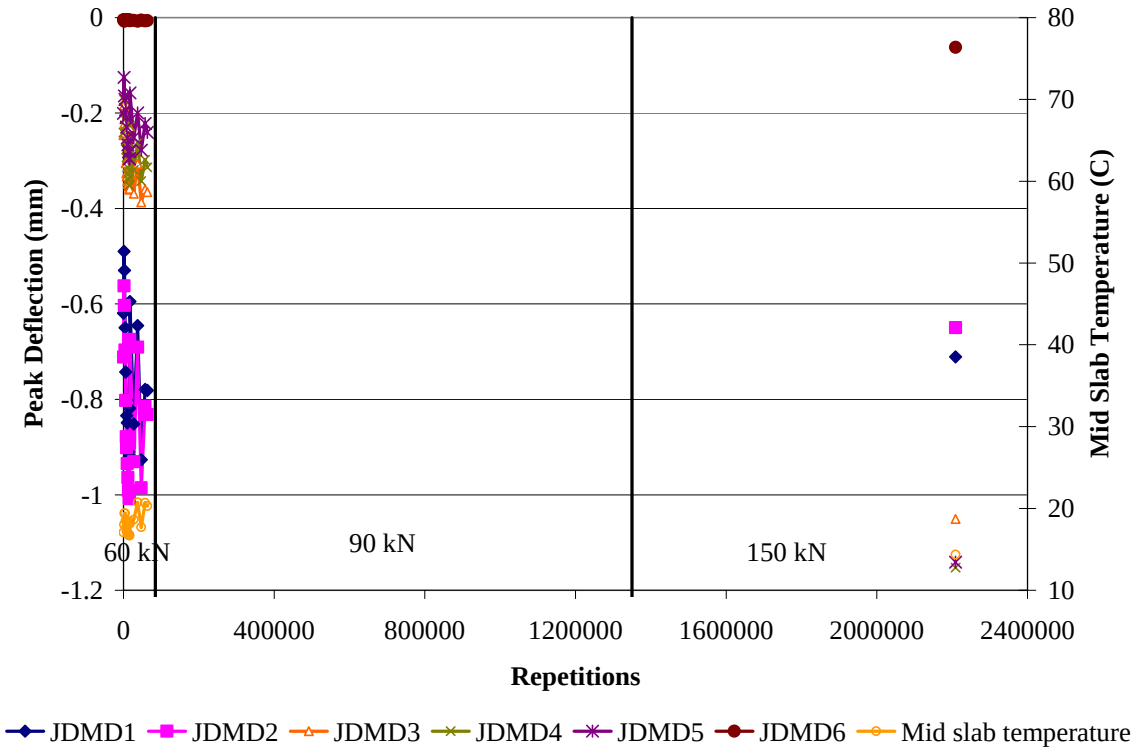

Figure 6.60. Maximum JDMD deflections with HVS measuring load of 60 kN on Section 558FD.

6.1.5.2 Vertical Joint Deflection vs. Mid-slab Temperature

The vertical JDMD deflection against the mid-slab temperature is shown in Figure 6.61 through Figure 6.64. Only JDMD deflections obtained under the HVS measuring load of 60 kN are included in these figures. From repetitions 3–63283 shown in the figures, it can be seen that there is a roughly linear relationship between vertical JDMD deflection and mid-slab temperature, while the vertical deflection decreases as the temperature increases. For JDMDs 1 and 2 (Joint 42), the deflection after 2,208,578 repetitions is not greater than those under the measuring load of 60 kN. However, for JDMD 4 and 5 (Crack 42), the deflection after repetitions of higher wheel loads is much higher, as has been observed from Sections 556FD and 557FD.

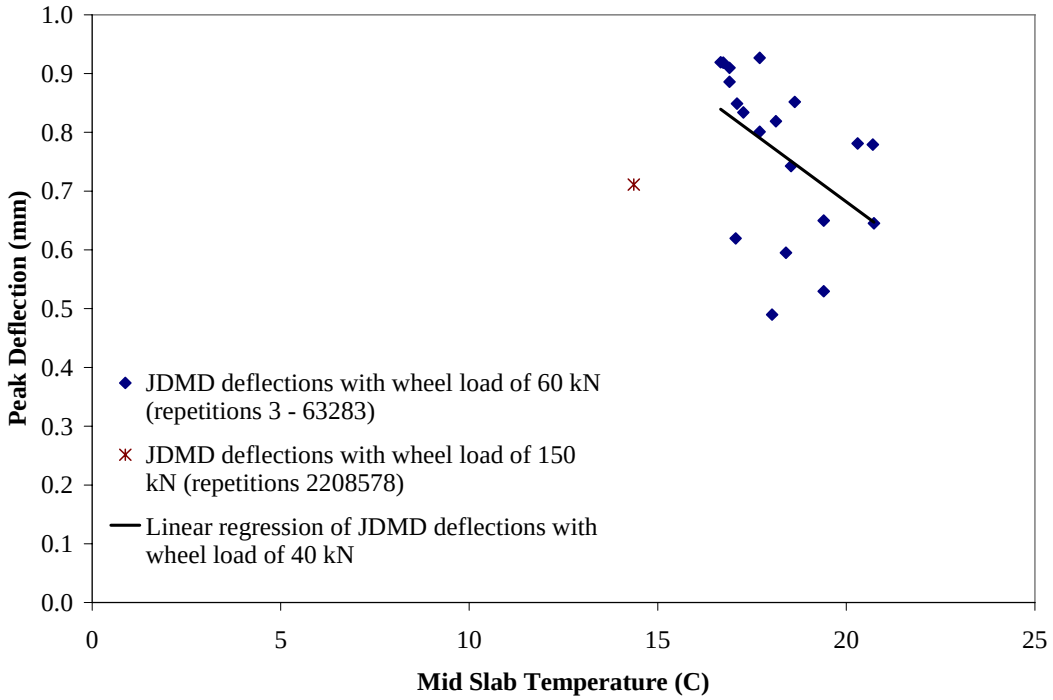

Figure 6.61. JDMD 1 Peak deflection vs. mid-slab temperature on Section 558FD (with measuring load of 60 kN; Joint 42, FRP dowel, 4/wheelpath).

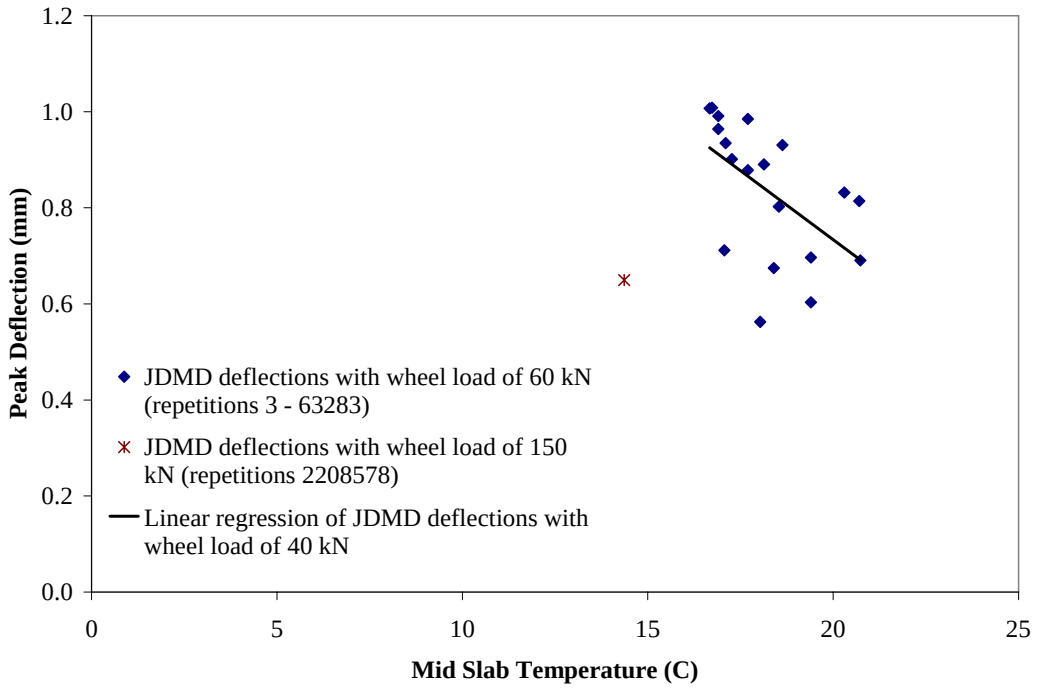

Figure 6.62. JDMD 2 Peak deflection vs. mid-slab temperature on Section 558FD (with measuring load of 60 kN; Joint 42, FRP dowel, 4/wheelpath).

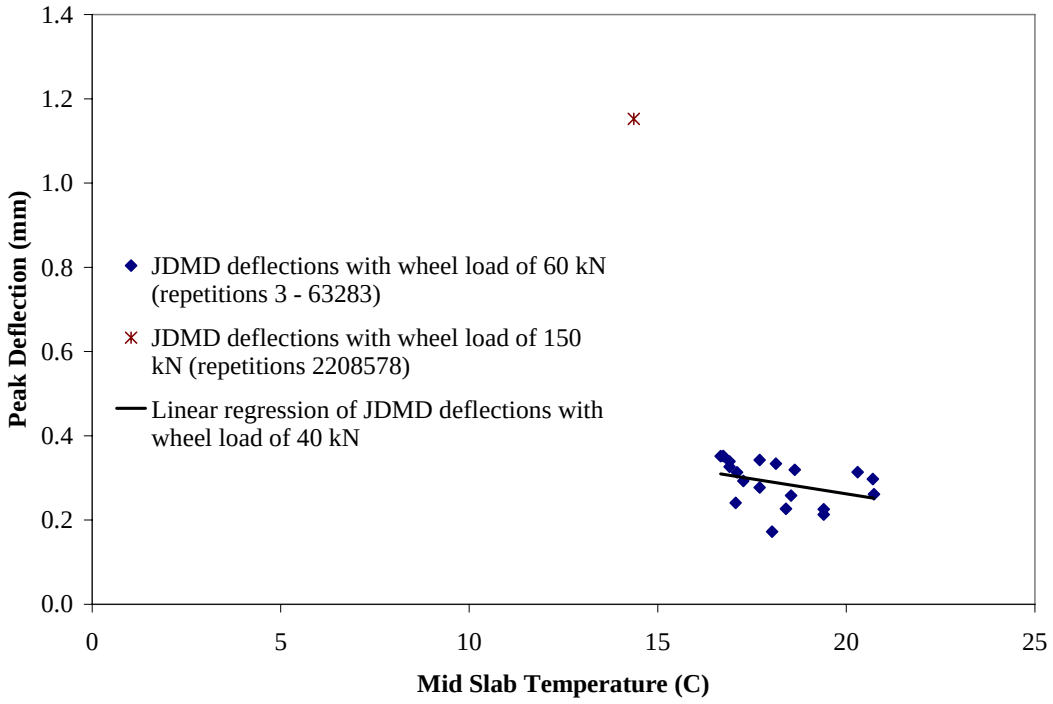

Figure 6.63. JDMD 4 peak deflection vs. mid-slab temperature on Section 558FD (with measuring load of 60 kN; Crack 2, FRP dowel, 4/wheelpath).

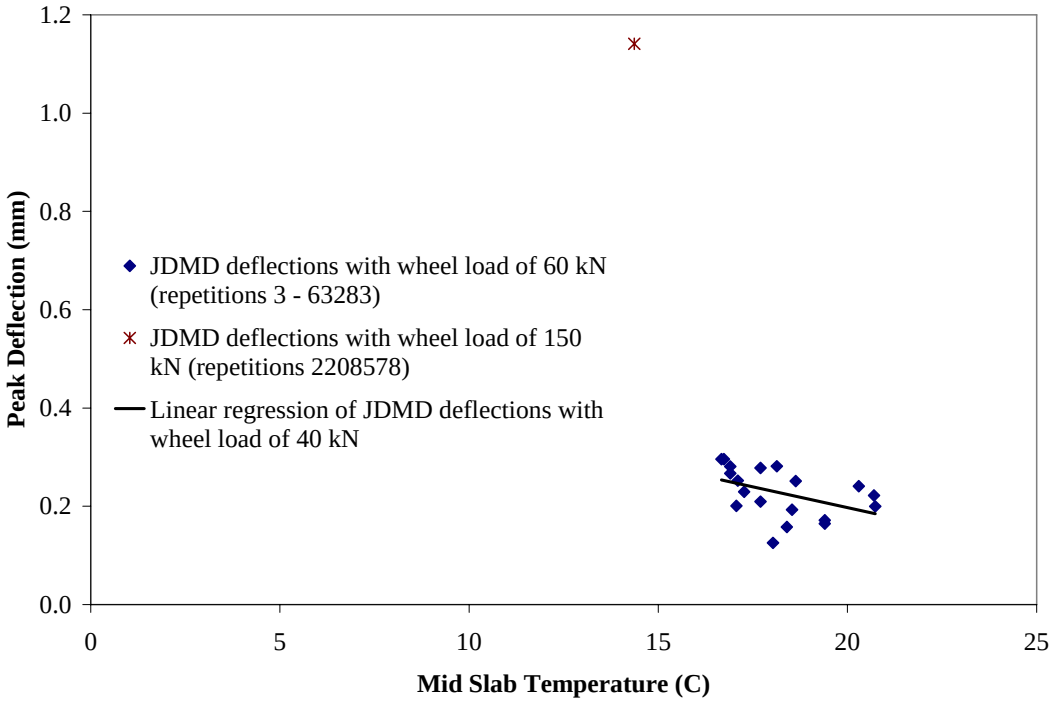

Figure 6.64. JDMD 5 peak deflection vs. mid-slab temperature on Section 558FD (with measuring load of 60 kN; Crack 2, FRP dowel, 4/wheelpath).

6.1.5.3 Load Transfer Efficiency

Load transfer efficiency (LTE) for all HVS repetitions together with mid-slab temperature for Section 558FD is shown in Figure 6.65. LTE with measuring load of 60 kN is shown in Figure 6.66. From these figures, it again appears that LTE increases with temperature, but doesn't change much with HVS wheel loading level or HVS repetitions. Most of the measured LTEs are higher than 80 percent; however, the JDMD 1 and JDMD 2 LTE values obtained from repetition 869,869 (Joint 42) are much lower than those obtained from other repetitions (62.2 percent for JDMD 1 and 74.6 percent for JDMD 2).

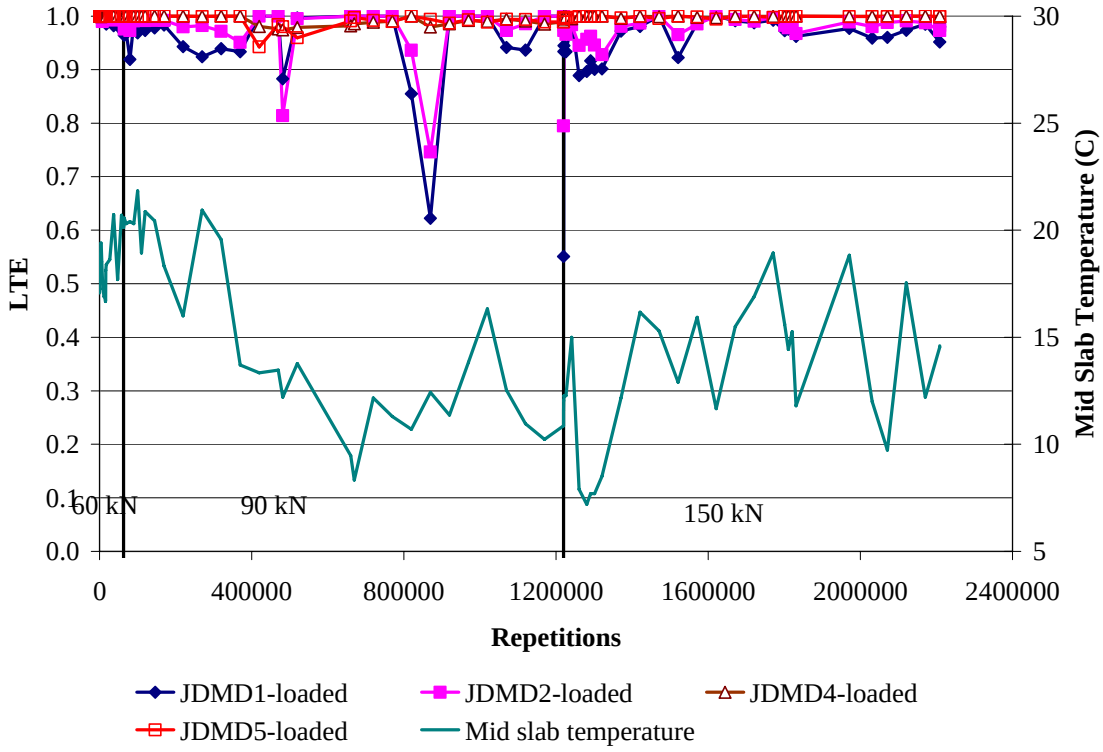

Figure 6.65. LTE under HVS trafficking loads on Section 558FD.

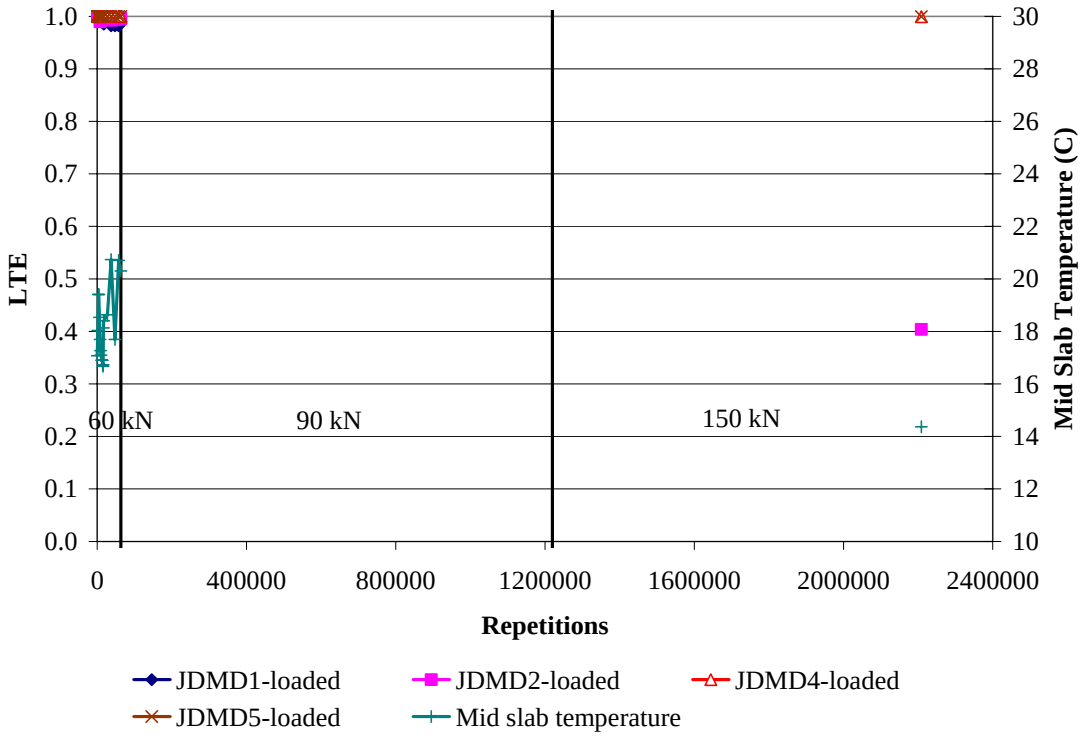

Figure 6.66. LTE under HVS loading with measuring load of 60 kN on Section 558FD.

6.1.5.4 LTE vs. Mid-Slab Temperature

The measured LTE against the mid-slab temperature are shown in Figure 6.67 through Figure 6.70. The LTEs shown in these figures are consistently high, and don't change with either temperature or HVS repetitions. In this test section, both Crack 2 and Joint 42 were DBR by FRP dowel bars, and it seems that FRP dowel bars work well to maintain a high LTE after millions of load repetitions. Detailed comparison among dowel bars made of different materials will be presented in Section 3.

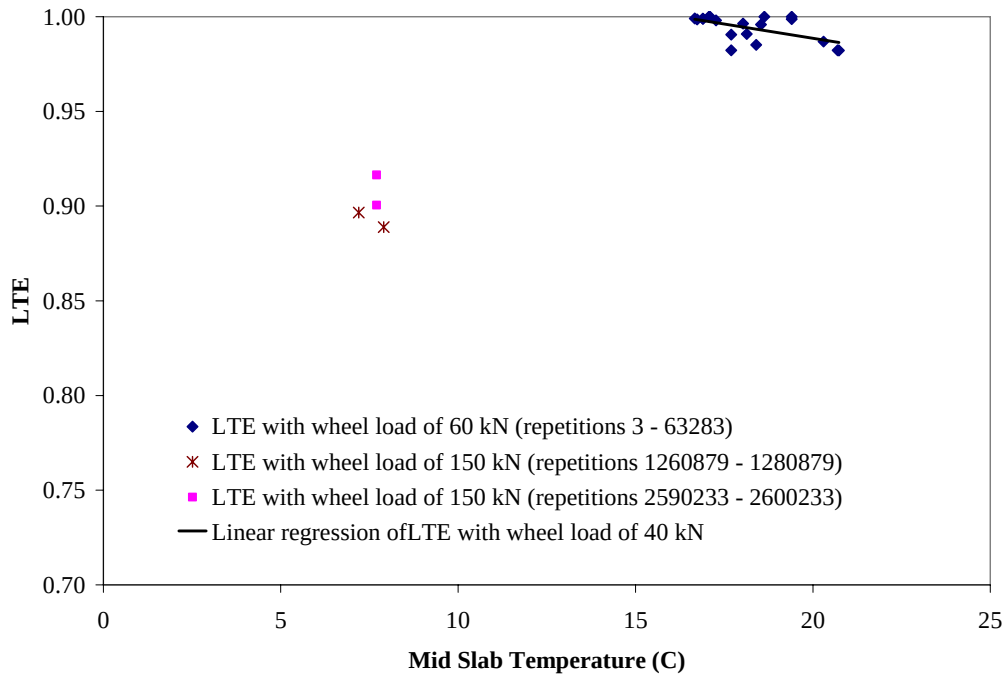

Figure 6.67. JDMD 1 LTE vs. mid-slab temperature on Section 558FD (with measuring load of 60 kN; Joint 42, FRP dowel, 4/wheelpath).

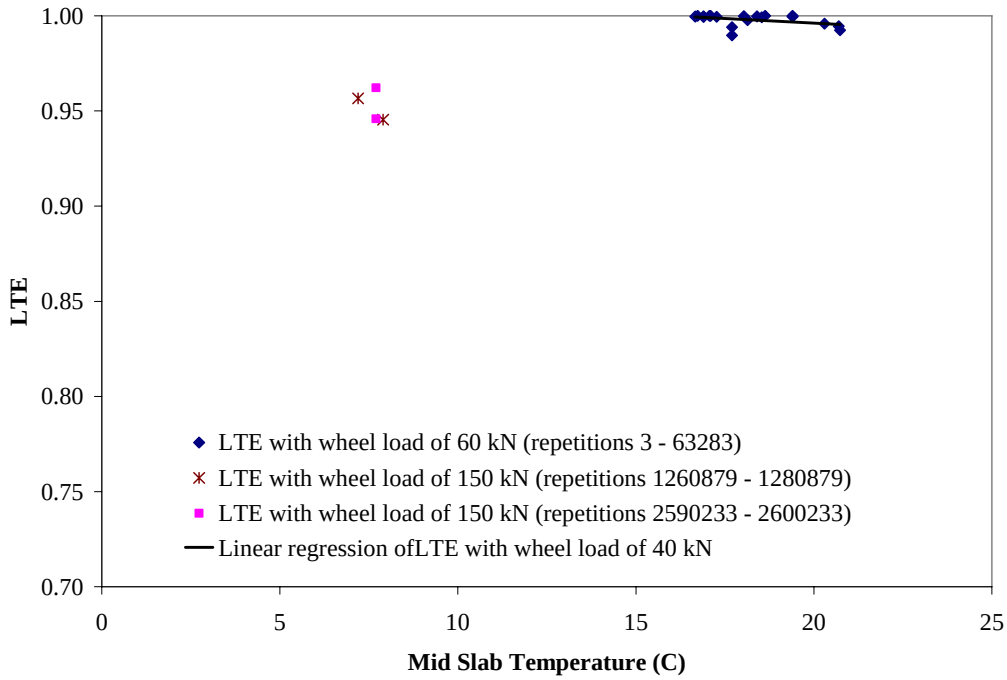

Figure 6.68. JDMD 2 LTE vs. mid-slab temperature on Section 558FD (with measuring load of 60 kN; Joint 42, FRP dowel, 4/wheelpath).

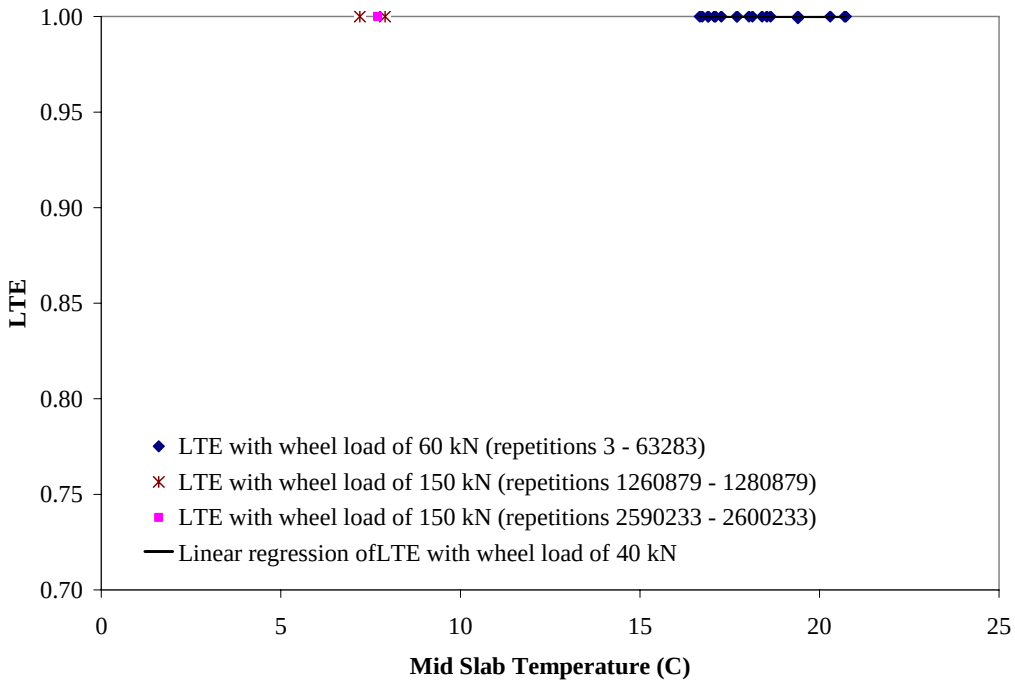

Figure 6.69. JDMD 4 LTE vs. mid-slab temperature on 558FD (with measuring load of 60 kN; crack 2, FRP dowel, 4/wheelpath).

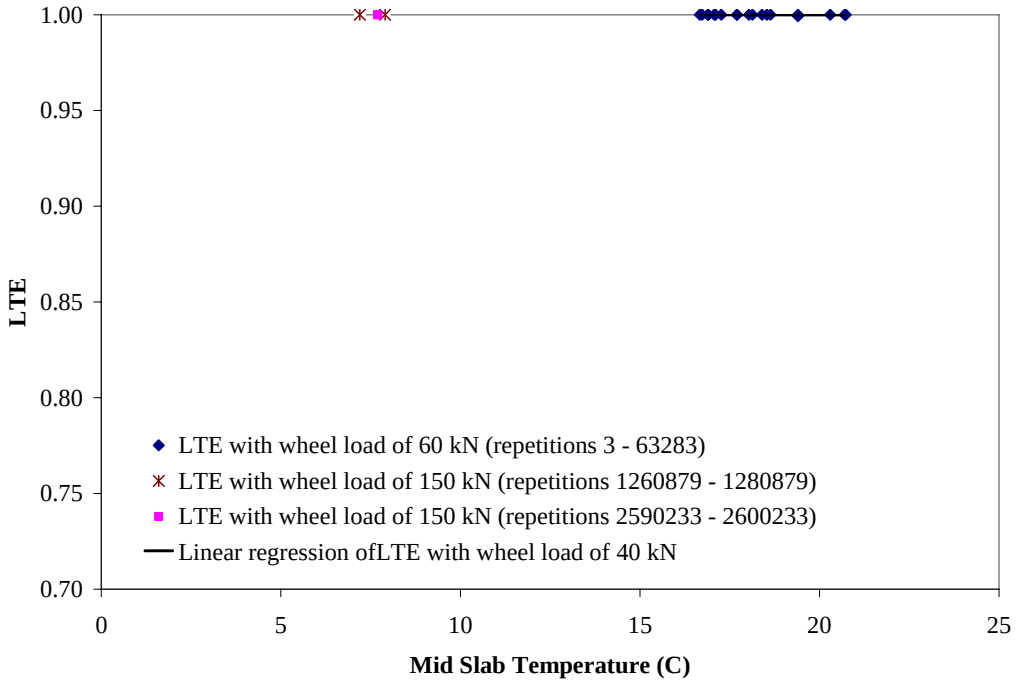

Figure 6.70. JDMD 5 LTE vs. mid-slab temperature on Section 558FD (with measuring load of 60 kN; crack 2, FRP dowel, 4/wheelpath).

6.1.5.5 Slab Cracking and Final Condition

Figure 6.71 shows the first new crack that developed on Section 558FD. This crack extended from the edge of the slab to the back of the outside DBR slot on Joint 42. The crack was on Slab 42 and was noted at 1.782 million load repetitions. Figure 6.72 shows a close-up of the same crack after 2.002 million load repetitions.

A mid-slab transverse crack appeared in Slab 42 between Crack 2 and Joint 42 at about 2.129 million repetitions, and then propagated towards Joint 42 as shown in Figure 6.73. The final condition of that crack and the dowel bar retrofitted Crack 2 can be seen in Figure 6.74 after 2.209 million load repetitions. Figure 6.75 shows a close-up of the final condition of Crack 2. The final condition of Slabs 41, 42, and 43 at the time of forensic coring can be seen in Appendix B.

Figure 6.71. First new crack on Section 558FD from slab edge to back of outside dowel bar slot on Joint 41 at 1.782 million load repetitions.

Figure 6.72. Close-up of first new crack after 2.002 million load repetitions.

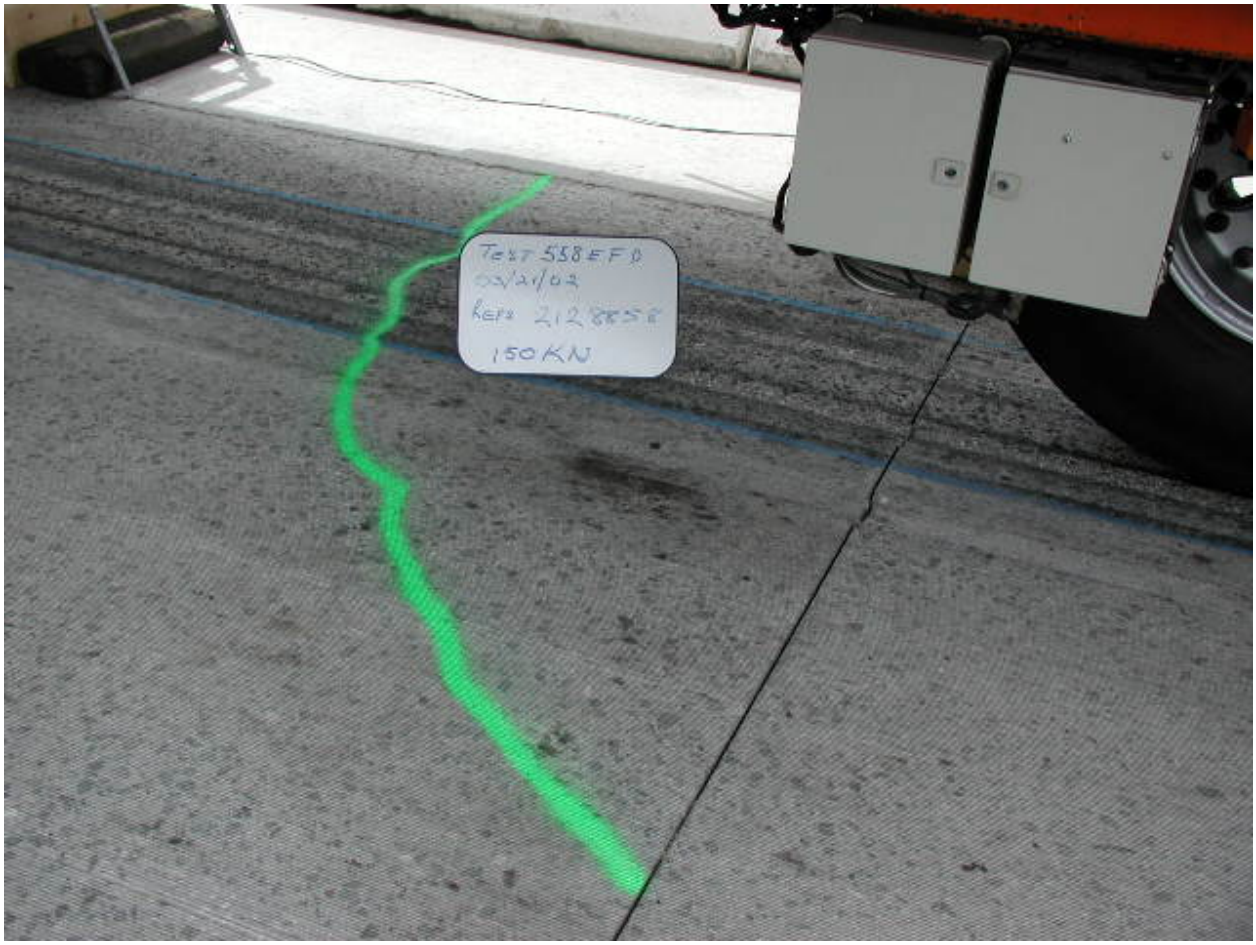

Figure 6.73 Mid-slab transverse cracking in Slab 42 near Joint 42 after 2.129 million repetitions.

Figure 6.74. Final condition of mid-slab transverse crack and Crack 2 after 2.209 million repetitions.

Figure 6.75. Close-up of final condition of Crack 2 at end of HVS loading after 2.209 million repetitions.

6.1.6 559FD HVS Test

The condition of Section 556FD prior to HVS testing in March 2002 is shown in Figure 6.76. Figure 6.77, Figure 6.78, and Figure 6.79 show close-ups of Joint 32, Crack 1, and Joint 33 prior to HVS testing.

JDMD locations and numbering for Section 559FD are shown in Figure 6.80.

The load history on Section 559FD is shown in Table 6.7. HVS loading on Section 559FD included the 60 kN dual wheel load, the 90 kN dual wheel load, and the 150 kN single aircraft wheel load, for a total of 2,001,497 repetitions. During the repetitions with wheel load of 150 kN, six repetitions at each data collection time were tested with a load of 60 kN.

Figure 6.76. HVS Test wection 559FD prior to HVS testing. Blue lines painted on surface show future HVS wheeltrack.

Figure 6.77. HVS Test Section 559FD, Joint 32, prior to HVS testing.

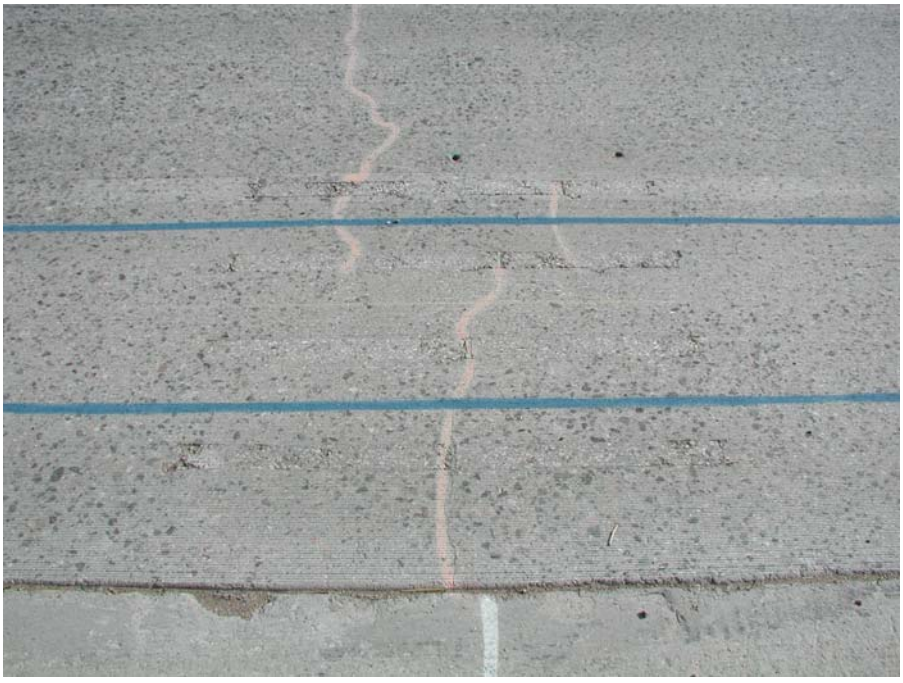

Figure 6.78. HVS Test Section 559FD, Crack 1, prior to HVS testing.

Figure 6.79. HVS Test Section 559FD, Joint 33, prior to HVS testing.

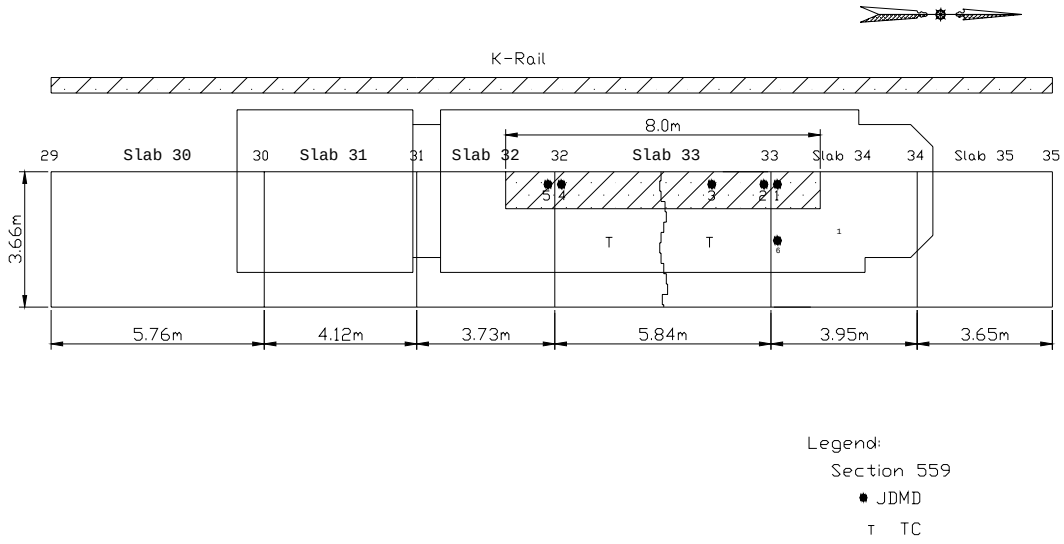

Figure 6.80. JDMD locations and numbering for Section 559FD.

Table 6.7. Load History on Section 559FD

Load (kN)	Tire/Wheel Type	Inflation Pressure (kPa)	From Repetition	To Repetitions	Repetitions
60	Dual truck	689.5	1	71,208	71,028
90	Dual truck	689.5	71,209	1,229,904	1,158,876
150	Single aircraft	1,450	1,229,905	2,001,497	771,593

Air temperature and relative humidity during testing of 559FD are shown in Figure 6.81. Extreme environmental conditions for 559FD are described in Table 6.8. The environmental condition during this test section can be summarized as cool and mildly humid. Mid-slab temperature and slab temperature gradient are shown in Figure 6.82 and Figure 6.83. Environmental conditions on Section 559FD were similar to those on Section 558FD, which was the intention to be able to compare different types of dowels under similar conditions.

Table 6.8. Extreme Environmental Conditions during HVS Testing of Section 559FD

	Air Temperature (°C)	Rainfall (mm)	Relative Humidity (%)
Maximum	23.3	91.19	100
Minimum	-0.1	0	9
Average	10.32	0.274	48.02

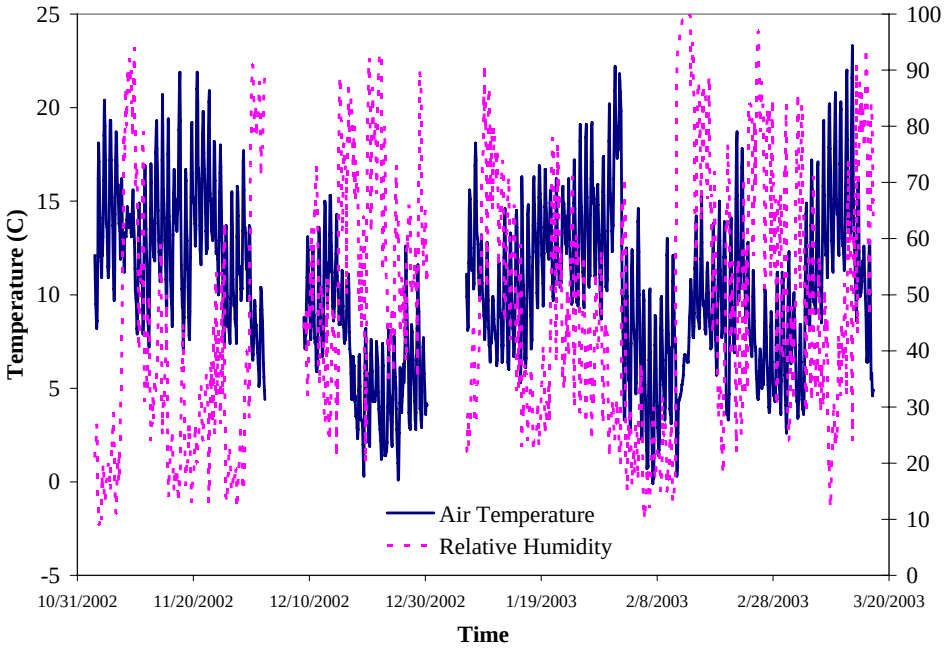

Figure 6.81. Air temperature and relative humidity during HVS Testing of Section 559FD.

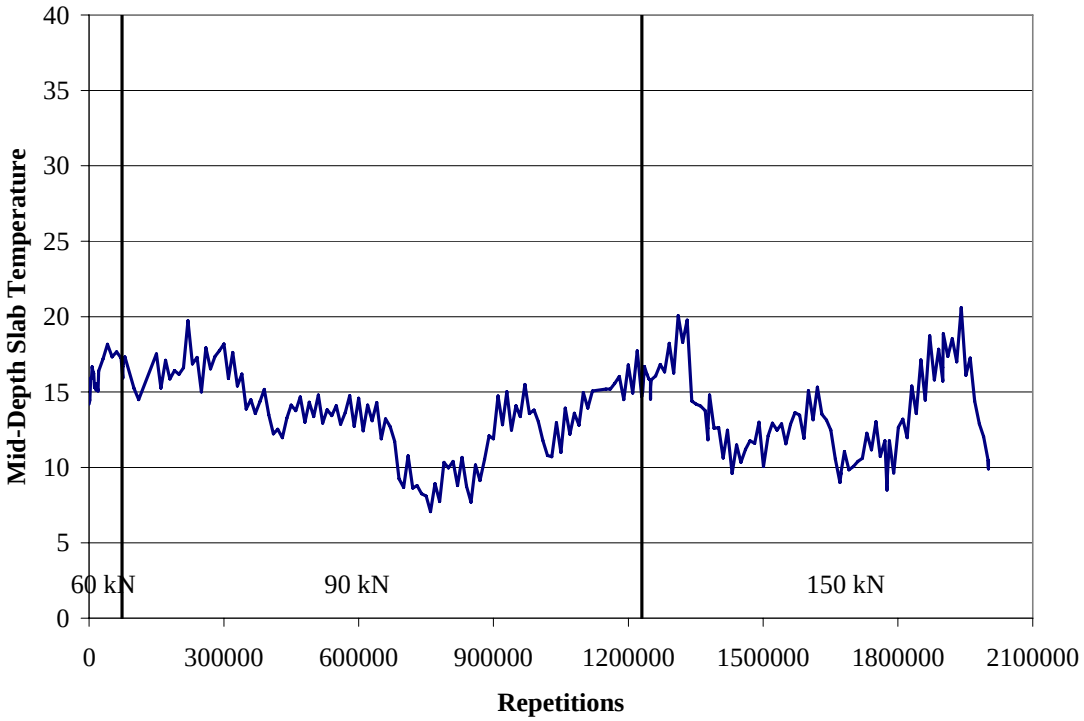

Figure 6.82. Mid-slab temperature for HVS Test Section 559FD.

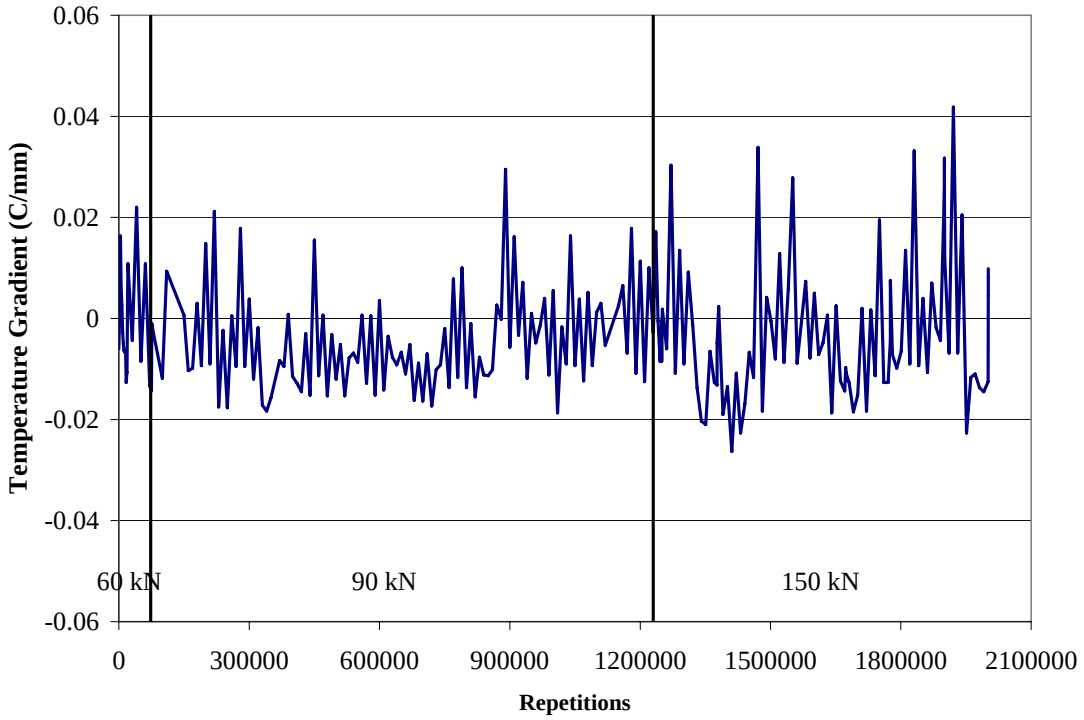

Figure 6.83. Slab temperature gradient for HVS Test Section 559FD.

6.1.6.1 Joint Maximum Deflection

Maximum JDMD deflections and the corresponding mid-slab temperatures for all repetitions are shown in Figure 6.84 under the HVS trafficking loads. Maximum JDMD deflections with the measurement load of 60 kN are shown in Figure 6.85.

From Figure 6.84 and Figure 6.85, it appears that vertical deflections (JDMD 1, 2, 4, and 5) increase considerably after repetitions with higher HVS loading level (90 kN and 150 kN). This indicates that the joints have been damaged under these HVS loading repetitions. Also, vertical JDMDs show greater deflection values under lower temperature, as expected.

Compared with vertical deflections, the horizontal deflections (JDMD 6) remain at a fairly stable level throughout the HVS test. Vertical deflection midway along the longitudinal slab edge (JDMD 3) fluctuates as the same trend with vertical deflections at the transverse joints, but with a smaller range.

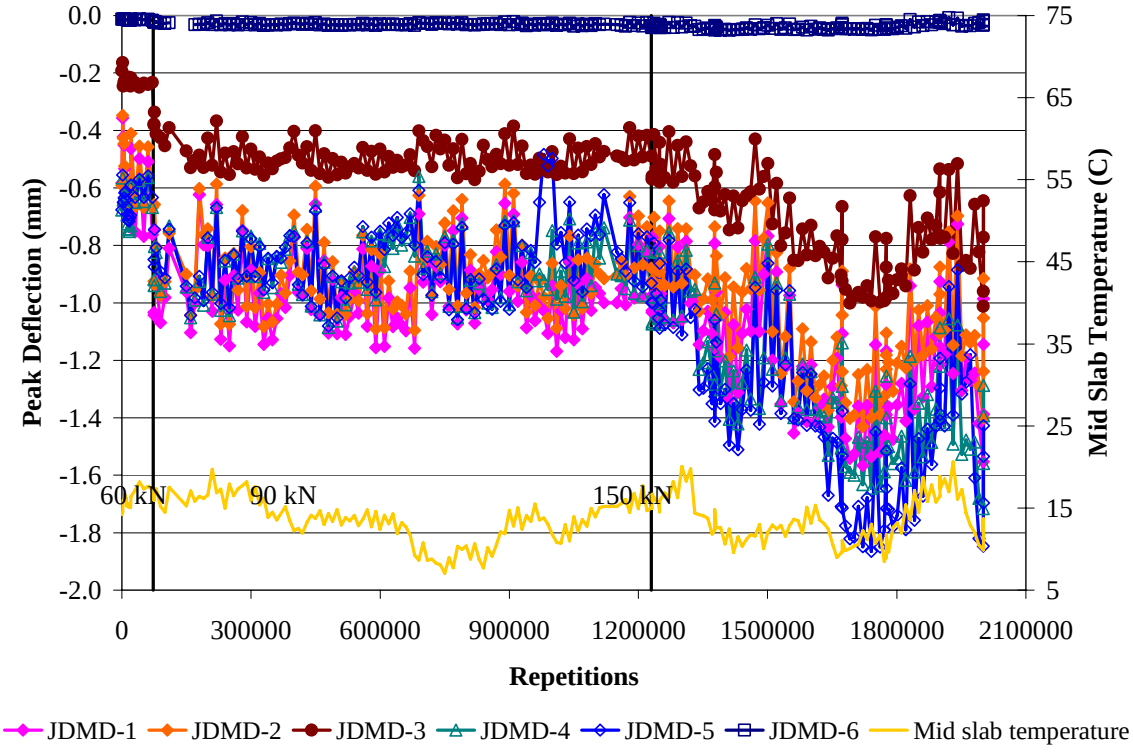

Figure 6.84. Maximum JDMD deflections on HVS Test Section 559FD under trafficking loads.

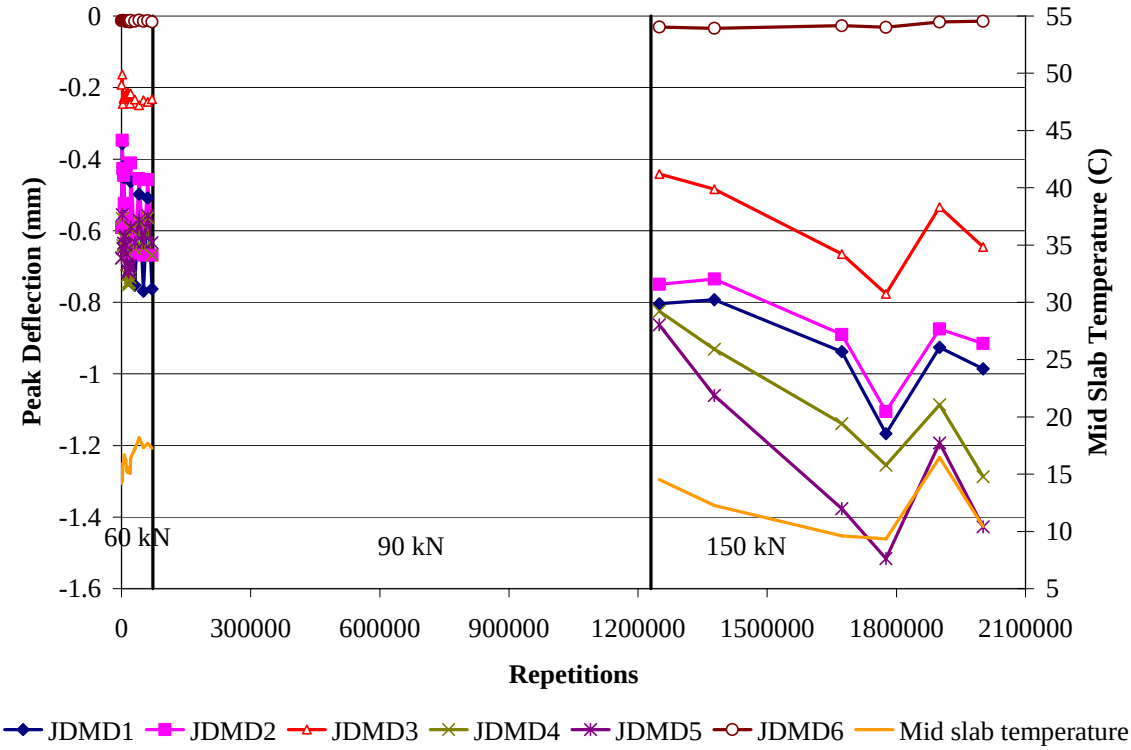

Figure 6.85. Maximum JDMD deflections with HVS measurement load of 60 kN on Section 559FD.

6.1.6.2 Vertical Joint Deflection vs. Mid-Slab Temperature

Vertical deflection against mid-slab temperature is shown in Figure 6.86 through Figure 6.89. Only deflections obtained under the measurement load of 60 kN are shown in these figures. From repetitions 0 through 71,028 (with wheel load of 60 kN), there exists a roughly linear relationship between JDMD peak deflection and corresponding mid-slab temperature. Except for Figure 6.86 (Joint 33, Slab 34), the regression lines have the same trend with those lines from Section 556FD–558FD: vertical deflection decreases as temperature increases. Within the same temperature range, the vertical deflections after repetitions of higher wheel load (90 kN and 150 kN) are obviously greater than those under the wheel load of 60 kN, indicating damage to the joint.

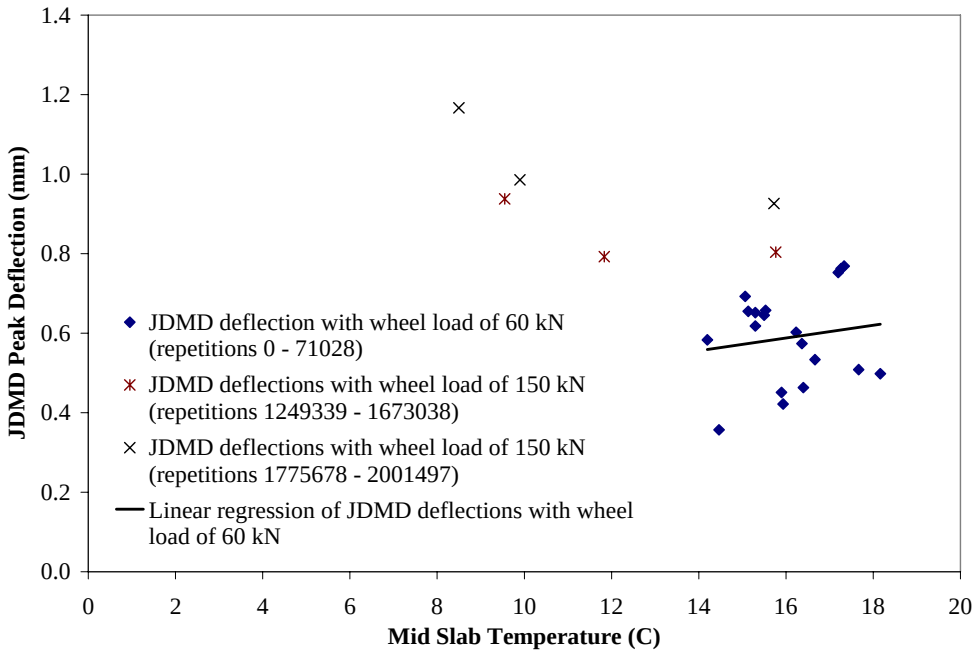

Figure 6.86. JDMD 1 peak deflection vs. mid-slab temperature on Section 559FD (with measuring load of 60 kN; Joint 33, hollow stainless dowel, 4/wheelpath).

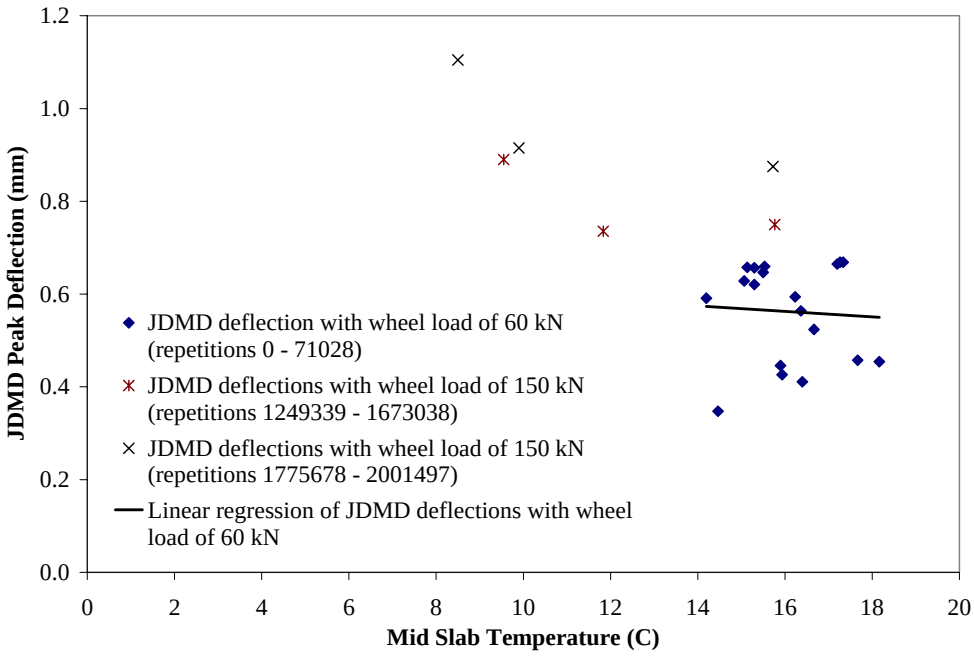

Figure 6.87. JDMD 2 peak deflection vs. mid-slab temperature on Section 559FD (with measuring load of 60 kN; Joint 33, hollow stainless dowel, 4/wheelpath).

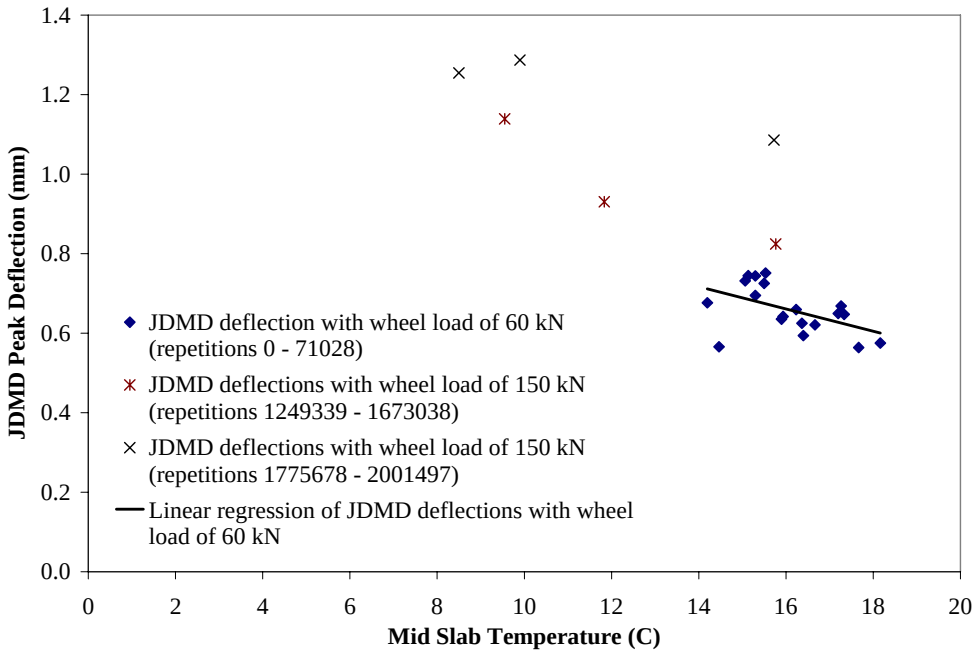

Figure 6.88. JDMD 4 peak deflection vs. mid-slab temperature on Section 559FD (with measuring load of 60 kN; Joint 32, epoxy-coated steel dowel, 4/wheelpath).

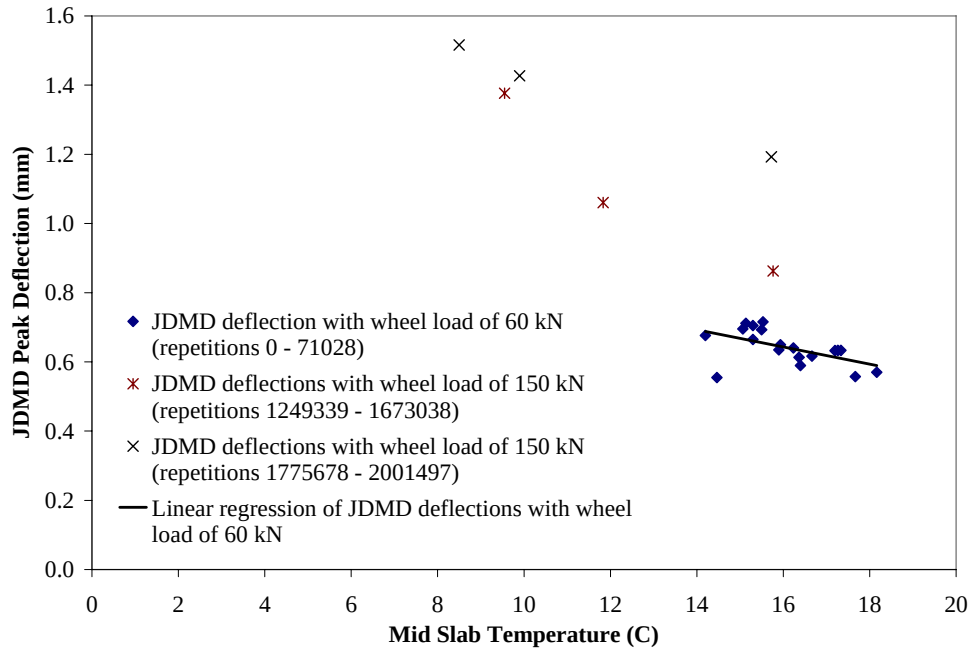

Figure 6.89. JDMD 5 peak deflection vs. mid-slab temperature on Section 559FD (with measuring load of 60 kN; Joint 32, epoxy-coated steel dowel, 4/wheelpath).

6.1.6.3 Load Transfer Efficiency

LTE for all the repetitions and mid-slab temperatures for Section 559FD are shown in Figure 6.90 under the HVS trafficking loads, while LTE with the measurement load of 60 kN are shown in Figure 6.91. Unlike JDMD peak deflection, LTE increases with temperature, but remains fairly stable as joints are subject to more repetitions and higher wheel loads. For all measured data, joint LTEs for 559FD are higher than 90 percent.

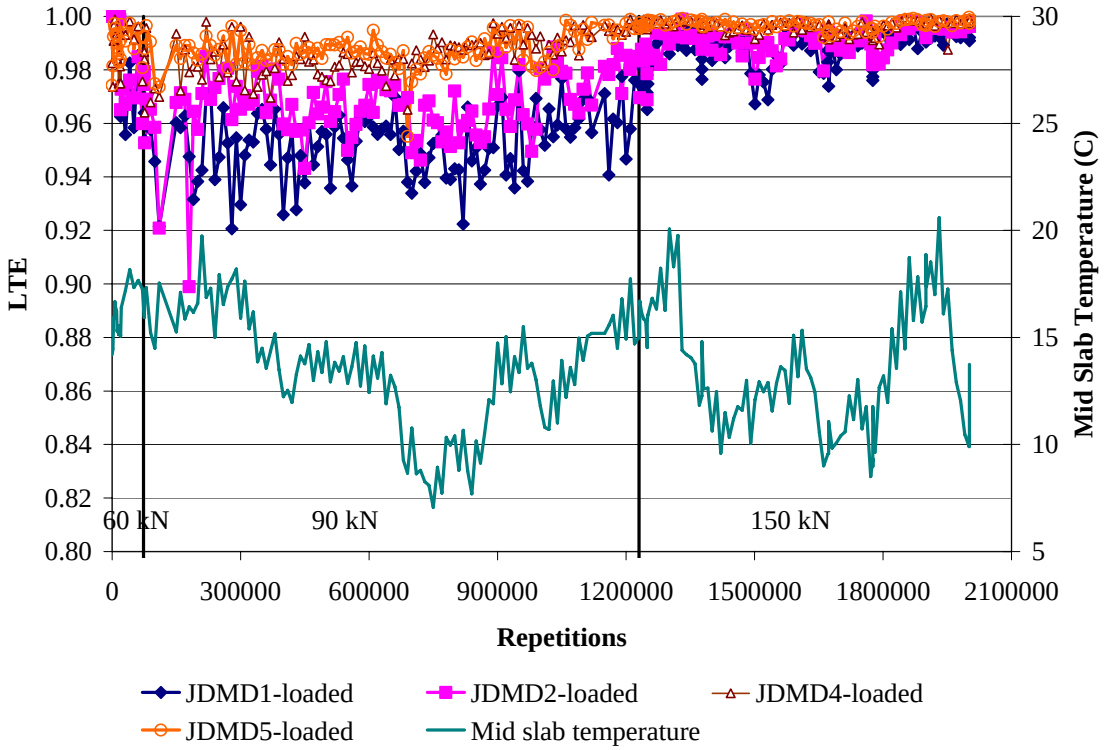

Figure 6.90. LTE for all repetitions under trafficking load on Section 559FD.

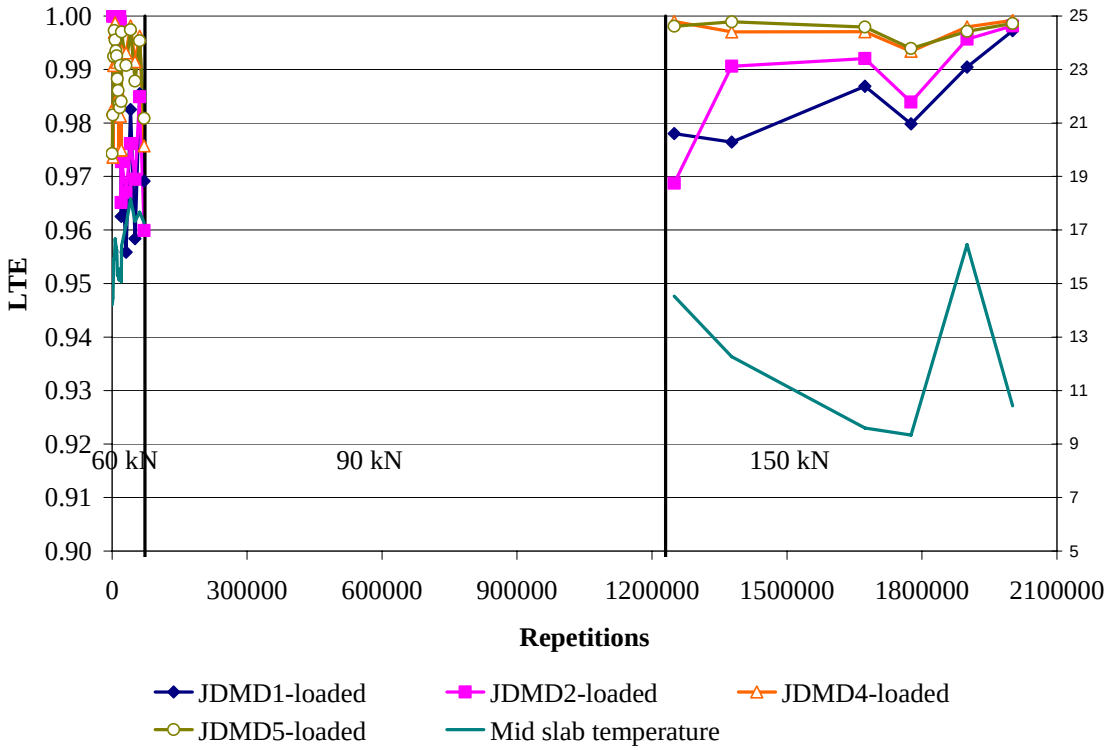

Figure 6.91. LTE under HVS measurement load of 60 kN on Section 559FD.

6.1.6.4 LTE vs. Mid-Slab Temperature

The joint LTE against the mid-slab temperature for Section 559FD are shown in Figure 6.92 through Figure 6.95. Only LTEs obtained under the measurement load (60 kN) are included in these figures. In Figure 6.94 and Figure 6.95 (Joint 32), the general trend is the same as what was found from Section 556FD to 558FD: LTE increases as temperature decreases. However, for Figure 6.92 and Figure 6.93 (Joint 33), the opposite trend is shown from the regression line of LTE with wheel load of 60 kN. From all these four figures, LTE is not reduced by millions of HVS repetitions. This joint is the only one in the test sections retrofitted with hollow stainless steel dowels.

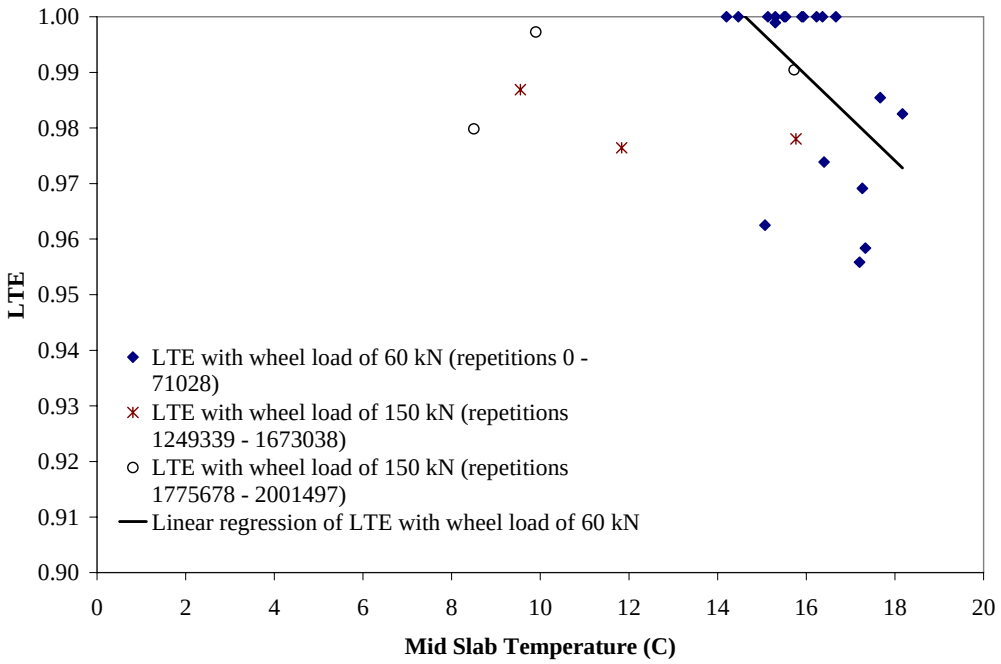

Figure 6.92. JDMD 1 LTE vs. mid-slab temperature on Section 559FD (with measuring load of 60 kN; Joint 33, hollow stainless steel dowel, 4/wheelpath).

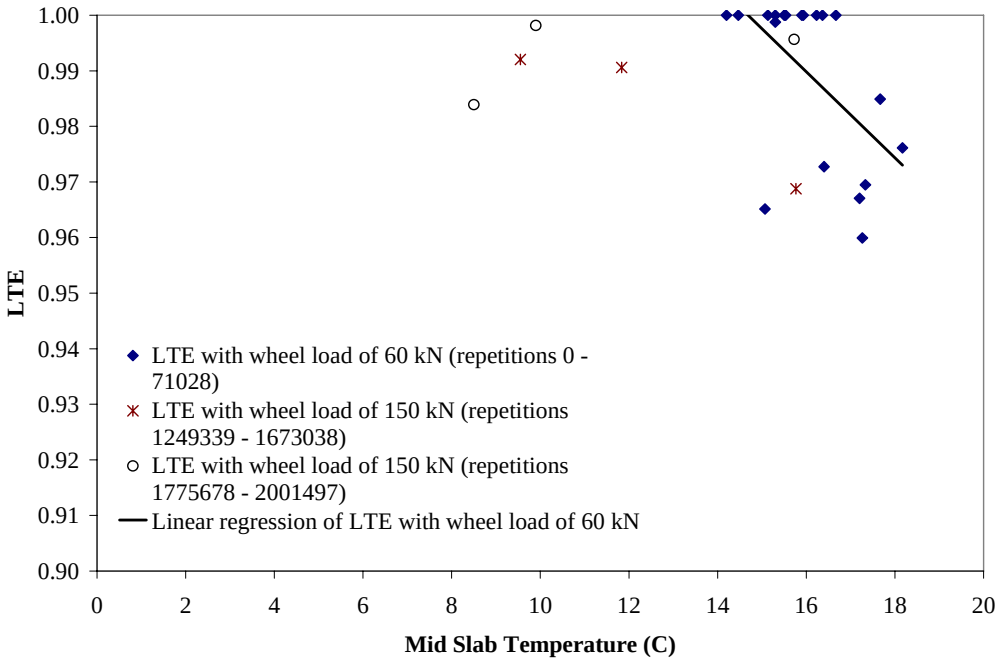

Figure 6.93. JDMD 2 LTE vs. mid-slab temperature on Section 559FD (with measuring load of 60 kN; Joint 33, hollow stainless steel dowel, 4/wheelpath).

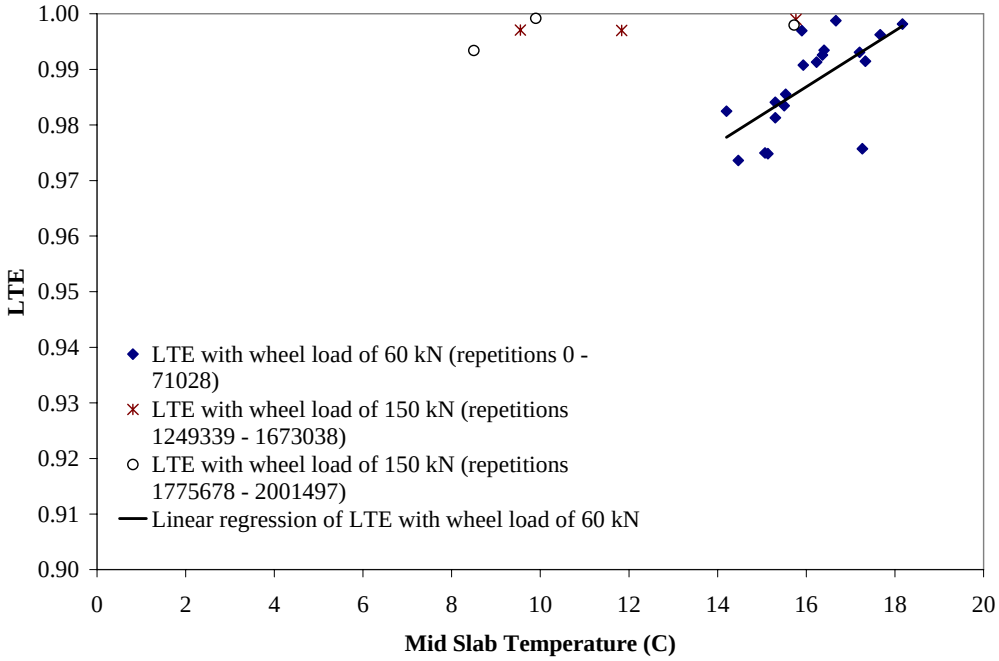

Figure 6.94. JDMD 4 LTE vs. mid-slab temperature on Section 559FD (with measuring load of 60 kN; Joint 32, epoxy-coated steel dowel, 4/wheelpath).

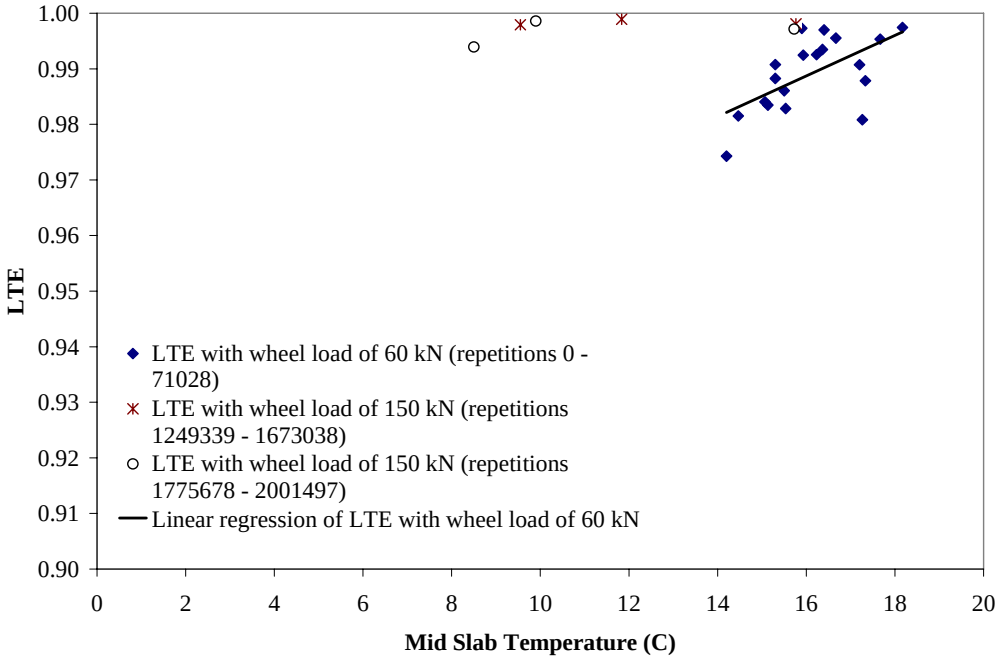

Figure 6.95. JDMD 5 LTE vs. mid-slab temperature on Section 559FD (with measuring load of 60 kN; Joint 32, epoxy-coated steel dowel, 4/wheelpath).

6.1.6.5 Slab Cracking and Final Condition

Figure 6.96 shows the final condition of Slab 33 at the end of HVS testing after 2.001 million load repetitions. It can be seen in the photograph that additional mid-slab transverse cracking developed around Crack 1. The final condition of the DBR on Joints 32 and 33 can also be seen in Figure 6.96. Figure 6.97 shows a close-up of the final cracking through the DBR on Crack 1. The final condition of Slabs 32, 33, and 34 at the time of forensic coring can be seen in Appendix B.

Figure 6.96. Final condition of Slab 33 showing additional cracking around Crack 1 after 2.001 million repetitions.

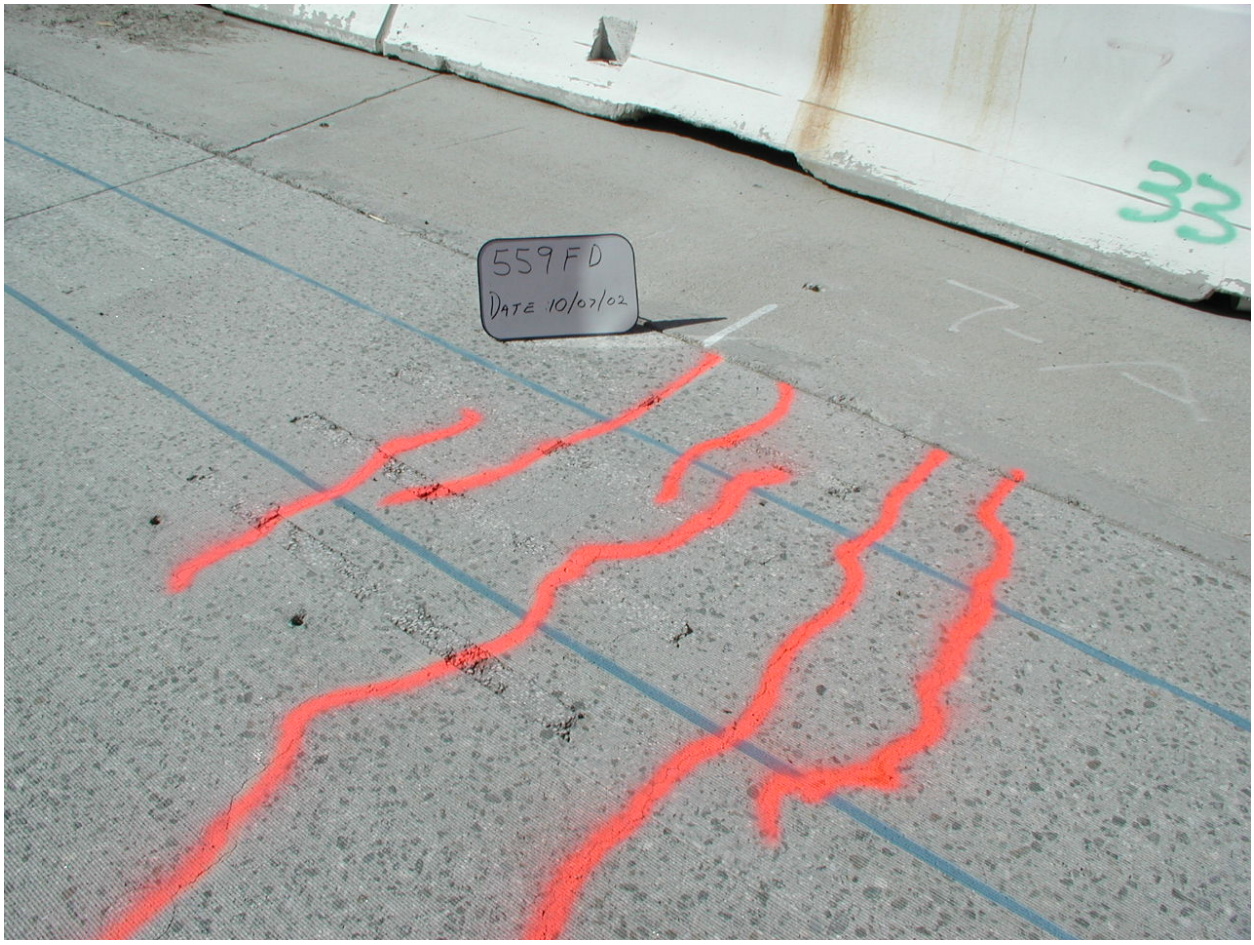

Figure 6.97. Close-up of final condition of Slab 33 and Crack 1.

6.2 FWD Results Analysis

6.2.1 April 2003

6.2.1.1 Backcalculated Stiffness

Pavement surface temperatures from April 2003 are summarized in Table 6.9 Backcalculated stiffness for concrete, support layer (base and subgrade), and subgrade k-values are shown in Table 6.10, based on center slab deflections.]

The FWD tests were performed from 1:35 p.m. to 2:52 p.m. on April 1, 2003 (daytime), and from 3:13 a.m. to 4:16 a.m. on April 2, 2003 (nighttime). Details of temperature and stiffness values for all the joints are shown in Figure 6.98 through Figure 6.100.

Table 6.9. Temperature Summary from April 2003

Location		Daytime		Nighttime	
		Average	**Standard Deviation**	**Average**	**Standard Deviation**
Center slab	Surface temperature (^oC)	33.4	1.4	10.3	0.8
	Air temperature (^oC)	18.7	0.6	6.8	0.5
Transverse joint	Surface temperature (^oC)	33.4	1.5	10.4	0.6
	Air temperature (^oC)	18.7	0.6	6.9	0.4

Table 6.10. Summary of Backcalculated Stiffnesses

		Daytime		Nighttime	
		Average	**Standard Deviation**	**Average**	**Standard Deviation**
Section 11 (Wide truck lane)	Concrete Stiffness E_{pcc} (MPa)	45,347	8,799	80,363	48,139
	Support stiffness $E_{sg+base}$ (MPa)	208	27	290	97
	Support k-value (MPa/m)	102	20	136	57
(Section 9) Doweled	Concrete Stiffness E_{pcc} (MPa)	46,934	8,224	59,463	20,329
	Support stiffness $E_{sg+base}$ (MPa)	225	38	234	93
	Support k-value (MPa/m)	110	20	110	51
Section 7 (DBR section)	Concrete Stiffness E_{pcc} (MPa)	42,905	8,771	53,668	23,076
	Support stiffness $E_{sg+base}$ (MPa)	213	34	225	79
	Support k-value (MPa/m)	106	21	111	52
All	Concrete Stiffness E_{pcc} (MPa)	44,975	8,658	62,515	31,913
	Support stiffness $E_{sg+base}$ (MPa)	216	34	245	92
	Support k-value (MPa/m)	107	21	117	54

It can be seen in Table 6.9 that the daytime pavement surface temperature is almost 23°C higher than the nighttime pavement surface temperature. Consequently, from Table 6.10 and Figure 6.98 through Figure 6.100 it can be seen that in general, the nighttime stiffness and k-values are much higher than the daytime values. For the average nighttime values of the whole test set, the concrete stiffness is 39.0 percent higher, the support layer stiffness is 13.3 percent higher, and subgrade k-values are 9.4 percent higher than the daytime average values. Again, the temperature influences the backcalculated concrete layer properties more because of slab curling caused by temperature gradients in the concrete slab, and has little influence on support layer (base and subgrade) properties except as they are affected by slab curl. As with April and October 2002 FWD test results, the subgrade/base support layers exhibit high linearity of stiffness with respect to load.

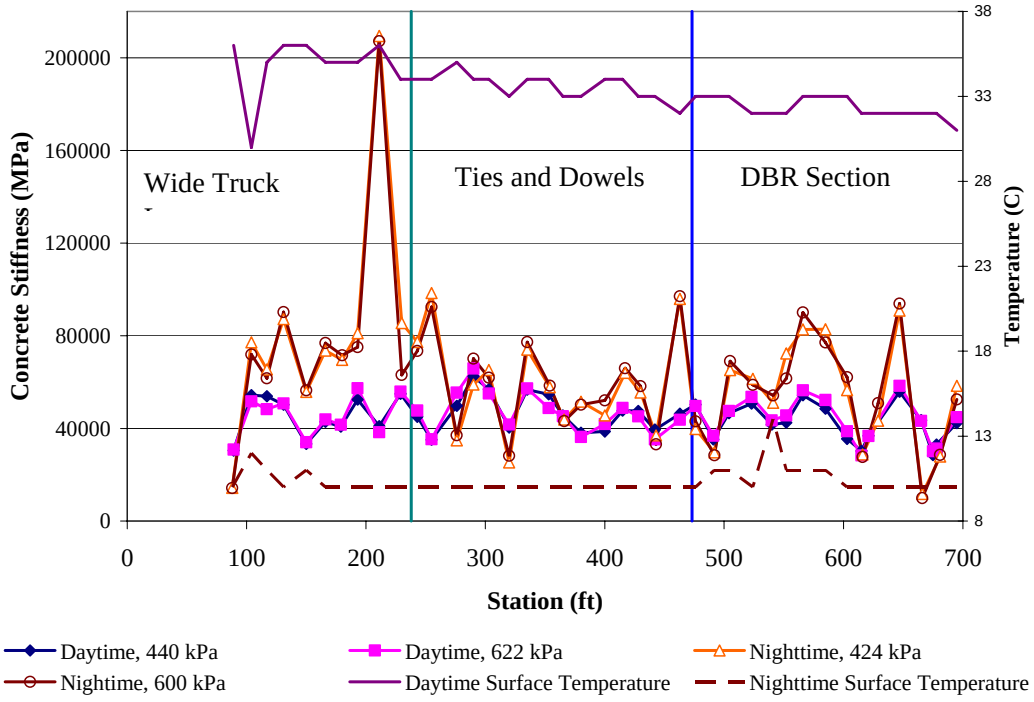

Figure 6.98. Backcalculated concrete stiffness from center slab deflection, April 2003.

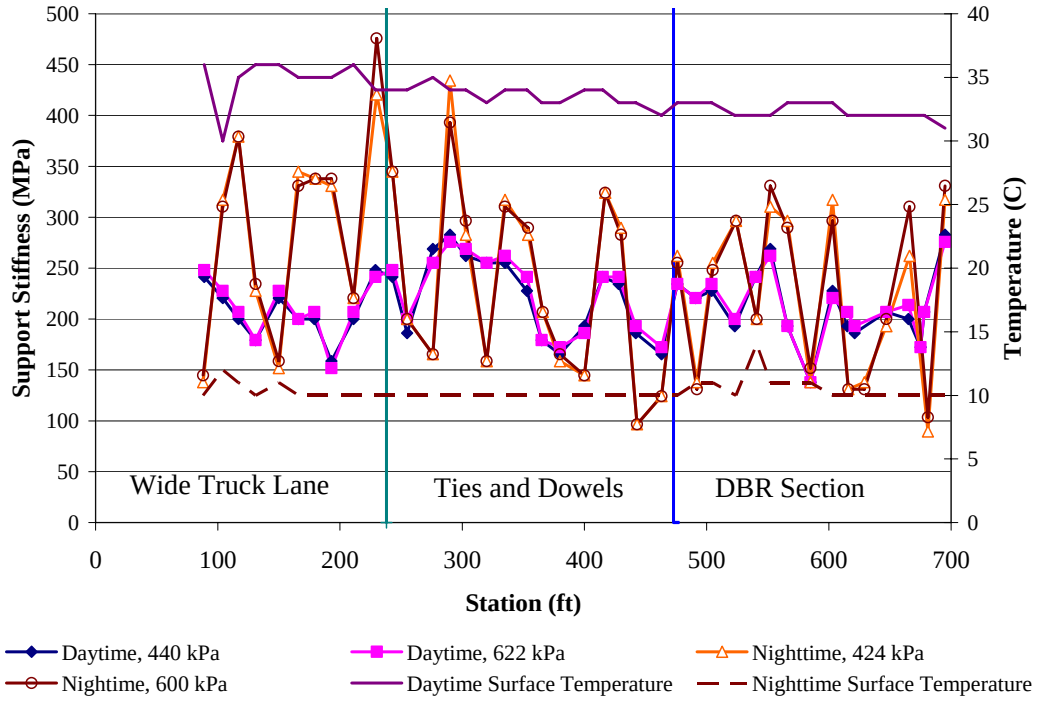

Figure 6.99. Backcalculated support layer stiffness from center slab deflections, April 2003.

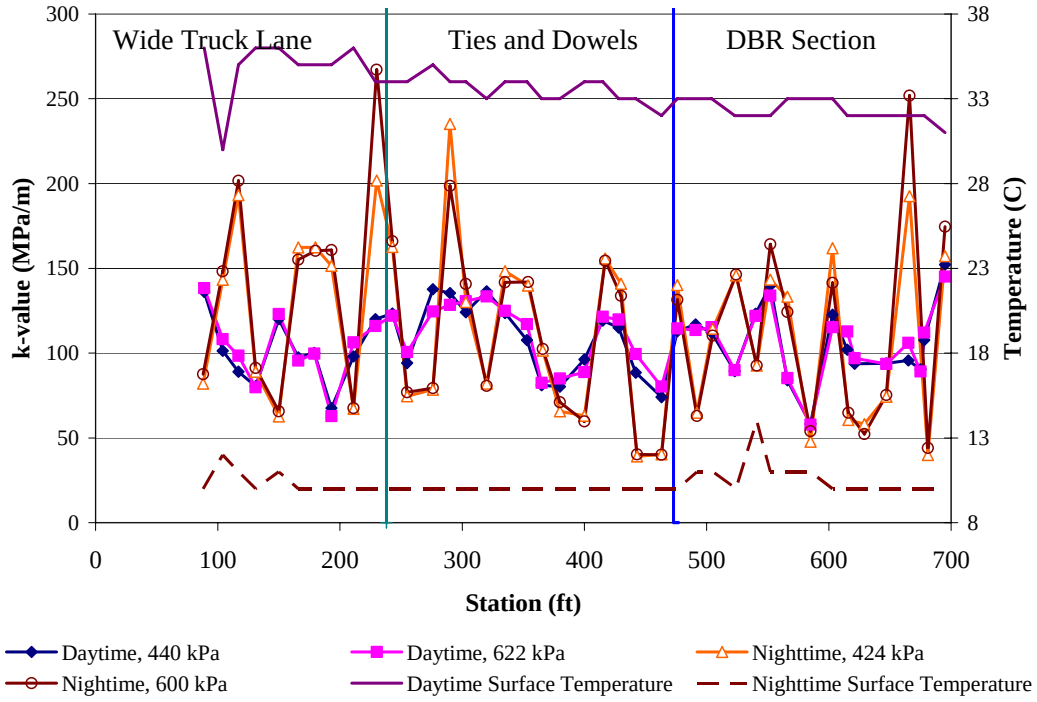

Figure 6.100. Backcalculated subgrade k-value from center-slab deflections, April 2003.

6.2.1.2 Load Transfer Efficiency

The daytime and nighttime measured load transfer efficiency from the April 2003 FWD tests for North Tangent is shown in Table 6.11 and Figure 6.101. In Table 6.11, only the LTE of DBR joints in Section 7 are included in "DBR joints." For Section 11 (wide truck lane) and Section 9 (initially doweled and tied), joint LTEs are consistently higher than 90 percent. During daytime, the average pavement surface temperature is 33.4°C and the LTEs under such a high temperature are always higher than 95 percent (Figure 6.101).

Table 6.11. LTE Summary from FWD Tests in April 2003

	Daytime		Nighttime	
	Average	**Standard Deviation**	**Average**	**Standard Deviation**
Wide truck lane	96.8%	0.8%	93.4%	1.3%
Ties and dowels	96.8%	0.7%	93.5%	1.6%
DBR joints	97.7%	1.3%	87.8%	5.0%

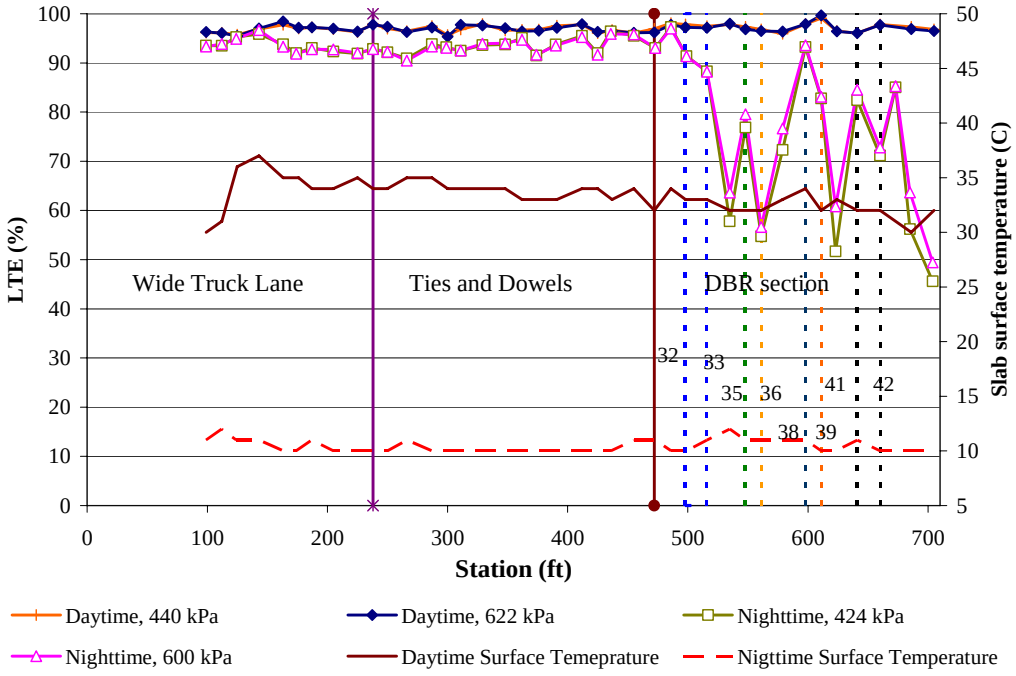

Figure 6.101. Load Transfer Efficiency, April 2003.

The average nighttime LTE values for DBR joints (Section 7) are significantly lower than those of Section 11 and Section 9 with their originally installed dowels. Details of nighttime joint LTEs for Section 7 are shown in Figure 6.101 and Table 6.12, with the latter showing both the undoweled and the DBR joint details. From Table 6.12, it can be seen that the average nighttime LTE of DBR joints is 12 percent higher than that of undoweled joints. Similar to the data shown in Table 5.11, Joint 36 has an LTE which is much lower than other joints; and this joint has only three dowel bars per wheelpath. If Joint 36 is not considered, it can be seen that the DBR joints have LTE values that are 3 to 21 percent greater than that of the undoweled joints.

Table 6.12. Average Nighttime LTE of Section 7 (DBR Section), April

		Joint no.	LTE	Average LTE of each dowel type	Overall Average LTE	Overall Standard Deviation
Doweled	ECS[1] dowel, 4pw[2]	32	91%	88%	81%	12%
		38	93%			
		39	83%			
		41	83%			
	ECS dowel, 3pw	35	78%	67%		
		36	56%			
	HSS[3] dowel, 4pw	33	88%	88%		
	FRP dowel, 4pw	42	72%	72%		
Un-doweled	31		97%	69%		17%
	34		61%			
	37		74%			
	40		56%			
	43		85%			
	44		60%			
	45		48%			

[1]: ECS: epoxy-coated steel
[2]: pw: per wheelpath
[3]: HS: hollow stainless steel

6.2.2 June 2003

6.2.2.1 Backcalculated Stiffness

Pavement surface temperatures from June 2003 are summarized in Table 6.13. Backcalculated concrete and support layer stiffness together with subgrade k-values are shown in Table 6.14. The FWD tests were conducted from 12:30 p.m. to 3:12 p.m. (daytime) and from 4:25 a.m. to 6:31 a.m. (nighttime). Average daytime pavement surface temperature is about 22^{o}C higher than nighttime average temperature. Details of temperatures and stiffness values for all the joints in North Tangent are shown in Figure 6.102 through Figure 6.104.

Nighttime concrete stiffnesses are higher than daytime stiffness values, as was the case from previous FWD testing, due to better contact between the slab and support layers at the center of the slab. For the whole test set average, nighttime concrete stiffness is 25.9 percent higher than daytime stiffness. From Figure 6.103 and Figure 6.104, there is not much difference between daytime and nighttime support stiffness as well as subgrade k-values.

Table 6.13. Temperature Summary from June 2003

Location		Daytime		Nighttime	
		Average	Standard Deviation	Average	Standard Deviation
Center slab	Surface temperature (^{o}C)	34.2	1.5	12.1	0.9
	Air temperature (^{o}C)	19.9	0.6	9.4	0.5
Transverse joint	Surface temperature (^{o}C)	34.2	1.2	12.2	0.9
	Air temperature (^{o}C)	19.9	0.6	9.4	0.6

Table 6.14. Summary of Backcalculated Stiffness, June 2003

		Daytime		Nighttime	
		Average	Standard Deviation	Average	Standard Deviation
Wide truck lane	Concrete Stiffness E_{pcc} (MPa)	42,021	16,065	57,533	18,185
	Support stiffness $E_{sg+base}$ (MPa)	273	41	316	116
	Support k-value (MPa/m)	151	34	164	69
Doweled	Concrete Stiffness E_{pcc} (MPa)	50,006	9,971	61,530	36,232
	Support stiffness $E_{sg+base}$ (MPa)	261	48	228	98
	Support k-value (MPa/m)	131	31	107	53
DBR section	Concrete Stiffness E_{pcc} (MPa)	45,127	10,174	53,588	30,233
	Support stiffness $E_{sg+base}$ (MPa)	266	42	210	93
	Support k-value (MPa/m)	139	27	102	57
All	Concrete Stiffness E_{pcc} (MPa)	45,718	12,694	57,551	28,369
	Support stiffness $E_{sg+base}$ (MPa)	267	43	50	111
	Support k-value (MPa/m)	140	31	123	67

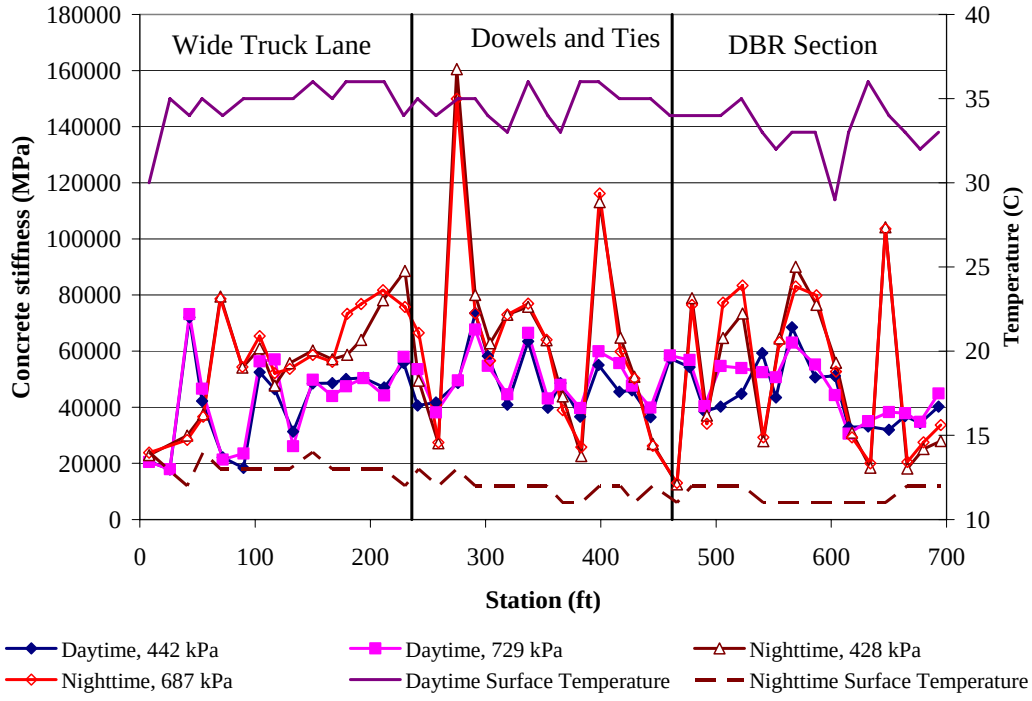

Figure 6.102. Backcalculated concrete stiffness from center slab deflection, June 2003.

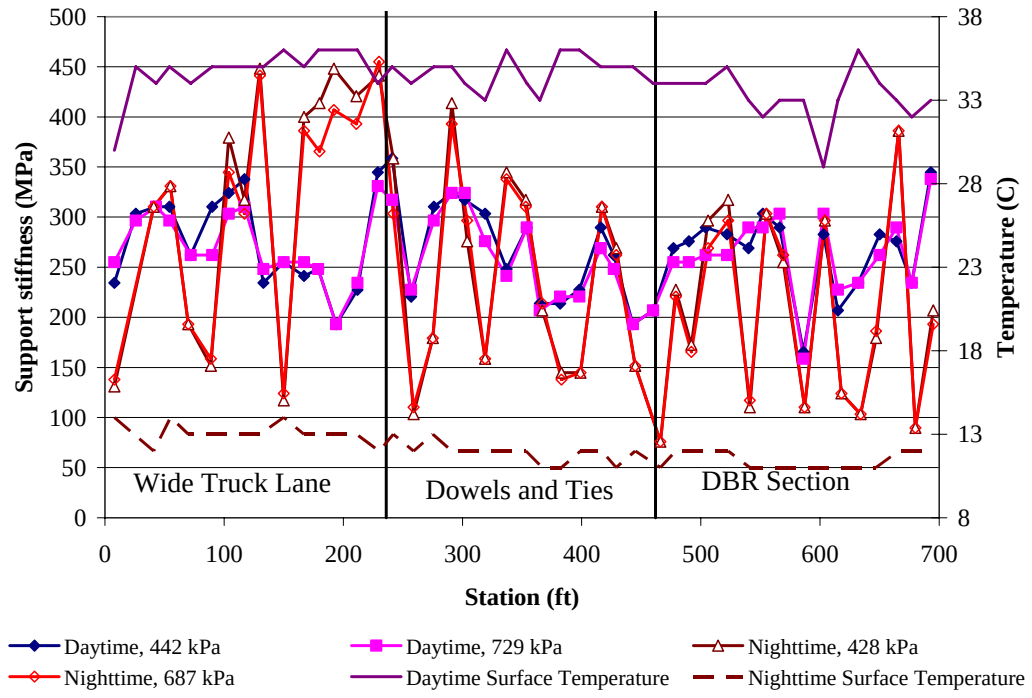

Figure 6.103. Backcalculated support layer stiffness from center slab deflections, June 2003.

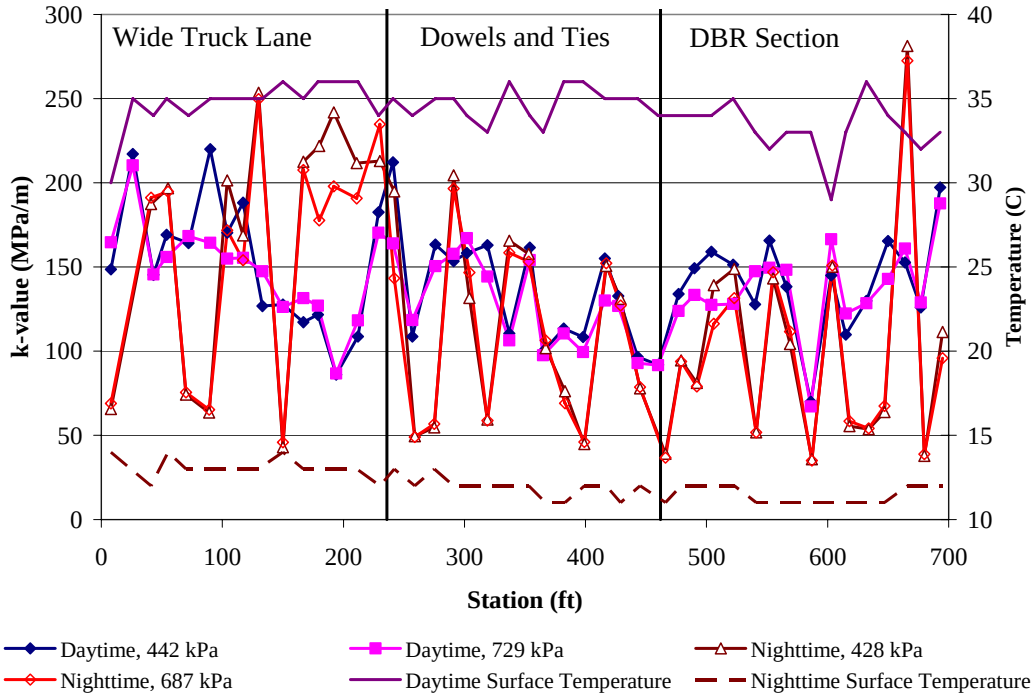

Figure 6.104. Backcalculated subgrade k-values from center slab deflections, June 2003.

6.2.2.2 Load Transfer Efficiency

Both daytime and nighttime measured load transfer efficiencies calculated from June 2003 FWD testing data are shown in Table 6.15 and Figure 6.105. Average daytime pavement surface temperature is 34.2°C, and all the daytime LTEs are higher than 95 percent. Average nighttime temperature is 12.2°C. Such a nighttime temperature is not extremely low; however, from Figure 6.105 it can be seen that even some joints in Section 11 (wide truck lane) and Section 9 (initially doweled and tied) show relatively low nighttime LTE. For the LTE backcalculated from the before-HVS FWD test data, joints in Section 11 and Section 9 always showed high LTE under low nighttime temperatures. Compared with those results, it seems that HVS testing damaged some joint LTEs in Section 11 and Section 9.

For Section 7 (DBR section), the average LTE is still lower than those of Section 11 and Section 9. However, the LTE for doweled joints in this section did not change much compared with the LTE calculated from previous FWD tests. More detailed comparison among different FWD test backcalculation results will be demonstrated in a later section. Details of nighttime joint LTEs for Section 7 are shown in Figure 6.105 and Table 6.16. In this FWD test, two dowel bar retrofitted cracks (Crack 1 and Crack 2) were also tested.

Table 6.15. LTE Summary from FWD Tests in June 2003

	Daytime		Nighttime	
	Average	**Standard Deviation**	**Average**	**Standard Deviation**
Wide truck lane	95%	1.4%	90%	10.8%
Ties and dowels	96%	1.1%	95%	4.2%
DBR section (doweled joints)	96%	1.4%	89%	12.3%

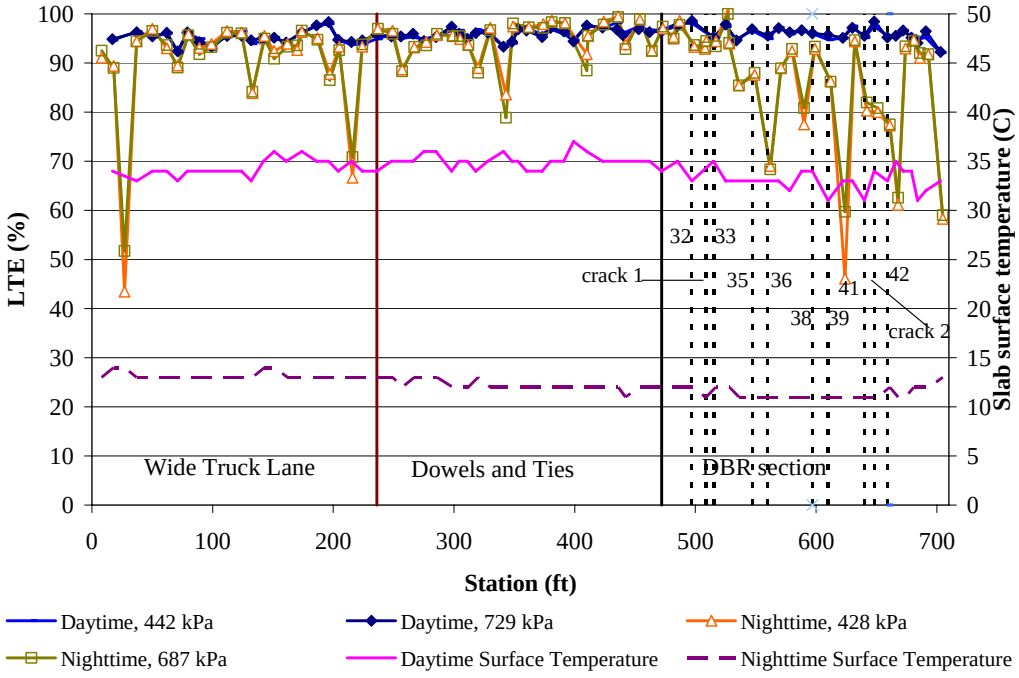

Figure 6.105. Load Transfer Efficiency, June 2003.

From Table 6.16, it can be seen that the average LTE for doweled joints is only 4.3 percent higher than that of undoweled joints. Compared with the LTE for the DBR section calculated from the April 2003 FWD test the average retrofitted joint LTEs are close, while the average unretrofitted joint LTE from June 2003 FWD test is 18.4 percent higher than that from the April 2003 FWD test. Such an LTE increase is possibly due to the minor temperature increase: the nighttime temperature for the June 2003 FWD test is 1.8°C higher. No other possible reason for the increase was identified. Again, Joint 36, which only has three dowels per wheelpath, showed the lowest LTE.

Table 6.16. Average Nighttime LTE of Section 7 (DBR Section), June 2003

	Dowel Type	Joint No.	LTE	Average LTE of Each Dowel Type	Overall Average LTE	Standard Deviation
Doweled	ECS[1] dowel, 4pw[2]	32	93%	88%	86%	8.4%
		38	93%			
		39	86%			
		41	81%			
	ECS dowel, 3pw	35	88%	78%		
		36	69%			
	HSS[3] dowel, 4pw	Crack 1	94%	94%		
		34	94%			
	FRP dowel, 4pw	Crack 2	80%	79%		
		42	77%			
Un-doweled	31		95%	81%		17%
	34		85%			
	37		93%			
	40		53%			
	43		93%			
	44		92%			
	45		59%			

1: ECS: epoxy-coated steel
2: pw: per wheelpath
3: HS: hollow stainless steel

6.2.3 February 2004

6.2.3.1 Backcalculated Stiffness

Air temperatures and pavement surface temperatures from February 2004 are shown in Table 6.17. Backcalculated layer moduli and k-values are shown in Table 6.18.

The FWD tests were performed from 12:25 p.m. to 1:00 p.m. (Daytime 1) and from 8:44 a.m. to 10:41 am (Daytime 2) on February 28, 2004. The Daytime 1 tests were only performed on Section 7 (DBR section). Pavement surface temperature and backcalculated layer stiffness for each joint are shown in Figure 6.106 through Figure 6.108. For this test, the Daytime 1 and Daytime 2 temperatures are very close. As a result, the Daytime 1 and Daytime 2 layer stiffnesses are relatively close to each other. Again, the measured stiffness and k-values do not change much with different FWD loads, which indicates the subgrade/base support can be considered to be linear.

Table 6.17. Temperature Summary from February 2004

Location		Daytime 1		Daytime 2	
		Average	**Standard Deviation**	**Average**	**Standard Deviation**
Center slab	Surface temperature (°C)	10.9	0.6	10.3	2.3
	Air temperature (°C)	11.4	0.4	10.6	2.1
Transverse joint	Surface temperature (°C)	10.9	0.5	10.3	2.3
	Air temperature (°C)	11.3	0.6	10.7	2.0

Table 6.18. Summary of Backcalculated Stiffnesses

		Daytime 1		Daytime 2	
		Average	**Standard Deviation**	**Average**	**Standard Deviation**
Wide truck lane	Concrete Stiffness E_{pcc} (MPa)	—	—	666,26	51,737
	Support stiffness $E_{sg+base}$ (MPa)	—	—	269	81
	Support k-value (MPa/m)	—	—	143	65
Doweled	Concrete Stiffness E_{pcc} (MPa)	—	—	54,477	35,488
	Support stiffness $E_{sg+base}$ (MPa)	—	—	249	82
	Support k-value (MPa/m)	—	—	126	53
DBR section	Concrete Stiffness E_{pcc} (MPa)	46,768	15,873	51,544	15,110
	Support stiffness $E_{sg+base}$ (MPa)	235	53	240	57
	Support k-value (MPa/m)	118	41	115	29

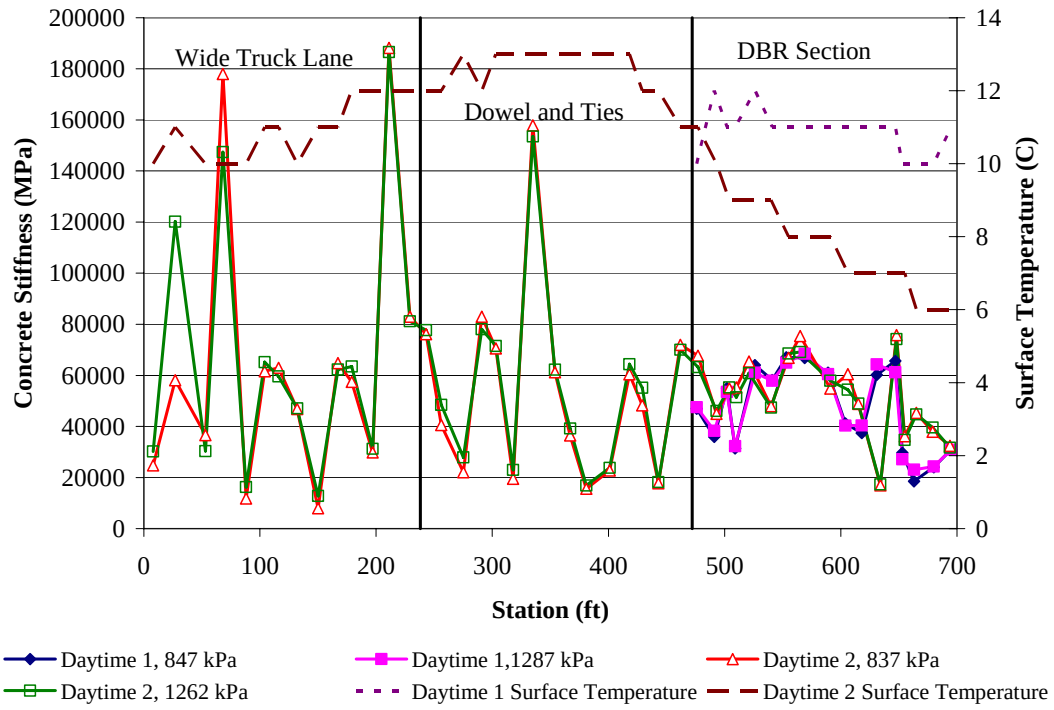

Figure 6.106. Backcalculated concrete stiffness from center slab deflection, Feb. 2004.

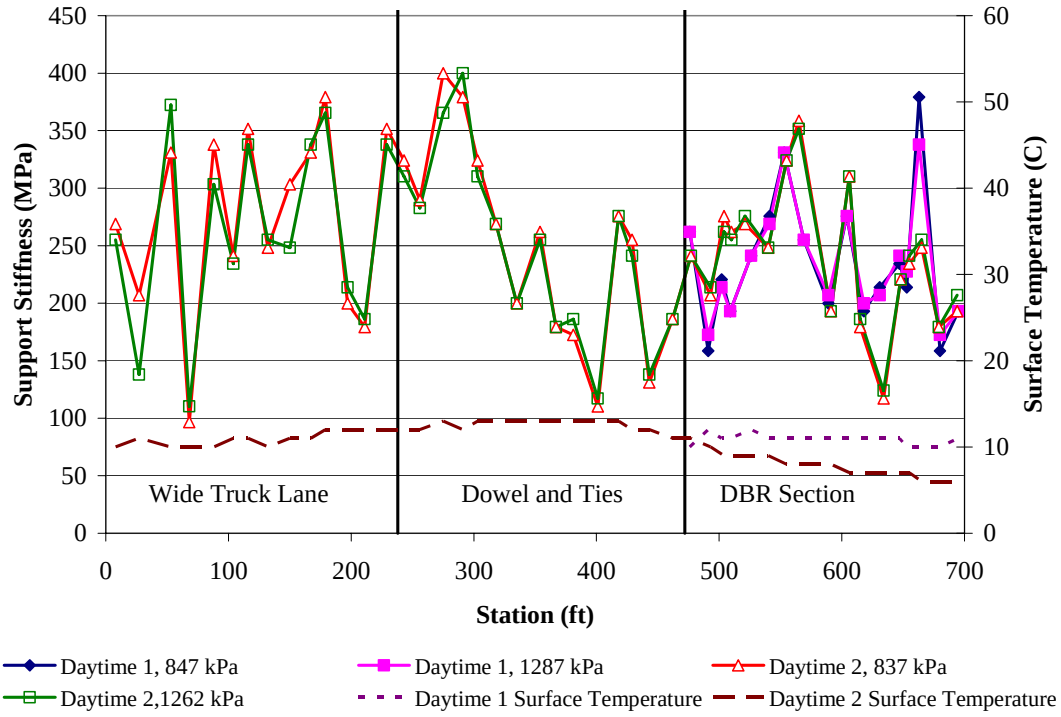

Figure 6.107. Backcalculated support layer stiffness from center slab deflections, Feb. 2004.

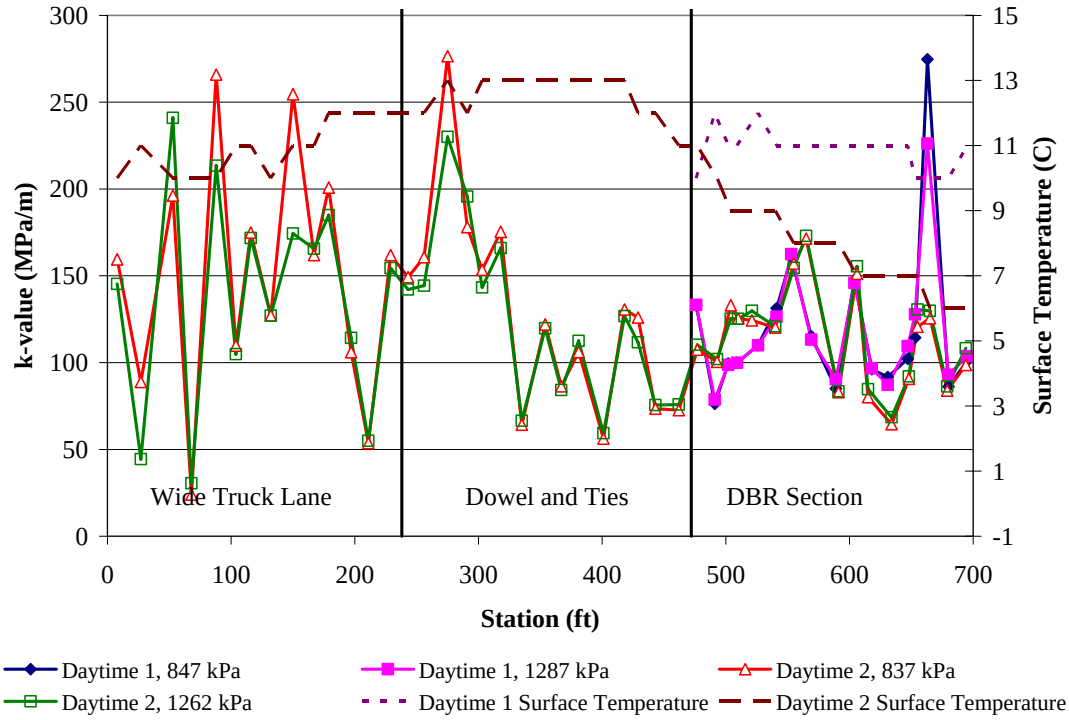

Figure 6.108. Backcalculated subgrade k-value from center slab deflections, Feb. 2004.

6.2.3.2 Load Transfer Efficiency

The Daytime 1 and Daytime 2 measured Load Transfer Efficiency from the February 2004 FWD tests for North Tangent are shown in Table 6.19 and Figure 6.109. All the LTEs for Section 11 (wide truck lane) and Section 9 (initially with dowels and ties) are above 90 percent. The air temperatures for both Daytime 1 and Daytime 2 tests are relatively low (around 11^{o}C), and the average LTEs for Section 7 (DBR section) are also much lower than those of Section 9 and 11. Details of joint LTEs for Section 7 are shown in Figure 6.109 and Table 6.20 for the eight joints and two cracks that were dowel bar retrofitted.

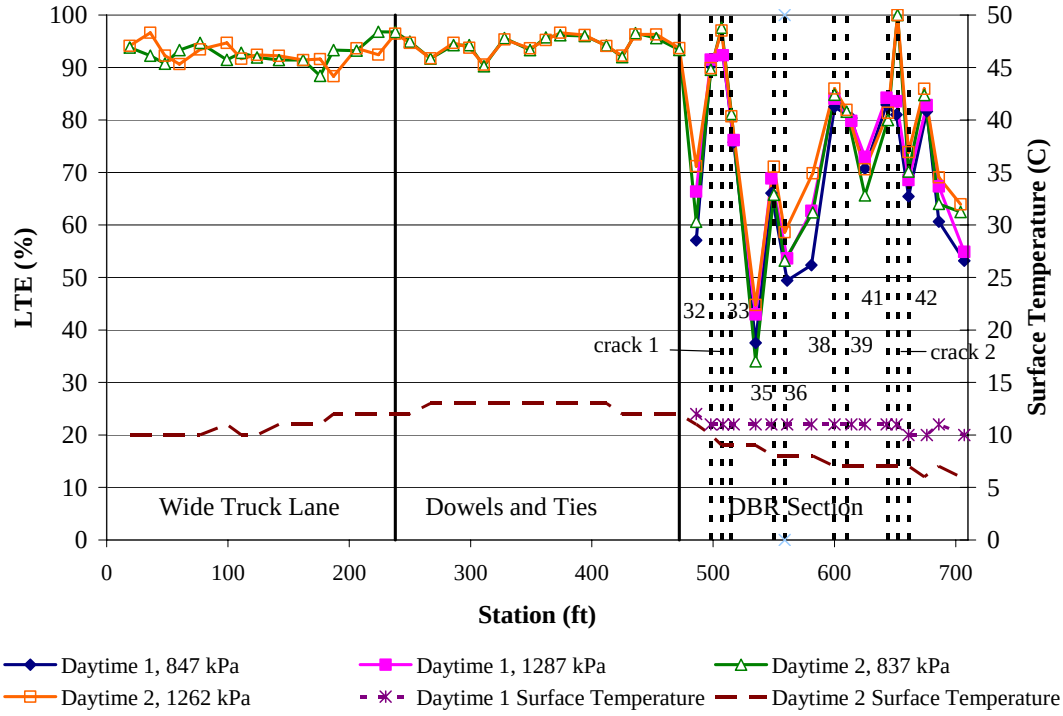

Figure 6.109. Load Transfer Efficiency, February 2004.

It can be seen from Table 6.20 that at a surface temperature of around 10.7°C, that the overall average LTE for doweled joints is 79 percent, 16 percentage points higher than the 63 percent for the undoweled joint LTE. This surface temperature is similar to that from April 2003 nighttime (10.4°C), and the average LTE values are also close to those from April 2003 nighttime (Table 6.12). However, compared to the LTE from June 2003 nighttime — which had an average surface temperature of 12.2°C (Table 6.16) — the average LTE for doweled joints is 6.3 percentage points lower and for undoweled joints it is 18 percentage points lower.

In summary, all of the FWD data generally show considerable improvement of deflections and LTE for the DBR joints, although the performance is not as good as that of the originally installed dowels on Sections 9 and 11. The data in Table 6.20 also indicate that joints with three dowels per wheelpath (Joints 35 and 36) exhibit lower LTEs than all the dowel bar retrofits with four dowels per wheelpath.

Table 6.19. LTE Summary from FWD Tests in February 2004

	Daytime 1		Daytime 2	
	Average	**Standard Deviation**	**Average**	**Standard Deviation**
Wide truck lane	—	—	93%	2%
Ties and dowels	—	—	94%	2%
DBR section (DBR joints only)	71%	15%	75%	15%

Table 6.20. Average LTE of Section 7 (DBR Section), February 2004

	Dowel Type	**Joint No.**	**LTE**	**Average LTE for Each Dowel Type**	**Overall Average LTE**	**Standard Deviation**
Doweled	ECS[1] dowel, 4pw[2]	32	90%	84%	79%	13%
		38	84%			
		39	81%			
		41	82%			
	ECS dowel, 3pw	36	54%	61%		
		35	68%			
	HSS[3] dowel, 4pw	33	78%	87%		
		crack 1	95%			
	FRP dowel, 4pw	crack 2	91%	80%		
		42	70%			
Un-doweled	31		64%	63%		13%
	34		40%			
	37		62%			
	40		70%			
	43		84%			
	44		65%			
	45		59%			

7 COMPARISON BETWEEN PALMDALE AND UKIAH DBR SECTIONS, AND UKIAH/PALMDALE DBR AND PALMDALE LLPRS SECTIONS USING FWD AND HVS RESULTS

This chapter presents focused comparisons of the measured performance of dowel types and number of dowels per wheelpath, DBR and originally installed dowels (OID), and the DBR performance of the Palmdale HVS test sections with that of the Ukiah test sections.

7.1 Comparison between Palmdale DBR Sections

7.1.1 FWD Results

7.1.1.1 Backcalculated Stiffness

Concrete slab stiffness, support layer stiffness, and subgrade moduli backcalculated from FWD data before and after DBR for Section 7 (DBR section) are shown in Table 7.1 and Figure 7.1, Figure 7.2, and Figure 7.3. The results are averaged across all slabs in the test section regardless of whether they had DBR or not, and split between daytime and nighttime without correction for actual temperatures.

As it has been discussed previously in this report (see Section 3.4), the layer stiffness and k-value are significantly influenced by the temperature and vertical temperature gradient in the slab. In general, pavement layers show higher stiffness under lower temperatures and the negative (cooler on top) temperature gradients that occurred at night. From Table 7.1 and Figure 7.1, Figure 7.2, and Figure 7.3, it can be seen that the layer moduli and k-value did not change much after DBR and HVS testing. Higher temperature and the associated positive (hotter on top) temperature gradients result in the edges of the slabs curling down, resulting in the slab being supported more on its corners. This reduces the contact pressure between the slab center and the underlying layer, which results in higher deflections and consequently lower backcalculated values for concrete slab stiffness, underlying layer stiffnesses, and k-values.

Table 7.1 Summary of Backcalculated Stiffness of DBR Section before and after DBR

			Concrete Stiffness E_{pcc} (MPa)	Support Stiffness $E_{sg+base}$ (MPa)	Support k-value (MPa/m)
Before DBR	Daytime	Average	52,421	214	100
		Standard Deviation	17,149	58	30
	Nighttime	Average	47,786	197	95
		Standard Deviation	26,982	71	37
After DBR, before HVS	Daytime	Average	47,784	248	129
		Standard Deviation	18,715	94	73
	Nighttime	Average	42,539	216	116
		Standard Deviation	22,739	94	79
After DBR, after HVS	Daytime	Average	44,968	237	121
		Standard Deviation	12,117	48	34
	Nighttime	Average	52,874	226	109
		Standard Deviation	22,032	77	48

Some cracking of the slabs due to HVS trafficking certainly changed the contact for those slabs and affected the average values presented in the table and figures.

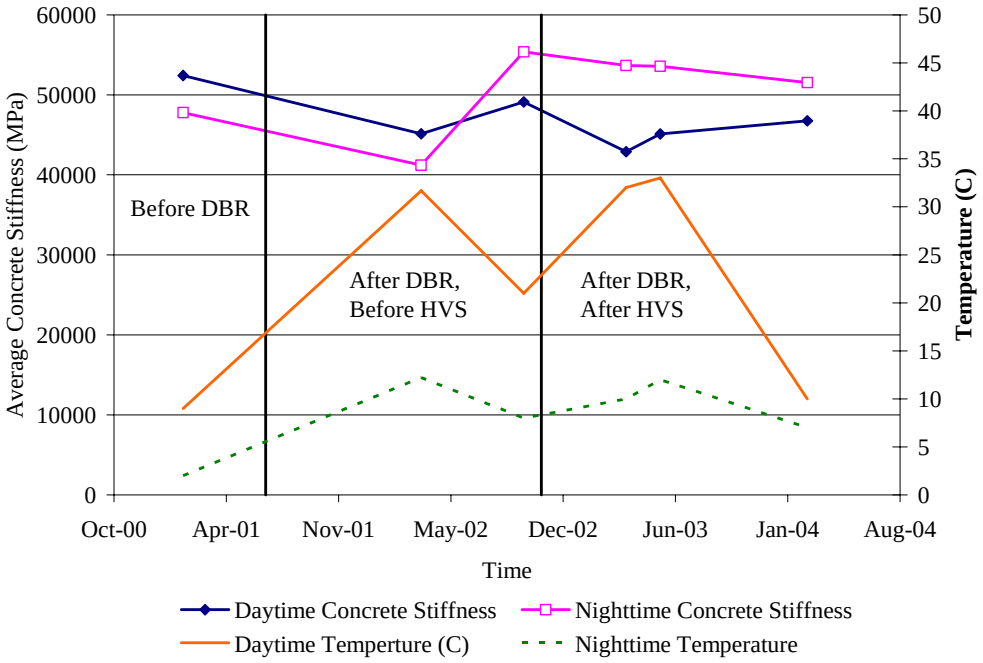

Figure 7.1. Backcalculated concrete stiffness before and after DBR.

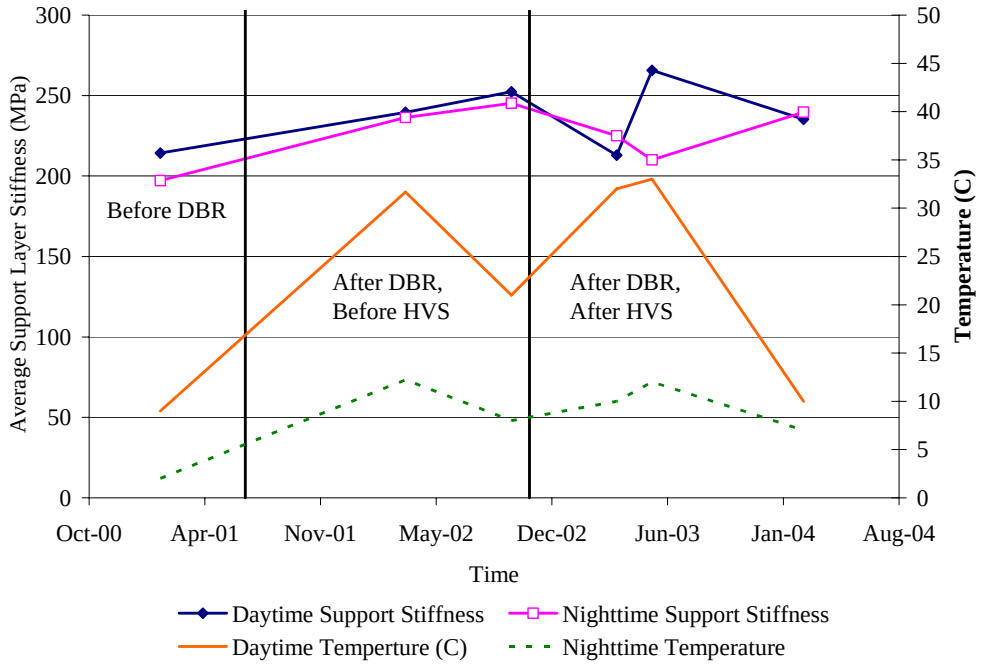

Figure 7.2. Backcalculated support layer stiffness before and after DBR.

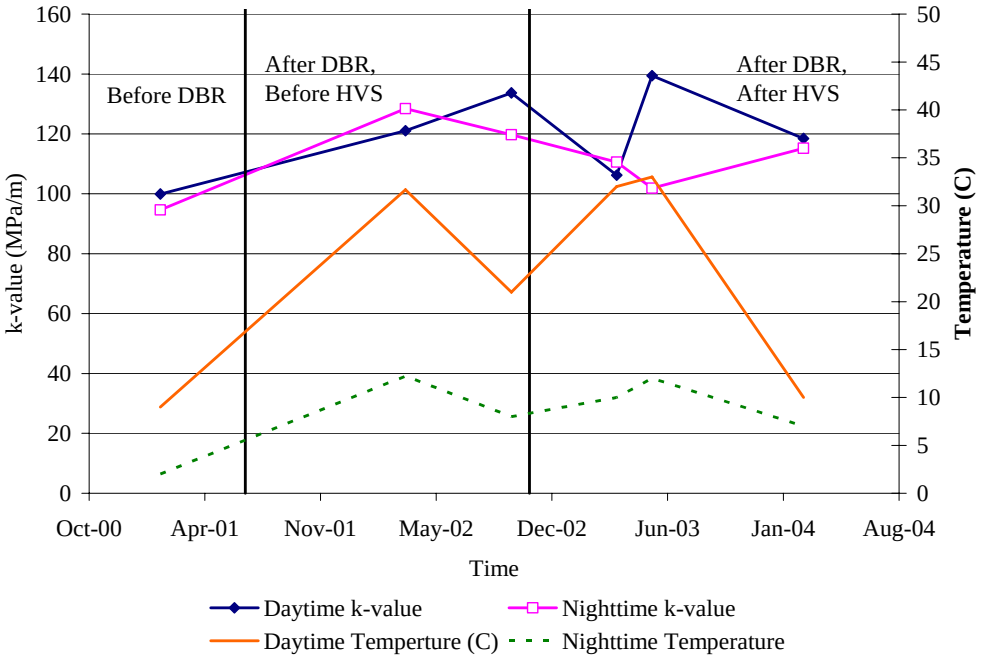

Figure 7.3. Backcalculated subgrade k-value before and after DBR.

7.1.1.2 Load Transfer Efficiency

LTE for DBR joints before DBR, after DBR but before HVS testing, and after DBR and HVS testing are shown in Figure 7.4 through Figure 7.11 for each retrofitted joint and crack. From these figures, it

appears that LTE for all retrofitted joints increased significantly after DBR, and was not significantly damaged after millions of HVS repetitions. It can also be seen that the expected trend of greater LTE values occurring at higher temperatures was also observed. As was discussed in Section 3.4 of this report, this is expected because higher temperatures cause the joint opening between slabs to close or even go into compression, thus producing very good aggregate interlock. Comparison among dowels made of different materials and different dowel bar amount per wheel path will be shown in Section 7.2.

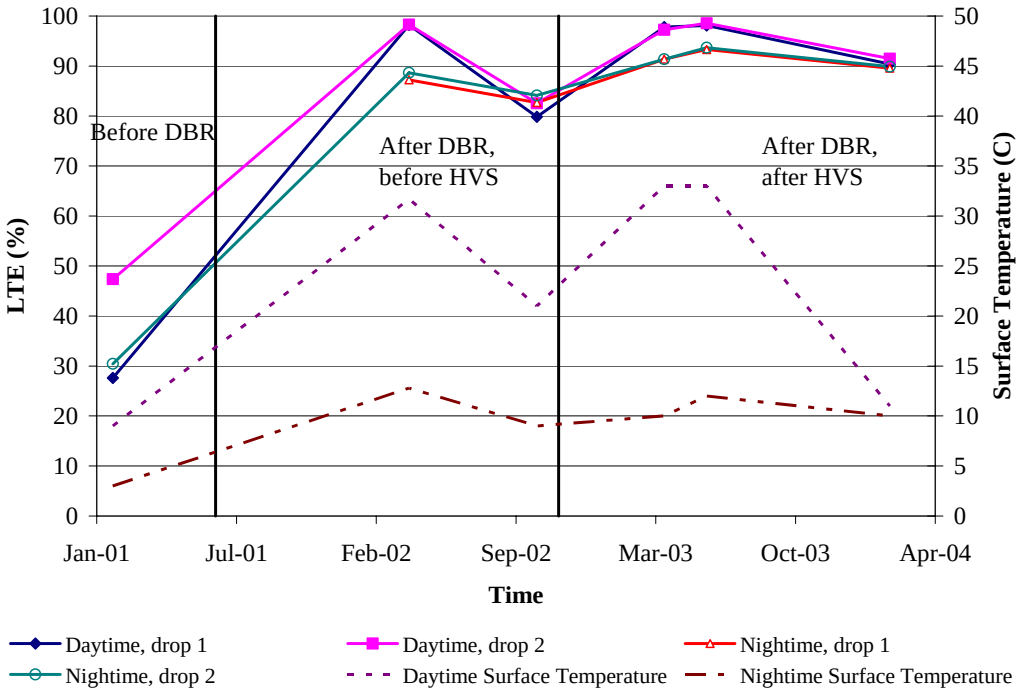

Figure 7.4. LTE from FWD before DBR, after DBR but before HVS testing, and after DBR and HVS testing for Joint 32 (epoxy-coated steel dowel, 4/wheelpath).

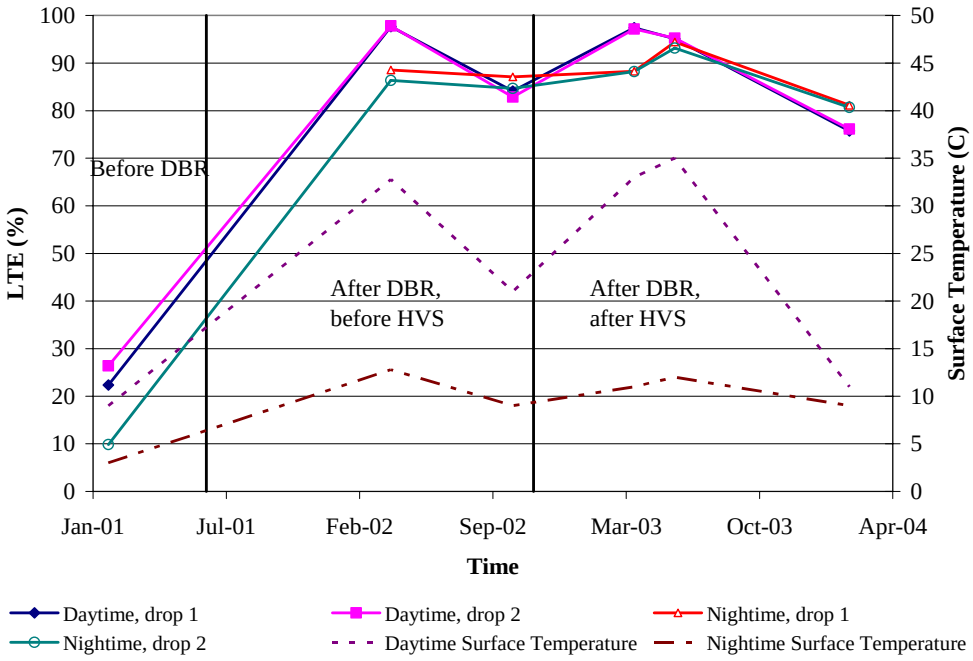

Figure 7.5. LTE from FWD before DBR, after DBR but before HVS testing, and after DBR and HVS testing for Joint 33 (hollow stainless steel dowel, 4/wheelpath).

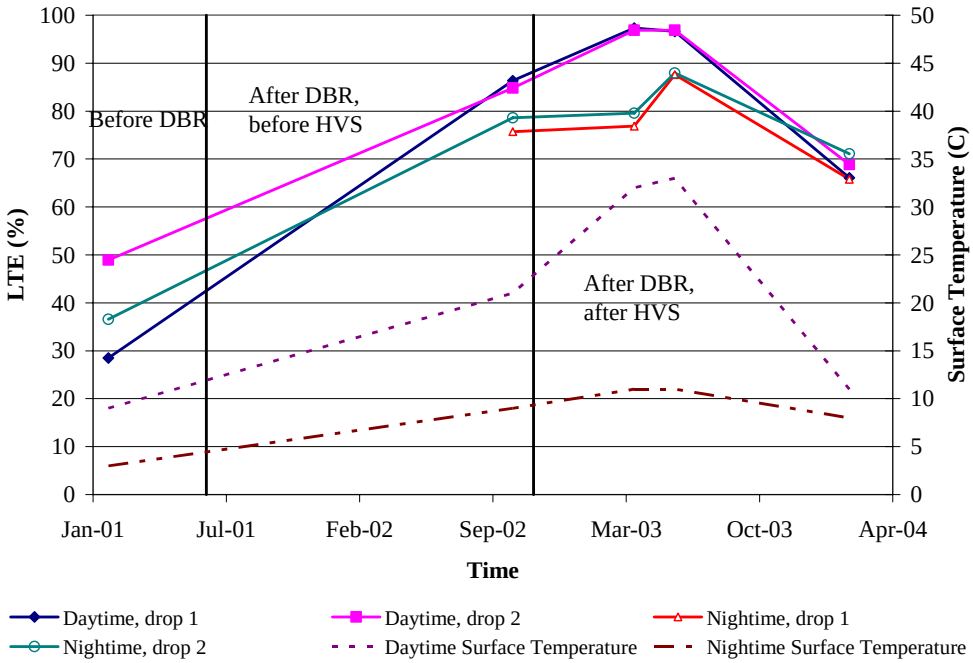

Figure 7.6. LTE from FWD before DBR, after DBR but before HVS testing, and after DBR and HVS testing for Joint 35 (epoxy-coated steel dowel, 3/wheelpath).

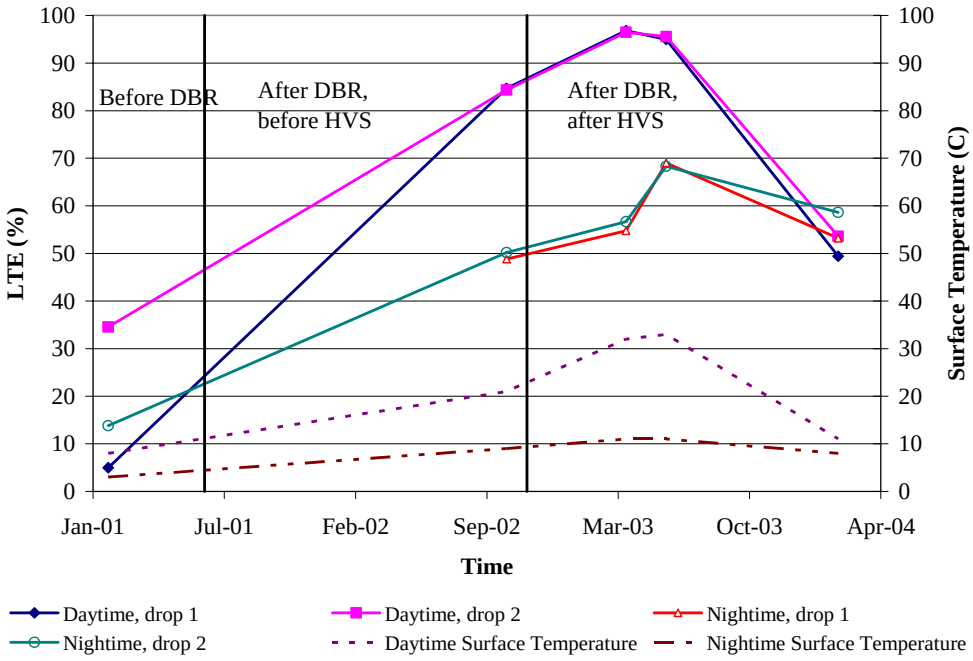

Figure 7.7. LTE from FWD before DBR, after DBR but before HVS testing , and after DBR and HVS testing for Joint 36 (epoxy-coated steel dowel, 3/wheelpath).

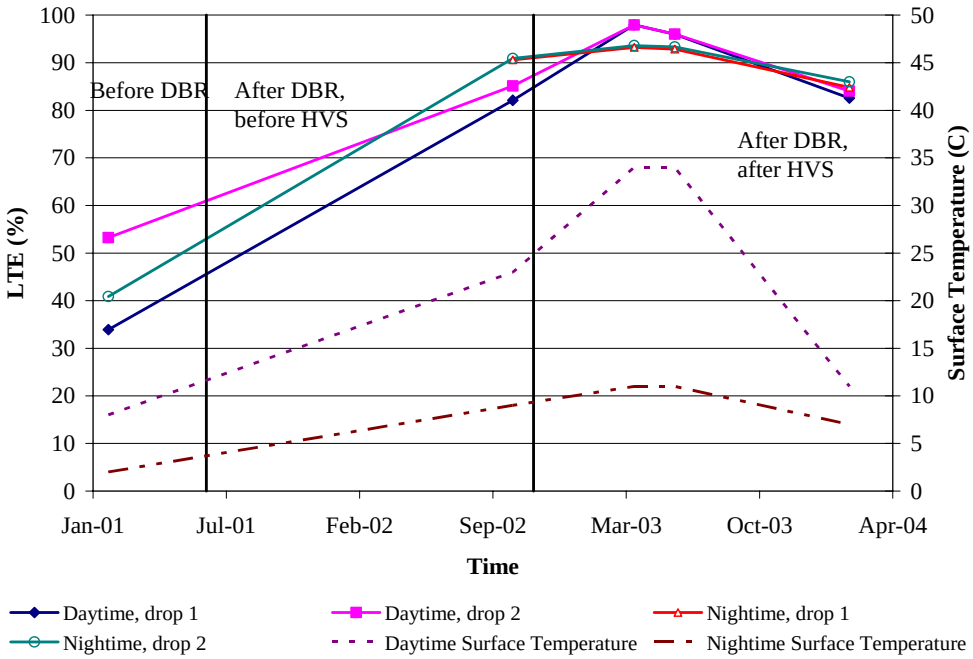

Figure 7.8. LTE from FWD before DBR, after DBR but before HVS testing , and after DBR and HVS testing for Joint 38 (epoxy-coated steel dowel, 4/wheelpath).

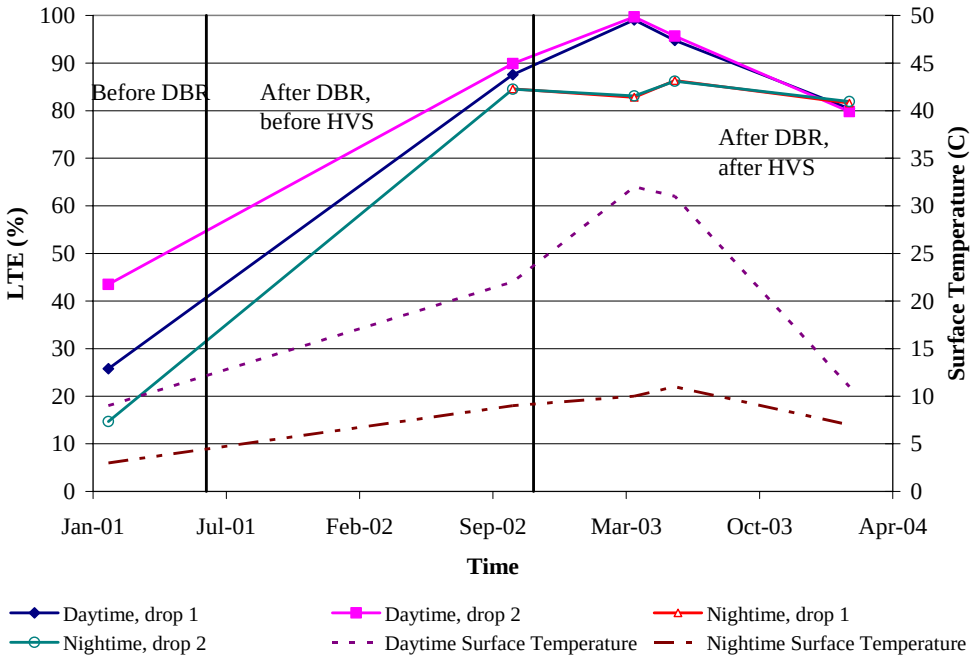

Figure 7.9. LTE from FWD before DBR, after DBR but before HVS testing , and after DBR and HVS testing for Joint 39 (epoxy-coated steel dowel, 4/wheelpath).

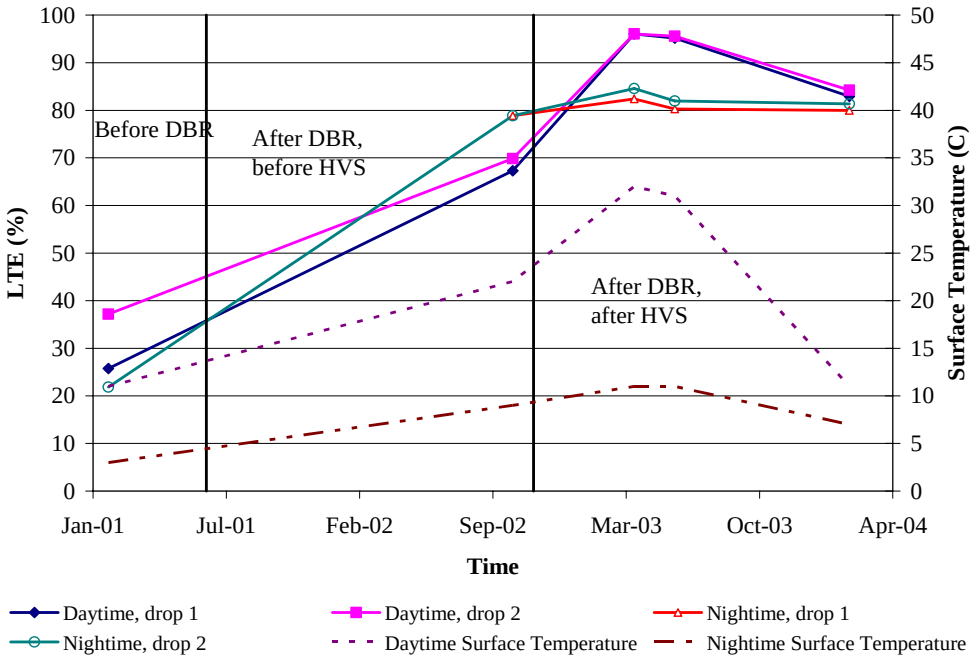

Figure 7.10. LTE from FWD before DBR, after DBR but before HVS testing , and after DBR and HVS testing for Joint 41 (epoxy-coated steel dowel, 4/wheelpath).

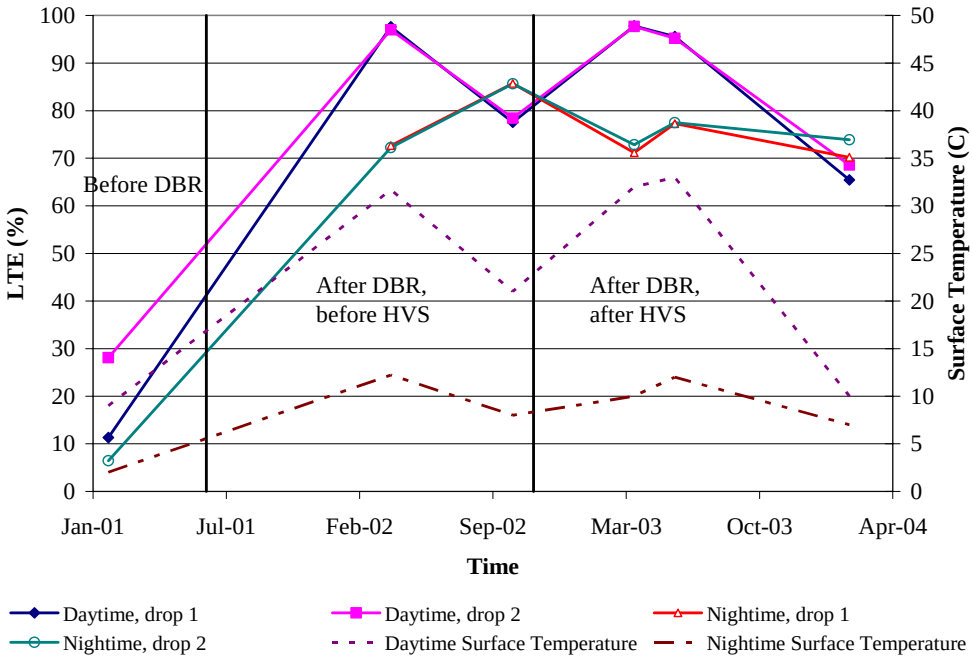

Figure 7.11. LTE from FWD before DBR, after DBR but before HVS testing , and after DBR and HVS testing for Joint 42 (FRP dowel, 4/wheelpath).

LTE from FWD testing versus surface temperature for HVS test sections before DBR, after DBR but before HVS loading, and after HVS loading on the joints DBR by different dowel bar types are shown in Figure 7.12 through Figure 7.15. It can be seen from the figures that when temperature is above 30°C, all DBR joints exhibit greater than 90 percent LTE. However, when temperature is below 15°C, the joints with three dowels show 10 to 20 percent less LTE than the joints with four dowels. The results also show that the HVS loading did little to damage the LTE on the DBR joints.

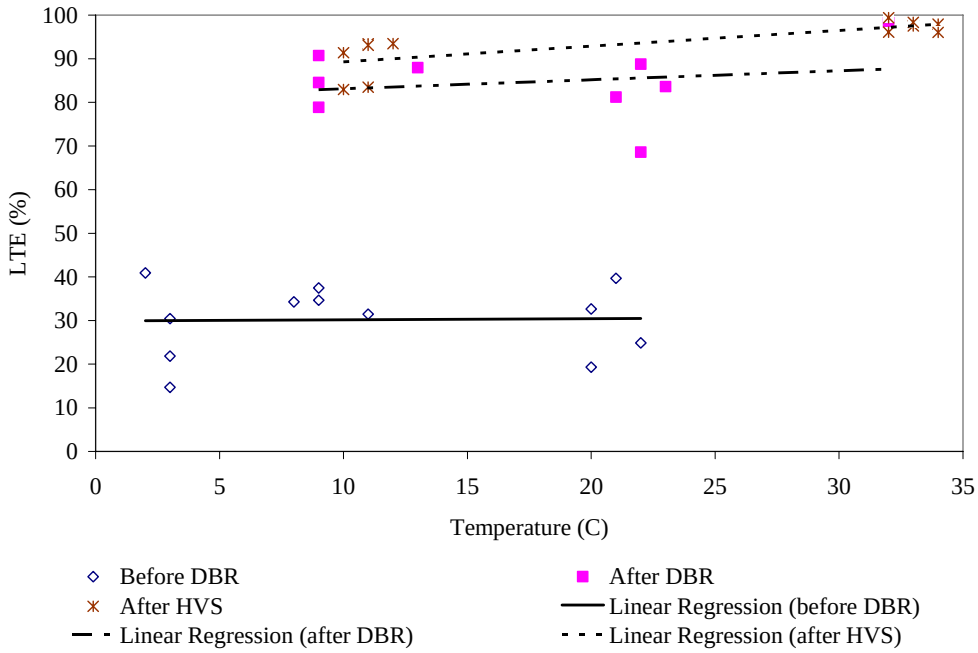

Figure 7.12. LTE vs. surface temperature for joints with four epoxy-coated steel dowels per wheelpath from FWD measurements.

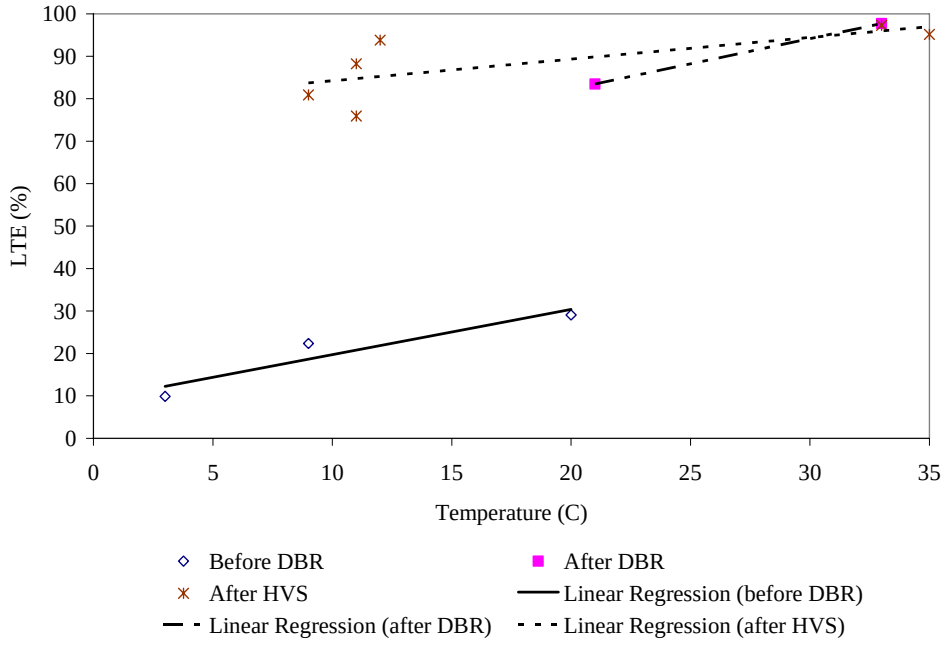

Figure 7.13. LTE vs. surface temperature for joints with four hollow stainless steel dowels per wheelpath from FWD measurements.

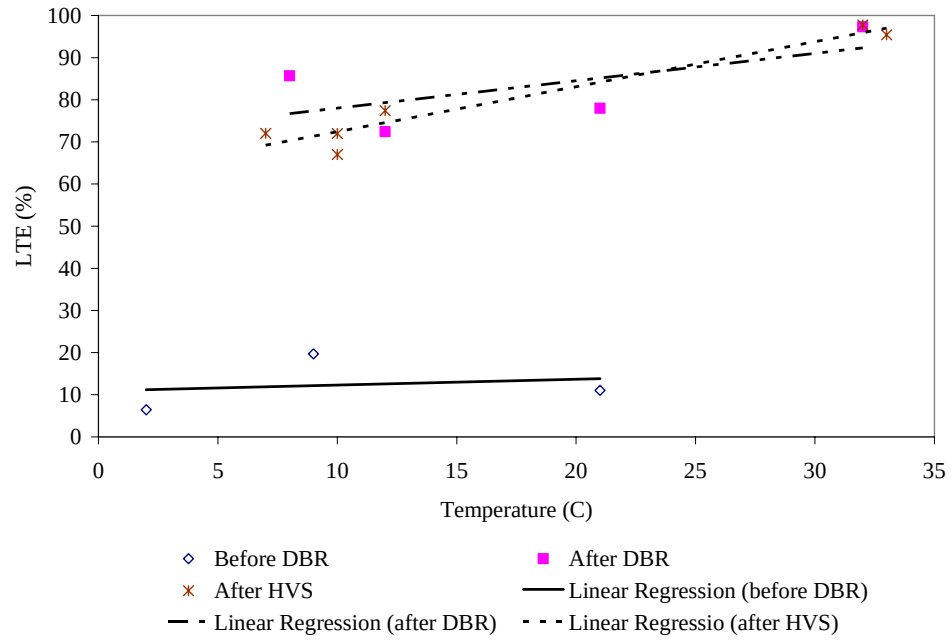

Figure 7.14. LTE vs. surface temperature for joints with four FRP dowels per wheelpath from FWD measurements.

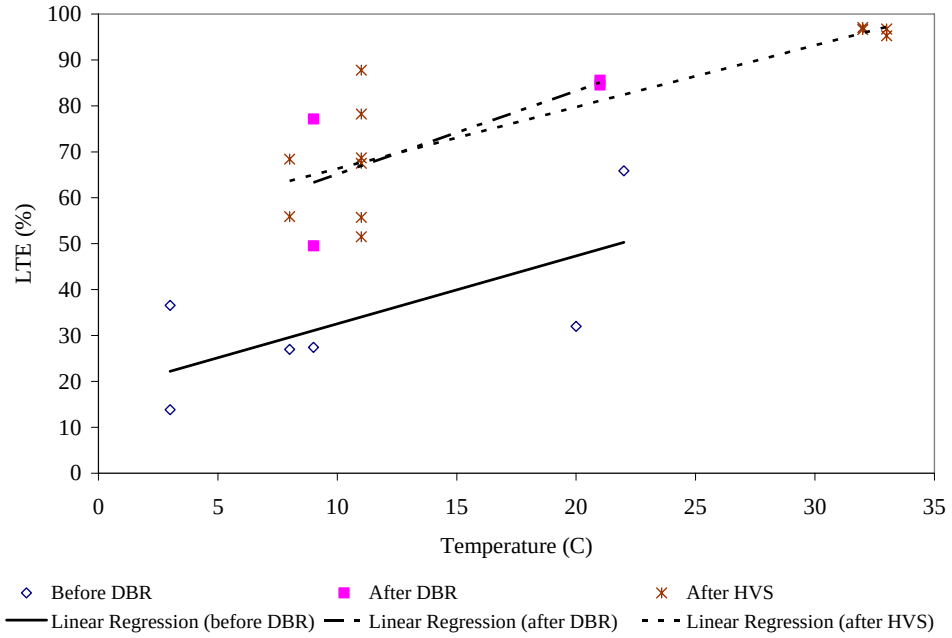

Figure 7.15. LTE vs. surface temperature for joints with three epoxy-coated steel dowels per wheelpath from FWD measurements.

7.1.2 Comparison of Palmdale DBR Section HVS Results

HVS testing results from the four Palmdale DBR test sections are summarized in Table 7.2.

7.1.2.1 JDMD Vertical Peak Deflection

Regression lines of JDMD vertical peak deflection for different HVS test sections have been shown in Figure 6.11 through Figure 6.14 (556FD), Figure 6.36 through Figure 6.39 (557FD), Figure 6.61 through Figure 6.64 (558FD), and Figure 6.86 through Figure 6.89 (559FD). In this section, regression lines for the joints with same dowel material and same dowel bar amount per wheelpath with measuring load of 60 kN are averaged into one line, and the resulting lines are shown in Figure 7.16.

From Figure 7.16, it can be concluded that joints with four epoxy-coated steel dowels per wheelpath give the smallest vertical deflections under HVS loading. It appears that using three dowels per wheelpath does not provide as much vertical deflection control, and neither do the alternative dowel types.

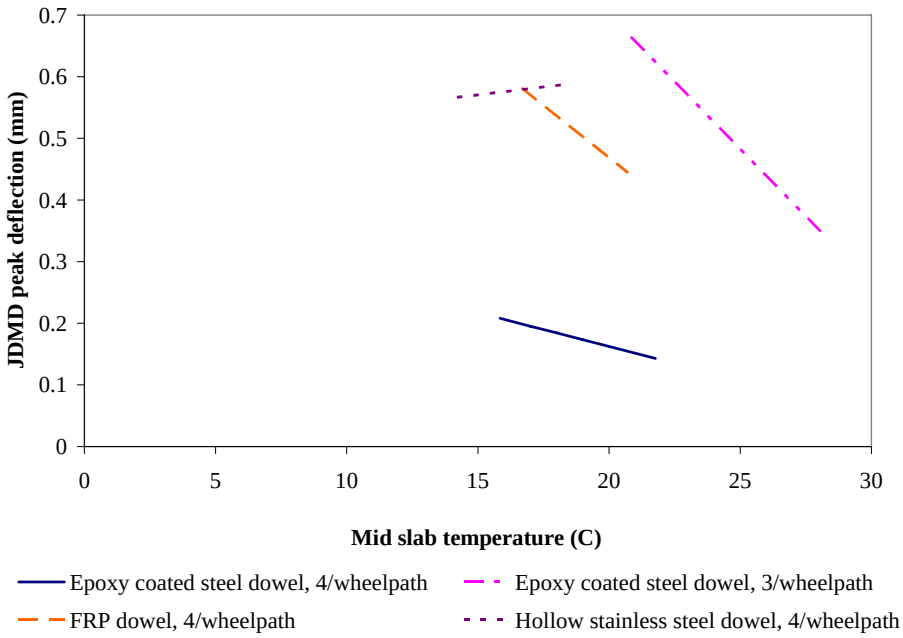

Figure 7.16. Comparison of JDMD vertical peak deflection regression lines under HVS loading, 60 kN testing load.

Table 7.2. HVS Testing Result Summary, under 60 kN testing load.

	556FD		557FD		558FD*		559FD*	
	Joint 38	**Joint 39**	**Joint 35**	**Joint 36**	**Crack 2**	**Joint 42**	**Joint 32**	**Joint 33**
Dowel Type	ECS, 4 pw		ECS, 3 pw		FRP, 4 pw		ECS, 4 pw	HSS, 4 pw
Average LTE	99.4%	99.3%	98.1%	98.6%	99.7%	97.1%	99.1%	97.5%
LTE Standard Deviation	0.6%	0.7%	2.4%	1.8%	0.7%	5.7%	0.7%	1.9%
Average peak deflection (mm)	0.78	0.79	0.95	0.91	0.85	0.99	1.04	0.98
Peak Deflection Standard Deviation (mm)	0.3	0.3	0.4	0.3	0.5	0.6	0.3	0.2
Average air temperature (^{o}C)	20.9		21.5		9.5		10.3	
Average mid-slab temperature (^{o}C)	24.4		24.8		15.1		13.7	
Average relative humidity	37%		35%		44%		48%	
Average rainfall (mm)	0.002139		0.000641		0.0835		0.274	

* Note that Joint 41 in Section 558FD was trafficked but did not have JDMD instrumentation. Crack 1 in Section 559 was also not instrumented.

7.1.2.2 Load Transfer Efficiency

Regression lines of LTE for different HVS test sections have been shown in Figure 6.17 through Figure 6.20 (556FD), Figure 6.42 through Figure 6.45 (557FD), Figure 6.67 through Figure 6.70 (558FD), and Figure 6.92 through Figure 6.95 (559FD). In this section, regression lines for the joints with same dowel material and same number of dowels per wheelpath are averaged into one line using data with measurement load of 40 kN, and the resulting lines are shown in Figure 7.17. From Figure 7.17 it can be seen that despite the dowel material, all joints with four dowels per wheelpath showed very high LTE values. Only joints with three dowels per wheelpath exhibited relatively low LTE, despite higher temperatures which would tend to increase.

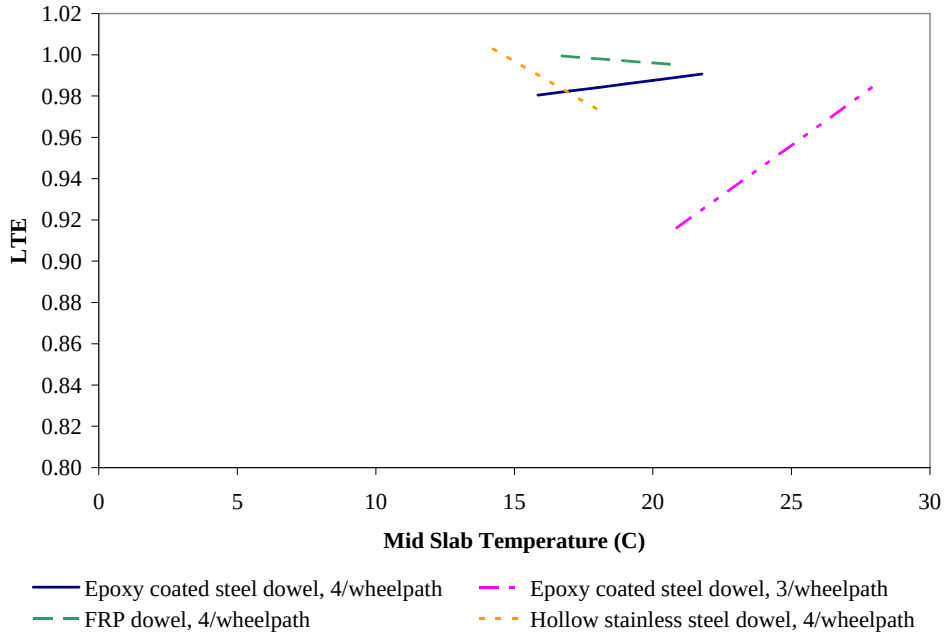

Figure 7.17. Comparison of LTE regression lines under HVS loading, 60 kN testing load.

7.2 Comparison between Palmdale DBR, Palmdale Originally Installed Dowels, and Ukiah DBR Using FWD and HVS Results

7.2.1 Comparison between Palmdale DBR and Originally Installed Dowel Sections

7.2.1.1 FWD Results, Comparison of Deflection and LTE

The backcalculated concrete stiffness, support layer stiffness, and subgrade k-value for the three original sections in North Tangent were previously shown in Table 5.2, Table 5.7, Table 6.10, Table 6.14, and Table 6.18. From these tables, it can be concluded that the layer moduli generally stay constant except for changes due to temperature and temperature gradients.

The average LTE for joints with originally installed dowel bars on Section 9 and 11 of the original Palmdale sections, which are on 0.3 m spacing across the joint per Caltrans specification

(eleven per joint or transverse crack), and four per wheelpath retrofitted epoxy-coated steel dowel bars are shown in Table 7.3. In this table, FWD tests in April and October 2002 were conducted after DBR but prior to HVS testing, and the results in the table compare joints with originally installed dowels that were not HVS tested with the untested DBR joints. FWD tests in April and June 2003 and February 2004 were conducted after DBR and HVS testing on the same DBR joints, and were compared with joints with originally installed dowels that had also been tested with the HVS.

It can be seen in Table 7.3 that when the temperature is above 33°C all joints have consistently high LTE, likely mostly carried by aggregate interlock, making the presence and installation (original or DBR) of dowels irrelevant. However, when temperatures are lower, the DBR joints had somewhat less LTE than joints with originally installed dowels, although still always greater than 80 percent and usually 85 to 90 percent. There is also greater variability in the LTE of the DBR joints. This may be due in part to the eight dowels in the joint for the DBR versus the eleven in the joints with originally installed dowels (OID). The HVS loading repetitions did not seem to significantly damage the LTE of the DBR joints or of the OID joints.

Table 7.3. Comparison of LTE for between Palmdale Originally Installed Dowel (OID) and Dowel Bar Retrofit (DBR) Joints

FWD Testing Date and Type of Joint		Daytime			Nighttime		
		Average LTE	Standard Deviation	Average Surface Temperature (°C)	Average LTE	Standard deviation	Average surface temperature (°C)
April 2002	OID joints	96%	1%	33.6	95%	2%	13.1
	DBR joints	98%	0%		83%	9%	
Oct. 2002	OID joints	94%	3%	23.2	95%	1%	9.4
	DBR joints	82%	6%		80%	12%	
April 2003	OID joints	97%	1%	33.4	94%	2%	10.4
	DBR joints	98%	1%		81%	12%	
June 2003	OID joints	96%	1%	34.2	95%	4%	12.2
	DBR joints	96%	1%		86%	8%	
Feb. 2004	OID joints	—	—	10.9	94%	2%	10.3*
	DBR joints	77%	12%		81%	13%	

* This is also daytime temperature. There are two daytime measurements but no nighttime measurement for this FWD test.

7.2.1.2 FWD Results, Reduction of Permanent Slab Warping Due to Shrinkage from DBR

It is known that concrete expands or contracts with changes in temperature or humidity, and that the top and bottom of a concrete slab expand/contract differently due to temperature or moisture gradients through the slab. Such non-uniform expansion or contraction results in curling and causes loss of contact between the slab and base. Curling, which causes stress in concrete slabs and greater deflection at joints, has five components: temperature gradient, moisture gradient, built-in temperature gradient, differential drying shrinkage, and creep. Effective built-in temperature difference (EBITD) is defined as the overall effect of all these components but the temperature gradient (24). Slabs with higher EBITD value have increased tensile stresses and joint and corner deflections.

The EBITD for all Palmdale HVS and FWD tests on the DBR sections were calculated following the procedure described by Rao and Roesler (24). In this project, the finite element program *EverFE* (29) was used to model the concrete slabs and calculate slab deflections under the the HVS wheel load and under the FWD plate load, in both cases using the measured slab temperatures to account for curling due to thermal gradients.

Table 7.4a shows EBITD calculated using deflections measured under the moving HVS wheel just after DBR using JDMDs at the corners and at the mid-slab edge. The predicted deflections assuming the -5.8°C EBITD together with measured deflections of JDMD 4 from Section 559FD are shown in Figure 7.18. The results show EBITD values between 0 and -9.9° C. EBITD values previously calculated by Rao and Roesler (24) for the same joints after the previous HVS test and prior to DBR were -33.3°C, -20.9°C and -21.8°C for JDMD2, JDMD3, and JDMD4, respectively. Comparison of these values suggests that DBR has the potential to significantly reduce the permanent curl of concrete slabs caused by differential shrinkage between the top and bottom of the slabs, which can reduce tensile stresses that cause fatigue cracking. However, the EBITD values calculated from before DBR seem very high and were not included in the table for this reason.

Table 7.4b shows EBITD calculated before DBR, after DBR and before HVS testing, and after HVS testing on the DBR sections using Falling Weight Deflectometer data and again following the procedure developed by Rao and Roesler. Not all joints are shown for each HVS test section and for each date because the presence of the HVS over the joints at the time of testing or because the deflections were too small to permit EBITD calculations. Small deflections mostly occurred during daytime testing when the top of the slab was hotter than the bottom of the slab, which caused the corners of the slabs to be in better contact with the top of the base.

The results in Table 7.4b for all of the joints indicate that DBR may cause some reduction in EBITD, but that difference is probably no more than about 2°C. If this change is real it will result in some reduction of tensile stresses that cause fatigue cracking in the slabs.

It is clear that most of the joints in the HVS test sections did not have an increase in EBITD after DBR. Grout was placed around the dowels in June in the early afternoon. Grout strength-gain data presented elsewhere in this report indicates that the grout would have set in the late afternoon and early evening, when the slab would have been close to its flattest position, which may be the reason that the EBITD values after DBR are somewhat lower than those before DBR. If the grout were to set at a time when the slabs have a highly negative temperature differential (colder on the top of the slab than on the bottom) then DBR could potentially lock in a high EBITD, which would tend to increase thermal stresses in the slab.

The results shown here suggest that EBITD should be calculated from deflection data taken before and after DBR on any future DBR projects to be able to more conclusively determine whether DBR has a significant effect on EBITD.

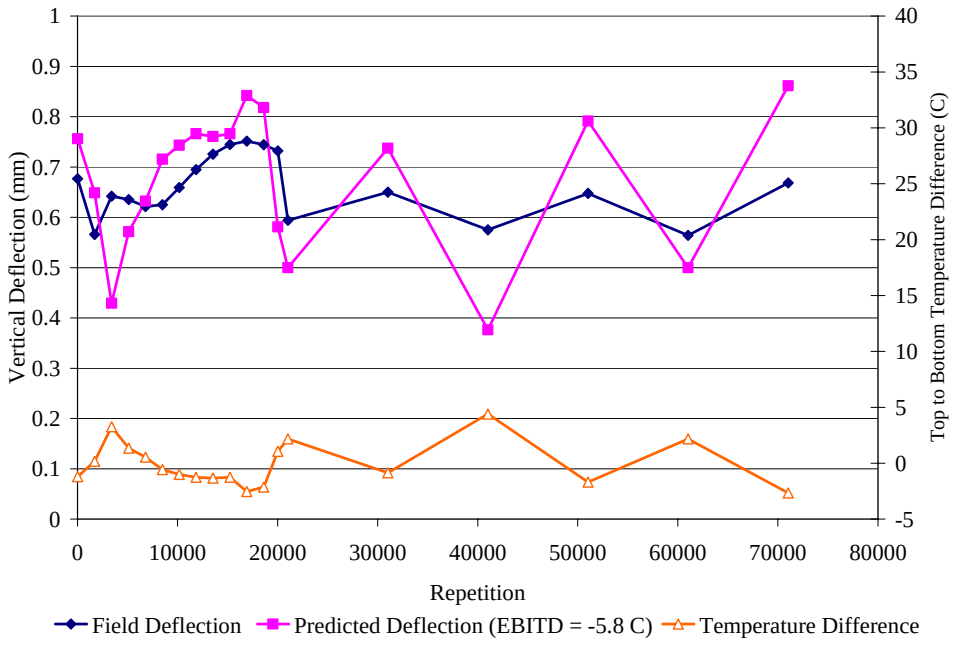

Figure 7.18 Example of matching of measured and calculated deflections to find EBITD.

Table 7.4. Calculated EBITD Before and After DBR

(a) EBITD Calculated from HVS Data

		HVS		
		JDMD2 (Right Corner)	**JDMD3 (Mid-slab Edge)**	**JDMD4 (Left Corner)**
After DBR, Before HVS testing	556FD (4 epoxy-coated steel dowels per wheelpath)	N/A	N/A	N/A
	557FD (3 epoxy-coated steel dowels per wheelpath)	0°C	0°C	0°C
	558FD (4 FRP dowels per wheelpath)	-9.9°C	-6.5°C	0°C
	559FD (one joint with four epoxy-coated steel dowels per wheelpath and one joint with four hollow stainless dowels per wheelpath)	-3.8°C	-3.8°C	-5.8°C

(b) EBITD Calculated from FWD Data for all Joints

			Joint 39 (556FD)		Joint 36 (557FD)		Joint 42 (558FD)		Joint 33 (559FD)		Joint 32 (559FD)	
			Day	Night	Day	Night	Day	Night	Day	Night	Day	Night
Before DBR	Drop 1		-7.5	-8.5	—	-6.3	—	-9.2	—	—	—	-8.1
	Drop 2		—	-6.6	—	—	—	—	—	—	—	—
After DBR, before HVS	Apr 2002	Drop 1	—	—	—	—	-5.5	-7.7	—	—	—	—
		Drop 2	—	—	—	—	—	-6.7	—	—	—	—
	Oct 2002	Drop 1	—	-5.9	—	-4.3	-6.9	-10.1	—	—	—	-3.7
		Drop 2	—	-5.6	—	-5.0	-6.1	-10.5	—	—	—	-4.4
After DBR, after HVS	Apr 2003	Drop 1	—	—	—	—	—	—	—	-7.0	—	-7.6
		Drop 2	—	—	—	—	—	—	—	—	—	-8.1
	Jun 2003	Drop 1	—	—	—	—	—	-8.7	—	—	—	-7.9
		Drop 2	—	—	—	—	—	-7.5	—	-6.4	—	-9.6

7.2.1.3 HVS Results, Comparison of Slab Curling due to Temperature Changes

The complete JDMD movements for a twenty-four-hour cycle without the HVS for 535FD (DBR section before DBR), 536FD (with originally installed dowels), 539FD (with widened truck lane and originally installed dowels), and 556FD (DBR section after DBR) are shown in Figure 7.19 through Figure 7.22. These sections were selected for this comparison because their 24-hour temperature differences without the temperature control box are similar to each other. It appears from the figures that with only temperature changing, the originally doweled section (Figure 7.20) and the DBR section (Figure 7.22) had less thermally induced deflection than the undoweled section (Figure 7.19) and widened-truck lane, originally doweled section (Figure 7.21).

These results indicate that DBR can help inhibit slab curling caused by temperature gradients. This will change tensile stresses in the slabs, the results of which must be further evaluated. The reduction of slab curling will definitely help reduce corner cracking.

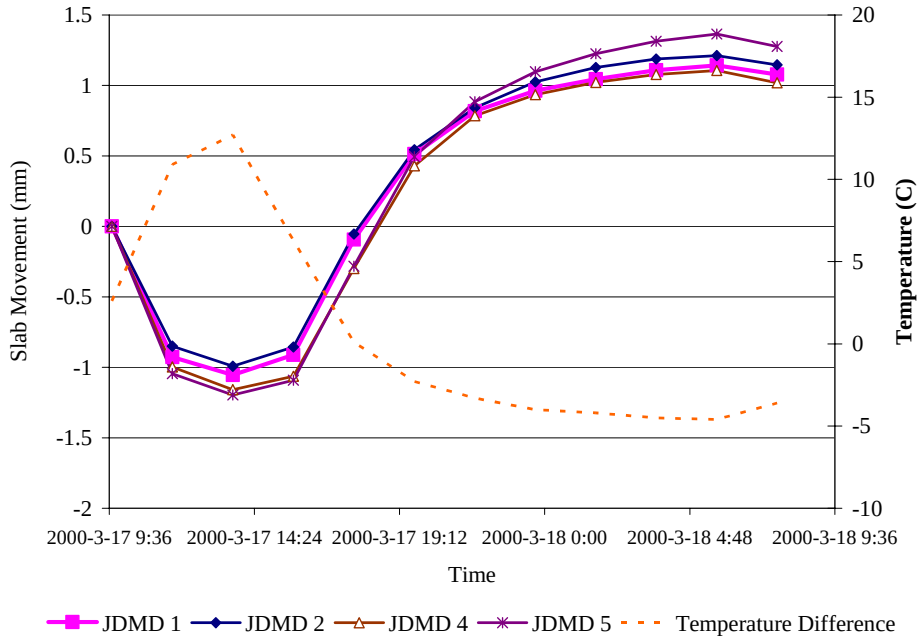

Figure 7.19. Corner deflections for Section 535FD (Section 7, DBR section before DBR) without temperature control box.

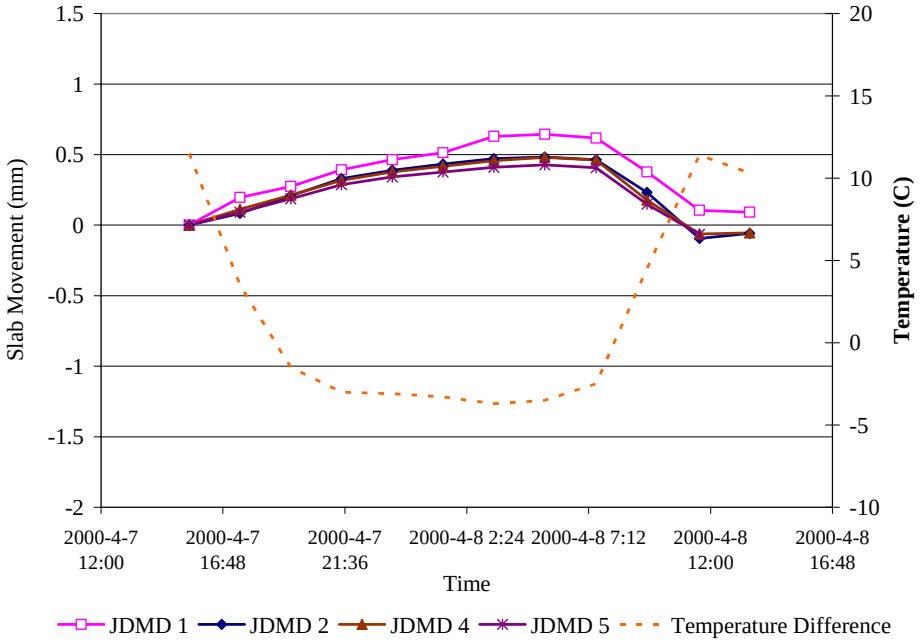

Figure 7.20. Corner deflections for Section 536FD (Section 9, with originally installed dowels) without temperature control box.

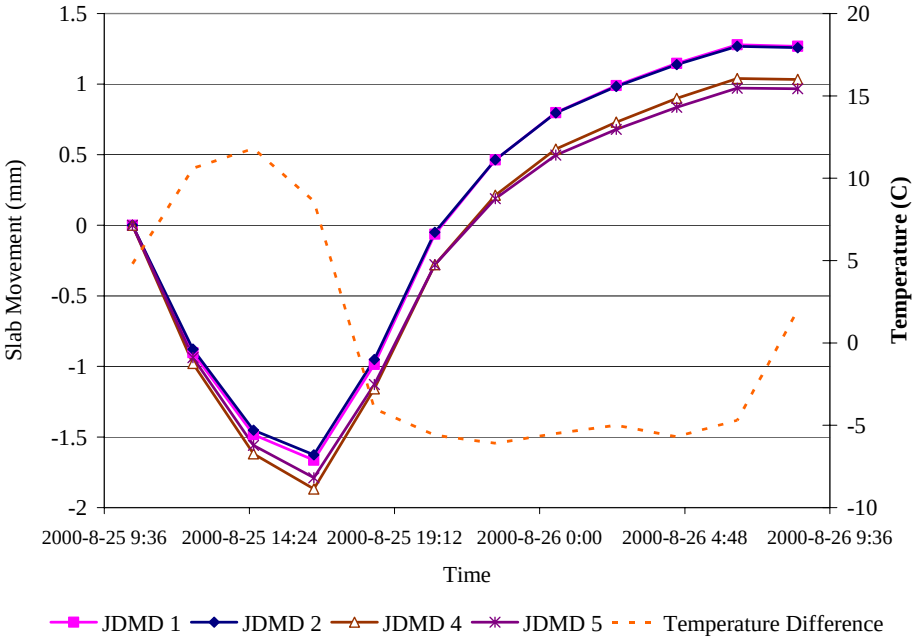

Figure 7.21. Corner deflections for Section 539FD (Section 11, with widened truck lane and originally installed dowels) without temperature control box.

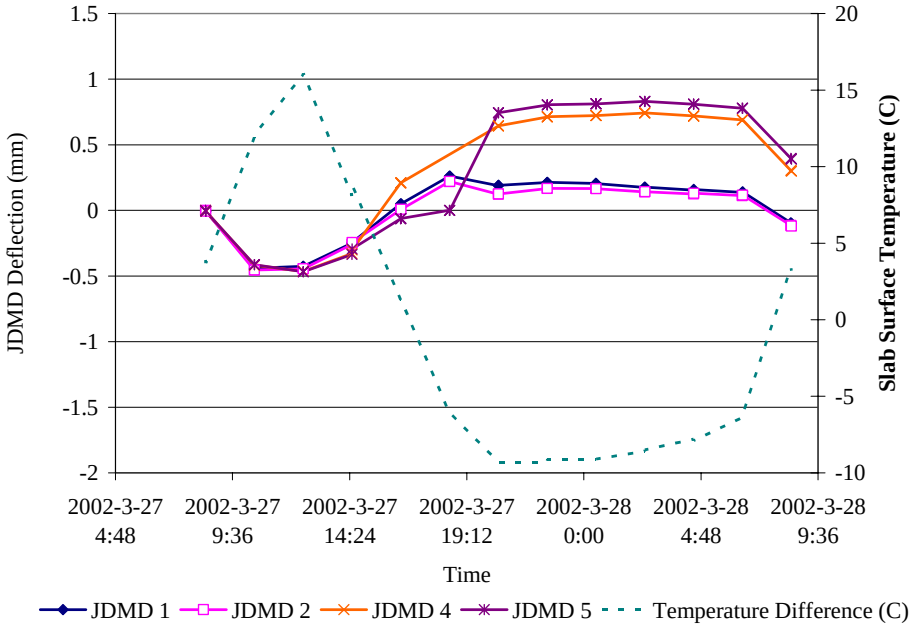

Figure 7.22. Corner deflections for Section 556FD (Section 7, DBR section after DBR) without temperature control box.

7.2.2 Comparison between Palmdale DBR and Ukiah DBR Sections Using FWD Results

Backcalculated layer moduli assuming a two-layer system (slab and underlying support layer) for after DBR but before HVS testing for Palmdale and Ukiah sections are shown in Table 7.5 and Table 7.6, respectively. The surface temperatures for the FWD tests of October 2002 (Palmdale) and February 2001 (Ukiah) are similar, and the backcalculated stiffnesses for the concrete slabs and support layers are too. The support layer k-values for the Ukiah and Palmdale sections are similar, despite the fact that Ukiah had a clay subgrade and Palmdale had a granular subgrade with bedrock not far below. However, both sections had same thickness of cement treated base (CTB), and it is expected that the CTB dominated the combined stiffness of the support layers. The construction specification for the Ukiah section built in the late 1960s called for greater unconfined compressive strength than did that of the Palmdale section built in 1998. The specification for the Palmdale CTB was the pre-1964 Caltrans specification.

LTE under a 40 kN load before and after DBR for the Palmdale and Ukiah sections are shown in Figure 7.23 and Figure 7.24. As expected, LTE increases with increased temperature. In both the Palmdale and Ukiah DBR sections, the joints showed much higher LTE after DBR construction, and the improved LTE wasn't damaged by HVS loading repetitions. For both sections, the undoweled (before DBR) joint LTE under relatively low temperatures (5 to 10°C) can be as low as 30 percent; while after DBR, the LTE is always greater than 85 percent.

Table 7.5. Backcalculated Stiffnesses for Palmdale DBR Sections

		Daytime		Nighttime	
		Average	**Standard Deviation**	**Average**	**Standard Deviation**
April 2002	Surface temperature (^oC)	33.6	1.2	13.1	0.5
	Concrete Stiffness E_{pcc} (MPa)	45,129	9,464	41,207	21,696
	Support stiffness $E_{sg+base}$ (MPa)	240	30	236	103
	Support k-value (MPa/m)	121	19	128	81
October 2002	Surface temperature (^oC)	23.1	1.9	9.3	0.7
	Concrete Stiffness E_{pcc} (MPa)	49,112	21,959	55,386	18,749
	Support stiffness $E_{sg+base}$ (MPa)	252	114	245	81
	Support k-value (MPa/m)	134	89	120	45

Table 7.6. Backcalculated Stiffnesses for Ukiah DBR Sections (Feb. 2001)

	Daytime		Nighttime	
	Average	**Standard Deviation**	**Average**	**Standard Deviation**
Surface temperature (^oC)	21.5	0.5	7.6	0.5
Concrete Stiffness E_{pcc} (MPa)	42,696	8,408	51,089	11,331
Support stiffness $E_{sg+base}$ (MPa)	181	36	276	51
Support k-value (MPa/m)	311	68	509	100

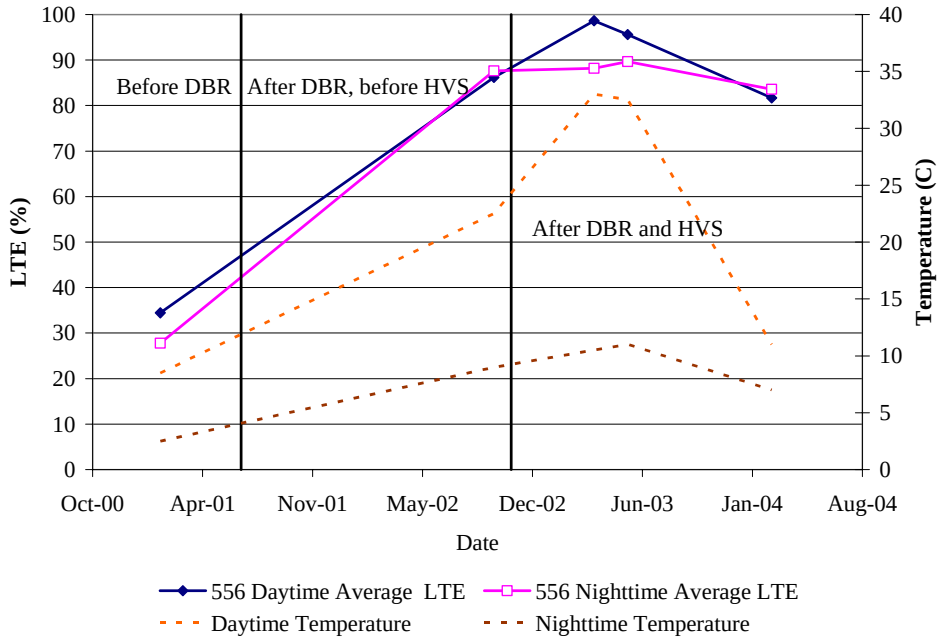

Figure 7.23. Load Transfer Efficiency across time for Palmdale DBR Section 556FD (four epoxy-coated steel dowels per wheelpath).

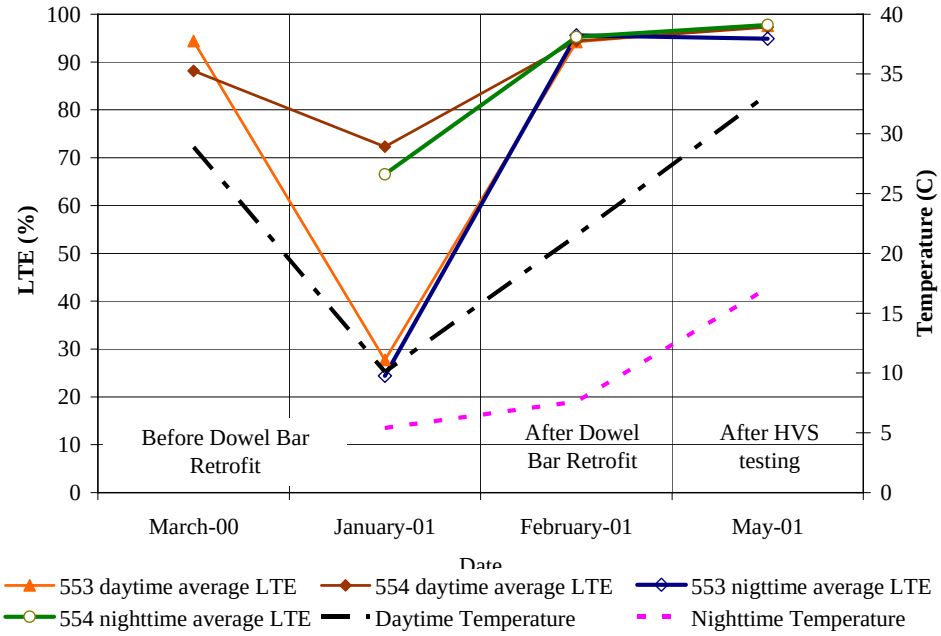

Figure 7.24. Daytime Load Transfer Efficiency across time for Ukiah DBR Sections 553FD and 554FD (four epoxy-coated steel dowels per wheelpath).

8 SUMMARY OF OBSERVATIONS AND FINDINGS

8.1 Observations and Findings

The following are based on tests and analyses presented in this report.

8.1.1 Construction and Materials (Chapter 2)

- Dowel bar retrofit (DBR) installation was successfully completed for all three types of dowels included in the study: epoxy-coated steel, hollow stainless steel cylinder filled with grout, and fiber-reinforced polymer (FRP) on pavement test sections previously trafficked with the HVS.
- The backfill grout material strength exceeded the Caltrans specifications requiring 3.5 MPa flexural strength at one day and 35 MPa compressive strength at one day. The specification of 21 MPa at three hours was not checked due to delays in testing; however, the material had a compressive strength of 37 MPa at eight hours, which indicates high early strength for the mix.
- The twenty-eight-day strengths for the backfill grout were high: 6.4 MPa flexural and 63 MPa compressive.
- Cores taken in the DBR slots after HVS testing was completed showed that all of the dowels cored were above the mid-depth of the slab and at least some were very near the top of the slab. These conditions indicate the test sections were not "perfect" and may resemble field construction in terms of dowel placement variability.
- Most of the dowel slots appear to be in good condition after construction, and after the heavy HVS trafficking that eventually resulted in fatigue cracking of the slabs. Observations after construction include the following:
  - Foam backer board slightly out of place on several joints.
  - Apparent segregation (lack of fine materials) in the grout in some slots.
  - Cracking on one set of slots that were placed across a set of unconnected, parallel transverse cracks. This may indicate what occurs if there is no clear joint or crack on which to place the foam backer board.
- Two years after construction and HVS testing was completed on all sections, transverse cracking was seen in the grout on some slots. Slight separation was seen between the grout and the slab on some slots but the grout did not come out of any slots and the cracks remained tightly interlocked.

8.1.2 FWD Results *after* Original HVS Testing and *before* DBR (Chapter 4)

- The average load transfer efficiency (LTE) in the Palmdale North Tangent test sections with originally installed dowels in the joints, some with a widened lane and others with a tied shoulder, was 91 percent — with almost no difference between daytime and nighttime measurements. The average LTE on the undoweled sections was 33 percent in the day at an average surface temperature of 10°C, and 25 percent at night at an average surface temperature of 3°C. The influence of temperature is expected, because higher temperatures result in slab expansion, which closes the joint and increases aggregate interlock at the joint.
- Temperature gradient has a significant effect on backcalculated stiffnesses, with higher slab and supporting layer stiffnesses and supporting layer k-values found from nighttime measurements. This is attributed to negative nighttime temperature gradients (cooler on top) in the concrete slabs, causing curl that places the slab center in closer contact with the supporting layers. The results agree with observations at the Ukiah DBR HVS sections.

8.1.3 FWD Results *after* DBR and *before* HVS testing (Chapter 5)

- The joints with originally installed dowels, many of which had been previously trafficked to slab-cracking failure, had high LTE, which was nearly insensitive to temperature. Average LTE was 96 percent at a slab surface temperature of 34°C; 94 percent at 13°C; 93 percent at 23°C; and 94 percent at 9°C. The standard deviation across the many joints in each section was always less than 2.5 percent.
- At higher temperatures the LTE of the undoweled and DBR joints was nearly the same as that of the originally installed dowel joints. The average LTE was 97 percent at 34°C, with no difference between undoweled and DBR joints. At 23°C, the average undoweled LTE was 85 percent, and the average DBR LTE was 82 percent.
- The undoweled joints had lower LTE than the DBR joints under cooler nighttime temperatures. The average LTE for the undoweled joints was 73 percent at 13°C; and 57 percent at 9°C. At 9°C, individual undoweled joint LTE ranged between 27 and 93 percent, indicating the inconsistency of relying on aggregate interlock for LTE. The greater values are likely joints that were not trafficked during the original HVS testing that did not have their aggregate interlock damaged.
- The DBR significantly improved the LTE of the previously undoweled joints, and reduced the sensitivity of the LTE to temperatures. The average LTE was 83 percent at 13°C; and 79 percent at 9°C.

- Three dowels per wheelpath typically had somewhat lower nighttime LTE than that of four dowels per wheelpath, regardless of the dowel type used for four dowels per wheelpath, although three dowels per wheelpath was generally much better than for undoweled joints.
- Backcalculated slab stiffnesses and the stiffnesses and k-values for the supporting layers were similar to those obtained before DBR, and generally showed the expected temperature sensitivity. As with all of the FWD results, the backcalculated stiffnesses and k-value appeared to have no load sensitivity (linear behavior).

8.1.4 Results of HVS Tests (Chapters 6 and 7)

- The failure criteria for the HVS test sections were: fatigue cracking of the concrete slab, or major damage to the DBR joints, or loss of LTE of the loaded joint or crack. All of the HVS test sections failed only by fatigue cracking of the concrete slab. Neither of the other two types of failure occurred on any of the test sections. HVS trafficking was stopped on each test section as shown below.

HVS Test Section	Joint or Crack Number	Type of Dowels	Number of Dowels	Number of HVS load repetitions
558FD	Joint 41	Epoxy-coated steel	Four per wheelpath	2,208,578
	Crack 2	Fiber reinforced polymer		
	Joint 42	Fiber reinforced polymer		
556FD	Joint 38	Epoxy-coated steel	Four per wheelpath	2,208,546
	Joint 39	Epoxy-coated steel		
557FD	Joint 35	Epoxy-coated steel	Three per wheelpath	1,121,600
	Joint 36	Epoxy-coated steel		
559FD	Joint 32	Epoxy-coated steel	Four per wheelpath	2,001,497
	Crack 1	Hollow stainless steel in one wheelpath; epoxy-coated steel in other wheelpath		
	Joint 33	Hollow stainless steel		

- Fatigue life of the slab with three dowels per wheelpath was substantially shorter than the other test sections that had four dowels per wheelpath. Fatigue life was similar for all three strategies with four dowels per wheelpath. Longer fatigue life, higher LTE, and lower deflections indicated better performance under these test conditions by four dowels per wheelpath when compared with three dowels per wheelpath.

The following observations about joint deflections and LTE are with respect to measurements made under HVS loading using Joint Deflection Measurement Devices (JDMD) mounted on the pavement during HVS testing. Larger joint vertical deflections and lower LTE correlate with increased rate of faulting and roughness development.

- As expected, all of the sections showed an increase in initial joint maximum vertical deflection with increase in load (60 to 90 to 150 kN).
- All of the sections showed a sensitivity of joint maximum vertical deflection to temperature, with deflections decreasing with increased temperature. This is expected and is caused by slab expansion closing the joint and increasing aggregate interlock at the joint.
- All of the DBR joints except one showed an increase in joint maximum deflection after HVS trafficking — measured using the same 60 kN measurement load — that could not be attributed to temperature changes. The increases came under the 90 and 150 kN loading. The only joint not showing an increase was in Section 558FD and had FRP dowels. The other joint with FRP dowels in the same section behaved the same as all the other joints.
- Four epoxy-coated steel dowels per wheelpath had much smaller joint vertical deflections than did the alternatives (four FRP dowels, four hollow stainless steel dowels, and three epoxy-coated steel dowels per wheelpath). The alternatives had deflections similar to each other. At comparable temperatures, three epoxy-coated steel dowels had the largest deflections.
- All of the sections showed a slight increase in initial LTE with increase in load (60 to 90 to 150 kN). Under HVS loading, and using the moving wheel definition of LTE described in the report, the LTE is nearly always greater than 90 percent on the DBR joints, regardless of temperature and load.
- All but one of the joints showed a sensitivity of LTE to temperature, with LTE increasing with increased temperature. This is expected and is caused by slab expansion closing the joint, and increasing aggregate interlock at the joint. The temperature susceptibility was very low compared to undoweled joints. The DBR joints with hollow stainless steel dowels showed no sensitivity to temperature.

- All of the DBR joints showed little or no decrease in LTE after HVS trafficking, as measured under the measuring load of 60 kN.
- Three epoxy-coated steel dowels per wheelpath had lower LTE than did all of the joints with four dowels per wheelpath, regardless of the type of dowel.

The following conclusions regarding joint deflections and LTE are with respect to measurements made using the FWD after HVS testing, from October 2002 through February 2004.

- The HVS trafficking caused almost no change in LTE for all of the DBR joints. Each of the dowel bar retrofit strategies tested by the HVS provided load transfer efficiency that was not substantially damaged by heavy traffic loading.
- Backcalculated stiffnesses from slab center deflection measurements showed the same day-to-night differences observed in the results from before DBR construction, as expected.

8.1.5 Comparison of DBR Joints with Originally Installed Dowel Joints at Palmdale from FWD Measurements (Chapter 7)

- When the temperature is above 33^{o}C all joints have consistently high LTE, likely mostly carried by aggregate interlock. Effects of dowels (original or DBR) are not apparent under these conditions.
- At lower temperatures, the DBR joints had somewhat less LTE than joints with originally installed dowels, although LTE was still always greater than 80 percent and was usually 85 to 90 percent with four dowels per wheelpath. There is also greater variability in the LTE between different DBR joints.

8.1.6 Reduction of Built-in Slab Curling from DBR (Chapter 7)

- The Equivalent Built-In Temperature Difference (EBITD) backcalculated on several slabs before and after DBR showed that the DBR may have reduced the EBITD by about 2C based on FWD deflections. EBITD is the permanent warping in the slab caused primarily by higher shrinkage at the surface than at the bottom. High EBITD increases tensile stresses in the slab that casue longitudinal and corner cracking. Further investigatin regarding the effect of DBR on EBITD is recommended, and should be based on FWD deflection measurements before and after DBR on future DBR projects.
- If a beneficial reduction in EBITD does occur, it would likely only occur when the DBR backfill grout sets during late afternoon and early evening when the temperature gradient in the slab is most positive (hotter on top) and the slab is the closest to being flat. Any future investigation of changes in EBITD caused by DBR should check to see if EBITD is dependent on the slab temperature gradient at the time that the backfill grout sets.

8.1.7 Comparison of DBR performance at Ukiah and Palmdale DBR HVS Test Sections (Chapter 7)

- LTE showed a trend towards being higher at Palmdale than Ukiah, which is partly a reflection of higher temperatures. Both locations showed a similarly small effect on LTE of HVS trafficking.
- Deflections at the joints for the Ukiah DBR sections were within the total range of those measured on the Palmdale DBR joints.
- The backcalculated concrete slab stiffnesses were similar at Ukiah and Palmdale. The underlying support stiffness was better at Palmdale than Ukiah, reflecting a more granular subgrade with bedrock below, compared to the clay subgrade at Ukiah.

REFERENCES

1. Maintenance Program, California Department of Transportation. 2004. “California, State of the Pavement Report, 2003.” Sacramento, CA.

2. Roberts, J., Marsh, R., and Herritt, K. Concrete Pavement Rehabilitation. Presentations at Workshop/Seminar. Ontario, California: July 16–18, 1997.

3. Carey, W., and Irick. P. 1960. “The Pavement Serviceability Performance Concept.” Highway Research Bulletin 250, Highway Research Board. Washington, D. C.

4. Hveem, F., 1960. “Devices for Recording and Evaluating Pavement Roughness.” Highway Research Bulletin 264, Highway Research Board. Washington, D. C.

5. Hudson, W. 1982. “Road Roughness: Its Elements and Measurement.” Transportation Research Record 836, Transportation Research Board. Washington, D. C.

6. Sayers, M., and Karamihas, S. 1998. The Little Book of Profiling, Basic Information about Measuring and Interpreting Road Profiles. University of Michigan, Ann Arbor, MI.

7. Janoff, M., Nick, J., and Davit, P. 1985. “Pavement Roughness and Rideability,” NCHRP Report 275, Transportation Research Board. Washington, D. C.

8. Zaniewski, J.P., Butler, Jr., B.C., Cunningham, G., Elkins, G. E., Paggi, M., and Machemehl, R. 1982. “Vehicle Operating Costs, Fuel Consumption and Pavement Type and Condition Factors,” PB82-238676, TRDF, FHWA, USDOT.

9. Sime, M., Ashmore, C., and Alavi, S. 2000. Tech Brief: WesTrack Roughness, Fuel Consumption and Maintenance Costs. Federal Highway Administration. Washington DC. FHWA-RD-00-052.

10. Harvey, J. T., Ali, A., Hung, D., Uhlmeyer, J., Popescu, L., Bush, D., Grote, K., Lea, J., and Scheffy, C. 2003. “Construction and Test Results from Dowel Bar Retrofit HVS Test Sections 553FD, 554FD, and 555FD: US 101, Ukiah, Mendocino County.” Draft report prepared for the California Department of Transportation. Pavement Research Center, Institute of Transportation Studies, University of California. UCPRC-RR-2003-03.

11. ARA, Inc., ERES Division, “Guide for Mechanistic-Empirical Design of New and Rehabilitated Pavement Structures,” Final Report NCHRP 1-37A, March 2004.

12 Darter, M., Smith, K., and Peshkin, D. 1991. “Field-Calibrated Mechanistic-Empirical Models for Jointed Concrete Pavements.” Transportation Research Record 1307, Transportation Research Board. Washington, D. C.

13. Yu, H., Darter, M., Smith, K., Jiang, J. and Khazanovich, L. 1996. “Performance of Concrete Pavements, Volume III – Improving Concrete Pavement Performance,” Final Report, Contract No. DTFH61-C-00053, Federal Highway Administration, McLean, Virginia.

14. Hoerner, T., Darter, M., Khazanovich, L., Titus-Glover, L., and Smith, K. 2001. “Improved Prediction Models for PCC Pavement Performance-Related Specifications, Volume I: Final Report,” FHWA-RD-00-130.

15. Harvey, J., Roesler, J., Farver, J., and Liang, L. September 1998. “Preliminary Evaluation of Proposed LLPRS Rigid Pavement Structures and Design Inputs,” Report for the California Department of Transportation, Institute of Transportation Studies, University of California, Berkeley, CA.

16. Hveem, F. N. 1949. “A Report of an Investigation to Determine Causes for Displacement and Faulting at the Joints in Portland Cement Concrete Pavements.” California Division of Highways, Materials and Research Department. Sacramento, CA.

17. Lea, J. and Harvey, J. T. August 2002 (Revision December 2004). **“**Data Mining of the Caltrans Pavement Management System (PMS) Database.” Draft report prepared for the California Department of Transportation. University of California Pavement Research Center, Institute of Transportation Studies. University of California, Berkeley and Davis. UCPRC-RR-2002-04.

18. McLeod, D. R., and Monismith, C. L. 1979. “Performance of Portland Cement Concrete Pavement.” Department of Civil Engineering, Institute of Transportation Studies, University of California, Berkeley, CA.

19. Wells, G. K., and Nokes, W. A. June 1991. “Synthesize PCCP Design Parameter Researched by Caltrans and Others.” California Department of Transportation, Division of New Technology, Materials, and Research, Office of Pavement.

20. Ventura, DFC. May 2003. “Durability Testing of LCB and CTB Materials Supplied by Caltrans.” Technical Memorandum prepared for the California Department of Transportation. University of California Pavement Research Center, Institute of Transportation Studies, University of California, Berkeley and Davis. UCPRC-TM-2003-02.

21. Mancio, M., Carlos, Jr., C., Zhang, J., Harvey, J. T., Monteiro, P. J. M., and Ali, A. May 2005. **“**Laboratory Evaluation of Corrosion Resistance of Steel Dowels in Concrete Pavement.” Draft report prepared for the California Department of Transportation. University of California Pavement Research Center, Institute of Transportation Studies, University of California, Berkeley and Davis. UCPRC-RR-2005-10.

22. University of California at Berkeley Pavement Research Center, Dynatest Consulting, Inc., Washington State Department of Transportation, University of Washington Seattle. August 2001. “Goal 7 Test Plan: Dowel Bar Retrofit Rehabilitation of Rigid Pavements.” Partnered Pavement Research Test Plan prepared for California Department of Transportation.

23. Roesler, J., Scheffy, C., Ali, A., and Bush, D. Final report submitted April 2000. **“**Construction, Instrumentation, and Testing of Fast-Setting Hydraulic Cement Concrete in Palmdale, California.” Report prepared for California Department of Transportation. University of California Pavement Research Center, CAL/APT Program, Institute of Transportation Studies, University of California, Berkeley. Draft report submitted March 1999. UCPRC-RR-2000-05.

24.Rao, S., and Roesler, J. May 2005. “Characterization of Effective Built-in Curling and Concrete Pavement Cracking on the Palmdale Test Sections.” Draft report prepared for the California Department of Transportation. University of California Pavement Research Center, Institute of Transportation Studies, University of California, Berkeley and Davis. UCPRC-RR-2005-04.

25. Heath, A., and Roesler, J. December 1999. “Shrinkage and Thermal Cracking of Fast Setting Hydraulic Cement Concrete Pavements in Palmdale, California.” Draft report prepared for California

Department of Transportation. University of California Pavement Research Center, CAL/APT Program, Institute of Transportation Studies, University of California, Berkeley.

26. Dynatest Corporation. March 1990. *ELMOD* 3.1 computer program.

27. Khazanovich, L., Darter, M I., and Yu, H. T. 2004. "Mechanistic-Empirical Model to Predict Transverse Joint Faulting." In Transportation Research Record: Journal of the Transportation Research Board (TRB), No. 1896: pp. 34-45. National Research Council: Washington D.C.

28. Plessis, L., Jooste, F., Keckwick, S., and Steyn, W. August 2005. **"**HVS Testing of the Palmdale Test Site, North Tangent Sections: Evaluation of Long Life Pavement Rehabilitation Strategies-Rigid." Draft report prepared for the California Department of Transportation. CSIR Transportek, Pretoria, Republic of South Africa. University of California Pavement Research Center, Institute of Transportation Studies, University of California, Berkeley and Davis. UCPRC-RR-2005-02.

29. Davids, W., Turkiyyah G. M., and Mahoney, J. P. 1998. "EverFE — Rigid Pavement Three-Dimensional Finite Element Analysis Tool." In Transportation Research Record: Journal of the Transportation Research Board (TRB), No. 1629: pp. 41-49. Washington D.C.

APPENDIX A:
LAYOUT OF DBR TEST SECTIONS

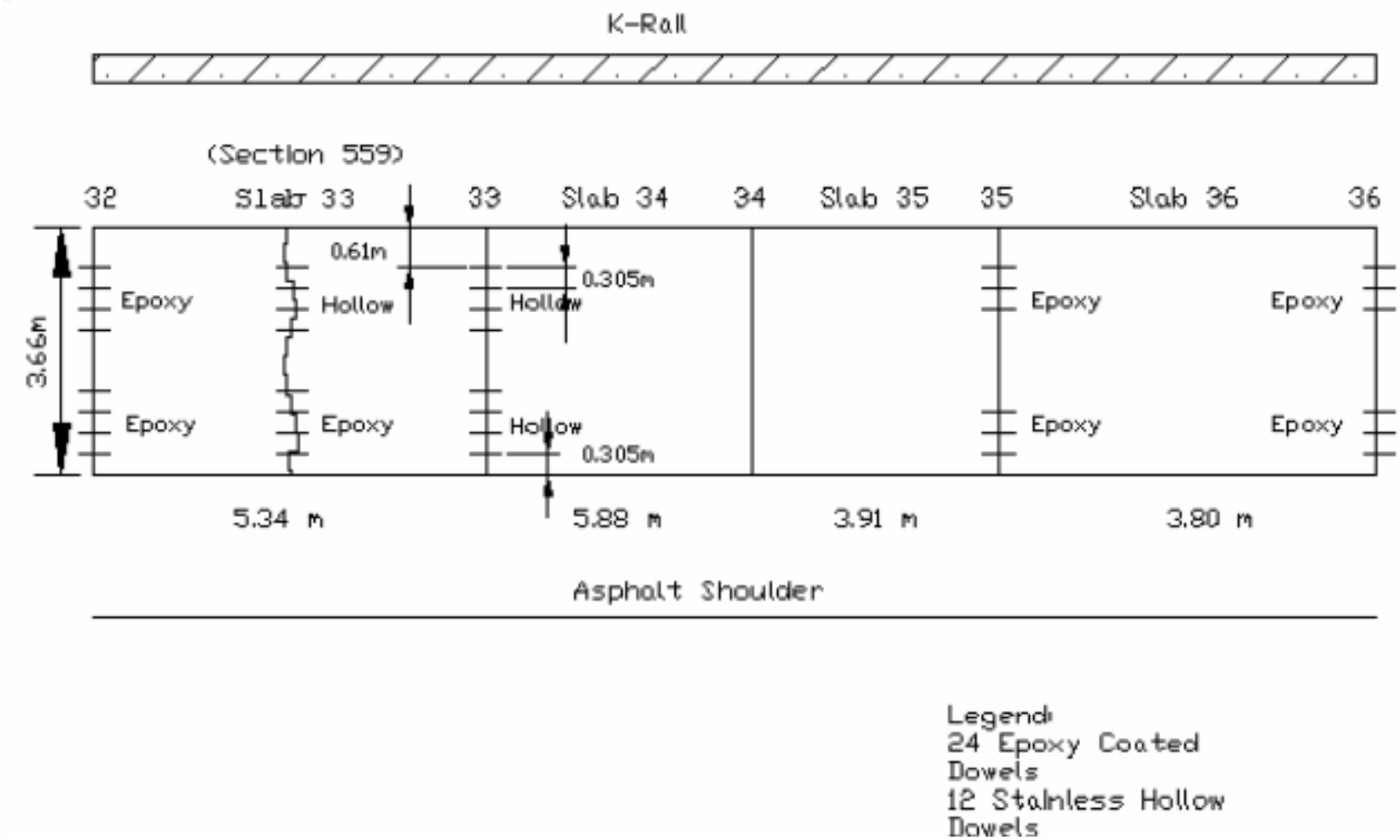

Figure A1. Slab Dimensions, Slab 33 – 36

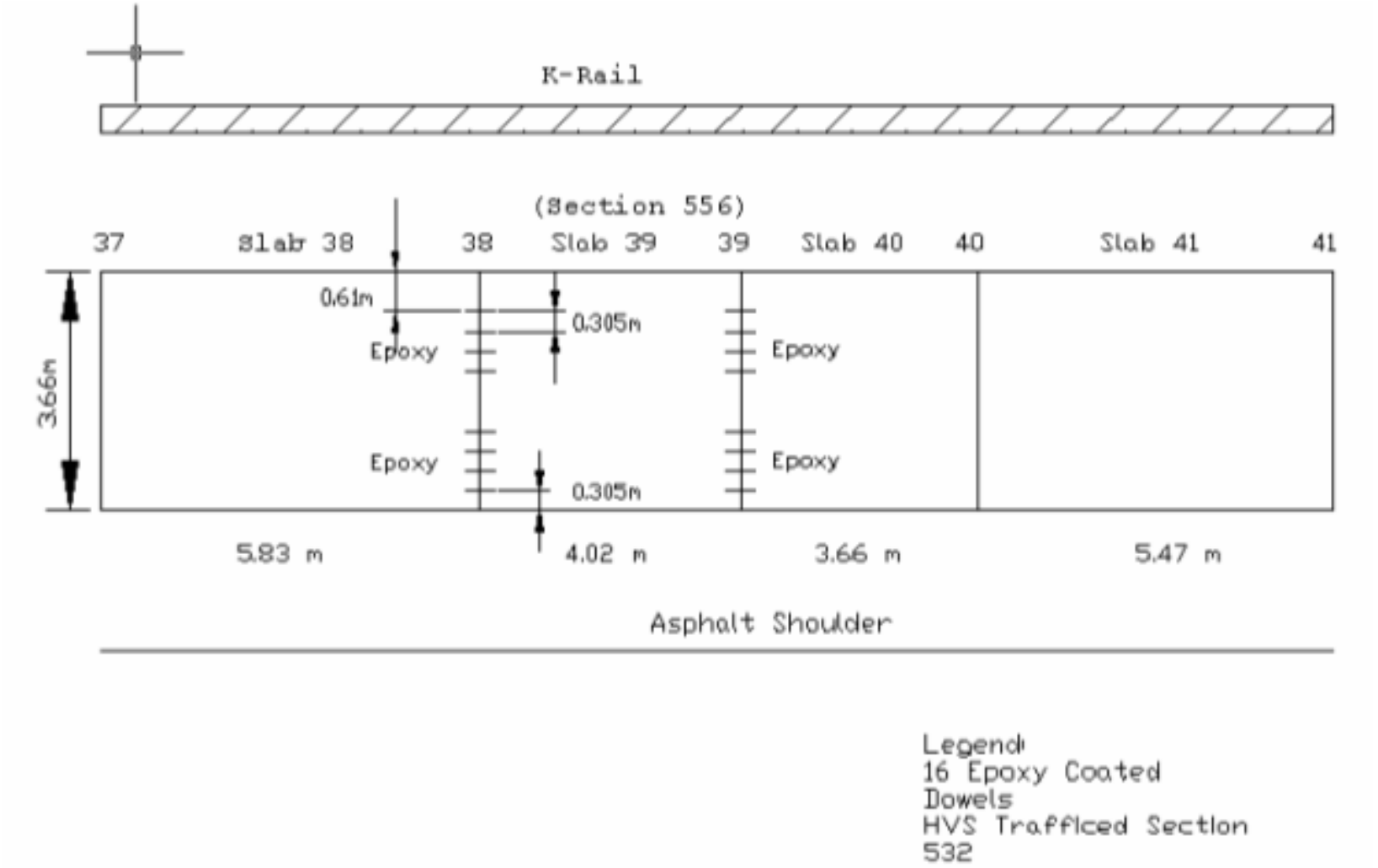

Figure A2. Slab Dimensions, Slab 38 – 41

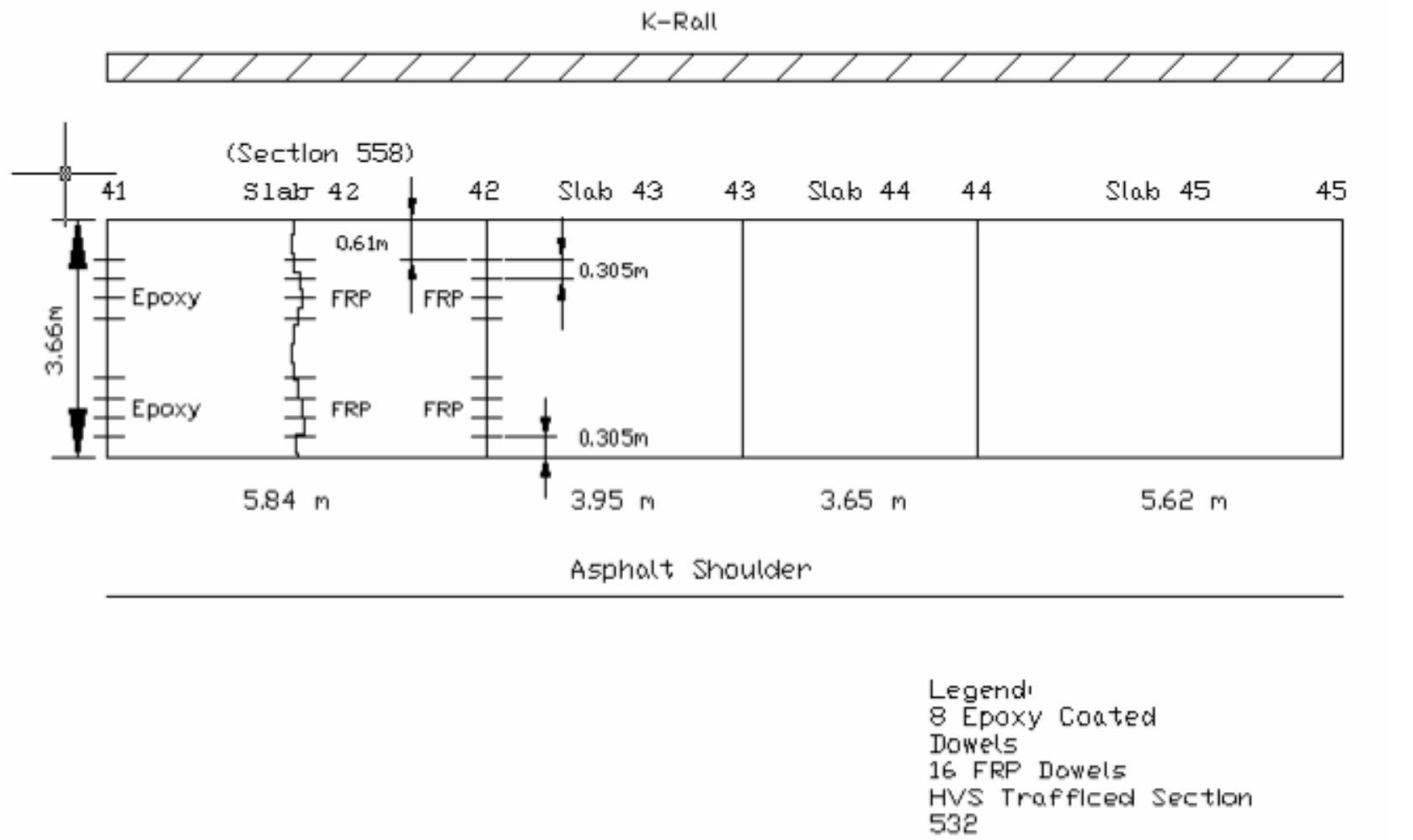

Figure A3. Slab Dimensions, Slabs 42 – 45

APPENDIX B:
OVERHEAD PHOTOGRAPHS OF HVS TEST SECTIONS AFTER TESTING

Appendix B. Figure 1. Slab 32 after DBR and HVS testing.

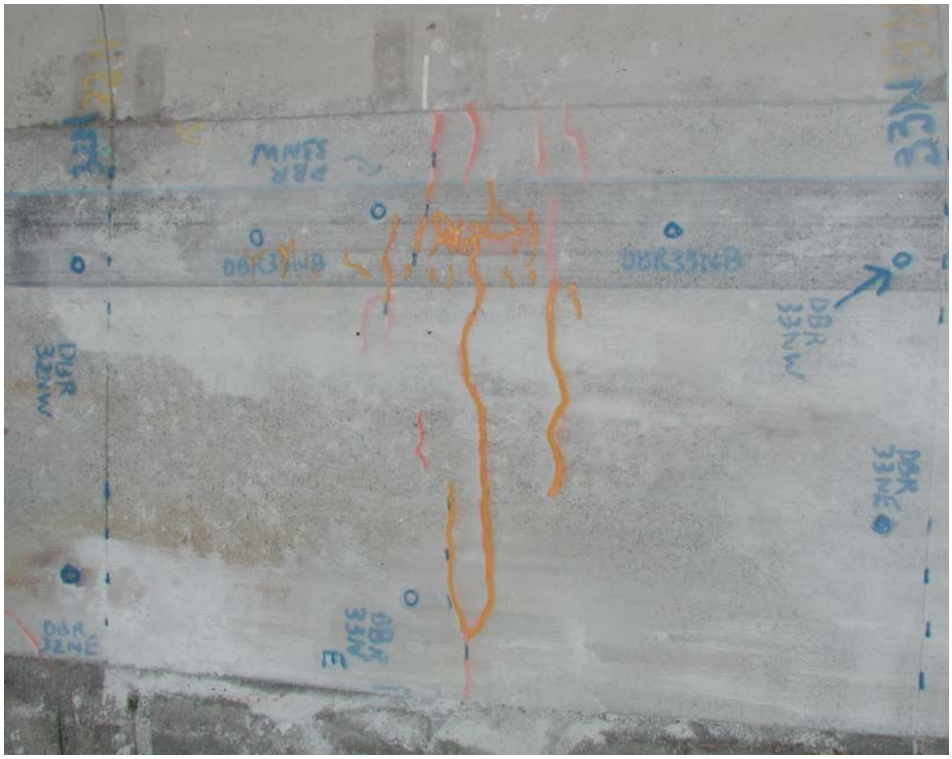

Appendix B. Figure 2. Slab 33 after DBR and HVS Testing.

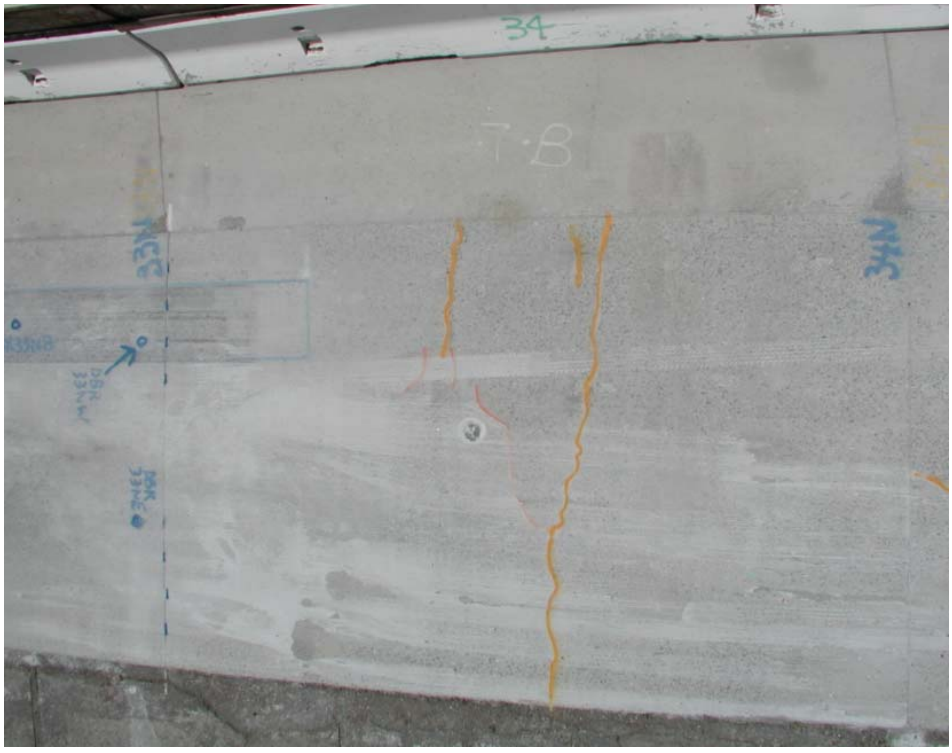

Appendix B. Figure 3. Slab 34 after DBR and HVS testing.

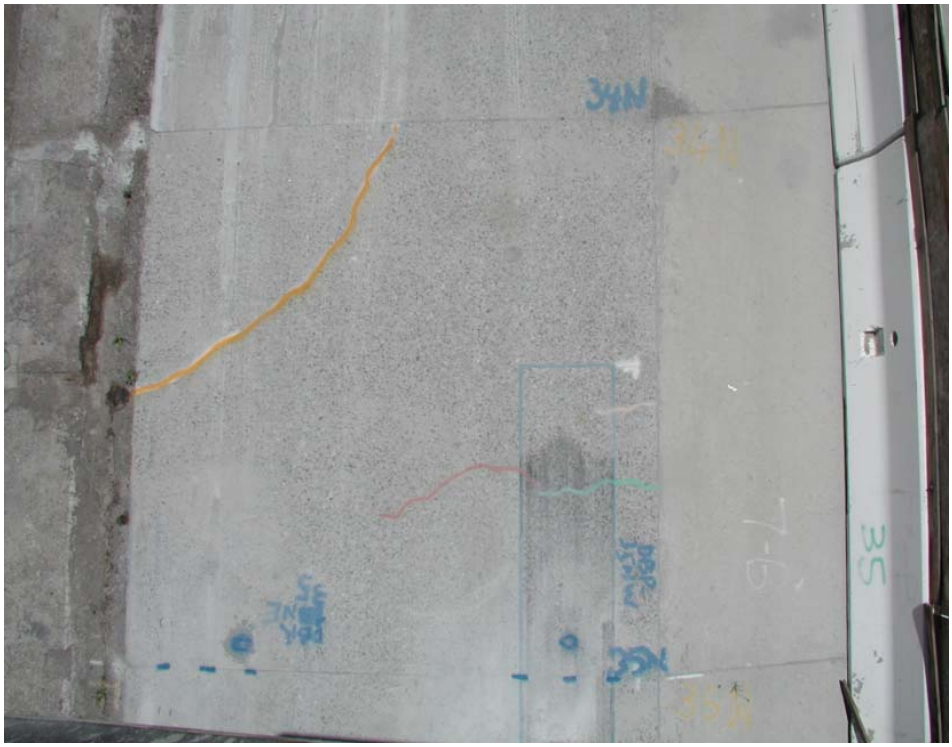

Appendix B. Figure 4. Slab 35 after DBR and HVS testing.

Appendix B. Figure 5. Slab 36 after DBR and HVS testing.

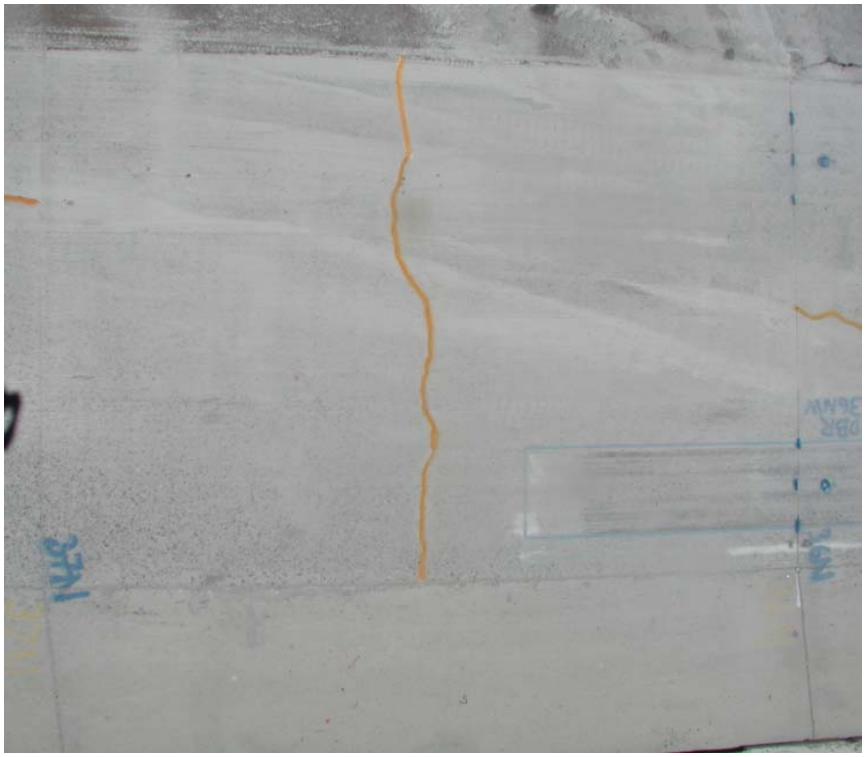

Appendix B. Figure 6. Slab 37 after DBR and HVS testing.

Appendix B. Figure 7. Slab 38 after DBR and HVS testing.

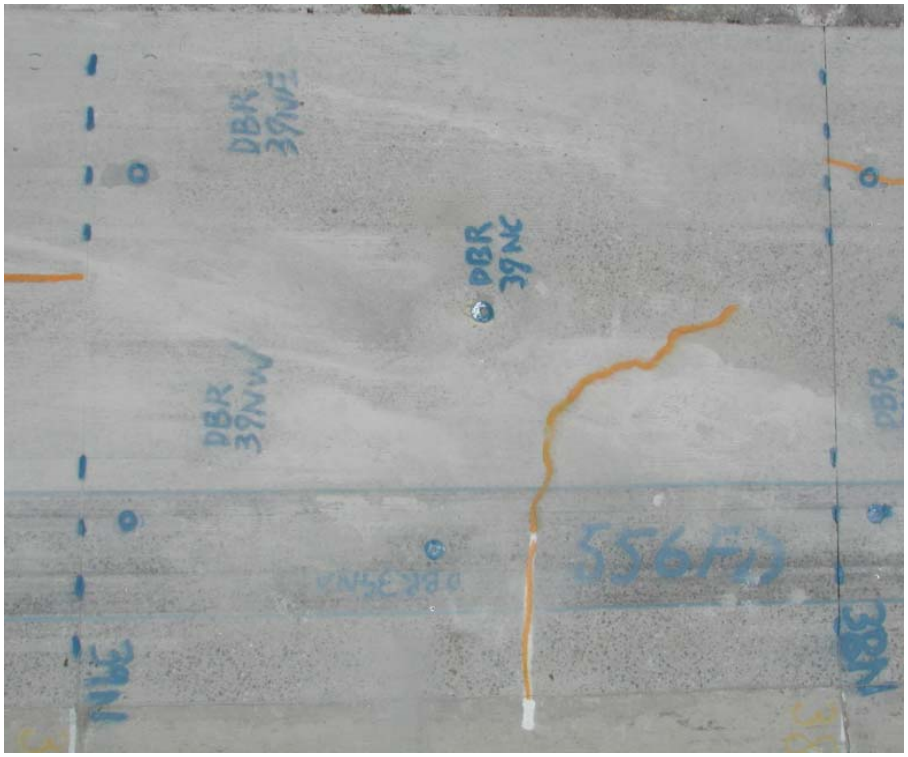

Appendix B. Figure 8. Slab 39 after DBR and HVS testing.

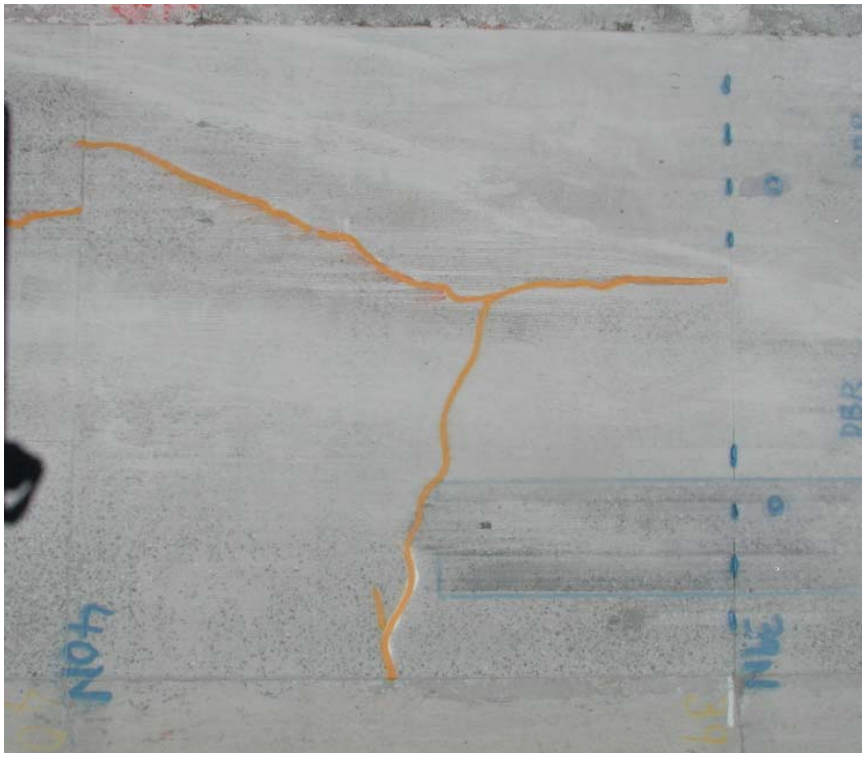

Appendix B. Figure 9. Slab 40 after DBR and HVS testing.

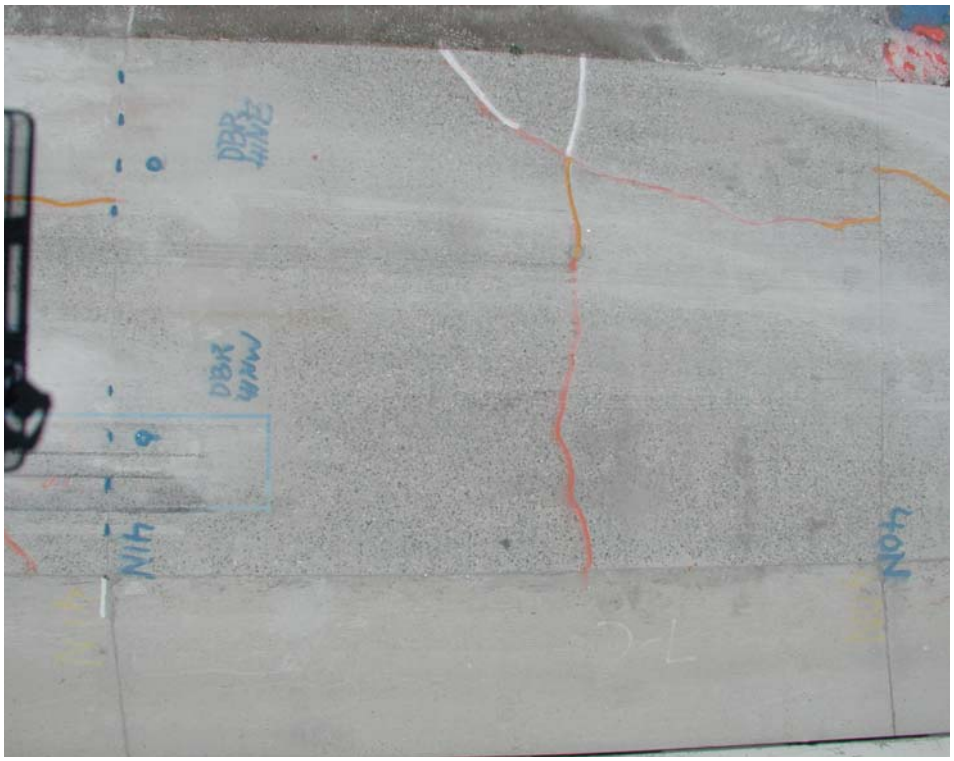

Appendix B. Figure 10. Slab 41 after DBR and HVS testing.

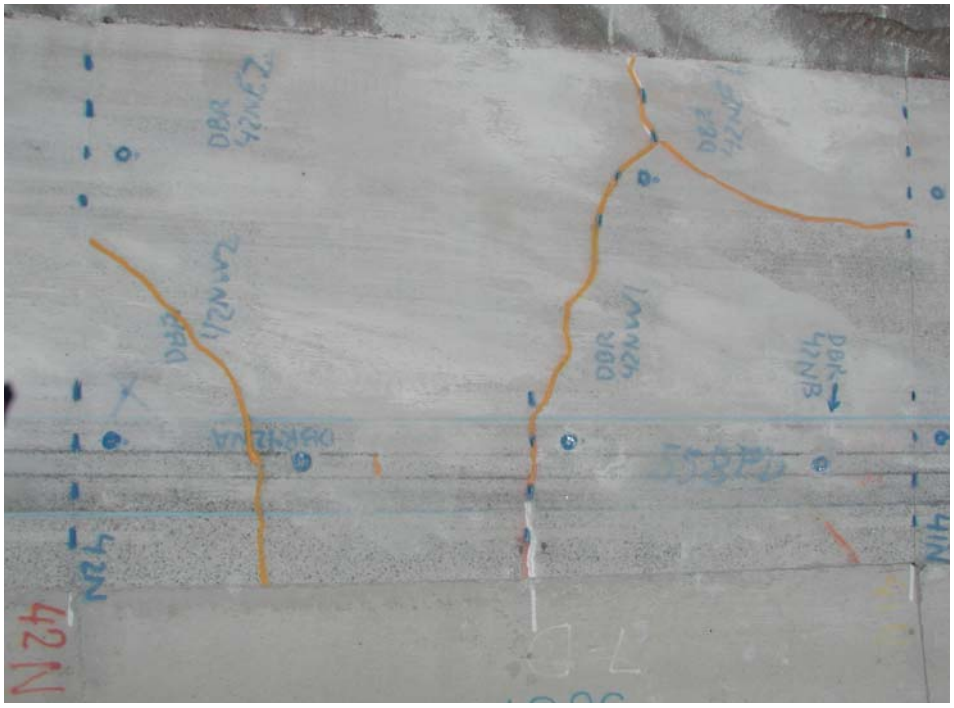

Appendix B. Figure 11. Slab 42 after DBR and HVS testing.

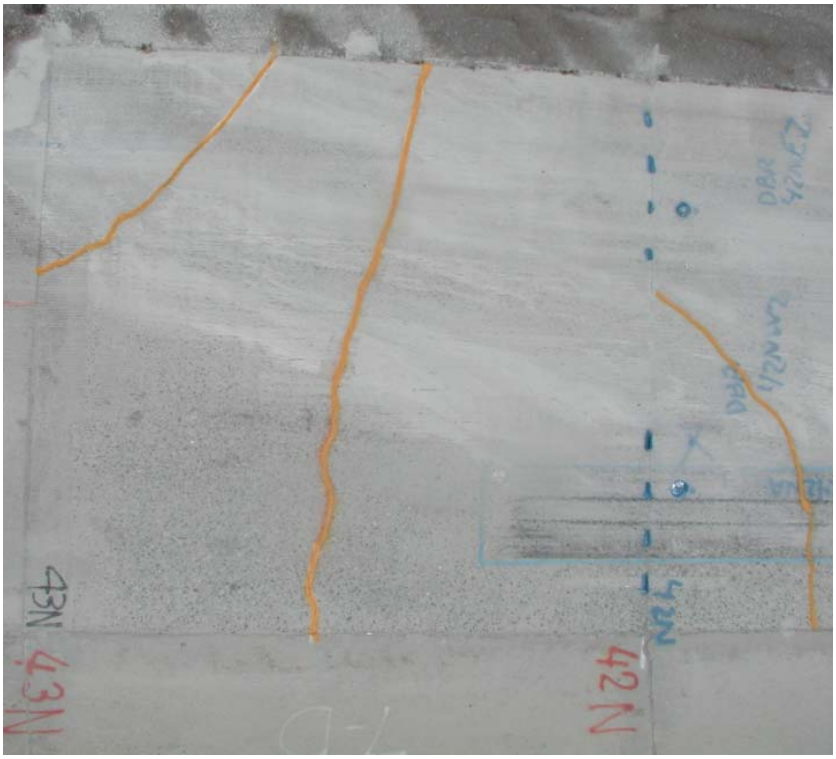

Appendix B. Figure 12. Slab 43 after DBR and HVS testing.

Appendix B. Figure 13. Slab 44 after DBR and HVS testing.

Appendix B. Figure 14. Slab 45 after DBR and HVS testing.

APPENDIX C:
GROUT STRENGTH DATA

Palmdale_DBR Flexural and Compression Strength

Batch Date:6/30/01

Flexural Strength

Specimen Name	Age (Days)	Date Tested	Depth (in)	Width (in)	Length (in)	Load (lb)	MR (Psi)	MR (Mpa)
PALMDALE_DBR-A-F	0.333	6/30/2001	6.13	6.00	18	5728	458.04	3.16
PALMDALE_DBR-B-F	0.333	6/30/2001	6.25	6.13	18	7151	537.98	3.71
PALMDALE_DBR-C-F	1	7/1/2001	6.02	6.20	18	6618	529.47	3.65
PALMDALE_DBR-D-F	1	7/1/2001	5.98	6.14	18	6279	514.72	3.55
PALMDALE_DBR-E-F	1	7/1/2001	5.93	6.18	18	7200	596.39	4.11
PALMDALE_DBR-F-F	7	7/7/2001	5.95	6.22	18	9682	792.77	5.47
PALMDALE_DBR-G-F	7	7/7/2001	6.00	5.91	18	8893	752.38	5.19
PALMDALE_DBR-H-F	7	7/7/2001	5.95	6.16	18	8994	743.62	5.13
PALMDALE_DBR-I-F	14	7/14/2001	6.00	6.00	18	11143	928.61	6.40
PALMDALE_DBR-J-F	14	7/14/2001	6.00	6.00	18	11388	949.03	6.54
PALMDALE_DBR-K-F	14	7/14/2001	6.00	6.00	18	11373	947.72	6.53
PALMDALE_DBR-L-F	28	7/28/2001	5.88	6.25	18	11487	958.50	6.61
PALMDALE_DBR-M-F	28	7/28/2001	6.00	6.25	18	11442	915.39	6.31
PALMDALE_DBR-N-F	28	7/28/2001	5.88	6.00	18	10588	920.29	6.35
PALMDALE_DBR-O-F	165	12/12/2001	6.00	6.00	18	13025	1085.41	7.48
PALMDALE_DBR-P-F	165	12/12/2001	6.00	6.14	18	12164	990.55	6.83
PALMDALE_DBR-Q-F	165	12/12/2001	5.94	6.10	18	12004	1003.94	6.92

Palmdale_DBR Flexural and Compression Strength **Batch Date:6/30/01**

Compressive Strength

Specimen Name	Age (Days)	Date Tested	Diameter(in)	Area (in^2)	Load (lb)	F'c (Psi)	F'c (Mpa)	Spec (Mpa)
PALMDALE_DBR-A-C	0.333	6/30/2001	4	13	67210	5351	36.90	21
PALMDALE_DBR-B-C	0.333	6/30/2001	4	13	67240	5354	36.91	21
PALMDALE_DBR-C-C	1	7/1/2001	4	13	74730	5950	41.02	-
PALMDALE_DBR-D-C	1	7/1/2001	4	13	78280	6232	42.97	-
PALMDALE_DBR-E-C	1	7/1/2001	4	13	77490	6170	42.54	-
PALMDALE_DBR-F-C	7	7/7/2001	4	13	93250	7424	51.19	-
PALMDALE_DBR-G-C	7	7/7/2001	4	13	95260	7584	52.29	-
PALMDALE_DBR-H-C	7	7/7/2001	4	13	97150	7735	53.33	-
PALMDALE_DBR-I-C	14	7/14/2001	4	13	109370	8708	60.04	-
PALMDALE_DBR-J-C	14	7/14/2001	4	13	107860	8588	59.21	-
PALMDALE_DBR-K-C	14	7/14/2001	4	13	101220	8059	55.57	-
PALMDALE_DBR-L-C	28	7/28/2001	4	13	113740	9056	62.44	-
PALMDALE_DBR-M-C	28	7/28/2001	4	13	115430	9190	63.37	-
PALMDALE_DBR-N-C	28	7/28/2001	4	13	113780	9059	62.46	-

APPENDIX D:
DEFLECTION DATA

Appendix D. Table 1. April 2002 Center Slab Deflection Summary (After DBR, Before HVS)

Daytime	Station (ft)	Pressure = 612 kPa			Pressure = 920 kPa			T_surface (C)	T_air (C)
		E1 (MPa)	E2 (MPa)	K-Value (MPa/m)	E1 (MPa)	E2 (MPa)	K-Value (MPa/m)		
	8.1	32046.8	220.6	118.9	35680.4	213.7	109.6	33.3	21.1
	27.1	39376.0	324.1	184.6	35059.9	303.4	173.7	31.7	21.7
	43.1	65155.5	248.2	112.2	62273.5	234.4	108.0	33.3	20.6
	55.1	64700.4	234.4	104.5	56088.9	227.5	106.9	33.9	21.7
	70.1	55909.6	255.1	121.3	54441.0	262.0	125.9	34.4	20.6
	88.1	41734.0	268.9	143.1	48449.5	268.9	138.9	33.9	21.1
	104.1	53386.1	220.6	103.2	59150.1	227.5	103.5	34.4	21.7
	116.1	52317.4	227.5	109.1	60949.7	227.5	102.4	34.4	21.1
	132.1	42692.4	227.5	116.0	43278.4	234.4	118.0	33.9	21.1
	150.1	36507.8	282.7	157.8	40768.7	296.5	163.9	35.6	21.1
	166.1	44691.8	199.9	95.9	44160.9	193.1	93.9	34.4	21.1
	179.1	44988.3	199.9	93.4	46994.7	199.9	93.1	35.0	20.6
	193.1	53055.2	158.6	67.1	55440.8	165.5	68.1	33.9	20.6
	211.1	58619.3	206.8	93.5	61315.1	213.7	93.4	33.3	20.6
	228.1	54096.3	262.0	128.2	53958.4	268.9	132.1	34.4	21.7
	243.1	50697.2	268.9	136.7	49959.4	296.5	151.5	33.3	21.1
	255.1	54999.5	275.8	136.1	58178.0	275.8	132.3	35.0	20.6
	275.1	50697.2	303.4	156.1	54192.8	303.4	154.6	35.0	20.6
	290.1	63052.6	296.5	145.5	65389.9	289.6	137.1	34.4	20.6
	302.1	53792.9	303.4	154.3	57460.9	303.4	154.1	33.9	20.6
	318.1	63080.2	282.7	136.0	57454.0	303.4	151.9	33.3	20.0
	335.1	62790.6	255.1	118.8	60205.0	268.9	129.0	34.4	20.0
	353.1	59474.2	241.3	113.5	58060.8	262.0	126.0	33.9	20.0
	365.1	47766.9	193.1	89.0	46767.2	186.2	87.9	32.8	20.0

	380.1	37576.4	213.7	108.3	36535.3	220.6	116.6	34.4	20.0
	400.1	57136.9	248.2	116.7	52338.1	255.1	127.5	34.4	20.0
	416.1	51965.8	268.9	132.6	48787.3	275.8	142.6	34.4	19.4
	427.1	48883.9	248.2	122.6	52489.8	248.2	120.5	33.3	19.4
	441.1	41278.9	213.7	104.5	44533.3	227.5	114.7	32.8	20.0
	460.1	51855.5	234.4	113.9	53510.2	255.1	123.8	32.8	19.4
	476.1	54254.9	234.4	109.0	53448.2	255.1	122.8	32.8	19.4
	489.1	38197.0	255.1	138.1	41658.1	248.2	127.7	31.7	18.9
	504.1	44905.6	275.8	143.6	49862.9	268.9	138.9	31.7	18.9
	523.1	53137.9	220.6	102.9	55723.5	234.4	109.2	32.2	19.4
	647.1	56902.5	234.4	110.5	59488.0	248.2	115.4	35.0	20.0
	663.1	32805.3	199.9	103.3	34563.4	220.6	116.1	31.7	20.0
	679.1	32260.6	186.2	95.0	34873.7	193.1	98.9	31.7	19.4
	695.1	40313.7	268.9	144.1	39672.4	289.6	161.8	31.1	20.6

Nighttime	**Station (ft)**	**Pressure = 603 kPa**			**Pressure = 931 kPa**				
		E1 (MPa)	**E2 (MPa)**	**K-Value (MPa/m)**	**E1 (MPa)**	**E2 (MPa)**	**K-Value (MPa/m)**	**T_surface (C)**	**T_air (C)**
	8.1	19712.1	158.6	86.7	19381.2	172.4	101.0	15.0	12.8
	27.1	19153.6	144.8	79.6	20553.3	158.6	88.9	13.9	12.8
	43.1	61949.4	393.0	207.2	69816.3	379.2	191.8	12.8	12.8
	55.1	62652.7	379.2	197.5	58219.4	393.0	213.9	13.3	12.8
	104.1	75297.7	241.3	105.6	75911.3	248.2	107.7	13.3	12.8
	116.1	53144.8	296.5	146.7	49869.8	289.6	148.5	13.3	13.3
	150.1	109392	199.9	71.0	108648.0	199.9	71.8	13.3	13.3
	167.1	57281.7	379.2	201.2	48346.1	420.6	243.1	13.3	12.8
	179.1	65555.4	365.4	182.8	58377.9	386.1	201.6	13.3	12.8
	194.1	76559.4	337.8	158.8	65038.3	365.4	183.2	13.3	12.2
	211.1	76049.2	386.1	191.5	77586.7	399.9	196.4	13.9	12.2
	229.1	77200.6	399.9	199.2	69974.9	324.1	154.1	13.3	12.8
	243.1	75787.2	324.1	149.4	97030.0	241.3	93.7	13.3	12.8
	255.1	86777.4	234.4	95.1	70236.9	193.1	79.2	13.3	12.2
	276.1	70829.9	186.2	73.6	63762.7	393.0	205.4	13.3	12.2

	290.1	69106.2	372.3	186.8	48973.5	282.7	143.2	12.8	12.8
	303.1	48980.4	282.7	143.5	95761.3	213.7	81.3	13.3	12.8
	318.1	88452.9	206.8	78.3	80455.0	324.1	144.6	12.8	12.2
	335.1	76187.1	330.9	153.4	67175.6	317.2	152.7	12.8	12.2
	354.1	72050.2	310.3	146.0	29557.8	193.1	104.3	13.3	12.2
	366.1	28682.2	199.9	109.6	72215.7	186.2	74.2	13.3	12.8
	380.1	71133.2	179.3	69.2	105062.0	227.5	86.1	12.8	12.8
	398.1	111585	227.5	82.2	51648.6	317.2	163.9	12.8	12.8
	418.1	48201.3	330.9	173.5	47311.8	241.3	117.7	12.8	12.2
	428.1	44126.5	248.2	126.6	15196.1	96.5	51.4	12.8	12.8
	442.1	13782.6	89.6	48.0	117983.0	165.5	55.3	12.8	12.2
	460.1	113626	158.6	52.8	47491.1	282.7	144.5	12.8	12.8
	476.1	43050.9	282.7	151.5	27565.3	151.7	75.4	12.8	12.2
	489.1	29040.7	137.9	67.5	63328.4	282.7	136.1	12.8	12.2
	504.1	65576.1	268.9	123.7	80675.6	275.8	119.7	12.8	12.2
	523.1	78214.2	255.1	112.9	18029.8	110.3	57.6	12.8	12.8
	663.1	19960.3	406.8	291.9	19753.5	441.3	319.6	12.8	12.2
	679.1	28213.4	117.2	54.7	30985.1	131.0	60.1	12.8	12.2
	695.1	36273.3	227.5	116.6	36232.0	220.6	111.0	12.8	12.2

Appendix D. Table 2. October 2002 Center Slab Deflection Summary (After DBR, Before HVS)

Daytime	Pressure = 434 kPa				Pressure = 704 kPa				T_surface (C)	T_air (C)
	Station (ft)	E1 (MPa)	E2 (MPa)	K-value (MPa/m)	Station (ft)	E1 MPa	E2 MPa	K-value MPa/m		
	S8.1	25827.8	248.21	148.05	S8.1	30826.47	234.42	126.92	27	18
	S27.1	15926.9	358.53	260.46	S27.1	20546.38	324.05	219.93	26	17
	S43.1	63728.3	434.37	234.15	S43.1	62935.37	420.58	228.41	25	18
	S55.1	53262	420.58	236.11	S55.1	53510.23	420.58	235.24	27	17
	S70.1	38479.7	296.47	161.61	S70.1	40934.19	296.47	158.09	25	16
	S88.1	51545.2	351.63	190.25	S88.1	55785.5	337.84	176.78	26	17
	S104.1	70133.5	420.58	219.78	S104.1	76649.05	386.11	191.23	27	17
	S117.1	61246.2	475.74	260.73	S117.1	61859.79	441.26	240.51	26	17
	S131.1	29640.6	199.95	105.67	S131.1	26434.51	206.84	115.90	25	16
	S150.1	14389.4	151.68	92.39	S150.1	16402.63	144.79	81.71	26	16
	S166.1	60977.3	406.79	215.80	S166.1	55206.34	420.58	230.11	25	16
	S179.1	53937.7	379.21	205.09	S179.1	47056.74	386.11	212.56	26	16
	S193.1	55323.6	296.47	147.31	S193.1	50628.22	303.37	156.24	24	16
	S211.1	69271.7	296.47	139.91	S211.1	66100.06	310.26	151.92	24	16
	S229.1	71546.9	399.90	201.37	S229.1	68644.23	399.90	201.05	23	16
	S243.1	65445.1	372.32	191.17	S243.1	68892.44	358.53	176.77	23	16
	S255.1	43209.5	172.37	77.56	S255.1	43119.83	172.37	79.38	23	15
	S276.1	30909.2	158.58	76.85	S276.1	28682.2	158.58	81.55	23	15
	S290.1	65052.1	372.32	191.44	S290.1	61066.89	379.21	197.51	23	15
	S303.1	55323.6	296.47	145.64	S303.1	52600.12	303.37	156.49	23	15
	S320.1	25303.8	117.21	57.85	S320.1	26186.3	117.21	56.96	23	15
	S335.1	72015.8	365.42	179.48	S335.1	69444.02	358.53	175.00	23	15
	S353.1	52448.4	399.90	223.95	S353.1	53468.86	393.00	218.48	23	15
	S365.1	12231.3	151.68	99.38	S365.1	13624.05	151.68	96.39	23	15
	S380.1	20229.2	144.79	76.51	S380.1	21111.76	137.90	75.13	23	15

	S399.1	87487.6	186.16	71.79	S399.1	89535.35	186.16	69.75	23	15
	S415.1	43995.5	337.84	187.79	S415.1	40348.14	358.53	203.86	23	15
	S428.1	40741.1	275.79	146.85	S428.1	43333.57	262.00	135.68	22	15
	S442.1	33749.9	117.21	52.27	S442.1	34432.43	124.11	52.86	22	14
	S463.1	51765.9	103.42	38.77	S463.1	54654.76	110.32	40.04	21	15
	S476.1	38983	234.42	123.85	S476.1	39279.45	234.42	119.75	21	15
	S491.1	55778.6	310.26	155.62	S491.1	62045.95	289.58	138.60	21	14
	S504.1	61563.3	330.95	163.20	S504.1	66355.17	317.16	154.41	22	14
	S523.1	69064.8	303.37	143.09	S523.1	66506.85	303.37	143.40	21	15
	S540.1	46160.4	399.90	233.75	S540.1	50145.59	386.11	216.47	22	15
	S552.1	38410.7	351.63	206.35	S552.1	49780.17	303.37	160.09	21	14
	S566.1	30047.4	144.79	70.94	S566.1	28551.2	151.68	76.69	21	15
	S566.1	67051.5	289.58	135.00	S566.1	46932.63	351.63	196.96	21	14
	S585.1	90169.7	179.26	65.37	S585.1	94837.42	179.26	63.60	21	14
	S603.1	22945.8	75.84	34.34	S603.1	24945.24	82.74	35.34	21	15
	S603.1	38831.3	227.53	118.90	S603.1	34108.38	241.32	130.89	21	15
	S615.1	41782.2	199.95	99.60	615.1	42878.51	213.74	106.36	22	15
	S629.1	14940.9	96.53	52.92	S629.1	15602.84	103.42	55.68	22	15
	S647.1	84695.2	179.26	67.73	S647.1	90576.46	186.16	70.11	22	15
	S665.1	16575	606.74	497.24	S665.1	32439.85	420.58	274.75	21	15
	S678.1	54027.3	186.16	82.66	S678.1	55571.77	193.05	84.85	21	15
Nighttime	Pressure = 414 kPa					Pressure = 668 kPa				
	Station	**E1**	**E2**	**K-value**	**Station**	**E1**	**E2**	**K-value**	**T_surface**	**T_air**
	(ft)	**MPa**	**MPa**	**MPa/m**	**(ft)**	**MPa**	**MPa**	**MPa/m**	**(C)**	**(C)**
	8.1	15678.68	89.63	46.16	8.1	15906.2	96.53	51.11	9	8
	27.1	11803.83	110.32	62.95	27.1	10900.6	110.32	67.14	9	8
	43.1	100567	455.05	219.86	43.1	103132	441.27	208.65	9	8
	55.1	42209.72	579.16	378.44	55.1	44857.3	530.90	337.13	9	8
	70.1	59129.46	165.47	69.33	70.1	60439.5	165.47	68.81	9	8
	88.1	44712.52	151.68	63.49	88.1	41927	158.58	71.64	11	7
	104.1	96437.01	330.95	147.35	104.1	92886.2	317.16	141.15	10	8
	116.1	45815.68	330.95	181.56	116.1	48842.5	310.26	164.61	9	8

	131.1	93492.95	165.47	58.97	131.1	98119.3	165.47	57.26	10	8
	150.1	43147.41	110.32	43.02	150.1	44843.5	110.32	44.10	10	8
	167.1	59329.41	586.05	345.24	167.1	69485.4	510.21	278.66	9	8
	179.1	74346.2	468.84	247.49	179.1	69161.3	482.63	261.04	10	8
	194.1	84709.02	386.11	185.54	194.1	91879.6	365.42	166.63	10	8
	229.1	82116.59	468.84	236.32	229.1	59687.9	551.58	318.99	10	8
	243.1	65010.69	365.42	185.58	255.1	120003	186.16	61.09	9	8
	255.1	122126.9	179.26	60.46	276.1	26262.1	110.32	49.14	10	8
	276.1	25586.45	103.42	46.81	290.1	90369.6	393.00	185.30	10	8
	290.1	74153.14	448.16	231.35	303.1	37721.2	234.42	120.61	9	8
	303.1	40479.14	220.63	110.66	318.1	28172	117.21	52.03	9	8
	318.1	28130.62	110.32	51.42	354.1	60839.4	372.32	192.79	9	8
	335.1	35011.59	482.63	322.87	366.1	22801	186.16	106.71	10	8
	354.1	57385.09	393.00	210.32	380.1	72608.7	117.21	40.30	9	7
	366.1	24214.4	186.16	105.47	418.1	65534.7	358.53	179.12	9	8
	380.1	72670.77	110.32	38.57	428.1	40892.8	220.63	109.67	9	8
	418.1	73187.88	344.74	165.92	442.1	21856.4	62.05	26.75	9	8
	428.1	35280.49	234.42	126.12	460.1	70581.7	213.74	89.35	10	8
	442.1	21821.92	62.05	26.82	476.1	46043.2	255.11	129.48	9	8
	460.1	71974.4	206.84	86.23	504.1	53303.4	303.37	150.63	10	8
	504.1	55337.34	303.37	153.15	523.1	66775.8	393.00	199.38	10	7
	523.1	69450.92	393.00	200.58	585.1	71540	241.32	105.27	9	8
	585.1	75407.99	234.42	98.90	614.1	29282	186.16	100.59	10	8
	604.1	33281.01	193.05	100.81	632.1	83819.6	137.90	49.16	9	8
	614.1	26613.77	179.26	99.66	679.1	45967.4	234.42	113.48	10	8
	632.1	76069.89	137.90	50.74						
	679.1	42513.09	241.32	124.53						

Appendix D. Table 3. April 2002 Joint Slab Deflection Summary (after DBR, before HVS)

Daytime	Station (ft)	LTE(%)		T_surface (C)	T_air (C)	Nighttime	Station (ft)	LTE(%)		T_surface (C)	T_air (C)
		Pressure = 613 kPa	Pressure = 959 kPa					Pressure = 603 kPa	Pressure = 931 kPa		
	18	96.83	95.52	32.2	21.1		17	90.28	90.05	17.2	12.8
	37	96.18	96.74	33.3	21.1		36	93.02	92.94	12.8	12.8
	50	98.31	97.56	33.9	21.1		48	92.27	92.00	12.8	12.8
	62	97.09	97.40	33.9	20.6		61	94.53	93.85	13.3	12.8
	80	97.05	95.16	34.4	21.1		79	94.74	94.96	13.3	13.3
	99	97.08	96.12	34.4	21.7		98	94.32	94.36	13.3	12.8
	112	95.65	95.65	33.9	21.1		111	92.75	91.88	13.3	12.8
	124	97.87	97.53	34.4	21.1		124	96.07	96.21	13.3	12.8
	143	97.87	98.59	34.4	21.1		143	96.69	96.50	13.3	12.8
	161	96.00	95.55	34.4	20.6		163	94.12	93.81	13.9	12.8
	176	98.21	96.45	34.4	20.6		176	90.21	90.09	13.3	12.8
	188	96.00	95.52	34.4	21.1		188	95.07	95.21	13.3	12.2
	206	97.49	97.66	34.4	21.1		206	92.17	92.17	13.3	12.8
	225	95.19	94.58	33.9	21.1		224	93.72	94.60	13.3	12.8
	238	95.85	96.30	33.9	21.1		238	93.89	93.81	12.8	12.8
	250	94.57	94.24	33.9	20.6		250	88.98	89.01	13.3	12.8
	268	95.42	95.80	35.0	20.0		267	97.96	96.71	13.3	12.8
	287	94.87	95.00	35.0	20.6		286	95.48	95.71	12.8	12.2
	300	94.48	95.16	34.4	20.6		299	94.29	93.98	13.3	12.2
	311	94.38	94.42	35.0	20.0		311	94.26	93.11	13.3	12.8
	329	95.38	95.24	34.4	20.0		330	96.10	95.20	13.3	12.8
	348	96.43	96.85	34.4	20.6		349	95.32	95.03	12.8	12.8
	361	96.46	97.04	32.8	19.4		362	97.62	97.39	12.8	12.8
	373	99.42	99.26	33.3	20.0		374	94.07	94.76	12.8	12.8
	394	95.03	95.65	35.0	20.0		394	93.29	92.92	13.3	12.2
	412	96.09	95.24	34.4	20.0		412	95.83	95.76	12.8	12.8

	425	94.06	94.31	33.9	20.0		426	93.98	94.17	12.8	12.8
	435	96.09	96.68	33.9	19.4		435	96.91	97.37	12.8	12.2
	453	95.95	95.20	33.3	20.0		453	98.92	98.08	12.8	12.2
	472	97.87	97.18	32.2	19.4		472	95.89	94.95	12.8	12.2
	486	96.84	96.93	31.7	19.4		486	94.68	94.52	12.8	12.2
	498	98.22	98.31	31.7	18.9		498	87.24	88.66	12.8	11.7
	516	97.65	97.82	32.8	19.4		515	88.55	86.35	12.8	12.2
	661	97.63	96.97	31.7	19.4		661	72.66	72.24	12.2	12.2
	674	95.87	95.03	32.8	19.4		675	59.15	62.55	12.8	12.2
	687	96.59	95.45	30.6	20.0		687	74.58	79.27	12.8	12.2
	705	94.77	93.90	31.1	20.0		705	58.50	58.24	12.8	12.2

Appendix D. Table 4. October 2002 Joint Slab Deflection Summary (after DBR, before HVS)

Day-time	Station (ft)	LTE (%)		T_surface (C)	T_air (C)	Night time	Station (ft)	LTE (%)		T_surface (C)	T_air (C)
		Pressure = 434 kPa	Pressure = 707 kPa					Pressure = 414 kPa	Pressure = 668 kPa		
	17	85.89	85.93	28	17		17	96.30	96.05	11	8
	37	85.38	85.11	25	17		36	92.58	92.43	9	8
	52	92.31	91.89	26	18		48	96.45	96.52	9	8
	62	91.30	91.53	25	17		61	91.54	91.52	9	8
	80	90.32	89.80	27	17		79	91.01	90.97	10	8
	99	93.06	93.04	26	17		98	91.14	91.12	10	8
	112	96.59	96.72	26	18		111	95.17	94.89	9	8
	125	88.64	88.26	26	17		124	93.25	92.94	10	8
	143	92.13	92.52	27	16		143	91.86	91.99	20	8
	163	93.12	92.56	25	16		162	91.00	90.69	10	8
	176	93.07	92.40	25	16		176	92.98	92.60	0	8
	187	95.86	95.65	24	16		188	91.43	91.87	10	8
	205	89.93	90.16	24	16		205	91.82	92.31	10	7
	225	93.98	94.03	24	16		224	91.78	91.45	10	8
	238	94.16	94.15	23	16		238	97.34	97.17	10	8
	250	90.91	91.04	23	15		250	96.05	96.03	10	8
	266	94.89	94.69	24	15		267	94.31	94.58	10	8
	287	92.06	90.43	23	15		286	93.33	93.17	9	8
	300	95.83	95.31	23	16		299	97.08	96.93	9	8
	311	91.67	91.04	23	16		311	96.37	96.42	9	8
	329	92.03	91.95	23	15		330	94.63	94.43	10	8
	348	94.41	94.12	23	15		349	92.86	93.14	9	8
	362	96.20	95.79	23	15		362	92.61	92.18	9	8
	376	90.82	90.55	22	15		374	94.53	94.22	9	8
	391	96.91	96.75	23	15		394	95.79	95.71	10	8

	412	94.38	93.90	23	15		412	95.91	95.82	9	8
	425	95.33	95.07	22	15		426	96.18	95.62	9	8
	437	97.67	97.83	22	15		435	95.51	94.74	10	8
	455	92.66	92.38	22	15		453	97.25	97.19	10	8
	472	92.39	92.41	21	15		472	95.60	95.02	10	8
	486	89.24	87.84	21	15		486	38.25	48.48	9	8
	498	79.85	82.55	21	15		498	82.71	84.12	9	8
	516	84.12	82.85	21	14		515	87.07	84.68	9	8
	535	95.03	94.77	22	14		535	69.93	75.33	9	8
	548	86.35	84.82	21	14		550	75.70	78.61	9	8
	561	84.68	84.34	21	14		559	48.81	50.19	9	8
	579	89.23	89.74	20	14		581	42.97	59.52	9	8
	598	82.12	85.12	23	15		600	90.58	90.87	9	8
	611	87.58	89.90	22	15		610	84.55	84.54	9	8
	623	59.76	61.58	22	15		625	30.93	22.51	9	8
	623	71.49	63.84	21	15		644	78.87	78.85	9	8
	641	67.31	69.88	22	15		661	85.71	85.64	8	8
	660	77.55	78.43	21	15		675	93.22	93.68	8	7
	675	93.38	93.70	21	15						

Appendix D. Table 5. April 2003 Center Slab Deflection Summary (after DBR, after HVS)

Daytime	Station (ft)	Pressure = 440 kPa			Pressure = 632 kPa				
		E1 (MPa)	E2 (MPa)	K-value (MPa/m)	E1 (MPa)	E2 (MPa)	K-value (MPa/m)	T_surface (C)	T_air (C)
	89	30419.68	241.32	136.12	30881.6	248.21	138.34	36	19
	104	54413.45	220.63	101.33	51676.2	227.53	108.23	30	19
	117	53861.87	199.95	89.00	48277.1	206.84	98.43	35	20
	131	50214.54	179.26	80.48	50835.1	179.26	79.88	36	19
	150	33294.8	220.63	120.04	34018.7	227.53	123.05	36	19
	166	42850.93	199.95	97.48	43864.5	199.95	95.59	35	20
	179	40768.72	199.95	100.12	41637.5	206.84	99.75	35	19
	193	52448.44	158.58	67.66	57281.7	151.69	62.83	35	19
	211	40947.98	199.95	98.01	38369.3	206.84	106.42	36	19
	229	54999.5	248.21	120.04	55882	241.32	116.08	34	19
	243	45029.68	241.32	123.30	47691.1	248.21	122.07	34	19
	255	35052.96	186.16	94.13	35315	199.95	100.55	34	19
	276	49711.22	268.90	137.62	55461.4	255.11	124.59	35	19
	290	62438.95	282.69	135.40	65893.2	275.79	128.42	34	19
	303	56805.93	262.00	124.09	55034	268.90	130.52	34	19
	320	40355.03	255.11	136.47	41727.1	255.11	133.40	33	19
	335	56750.77	255.11	123.67	57274.8	262.00	124.96	34	20
	353	54737.5	227.53	107.74	48808	241.32	117.14	34	19
	365	45567.47	179.26	81.01	45250.3	179.26	82.49	33	19
	380	38086.65	165.47	80.23	36321.6	172.37	85.05	33	19
	400	38658.92	193.05	96.23	41837.4	186.16	88.88	34	19
	415	47753.11	241.32	119.22	48821.8	241.32	121.42	34	19
	428	47560.05	234.42	114.98	45174.5	241.32	119.80	33	19
	442	39527.66	186.16	88.50	35252.9	193.05	99.47	33	19
	463	46360.37	165.47	74.02	43754.1	172.37	80.31	32	19

	476	50297.27	234.42	112.97	49697.4	234.42	114.59	33	18
	491	35252.91	220.63	116.87	36818	220.63	113.58	33	19
	504	46608.58	227.53	112.09	47518.7	234.42	115.33	33	18
	523	50690.28	193.05	89.33	53593	199.95	89.96	32	18
	540	41685.72	241.32	123.23	43478.4	241.32	121.95	32	18
	552	42471.72	268.90	139.92	45622.6	262.00	133.91	32	18
	566	54330.71	193.05	84.03	56447.4	193.05	85.26	33	18
	585	48539.11	137.90	58.25	52289.9	137.90	57.82	33	18
	603	35514.91	227.53	122.69	38762.3	220.63	115.35	33	19
	615	30316.26	193.05	101.99	28309.9	206.84	112.79	32	18
	621	36797.33	186.16	93.73	36700.8	193.05	97.04	32	18
	647	55861.35	206.84	94.07	58384.8	206.84	93.63	32	18
	665	43581.78	199.95	95.68	43216.4	213.74	106.02	32	18
	675	28475.36	172.37	90.40	30088.7	172.37	89.17	32	18
	678	33074.16	206.84	107.75	31281.5	206.84	112.10	32	18
	695	42375.19	282.69	152.19	44891.8	275.79	145.06	31	18
Nighttime	**Station (ft)**	**Pressure = 428 kPa**			**Pressure = 687 kPa**			**T_surface (C)**	**T_air (C)**
		E1 (MPa)	**E2 (MPa)**	**K-Value (MPa/m)**	**E1 (MPa)**	**E2 (MPa)**	**K-Value (MPa/m)**		
	88	14292.84	137.90	82.08	14237.68	144.79	87.55	10	7
	104	77159.26	317.16	143.20	71884.77	310.26	148.21	12	7
	117	65486.43	379.21	193.24	61618.47	379.21	201.58	11	7
	131	87198.03	227.53	89.09	90231.72	234.42	91.22	10	7
	150	55764.82	151.68	62.74	56447.40	158.58	65.78	11	7
	166	73587.77	344.74	162.35	76862.78	330.95	155.11	10	7
	180	69637.08	337.84	162.47	71533.14	337.84	160.34	10	8
	193	81123.75	330.95	151.49	75097.73	337.84	160.77	10	7
	211	209407.70	220.63	67.19	207097.90	220.63	67.64	10	7
	230	85460.55	420.58	201.70	63121.53	475.74	267.17	10	7
	243	77338.52	344.74	162.65	73408.51	344.74	165.94	10	7
	255	98450.28	199.95	74.66	92382.89	199.95	76.98	10	7
	276	34887.49	165.47	78.54	37045.55	165.47	79.42	10	7
	290	58977.78	434.37	235.12	70112.81	393.00	198.64	10	7

	303	65196.85	282.69	130.08	61859.79	296.47	140.81	10	7
	320	25331.35	158.58	82.06	28206.46	158.58	80.72	10	6
	335	74022.14	317.16	148.33	77297.15	310.26	141.82	10	7
	354	57778.09	282.69	139.87	58453.78	289.58	141.94	10	7
	366	43795.52	206.84	101.48	43140.51	206.84	102.53	10	7
	380	51503.86	158.58	65.69	50255.91	165.47	71.01	10	7
	400	45560.57	144.79	63.10	52103.70	144.79	59.77	10	7
	417	63997.16	324.05	155.78	65920.80	324.05	154.44	10	7
	430	55557.98	289.58	140.86	58240.04	282.69	133.79	10	6
	443	36935.23	96.53	39.09	33122.43	96.53	40.35	10	7
	463	95926.80	124.11	40.32	97078.22	124.11	40.04	10	6
	476	39720.71	262.00	140.08	43057.78	255.11	131.47	10	6
	492	29599.20	137.90	64.85	28447.78	131.00	62.97	11	6
	505	65176.17	255.11	114.41	69044.13	248.21	110.37	11	7
	524	61425.42	296.47	145.78	58826.09	296.47	146.34	10	6
	541	51076.38	199.95	92.71	54227.29	199.95	92.67	14	7
	552	72360.51	310.26	143.32	61521.94	330.95	164.26	11	7
	566	82688.86	296.47	133.27	90045.57	289.58	124.24	11	7
	585	82812.96	137.90	47.78	77076.52	151.68	53.93	11	7
	603	56468.08	317.16	161.92	62163.16	296.47	141.40	10	6
	616	28709.78	131.00	60.59	27654.88	131.00	64.84	10	7
	629	43340.46	137.90	58.18	50917.80	131.00	52.30	10	6
	647	90886.73	193.05	74.33	93844.58	199.95	75.30	10	6
	666	11734.88	262.00	192.66	9949.14	310.26	251.78	10	6
	681	27827.25	89.63	40.00	28592.57	103.42	44.06	10	6
	695	58343.46	317.16	157.27	52489.81	330.95	174.58	10	7

Appendix D. Table 6. June 2003 Center Slab Deflection Summary (After DBR, After HVS)

	Station (ft)	Pressure = 442 kPa			Pressure = 729 kPa			T_surface (C)	T_air (C)
		E1 (MPa)	E2 (MPa)	k-value (MPa/m)	E1 (MPa)	E2 (MPa)	k-value (MPa/m)		
Daytime	8	20732.54	234.42	148.53	20498.12	255.11	164.60	30	21
	26	17795.38	303.37	217.07	17953.96	296.47	210.42	35	21
	43	72043.35	310.26	145.34	73187.88	310.26	145.58	34	20
	54	42223.51	310.26	169.05	46594.79	296.47	155.97	35	21
	72	22139.07	262.00	164.20	21346.18	262.00	168.33	34	21
	90	18422.80	310.26	219.96	23518.03	262.00	164.36	35	21
	104	52517.39	324.05	170.35	56392.24	303.37	154.87	35	20
	117	46450.00	337.84	188.18	57061.03	310.26	155.51	35	21
	133	31371.16	234.42	126.80	26144.93	248.21	147.38	35	20
	150	48456.37	255.11	127.70	49793.96	255.11	126.26	36	20
	167	48642.53	241.32	117.22	43988.57	255.11	131.47	35	20
	179	50055.96	248.21	121.64	47463.53	248.21	127.02	36	21
	194	50504.12	193.05	86.04	50331.75	193.05	86.77	36	20
	212	47091.21	227.53	108.72	44167.83	234.42	118.35	36	20
	229	55757.92	344.74	182.52	57984.93	330.95	170.33	34	20
	241	40637.72	358.53	212.13	53599.86	317.16	163.90	35	20
	257	41685.72	220.63	108.67	38162.50	227.53	118.46	34	20
	276	48690.80	310.26	163.32	49573.32	296.47	150.44	35	20
	291	73532.62	324.05	153.43	67672.07	324.05	157.85	35	20
	302	58246.93	317.16	158.21	54806.45	324.05	167.04	34	20
	319	40885.93	303.37	162.95	44615.99	275.79	144.32	33	20
	337	63452.48	248.21	110.52	66479.28	241.32	106.41	36	20
	354	39831.03	289.58	161.53	43099.15	289.58	154.09	34	20
	365	48594.27	213.74	99.91	47980.64	206.84	97.52	33	20
	382	36645.65	213.74	113.38	39720.71	220.63	110.50	36	20
	398	55020.18	227.53	108.38	59901.68	220.63	99.39	36	20
	416	45512.31	289.58	155.06	55723.45	268.90	130.05	35	20

	427	46070.79	262.00	132.65	47704.84	248.21	126.78	35	20
	443	36466.39	193.05	96.71	39941.35	193.05	92.85	35	20
	460	57460.93	206.84	91.83	58474.46	206.84	91.58	34	20
	477	54289.34	268.90	133.93	56833.51	255.11	123.85	34	20
	490	38500.34	275.79	149.26	40375.72	255.11	133.35	34	19
	504	40272.29	289.58	159.07	54703.03	262.00	127.47	34	19
	522	44829.73	282.69	151.34	54006.66	262.00	128.04	35	19
	540	59322.52	268.90	127.83	52476.02	289.58	147.38	33	19
	552	43436.99	303.37	165.75	50717.86	289.58	149.54	32	20
	566	68527.02	289.58	138.31	63018.11	303.37	148.31	33	19
	586	50676.49	165.47	69.97	55254.61	158.58	67.14	33	20
	603	51131.54	282.69	145.01	44305.73	303.37	166.40	29	19
	615	32894.90	206.84	109.78	30585.16	227.53	122.31	33	19
	632	33115.53	234.42	129.91	35052.96	234.42	128.42	36	20
	650	31957.21	282.69	165.35	38307.29	262.00	142.84	34	19
	664	36928.33	275.79	152.68	37900.50	289.58	160.95	33	19
	677	34342.80	234.42	125.99	34811.64	234.42	128.93	32	19
	693	40265.40	344.74	197.26	44960.73	337.84	187.76	33	19
Nighttime	**Station (ft)**	**Pressure = 428 kPa**			**Pressure = 687 kPa**			**T_surface (C)**	**T_air (C)**
		E1 (MPa)	**E2 (MPa)**	**k-value (MPa/m)**	**E1 (MPa)**	**E2 (MPa)**	**k-value (MPa/m)**		
	8	22994.03	131.00	65.67	23848.98	137.90	68.93	14	11
	41	29902.57	310.26	187.41	28406.41	310.26	191.13	12	10
	55	37466.13	330.95	196.75	36624.97	330.95	194.71	14	10
	70	79496.58	193.05	74.20	78689.90	193.05	75.57	13	10
	89	54144.55	151.68	63.47	54399.66	158.58	65.23	13	10
	104	61025.52	379.21	201.45	65327.85	344.74	171.82	13	10
	117	47739.32	317.16	168.78	52186.44	303.37	153.99	13	10
	130	55682.08	448.16	253.51	53682.60	441.26	249.72	13	10
	150	60267.10	117.21	42.92	58646.83	124.11	45.86	14	9
	167	57150.67	399.90	212.46	56150.93	386.11	207.57	13	10
	180	58701.99	413.69	221.89	73311.98	365.42	177.66	13	10
	192	64045.43	448.16	241.89	76835.21	406.79	197.83	13	10

	211	78152.11	420.58	211.73	81758.06	393.00	190.76	13	9
	230	88563.19	441.26	212.97	75732.04	455.05	234.87	12	9
	242	49463.01	358.53	194.92	66499.96	303.37	143.27	13	9
	259	27158.46	103.42	49.39	27454.93	110.32	48.96	12	9
	275	160530.70	179.26	54.70	149954.14	179.26	56.82	13	10
	291	79999.90	413.69	204.46	73546.41	393.00	196.54	12	9
	304	62845.74	275.79	131.53	56605.98	296.47	146.70	12	9
	319	73015.51	158.58	59.39	72994.82	158.58	58.78	12	9
	337	75800.99	344.74	165.62	76938.63	337.84	158.43	12	9
	353	63900.64	317.16	157.84	64079.90	310.26	153.08	12	9
	367	43878.25	206.84	101.78	38989.87	213.74	106.35	11	9
	383	22628.60	144.79	76.26	25772.61	137.90	69.05	11	9
	399	113101.64	144.79	44.91	116169.81	144.79	46.04	12	9
	417	64817.64	310.26	150.53	59887.89	310.26	152.25	12	9
	429	50869.54	268.90	131.07	50317.96	262.00	127.13	11	9
	445	26896.46	151.68	77.96	26220.77	151.68	78.68	12	9
	466	12500.20	75.84	39.08	13065.57	75.84	36.67	11	9
	479	78862.27	227.53	94.48	76483.57	220.63	93.88	12	9
	492	37004.18	172.37	81.19	34163.54	165.47	78.98	12	9
	506	64707.32	296.47	139.21	77269.58	268.90	116.28	12	9
	523	73394.72	317.16	148.88	83392.12	296.47	131.43	12	9
	541	27903.09	110.32	51.77	29282.05	117.21	51.79	11	9
	555	64569.43	303.37	143.20	63218.05	303.37	146.92	11	9
	569	90059.36	255.11	104.29	83012.91	262.00	111.60	11	9
	587	76497.36	110.32	35.85	79862.01	110.32	35.00	11	9
	604	55868.24	296.47	150.12	52710.44	296.47	150.93	11	9
	618	30909.21	124.11	55.45	29254.47	124.11	58.37	11	9
	634	18457.27	103.42	53.72	20022.38	103.42	54.15	11	9
	647	104138.46	179.26	63.81	103579.98	186.16	67.46	11	10
	666	18126.32	386.11	281.26	20498.12	386.11	272.50	12	10
	680	25110.72	89.63	37.83	27544.57	89.63	38.85	12	10
	695	28020.31	206.84	111.36	33708.48	193.05	95.85	12	10

Appendix D. Table 7. February 2004 Center Slab Deflection Summary (After DBR, After HVS)

	Station (ft)	Pressure = 847 kPa			Pressure = 1287 kPa			T_surface (C)	T_air (C)
		E1 (MPa)	E2 (MPa)	k-value (MPa/m)	E1 (MPa)	E2 (MPa)	k-value (MPa/m)		
Daytime 1	476	46953.32	262.00	132.99	47511.79	262.00	133.30	10	13
	491	35928.59	158.58	76.33	38334.87	172.37	78.73	12	12
	502	54978.82	220.63	99.46	53489.55	213.74	98.70	11	12
	509	31419.42	193.05	99.90	32260.58	193.05	99.91	11	12
	526	63955.79	241.32	110.17	60977.26	241.32	109.95	12	11
	541	58198.67	275.79	131.42	57888.40	268.90	126.44	11	12
	553	67044.65	330.95	160.57	64934.85	330.95	162.45	11	11
	569	66844.70	255.11	115.21	68464.97	255.11	113.31	11	11
	589	61025.52	199.95	85.04	60508.41	206.84	90.36	11	11
	604	41251.35	275.79	147.56	40348.14	275.79	145.90	11	11
	618	37404.07	193.05	96.19	40396.40	199.95	96.79	11	12
	631	60198.15	213.74	91.79	64266.06	206.84	87.15	11	11
	647	65645.01	234.42	102.18	61218.57	241.32	109.47	11	11
	653	29702.63	213.74	114.37	27179.14	227.53	127.83	10	11
	663	18540.01	379.21	274.67	23056.08	337.84	226.13	10	11
	680	24021.34	158.58	86.17	24366.08	172.37	93.02	10	11
	695	30929.89	193.05	100.92	30874.74	193.05	103.67	11	11
Daytime 2	Station (ft)	Pressure = 837 kPa			Pressure = 1262 kPa			T_surface (C)	T_air (C)
		E1 (MPa)	E2 (MPa)	k-value (MPa/m)	E1 (MPa)	E2 (MPa)	k-value (MPa/m)		
	8	24752.19	268.90	159.48	30185.26	255.11	145.36	10	11
	27	58109.04	206.84	88.79	120189.46	137.90	44.43	11	12
	53	36590.49	330.95	196.17	30336.94	372.32	240.93	10	12
	68	177974.44	96.53	24.01	147430.65	110.32	30.50	10	12
	88	11810.72	337.84	265.86	16313.00	303.37	213.44	10	12
	104	61590.89	241.32	109.77	65196.85	234.42	104.95	11	13

	116	62942.26	351.63	174.87	59632.78	337.84	171.81	11	13
	132	46808.53	248.21	127.16	47077.42	255.11	127.08	10	13
	150	7935.87	303.37	254.61	12789.78	248.21	174.37	11	13
	167	64790.06	330.95	161.95	62252.79	337.84	165.61	11	12
	179	57454.04	379.21	200.80	63459.37	365.42	184.95	12	13
	197	29812.94	199.95	105.99	31247.05	213.74	114.25	12	12
	211	188206.26	179.26	53.71	186523.94	186.16	54.98	12	13
	229	82943.96	351.63	161.91	81178.90	337.84	154.43	12	13
	243	76090.57	324.05	149.26	77676.37	310.26	142.09	12	13
	256	40582.56	289.58	160.71	48463.27	282.69	144.32	12	13
	275	22104.60	399.90	276.47	27889.30	365.42	230.00	13	13
	291	82964.65	379.21	177.99	78076.26	399.90	195.65	12	12
	303	70547.18	324.05	153.46	71533.14	310.26	143.27	13	12
	318	19491.49	268.90	175.29	22973.34	268.90	166.01	13	12
	335	157862.42	199.95	64.28	153484.25	199.95	66.47	13	12
	354	61246.15	262.00	121.96	62197.63	255.11	119.70	13	11
	367	36493.97	179.26	86.40	39231.18	179.26	84.23	13	12
	381	15637.32	172.37	106.16	16871.48	186.16	112.46	13	12
	401	22794.08	110.32	56.28	23821.40	117.21	59.34	13	12
	418	60439.47	275.79	130.60	64383.27	275.79	126.80	13	11
	429	48311.58	255.11	126.04	55116.71	241.32	111.76	12	10
	443	17788.48	131.00	73.40	18236.64	137.90	75.52	12	10
	462	71953.72	186.16	72.63	70050.76	186.16	75.88	11	10
	477	67720.33	241.32	107.51	63259.42	241.32	110.29	11	10
	493	44960.73	206.84	100.47	46063.89	213.74	102.06	10	8
	504	54923.66	275.79	133.04	55316.66	262.00	125.38	9	9
	510	55302.87	262.00	125.30	51393.54	255.11	125.19	9	8
	521	65403.69	268.90	124.38	60873.84	275.79	129.77	9	9
	540	47925.48	248.21	120.15	47360.11	248.21	120.82	9	8
	555	66865.38	324.05	157.08	68527.02	324.05	154.61	8	8
	565	75345.94	358.53	171.39	69154.44	351.63	173.04	8	8
	591	54827.13	193.05	82.92	57867.72	193.05	83.54	8	8

	606	60508.41	310.26	151.16	54406.55	310.26	155.50	7	8
	615	48794.22	179.26	80.09	48973.48	186.16	84.73	7	8
	634	16981.79	117.21	64.49	17305.85	124.11	68.55	7	7
	648	75745.83	220.63	90.79	74201.41	220.63	92.07	7	8
	655	36169.91	234.42	120.64	34715.12	241.32	130.60	7	7
	665	45277.89	248.21	125.54	44698.73	255.11	129.79	6	8
	679	37962.55	179.26	83.96	39548.34	179.26	86.25	6	8
	694	32419.16	193.05	98.66	31709.00	206.84	108.29	6	8

Appendix D. Table 8. April 2003 Joint Slab Deflection Summary (After DBR, After HVS)

Daytime	Station (ft)	LTE (%)		T_surface (C)	T_air (C)	Nighttime	Station (ft)	LTE (%)		T_surface (C)	T_air (C)
		Pressure = 440 kPa	Pressure = 632 kPa					Pressure = 424 kPa	Pressure = 600 kPa		
	99	96.15	96.30	30	19		99	93.51	93.33	11	7
	112	96.09	96.06	31	20		112	93.46	93.84	12	7
	125	95.74	95.49	36	19		124	95.24	94.87	11	7
	143	96.89	97.00	37	19		143	95.86	96.67	11	7
	163	97.75	98.43	35	19		163	93.79	93.28	10	7
	176	97.00	97.14	35	19		174	92.00	91.87	10	8
	187	97.21	97.21	34	19		187	93.02	92.77	11	7
	205	96.89	96.97	34	19		205	92.31	92.73	10	7
	225	96.30	96.37	35	19		225	91.89	92.02	10	7
	238	97.92	97.78	34	19		238	92.83	92.80	10	7
	250	96.97	97.38	34	19		250	92.12	92.24	10	7
	266	96.43	96.30	35	19		266	90.91	90.48	11	7
	287	97.48	97.18	35	19		287	93.79	93.33	10	7
	300	95.65	95.34	34	19		299	93.17	93.06	10	7
	311	96.83	97.75	34	19		311	92.49	92.50	10	7
	329	97.93	97.61	34	19		329	93.63	93.90	10	7
	348	96.61	97.08	34	19		348	93.71	93.98	10	7
	362	96.70	96.39	33	20		362	95.05	94.69	10	7
	376	96.77	96.55	33	19		374	91.49	91.64	10	7
	391	97.56	97.14	33	19		390	93.72	93.52	10	7
	412	97.74	97.89	34	19		412	95.51	95.27	10	7
	425	96.05	96.33	34	19		425	92.00	91.65	10	6
	437	96.67	96.47	33	19		436	96.40	95.90	10	7
	455	96.06	96.09	34	19		455	95.52	95.80	11	7
	472	96.92	96.17	32	18		473	93.02	93.02	11	7
	486	98.06	97.74	34	18		486	97.30	96.95	10	6
	498	97.82	97.23	33	18		499	91.37	91.37	10	7

	516	97.44	97.14	33	18		516	88.28	88.22	11	7
	535	97.81	97.96	32	18		535	57.78	63.61	12	7
	548	97.33	96.86	32	18		548	76.85	79.58	11	7
	561	96.82	96.46	32	19		561	54.76	56.66	11	7
	579	95.91	96.36	33	18		579	72.29	76.67	11	7
	598	97.94	97.90	34	19		598	93.21	93.59	11	7
	611	99.07	99.68	32	19		611	82.81	83.12	10	6
	624	96.47	96.39	33	18		623	51.69	60.85	10	7
	641	96.05	96.06	32	18		641	82.40	84.55	11	6
	660	97.80	97.71	32	18		660	71.17	72.83	10	7
	686	97.35	96.89	30	18		673	85.00	85.28	10	6
	705	96.80	96.46	32	18		685	56.20	63.64	10	6
							704	45.57	49.44	10	6

Appendix D. Table 9. June 2003 Joint Slab Deflection Summary (After DBR, After HVS)

Daytime	Station (ft)	LTE (%)		T_surface (C)	T_air (C)	Nighttime	Station (ft)	LTE (%)		T_surface (C)	T_air (C)
		Pressure = 442 kPa	Pressure = 729 kPa					Pressure = 428 kPa	Pressure = 687 kPa		
	17	94.66	94.83	34	20		8	91.08	92.50	13	11
	37	96.35	96.27	33	20		18	89.42	88.96	14	11
	50	95.29	95.38	34	20		27	43.44	51.74	14	11
	62	96.05	96.12	34	20		37	94.40	94.42	13	11
	71	92.19	92.38	33	21		50	96.95	96.51	13	10
	79	96.05	96.21	34	22		62	92.97	93.65	13	10
	89	94.92	94.23	34	22		71	89.50	89.04	13	10
	99	92.80	93.27	34	20		80	95.86	95.62	13	10
	112	96.05	95.52	34	20		89	93.07	91.79	13	10
	124	96.45	95.58	34	20		99	93.88	93.22	13	10
	132	93.91	94.62	33	20		112	96.50	96.15	13	10
	142	94.49	95.15	35	20		124	96.20	96.03	13	10
	151	95.16	95.15	36	20		133	83.87	84.15	13	10
	161	94.19	94.16	35	20		143	95.51	94.95	14	10
	174	96.13	96.22	36	20		151	92.41	90.87	14	10
	186	97.50	97.66	35	20		162	93.92	93.33	13	10
	196	97.96	98.33	35	20		170	92.63	93.59	13	9
	204	94.57	94.74	34	20		174	96.33	96.59	13	10
	215	93.75	94.29	35	19		187	95.06	94.74	13	9
	224	93.81	94.57	34	20		197	87.74	86.51	13	10
	236	94.92	95.77	34	20		205	93.33	92.61	13	9
	248	95.73	95.38	35	20		216	66.67	70.85	13	9
	256	95.10	95.40	35	20		224	93.33	93.75	13	10
	266	95.24	95.95	35	20		237	96.95	96.97	13	9
	275	94.85	94.48	36	20		249	96.60	95.90	13	9
	285	95.50	95.29	36	20		257	88.72	88.29	12	10
	298	96.61	97.41	34	20		267	93.15	93.28	13	9

	304	96.63	95.95	35	20		277	94.27	93.56	13	9
	311	95.00	94.90	35	20		286	95.65	95.93	13	9
	318	96.77	96.10	34	20		299	95.61	95.42	12	9
	328	96.50	96.17	35	21		305	94.87	95.45	12	9
	341	93.44	93.33	36	20		312	93.64	93.68	12	9
	348	94.02	94.30	35	20		320	88.98	88.00	13	9
	353	96.91	96.86	35	20		330	97.18	96.67	12	9
	360	97.01	96.63	34	20		343	83.58	78.87	12	9
	373	95.87	95.29	34	20		349	97.44	98.02	12	9
	380	96.92	97.14	35	20		362	97.25	97.27	12	9
	391	95.87	96.45	35	20		374	97.92	97.14	12	9
	399	94.66	94.39	37	20		381	98.63	98.28	12	9
	410	97.64	97.61	36	20		392	98.06	98.16	12	9
	423	97.01	97.22	35	20		410	91.79	88.46	12	9
	435	98.25	96.81	35	20		411	95.50	95.53	12	9
	440	96.06	95.65	35	20		424	98.43	97.81	12	9
	453	97.44	96.88	35	20		436	99.47	99.34	12	9
	462	96.64	96.30	35	20		442	93.81	92.83	11	9
	472	96.72	96.48	34	20		454	98.82	98.92	12	9
	485	97.99	97.54	35	19		464	92.49	92.42	12	9
	497	98.11	98.54	33	20		473	97.01	97.42	12	9
	515	95.08	95.24	35	19		482	95.33	94.94	12	9
	525	97.39	97.85	33	19		487	98.56	97.74	12	9
	534	94.81	94.59	33	19		499	93.29	93.66	12	9
	547	96.61	96.88	33	20		508	92.86	93.16	11	9
	560	94.96	95.58	33	20		509	94.44	94.51	11	9
	569	97.22	97.10	33	19		517	94.42	93.40	12	9
	578	95.89	96.27	32	19		527	100.72	100.00	12	9
	588	96.55	96.66	34	19		528	93.94	94.04	12	9
	597	96.00	96.03	34	19		536	85.45	85.43	11	9
	610	94.74	95.68	31	19		549	87.61	87.95	11	9
	622	95.06	95.09	33	19		562	69.01	68.31	11	9

	630	97.50	97.20	33	20		571	89.06	88.89	11	9
	640	95.18	95.56	31	19		580	92.42	92.86	11	9
	648	97.44	98.43	34	19		590	77.49	80.84	11	9
	659	95.56	95.21	33	20		599	92.86	93.30	11	9
	666	95.58	95.56	35	20		612	86.30	86.19	11	9
	672	96.55	96.64	34	20		624	46.10	59.73	11	9
	679	95.50	95.14	34	20		632	94.40	94.66	11	9
	684	95.05	94.05	31	19		642	80.27	81.95	11	9
	691	95.15	96.43	32	19		651	80.00	80.82	11	10
	703	92.11	92.22	33	20		661	77.28	77.50	12	10
							668	61.11	62.56	11	10
							674	92.94	93.39	11	10
							681	94.70	94.51	12	10
							686	91.06	92.00	12	10
							693	91.71	91.78	12	10
							705	58.26	59.02	13	9

Appendix D. Table 10. February 2003 Joint Slab Deflection Summary (After DBR, After HVS)

Daytime 1	Station (ft)	LTE (%)		T_surface (C)	T_air (C)	Daytime 2	Station (ft)	LTE (%)		T_surface (C)	T_air (C)
		Pressure = 847 kPa	Pressure = 1287 kPa					Pressure = 837 kPa	Pressure = 1262 kPa		
	486	57.08	66.35	12	13		19	93.79	94.12	10	12
	498	90.40	91.47	11	12		36	92.27	96.61	10	12
	508	92.37	92.35	11	12		48	90.71	92.25	10	12
	517	75.76	76.15	11	12		60	93.33	90.63	10	13
	535	37.54	42.95	11	11		77	94.67	93.44	10	12
	548	66.08	68.86	11	11		99	91.45	94.69	11	13
	561	49.40	53.62	11	11		111	92.82	91.67	10	13
	581	52.35	62.67	11	11		124	91.91	92.39	10	12
	600	82.55	84.04	11	11		142	91.41	92.23	11	12
	614	80.39	79.81	11	11		162	91.41	91.42	11	12
	625	70.76	72.95	11	11		176	88.40	91.60	11	13
	643	82.91	84.23	11	11		187	93.33	88.34	12	13
	651	80.99	83.57	11	11		206	93.23	93.64	12	13
	661	65.43	68.57	10	11		224	96.82	92.44	12	13
	676	81.64	82.82	10	11		238	96.76	96.45	12	13
	686	60.63	67.36	11	11		250	94.93	94.69	12	13
	707	53.20	54.87	10	11		267	91.70	91.73	13	13
							286	94.27	94.67	13	13
							299	94.29	93.77	13	12
							311	90.23	90.54	13	12
							328	95.60	95.32	13	12
							349	93.33	93.67	13	12
							362	95.75	95.22	13	12
							374	96.15	96.63	13	11
							394	96.00	96.17	13	11
							412	94.20	94.09	13	11
							425	91.98	92.24	12	11

							436	96.55	96.28	12	10
							453	95.60	96.31	12	10
							472	93.38	93.70	12	10
							486	60.59	71.19	11	9
							498	89.60	89.87	10	9
							507	97.58	97.04	9	9
							515	81.13	80.69	9	9
							535	34.03	44.76	9	9
							550	65.77	71.08	8	9
							559	53.21	58.61	8	9
							582	62.40	69.85	8	8
							600	84.81	85.97	7	8
							610	81.60	81.92	7	8
							625	65.62	70.61	7	7
							644	80.00	81.36	7	8
							652	100.00	100.00	7	8
							661	70.19	73.89	7	7
							674	84.75	85.94	6	8
							686	64.00	69.08	7	8
							704	62.48	63.92	6	8

APPENDIX E:
CONSTRUCTION SPECIFICATIONS AND SPECIAL PROVISIONS

10-1. Retrofit dowels for concrete pavement joints

General. – Epoxy-coated, round dowels shall be placed in existing concrete pavement at transverse joints at the locations as shown on the plans, and in accordance to the provisions in Section 40, "Portland Cement Concrete Pavement," and these special provisions. Three (Four) dowels per wheel path shall be installed.

Pre-Construction Conference (Dowel Retrofit). – Supervisory personnel of the Contractor and any subcontractor who are to be involved in the concrete dowel retrofit work shall meet with the Engineer, at a mutually agreed time and location, to discuss methods of accomplishing all phases of the dowel retrofit work.

Materials. – Materials shall conform to the following:

Dowels. – Dowels at transverse joints shall be placed as shown on the plans. Dowel bars shall be smooth round epoxy coated steel conforming to the requirements of ASTM Designation: A 36M and shall conform to the details shown on the plans and the provisions in Section 75-1.02, "Miscellaneous Iron and Steel" of the Standard Specifications, except galvanization will not be required. Dowels shall be epoxy coated over the entire bar and shall conform to the provisions of Section 52-1.02B, "Epoxy Coated Bar Reinforcement," of the Standard Specifications, except that references made to ASTM Designation D 3963 shall be changed to ASTM Designation A 934.

Dowels shall be 460 mm ±6 mm in length and free from burrs or other deformations detrimental to free movement of the bars in the concrete. Dowels shall be a nominal 38 mm in diameter for pavement thickness greater than or equal to 215 mm and shall be a nominal 2 mm in diameter for pavement thickness less than 215 mm. Alternative dowels may be required by the Engineer, and will be supplied by the Engineer.

Bond Breaker. – Dowels shall be lubricated with a bond breaker over the entire bar. A bond breaker application of petroleum paraffin based lubricant or white pigmented curing compound shall be used to coat the dowels completely prior to concrete placement. Oil or asphalt based bond breaker shall not be allowed. Petroleum paraffin based lubricant shall be (1) Dayton Superior DSC BB-Coat, or (2) Valvoline Tectyl 506 or an approved equal. Petroleum paraffin based lubricant shall be factory applied. White pigmented curing compound shall be in accordance to ASTM Designation: C309, Type 2, Class A, and shall contain 22 percent minimum nonvolatile vehicles consisting of at least 50 percent paraffin wax. Curing compound shall be applied in two separate applications. Each application of curing compound shall be applied at the approximate rate of one liter per 3.7 m^2.

Expansion Cap. – Expansion caps shall be tight fitting, commercial quality non-metallic, non-organic material that will allow for 6 mm (minimum) of movement at each end of the bar.

Caulking Filler. – Caulking filler used for sealing the traverse joint at the bottom and sides of the slot shall be a silicone caulk containing a minimum of 50 percent silicone and is

designated as a concrete sealant. Caulking filler shall be in accordance to ASTM Designation C834.

Foam Core Insert. – The foam core insert shall be closed cell foam faced with poster board material or plastic faced material on each side, and/or rigid styrofoam material capable of remaining in a vertical position and tight to all edges during the placement of the fast setting grout.

Dowel Bar Support Chairs. – Chairs for supporting the dowel bars shall be either completely epoxy coated steel in accordance with ASTM Designation A 884 or shall be fabricated or commercial quality nonmetallic, non-organic material. The dowel bar support chairs shall firmly hold the dowels centered in the slots during grout backfill operations. Dowel supports shall be designed to hold the bar 13-mm above the bottom of the slot while the slot backfill is placed and consolidated.

Fast Setting Grout. – Fast setting grout materials shall conform to Section 90, "Portland Cement Concrete," of the Standard Specifications and shall be either (1) magnesium phosphate concrete, either single component (water activated) or dual component (with a prepackaged liquid activator); or (2) modified high alumina based concrete; or (3) portland cement based concrete, as approved by the Engineer. Magnesium phosphate concrete, modified high alumina based concrete or portland cement base concrete shall conform to the following requirements:

Property	Test Method	Requirements
Compressive Strength		
at 3 hours, MPa	California Test 551	21 min.
at 24 hours, MPa	California Test 551	35 min.
Flexure Strength		
at 24 hours, MPa	California Test 551	3.5 min.
Bond Strength; at 24 hours		
SSD Concrete, MPa	California Test 551	2.1 min.
Dry Concrete, MPa	California Test 551	2.8 min.
Water Absorption. %	California Test 551	10 max.
Abrasion Resistance		
at 24 hours, grams	California Test 550	25 max.
Drying Shrinkage at 4 days, %	ASTM Designation: C 596	0.13 max.
Soluble Chlorides by mass, %	California Test 442	0.05 max.
Water Soluble Sulfates by mass, %	California Test 417	0.25 max.

Clean, uniform rounded aggregate filler may be used to extend the pre-packaged concrete. The moisture content of the aggregate shall not exceed 0.5 percent. Grading of the aggregate shall conform to the following:

Sieve size	Percentage Passing
9.5 mm	100
1.18 mm	0-5

The amount of aggregate filler shall conform to the manufacturer's recommendation, but in no case shall the concrete strengths be less than that specified for magnesium phosphate concrete.

Magnesium phosphate concrete shall be formulated for minimum initial set time of 15 minutes and minimum final set time of 25 minutes at 21°C. The materials, prior to use, shall be stored in a cool, dry environment.

Mix water used with water activated material shall conform to the provisions in Section 90-2.03, "Water."

The quantity of water for single component type or liquid activator (for dual component type) to be blended with the dry component, shall be within the limits recommended by the manufacturer and shall be the least amount required to produce a pourable batter.

Addition of retarders, when required and approved by the Engineer, shall be in conformance with the manufacturer's recommendations.

Before using grout material that has not been previously approved, a minimum of 20 kg shall be submitted to the Engineer for testing. The Contractor shall allow 30 days for the testing. Each shipment of concrete material that has been previously approved shall be accompanied by a Certificate of Compliance as provided in Section 6-1.07, "Certificates of Compliance."

Silicone Joint Sealant. – Low modulus silicone joint sealant shall be furnished in a one-part silicone formulation. Acid cure sealants shall not be used. The compound shall be compatible with the surface to which it is applied and shall conform to the following requirements:

Specification	Test Method	Requirement
Tensile stress, 150% elongation, 7-day cure at 25°±1°C and 45% to 55% R.H.[e]	ASTM D 412 (Die C)	310 kPa max.
Flow at 25°±1°C	ASTM C 639[a]	shall not flow from channel
Extrusion Rate at 25°±1°C	ASTM C 603[b]	75-250 gms/min.
Specific Gravity	ASTM D 792 Method A	1.01 to 1.51
Durometer Hardness, at -18°C Shore A, cured 7 days at 25°±1°C	ASTM C 661	10 to 25
Ozone and Ultraviolet Resistance, after 5000 hours	ASTM C 793	No chalking, cracking or bond loss
Tack free at 25°±1°C and 45% to 55% R.H.[e]	ASTM C 679	less than 75 minutes
Elongation, 7 day cure at 25°±1°C and 45% to 55% R.H.[e]	ASTM D 412 (Die C)	500 percent min.
Set to Touch, at 25°±1°C and 45% to 55% R.H.[e]	ASTM D 1640	less than 75 minutes
Shelf life, from date of shipment	---	6 months min.
Bond, to concrete mortar-concrete briquets, air cured 7 days at 25°±1°C	AASHTO T 132[c]	345 kPa min.
Movement Capability and Adhesion, 100% extension at -18°C after, air cured 7 days at 25°±1°C, and followed by 7 days in water at 25°±1°C	ASTM C 719[d]	No adhesive or cohesive failure after 5 cycles

Notes:
a ASTM C 639 Modified (15 percent slope channel A).
b ASTM C 603, through 3-mm opening at 345 kPa.
c Mold briquets in accordance with AASHTO Designation: T 132, sawed in half and bonded with a 1.5 mm maximum thickness of sealant and tested in accordance with AASHTO Designation: T 132. Briquets shall be dried to constant mass at 100±5°C.
d Movement Capability and Adhesion: Prepare 305 mm × 25 mm × 75 mm concrete blocks in accordance with ASTM Designation: C 719. A sawed face shall be used for bond surface. Seal 50 mm of block leaving 12.5 mm on each end of specimen unsealed. The depth of sealant shall be 9.5 mm and the width 12.5 mm.
e R.H. equals relative humidity.

The silicone joint sealant shall be formulated to cure after application, on grades of up to 15 percent, recessed below the final surface as shown on the plans.

A Certificate of Compliance for the silicone sealant shall be furnished to the Engineer in accordance with the provisions of Section 6-1.07, "Certificates of Compliance," of the Standard Specifications. The certificate shall also be accompanied with a certified test report of the results of the required tests performed on the sealant material within the previous 12 months prior to proposed use. The certificate and accompanying test report shall be provided for each lot of silicone joint sealant prior to use on the project.

Construction Requirements. – The Contractor shall install the dowel bars in the existing portland cement concrete pavement as shown in the plans and according to the following requirements:

Slot Cutting. – Slots shall be cut in the pavement to place the center of the dowel bar at mid-depth in the pavement slab as directed by the Engineer. The slots shall be parallel to each other and to the centerline of the roadway with a maximum tolerance of 6-mm. Contractor shall employ saws equipped with gang mounted diamond blades to provide the desired width and capable of making three (or four) slots simultaneously. Slots shall not be cut more than four hours prior to concrete slot removal. After initial slot cutting, no traffic shall be allowed over these cuts. A minimum of three (or four) slots in each wheel path will be required. Skewed joints or cracks may require slot longer than the length specified in the plans. No additional compensation shall be made for additional length or any component of the dowel bar retrofit beyond limits as shown on the plans. Pickup and removal of debris concrete, water residue, or paste shall be immediate. It shall include the use of high power, mobile, vacuum cleaning machine capable of removing all displaced material with a minimum of dust.

Break out slot concrete. – Concrete removal operations and the equipment used to remove the concrete shall not damage the pavement to remain. If the concrete removal operations causes damage, as determined by the Engineer, to the pavement that is to remain, the concrete removal operations shall be discontinued. Concrete removal operations shall not resume until the Contractor has taken corrective measures, approved by the Engineer. Damage to the concrete to remain shall be repaired or replaced, as determined by the Engineer, at the Contractor's expense to a condition prior to removal operations.

Any jack (chipping) hammers used to break loose the concrete between the saw cuts shall not be greater than the 14-kg class. If the pavement is damaged by the 14-kg hammer, the Contractor will be required to use a 7-kg hammer. After removal of large concrete pieces by jack hammering, the Contractor shall use small hammerhead to chip off rocks and burrs from the slot bottom to produce a level surface for dowel to sit.

Slot Cleaning and Preparation. – All exposed surfaces and cracks in the slot shall be cleaned using sand blasting to remove debris and to clean surfaces such that clean aggregate is exposed. Where sand blasting operations are being performed within 3 meters of a lane occupied by public traffic, the residue, including dust, shall be removed immediately after contact between the sand and the surface being treated. Such removal shall be by a vacuum attachment operating concurrently with the sand blasting operation. In all other instances, all debris or residue in the slot shall be vacuumed prior to bar installation.

Immediately after vacuuming all debris from the slot, the slots shall be finally cleaned with moisture-free, oil-free compressed air having a minimum pressure of 620 Kpa.

Seal Joints and Cracks in Slot. – The Contractor shall seal the existing transverse joint at the bottom and the sides of the slot with caulking filler. This caulking filler shall be placed to a minimum of 13 mm beyond the edges of the slot in the existing transverse joint.

Any other cracks within the slot shall also be filled with caulking filler. 1300 parts per million of sulfates as SO_4, nor shall it contain any impurities in a sufficient amount to cause discoloration of the concrete or produce etching of the surface.

Water from core drilling operations shall not be permitted to fall on public traffic, to flow across shoulders or lanes occupied by public traffic, or to flow into gutter or other drainage facilities.

Joint Sealing. – Joint sealing shall be completed as specified elsewhere in these special provisions and as shown on the plans.

Removing old sealant. – The Contractor shall remove the existing sealant by manual removal, sawing, plowing or cutting. Contractor shall propose method of removal to the Engineer for approval 7 working days before actual sealant removal. No sealant removal by the Contractor shall take place until the Engineer approves the sealant removal method. V-shaped plows shall not be allowed when using plowing method. Only rectangular plows shall be allowed if plowing method is used. Any removal method selected shall not damage the existing sealant reservoir.

Shaping the reservoir. – The Contractor shall repair minor spalling along joint faces as shown on the plans. Contractor shall use vinyl concrete patching compound as specified elsewhere in these special provisions.

Cleaning the reservoir. – The Contractor shall thoroughly clean the reservoir of any dust, dirt, or visible traces of old sealant. Chemical solvents shall not be used to wash the joint reservoir. Immediately after sawing, plowing or cutting, or manual removal, any slurry or remaining debris from these removal operations shall be cleaned away. This cleaning operation shall be performed in one direction to minimize contamination of surrounding areas. Pavement surface moisture shall be removed at the joints by means of compressed air or moderate hot compressed air or other means approved by the Engineer. Drying procedures that leave a residue or film on the joint wall shall not be used. After the joint has dried sufficiently, sandblast the joint to remove any remaining residue. Sandblasting straight into the joint shall not be allowed. The sandblast nozzle shall be pointed close to the surface at an angle to clean each joint face. A minimum of one pass along each reservoir face shall be made. To ensure that the reservoir is clean after sandblasting, the joint shall be air blasted to remove sand, dirt, and dust no longer than one hour before placement of sealant. Compressed air used to air blast the joint shall not introduce oil into the joint. If oil is accidentally introduced into the joint, the Contractor shall begin the joint cleaning process again until the satisfaction of the Engineer is met that the joint is

clean. Compressed air shall deliver air at a minimum of 3.40 m^3 per minute and develop at least 0.62 MPa nozzle pressure. A vacuum sweeper shall be used to remove all debris or contaminants from the surrounding pavement surfaces after air blasting.

Backer rod installation. – Backer rods shall be installed after joint cleaning. The backer rod must have a diameter at least 25% greater than the reservoir width. Backer rod shall be installed as shown on the plans and shall be expanded, closed-cell polyethylene foam that is compatible with the joint sealant so that no bond or adverse reaction occurs between the rod and sealant. Backer rod shall be installed when the temperature of the portland concrete pavement is above the dew point of the air and when the air temperature is 4°C or above. Backer rod shall be installed when the joints to be sealed have been properly patched, cleaned and dried, as determined by the Engineer. Methods of placing backer rod that leave a residue or film on the joint walls, shall not be used.

Cleanliness inspection. – Before installing sealant, the reservoir sidewalls shall be checked for cleanliness by the Engineer. The Engineer shall check for dirt and dust by wiping the sidewalls with their fingers. If any traces of contamination are found, the Contractor shall reclean the joint.

Placing dowel assembly in Slot. – Any dowel bar surface contaminant shall be cleaned prior to application of the bond breaker. The dowel bars shall be lightly coated with the bond breaking compound prior to placement. The Contractor shall not allow the bond breaking compound to drip onto the slot walls or bottom if wax curing compound is used. The bar chair shall provide a minimum of 13-mm clearance between the bottom of the dowel bar and the bottom of the slot. The dowel bars shall be placed to the depth shown on the plans, parallel to the traffic lane centerline and the top of the roadway surface, and at the middle of the slot, all within a tolerance of 6 mm. Dowels shall be centered at the transverse joint, such that not less than 205 and not more than 255 mm of the dowel extend into each adjacent panel. The chair shall hold the dowel bar securely in place during placement of the fast setting grout.

The foam core insert shall be placed at the middle of the dowel bar to maintain the transverse weakened plane joint. The existing joint sealant is to be removed to accommodate the 6 to 13 mm thick foam core board with two 13 mm by 13 mm tabs. The tabs are required to stabilize the foam core insert during backfilling with fast setting grout. The foam core insert shall be capable of remaining in a vertical position and tight to all edges during the placement of the fast setting grout.

Mixing Fast Setting Grout. – The Contractor shall mix fast setting grout in accordance to the manufacturer's instructions and these special provisions.

The components of prepackaged, dual component (with a prepackaged liquid activator) magnesium phosphate shall be combined by mixing the units completely as supplied by the manufacturer. Portion of units shall not be used. Water shall not be added to dual component magnesium phosphate.

Magnesium phosphate grout shall not be mixed in containers or worked with tools containing zinc, cadmium, aluminum, or copper. Modified high alumina based grout shall not be mixed in containers or worked with tools containing aluminum.

Placing Fast Setting Grout. – The Contractor shall fill the slot (with the installed dowel bar with caps, chairs, joint filler material, and silicone caulk in place) with the fast setting grout. The grout shall be vibrated with a small hand held vibrator capable of thoroughly consolidating

the grout material into the slot and around the dowel bars. All grout shall be placed while fresh, and before the grout has taken an initial set.

Grout shall not be re-tempered. Finishing tools that are cleaned with water shall be thoroughly dried before working the grout.

The surface temperature of the areas to receive the concrete shall be 5°C or above when grout is placed. Methods that are proposed to heat said surfaces are subject to approval by the Engineer. The contact surfaces to receive magnesium phosphate grout shall be dry. The contact surfaces to receive modified high alumina based grout or portland cement based grout may be damp but not saturated.

Finishing Grout. – The surface of backfilled dowel bar slots shall be slightly rounded above the existing concrete surface, which will be trimmed during subsequent grinding work.

Curing Grout. – Fast setting grout shall be cured in conformance with the provisions in Section 90.7.01B, "Curing Compound Method," of the Standard Specifications.

Saw Cut. – The existing sealant (if any) shall be removed and disposed of. Transverse contraction joints shall be sawed or routed as shown in the plans. Procedures for sealant removal, saw cutting or routing the joint shall conform to "Concrete Pavement Joint Resealing," elsewhere in these special provisions.

Grind Pavement. – Pavement shall be ground, after transverse weaken plane joints are sawn, to smoothness and/or finishing requirements as specified in Section 42 of the Standard Specifications for "Groove and Grind Pavement" and elsewhere in these special provisions. Each transverse joint with the completed grouted backfilled slots shall be ground smooth within 30 calendar days from the initial concrete slot cutting. The Contractor shall grind the width of the pavement lane(s). All grout backfilled slots must have a minimum cure time of 12 hours before any grinding.

All dowel bars misaligned or damaged by the Contractor shall be repaired or replaced at the expense of the Contractor.

Once the Contractor has removed the concrete from the slots, these slots must be completed within the same work shift with the dowel and the fast setting grout place into the slot in accordance with these special provisions. In no case, shall the Contractor leave any slot unfilled prior to opening to traffic.

All removed material or material generated by the Contractor's operations shall be disposed of outside the right-of-way in accordance with Section 7-1.13 "Disposal of Material Outside the Highway Right of Way," of the Standard Specifications.

Measurement and Payment. – The quantity of dowel bar retrofit to be paid for will be agreed to in writing by the Engineer and Contractor prior to commencement of work.